Université des Sciences et Technologies de Lille
UFR des Sciences de la Terre
UMR CNRS PBDS

n° ordre : 3916

*THESE*

pour obtenir le grade de

**Docteur de l'Université de Lille I**

***En Dynamique et Environnement Sédimentaires***

présentée et soutenue publiquement par

**M. Naze-Nancy MASALEHDANI**

Le : 20 décembre 2006

Titre :

# Coal fires associated with the coal waste heaps in the Nord-Pas-de-Calais region, France
# The environmental pollution and resulting by-products

**JURY**

| | | |
|---|---|---|
| **Florias MEES** | **Université de Gant** | **Rapporteur** |
| **Bernard GUY** | **Ecole des Mines de St. Etienne** | **Rapporteur** |
| **Fabrice CAZIER** | **Université du Littoral** | **Examinateur** |
| **Yves PAQUETTE** | **INERIS, St. Etienne** | **Examinateur** |
| **Michel DUBOIS** | **Université de Lille I** | **Examinateur** |
| **Jean-Luc POTDEVIN** | **Université de Lille I** | **Directeur** |

**Science Times** Tuesday, January 15, 2002

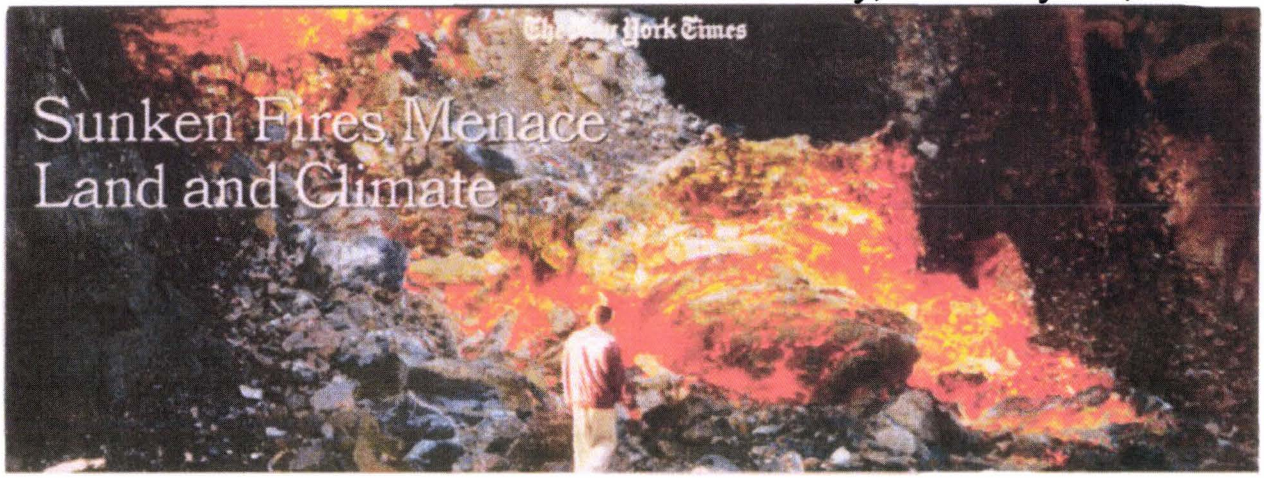

An open pit coal mine in northern China is being mined for coal even as it burns (Prakash, 2002).

Surface fire in the western part of the Jharia coalfield, India (Prakash, 2002).

**"The problems that exist in the world today cannot be solved by the level of thinking that created them"**

**Albert Einstein**

# TABLE OF CONTENTS

## CHAPTER VI (ARTICLE N°4, CASE STUDY): MINERALOGY AND PETROGRAPHY OF IRON-RICH SLAGS AND PARALAVAS FORMED BY SPONTANEOUS COAL COMBUSTION, ROTOWARO COALFIELD, NORTH ISLAND, NEW ZEALAND 185

# SUMMARY IN FREANCH

La demande croissante en énergie et la découverte d'énormes réserves de charbon dans le nord de la France ont contribué à l'extraction intensive du charbon depuis 200 ans. L'exploitation souterraine a engendré la formation de terrils en surface, et très souvent aux abords de l'habitat local, sans précautions particulières prises en matière de protection de l'environnement. Ces énormes amas de déchets miniers contiennent des matériaux inflammables et sont peu compacts, ce qui favorise la circulation d'air. Ils sont ainsi susceptible de subir des phénomènes d'auto combustion ou de participer aux incendies initiés par les forêts ou les ordures ménagères. Le fait que ces types de déchets miniers sont des matériaux combustibles et ces risques-là sont liés à la pollution des cours d'eau, nappes phréatiques et sols, sont encore peu pris en compte en région Nord-Pas-de-Calais.

Le « coal fires » sont signalés pratiquement de par le monde et ils sont des phénomènes catastrophiques générant, en particulier, d'importantes émissions de gaz et particules nocifs, des affaissements de terrain, la formation de sédiments métamorphisiés et fondus (« the porcellanites, the slags et the paralavas », de produits de condensation responsables de la pollution des nappes phréatiques et des sols. Les conséquences de tels phénomènes sur les populations peuvent être dramatiques : taux de mortalité élevé, déplacement massif des populations entraînant la désertification des agglomérations, destruction de l'écosystème par exemple en Chine, Inde, U.S.A. et Afrique du Sud, notamment. L'exploitation industrielle du charbon a favorisé la multiplication de ces phénomènes.

Depuis ces cinq dernières années, sont apparus des articles dans des revues spécialisés, ainsi que sur internet, décrivant les implications de ces mises à feu spontanées sur l'environnement et la santé publique. Néanmoins ces informations restent encore insuffisantes, notamment dans le domaine de la santé publique, alors que les implications, quasi similaires, de l'utilisation domestique du charbon ont été largement décrites (en Chine par exemple). Outre ces conséquences à court ou moyen terme sur les populations et l'écosystème, l'émission massive de gaz à effet de serre ($CH_4$ et $CO_2$) venant part des mines de charbon en combustion peut contribuer gravement, au cours de ce siècle, au réchauffement de la planète.

Naturellement les scientifiques se doivent de publier les résultats de leur travail de recherche, du moins sur l'aspect santé publique, afin d'informer les pouvoirs publics sur les dangers présentés par ces émanations toxiques. Une première conférence internationale faisant le point sur les recherches en cours s'est tenue en 2005 à Pékin sous l'égide de l'UNESCO. Invitée à y participer, j'ai présenté les premiers résultats de ce travail.

En l'absence de thématique au niveau national sur ce sujet en France, ce projet intitulé "Coal fires associés aux terrils miniers de la région Nord-pas-De-Calais, France : Pollution environnementale et produits secondaires" a été soumis par cet auteur au laboratoire de « Processus et Bilans des Domaines Sédimentaires » département de géologie de l'université de Lille1, sans support financier. Deux terrils en activité ont été choisis pour cette étude : il s'agit du terril n°76 situé à Avion et du terril n°83, aujourd'hui à l'abandon, situé à Fouquières les-Lens. Le terril n°76 est un terril conique qui est en combustion depuis 1987. Evidement, aucune végétation ne pousse à la surface des zones de combustion. Le terril n°83 est un terril tabulaire qui a été exploité pour ces schistes noirs et rouges pour les travaux routiers par la société Terril S.A. puis a été abandonné. Ce site est déclaré zone dangereuse et a été fermé au public par des grillages en 2002.

Un autre terril, n° 144 à Rieulay a été choisi pour un travail en minéralogie. Quelques minéraux secondaires ainsi que des débris métamorphisés ont également été échantillonnés sur ce terril pour comparaison. Ceci nous a permis d'estimer les températures de "baking" des débris et de certains minéraux néo-formés. Il s'agite de l'un des plus anciens terrils de la région. De forme allongée ce terril est contient suffisamment de charbon pour être à nouveau exploite. A l'inverse des deux précédents terrils, la combustion sur ce dernier terril est mise intentionnellement par l'industrie à des fines commerciales (exploitation de schiste rouge).

Les porcellanites, "slags" et "paralavas" échantillonnées sur une mine de charbon ayant subi une combustion spontanée dans l'île du Nord de Nouvelle-Zélande ont, par ailleurs, contribué à identifier des assemblages minéraux uniques témoins de ces évènements. On note que les "slags" sont Fe-riche et contiennent des phases cristallines telles que magnetite, hematite, hercynite, titaniferous magnetite, fayalite et ± verre. Les "paralavas" sont Si-riche, et ils contiennent fayalite, orthoferrosilite, anorthite, cristobalite, tridymite et du verre. Etude de ces phases minérales dans ces échantillons indiquent que ces sédiments one été formés à très haute température voir $\geq$1600°C. La source de Fe nécessaire pou produire ces Fe-riches "slags" est une énigme car les sédiments originaux ne sont pas riches en Fe. Nous études montent que le fer a été mobilisé et concentré pendant les processus de pyrometamorphisme et de combustion. Les sédiments "slags" exceptionnellement riches en fer étudiés ici sont plutôt très

rares et les exemples de Rotowaro représentent les "slags" naturels les plus riches en Fe jamais connus de l'environnement "combustion metamorphic".

De nombreux résultats présentés dans cette thèse ont fait l'objet de communications (orales ou par voie posters) lors de conférences au niveau national ou international (voir bibliographie). Une partie des résultats donnés dans les chapitres 3 et 4 a été présentée lors de la première conférence internationale, déjà citée. L'article final sera publié par l'UNESCO dans "ERSEC Ecological Book Series N°4". L'article reproduit dans le chapitre 6 est, quant à lui, accepté pour publication dans "Coal Fires Book Special Edition by the American Geological Society". L'article reproduit dans le chapitre 3 est en cours de révision pour la revue "Environmental Pollution Journal". A l'invitation des éditions Elsevier, l'article reproduit dans le chapitre 4 contribuera au premier "World Atlas of Coal Fires". Ce dernier article remanié sera bientôt soumis pour publication dans une revue internationale.

**Le présent document est organisé comme suit**:
Le chapitre 1 propose un aperçu général des terrils en région Nord-Pas-de-Calais. Il y est décrit également le phénomène de combustion spontanée dans les terrils, ses causes et mécanismes. Le chapitre 2 présente les différents modèles élaborés pour décrire ce phénomène. Ils montrent clairement la propension qu'ont les matériaux constituant le terril à s'embraser spontanément. Le chapitre 3 présente les résultats d'analyse in situ de gaz émis des deux terrils sélectionnés. L'étude des formations minérales secondaires issues du dégazage des terrils en combustion fera l'objet du chapitre 4. L'analyse des inclusions fluides présentes dans les cristaux de sulfate de sodium est présentée dans le chapitre 5. Le chapitre 6 décrit la minéralogie et la pétrographie des "paralavas" et "slags" riches en fer de Nouvelle-Zélande. Les similarités avec les résultats du présent travail, recueillis sur les sites miniers du nord de la France, sont particulièrement soulignées. En conclusion de ce travail, chapitre 7, sont données quelques pistes afin de prévenir et lutter contre ces phénomènes.

Ce travail est le fruit d'une collaboration étroite entre divers laboratoires et organismes de recherche Français, dont l'Université de Lille 1, l'Université du Littoral (Dunkerque), l'Université de Paris VI, Jussieu, l'Ecole des Mines de Douai et l'INERIS, St. Etienne, et internationaux, dont «UNESCO, Beijing, China ; Auckland University, New-Zealand; Université de Gant, Belgium; the Geological Society of America and East Georgia College, Swainsboro, Georgia, the United States of America; et CSIRO, Sydney Australia».

La dégradation générale des deux terrils étudiés dans la région Nord-Pas-de-Calais est liée à la combustion des matériaux (du charbon et débris des schistes Carbonifères) riches en matière organique (carbone organique). La combustion modifie la résistance, la composition et la cohérence des matériaux du terril et s'accompagne d'une réduction de volume conséquente. Elle se signale comme suit : apparition de fentes de tension et d'ouvertures circulaires, développement de fissures superficielles, présence de fumerolles, débris de schistes oxydés rouges et métamorphisés, émission de divers gaz (et vapeur d'eau), et dépôts de sels minéraux secondaires. Les propriétés physiques et chimiques des matériaux constituant les terrils sont à l'origine de ces phénomènes de combustion, ces propriétés contrôlent l'avancée de la combustion. On peut dresser comme suit une liste des principaux facteurs intervenant dans le déclenchement de ces phénomènes:

- qualité du charbon ("rank") et sa matière volatile (MV)
- taux d'humidité du charbon
- composition pétrographique
- composition pétrographique des schistes Carbonifères et leur teneur en charbon organique
- taux de pyrite dans le charbon et dans des schistes Carbonifères
- méthode minière (l'exploitation du charbon), la construction de terril (l'influence de la taille), la granulométrie des schistes Carbonifères, et la circulation d'air
- conditions atmosphériques

Des mesures de température de surface, régulièrement espacées sur une période d'un an, ont été faites près de fumerolles du terril 76. Les températures mesurées de 40 à 255.7°C ont montrées que la combustion est ainsi plus active au NE et du SE du terril. Il faut bien préciser encore qu'il s'agit de températures mesurées en surface, et que donc elles sont différentes de celles auxquelles les débris ont été soumis (voir ci-dessous).

Les schistes Carbonifères du terril 76 en plus de pyrite et de carbone d'origine organique sont composés de quartz, kaolinite, muscovite, illite, ± gypse, ± siderite, ± chlorite. Ces débris ont été transformés suite à l'altération thermique et à la déshydrations totale à des températures comprises entre 500 et 900°C à la pression atmosphérique en débris rougeâtres "the porcellanites" riches en hématite et contenant du quartz. Par contre les grès à quartz ont peu été affectés par la combustion. De plus, pas de trace significative de débris de roches fondues ("the slags et the paralavas"), ce qui indique que la température n'a pas excédé 900°C dans ce terril, comme le confirme l'étude suivante menée en laboratoire.

Il a été constaté que les minéraux argileux se déshydratent les premiers à 500°C. A cette température, l'eau moléculaire et les ions OH sont évacués de la kaolinite, comme le montrent les clichés de XRD. Les processus de dégradation de l'illite, de la muscovite et de la calcite commencent vers 700°C, à 900°C ces minéraux disparaissent. A 1200°C, apparaissent de nouvelles phases, la mullite, la cordiérite, le spinelle, la tridymite. Les échantillons présentent alors une surface ("ropy"), parsemée de vésicules sphériques de diamètre pouvant atteindre 2 mm et significatives du dégazage de l'échantillon.

Ces résultats expérimentaux ont démontré que, contrairement au terril 76, le terril 144 à Rieulay a été soumis à des températures élevées ($\geq$1200°C), puisqu'il y a été trouvé la plupart des minéraux de hautes températures énumérés ci-dessus.

Trois séries de mesures de composition des gaz éjectés des fumerolles du terril n°76 (deux pour le terril n°83) ont été effectuées in-situ par la "chamber method". L'obectif de cette étude a été de mesurer les quantités de divers gaz contenus dans les émanations gazeuses se dégageant du sol de ces deux terrils. La température et la composition des gaz en $H_2S$, $SO_2$, $NO_x$, CO, $CO_2$, hydrocarbures, $O_2$ et $H_2O$ ont ainsi pu être déterminées.

Le $H_2S$ est piégé par barbotage dans de la soude 0.5 N. On fait ensuite réagir la solution obtenue avec du N,N-diméthyl-p-phénylènediamine oxalate pour former du bleu de méthylène. L'analyse est réalisée par spectroscopie UV (absorbance à 665 nm), l'intensité de la couleur bleue développée lors de la réaction étant proportionnelle à la concentration en $S^{2-}$. Les solutions de barbotage (soude 0.5 N) obtenues lors des prélèvements effectués pendant la première campagne de mesure, sont analysées par spectroscopie UV/Visible selon la méthode décrite précédemment. Afin de quantifier les sulfures présents, on a tout d'abord réalisé le spectre UV d'une solution standard de sulfure.
Si le tracé en bleu démontre un pic d'absorption à 665 mm (caractéristique des sulfures), les deux autres tracés restent plats dans cette zone de longueur d'onde. On ne détecte donc pas de sulfure dans nos solutions de barbotage. Lors de la seconde campagne de mesures, des analyses complémentaires ont réalisées sur les condensats recueillis dans le piège froid. Ces mesures sont effectuées afin de vérifier que les sulfures ne sont pas piégés dans les condensats avant leur arrivée dans les barbotages. On ne détecte pas de sulfure dans ces solutions.

Les teneurs et compositions des différents gaz ont été comparées entre elles et évaluées par rapport à la TLV (Threshold limit value), afin de déterminer l'impact négatif de ces gaz sur la santé publique et l'environnement. Comme expliqué ci-dessus dans le texte, les températures mesurées montrent de fortes disparités, ce qui dénote des conditions de combustion très différentes pour les deux sites étudiés. Le résultat le plus significatif est la teneur en $CO_2$, 7%, qui excède de beaucoup la TLV. $SO_2$ (<5 à 25ppmv) et NOx (8 à 25ppmv) sont également au dessus de la TLV. CO, avec des teneurs de l'ordre de 20-110 ppmv, est, pour sa part, à la limite de la TLV. Par contre, $H_2S$ n'a jamais été détecté. $CH_4$, le principal hydrocarbure détecté, a été mesuré à des teneurs de (47 à 260 ppmv) donc au dessous de la limite d'explosion. L'accès au public ne doit pas être pour autant autorisé, en raison de la faible teneur en $O_2$ (<1% à 19%) autour des cavités de gaz de ces sites.

Des études en laboratoire sur l'oxydation de charbons bitumeux moyennement volatile et de schistes Carbonifères du terril n°76 ont également été entreprises. Elles ont montré que la concentration et le mode d'émission des gaz dépendent fortement du ″rank″ et de la température. Par exemple, plus la température augmente, plus la teneur en CO augmente. C'est aussi vrai pour certains hydrocarbures comme le méthane et l'éthylène. L'étude a également montré que les schistes Carbonifères sont sources d'émissions de gaz, tels $SO_2$, CO, $O_2$, et de chaleur ($CO_2$). Les tests d'oxydation des charbons bitumeux ont quant à eux montré que ces échantillons subissaient, d'abord une perte puis une reprise de masse. Ce phénomène peut s'expliquer par la formation initiale de gaz qui restent piégés dans le solide et se condensent pour donner des sulfates.

Durant les trois années de collecte d'échantillons sur le terril n°76, 21 phases minérales différentes ont été identifiées sous forme d'incrustations déposées principalement sur les débris de schistes thermiquement altérés et autour des fumerolles. Les minéraux les plus abondants sont la thenardite et la bloedite, suivis de la konyaite, la glauberite, l'aphthitalite, la langbeinite, l'arcanite, le gypse, l'epsomite, l'hexahydrite, l'alunogen, la kalinite, la pickeringite, l'haltrichite, la tschermigite, la mascagnite, la lecontite, de même que des halides (salammoniac, halite) et du soufre natif. Enfin, la description de deux nouvelles espèces minérales est actuellement en cours. Les éléments chimiques majeurs entrant dans la composition des dépôts minéraux près des fumerolles sont: $SO_4$, $NH_4$, $H_2O$, Cl, Mg, K, Na, Al, Ca, Fe, Mn et S.

Il est tentant de dire que ces phases minérales secondaires qui se forment sur le terril n°76 en combustion ainsi que l'origine du processus de leur formation sont analogues aux minéraux qui se forment autour des fumerolles sur les volcans. Ces assemblages minéraux ont été produits par altération hydrothermale de débris sédimentaires (schiste Carbonifères) par des solutions aqueuses légèrement acides (pH entre 4 et 5.5) suite à la combustion. Ainsi, la plupart des incrustations et des phases cristallines ont été déposées dans un environnement saturé en vapeur d'eau, à des températures comprises entre 40 et 265°C (voir ≤300°C). Les minéraux formés près des fumerolles ont été produits à partir du refroidissement de gaz (S, N, O, C et vapour d'eau) en surface du terril. Il a été démontré que les phases minérales déposées à haute température (≥ 300°C) sont moins abondantes que celles déposées à basse température (≤120°C°). La différence en température contrôle la nature de différente phase minérale secondaire qui se forme sur le terril n°76 à Avion.

Il faut bien préciser que le processus de minéralisation s'est effectué par étapes à partir d'une solution chimique complexe. "Salammoniac" s'est formé par sublimation tandis que thenardite, bloedite, aphthitalite, langebeinite, arcanite, glauberite, halite, gypse, epsomite, pickeringite, alunogen, tschermigite, mascagnite et soufre natif se sont formés par condensation (c'est-à-dire lors du processus de refroidissement d'un système gaz-liquide). Konyaite et hexahydrite sont des produits d'altération minérale partielle: on peut penser qu'une phase de déshydratation est intervenue immédiatement après que le dépôt se soit mis en place, ou bien après échantillonnage. L'hydratation partielle de bloedite a produit le konyaite et la déshydratation partielle d'epsomite a produit l'hexahydrite. La kalinite provient certainement de la déshydratation du "K-alum", et la lecontite pourrait être un produit d'altération de la phase native "ammonium aphthitalite".

La présence d'inclusions fluides dans la thénardite de l'échantillon AV1443d permet de confirmer que la cristallisation dans cet échantillon a bien eu lieu à basse température (≤150°C), en milieu aqueux à haute salinité dominée par $Na_2SO_4$ et NaCl dans l'assemblage thenardite-bloedite-aphthitalite. Toutes les inclusions observées on une origine primaire ou "pseudosecondaire".

Les variations constatées dans les assemblages minéraux du terril n°76 sont liées: à la variabilité de la teneur en charbon d'un site à l'autre, à l'influence de l'interaction gaz-roche sur la chimie des gaz éjectés, à des différences dans la température et la vitesse de refroidissement de ces gaz, aux changements de conditions atmosphériques (saison, pluie etc), et enfin, à la composition de la solution aqueuse.

On a constaté que les sulfates et les halides dont il est question ici sont tous solubles dans l'eau désionisée sans laisser de résidu solide. Sur le terrain, les efflorescences minérales sont donc immédiatement dissoutes dès les premières averses suivant leur formation. Tous les minéraux secondaires décrits pour le terril n°76 pourraient avoir un impact négatif sur la santé publique ainsi que sur l'environnement. En particulier les sulfates qui, en plus des éléments S et N, contiennent des traces de métaux lourds, As, Ba, Cu, Mo, Cs, Ni, Rb, Th, U etc. Les sels produits par ces phénomènes d'autocombustion sont donc des facteurs de pollution des nappes phréatiques (par les nitrates et nitrites en particulier) et des sols, contaminant ainsi les cultures environnantes avec risques réels de passage dans la chaîne alimentaire et menace directe sur la faune et la flore.

La dissolution lente des minéraux composant de Na-Mg-sulfates (thénardite, bloedite etc.), $NH_4$-halide (salammoniac), et $NH_4$-$SO_4$-sulfates (mascagnite, tschermigite, lecontite) et leur précipitation dans des sols (terre cultivée) et dans des nappes phréatiques peut augmenté le taux de sale dans ces zones. L'interaction de gaz avec l'oxygène ambiant résulte en précipitation de $NO^{3-}$ et $NO^{2-}$, de plus, leur migration dans la nappe phréatique peut augmenter le taux de nitrogène et s'avérer un facteur aggravant de pollution. Des mesures effectuées sur l'eau pompée in-situ dans la nappe du terril même, ont révélés des teneurs élevées en nitrates donc supérieure à TLV autorisé à 45 mg/l. Tandis que la teneur en arsenic, pour le moment se situait en dessous de la limite légale de TLV 0.05 mg/l.

Il est donc important d'insister sur le fait que ces formations de sels sur les terrils en auto combustion présentent des risques environnementaux et de santés. Il nous semble urgent, que des études scientifiques soient menées, où la combustion liée aux mines de charbons ou aux terrils miniers se produit, afin de déterminer la nature chimique des phases contenant des éléments nocifs et toxiques ainsi que leurs interactions mutuelles.

La plupart des sulfates décrits dans ce travail, ainsi que l'étude portant sur les inclusions fluides dans la thénardite, constituent une première approche originale des effets induits par les gaz émis des terrils et des mines de charbon en autocombustion. Cette étude, forcément limitée dans le temps, n'a pas pu circonscrire tous les aspects liés à ces phénomènes situés à la frontière de plusieurs domaines scientifiques. Les points suivants devraient être abordés ou développés au cours d'études ultérieures:

1) mesure (régulière) in-situ des gaz éjectés avec quantification des gaz à effet de serre et des flux thermiques (en particulier sur le terril n°83)
2) analyses de l'eau produite par condensation afin de préciser les phénomènes de transports ioniques (métaux lourds en particulier)

3) tests en laboratoire sur les schistes Carbonifères afin d'établir des modèles de sources de chaleur ($CO_2$) potentiels pour les terrils à risque

4) échantillonnage et analyses réguliers de l'eau du robinet et des nappes phréatiques dans l'environnement des terrils (76, 83, 144, en particulier)

5) étude approfondie des processus autour de la formation des minéraux secondaires produits à partir des émissions gazeuses

6) enfin, nous recommandons expressément d'entreprendre une étude ciblée sur les problèmes de pollution de l'eau et des sols dans l'environnement du terril n°144 à Rieulay. Ce site ainsi que les ″taillings″ pourraient être particulièrement chargé en sulfures et As-pyrite surtout en métaux lourds.

La combustion du charbon comme source d'énergie est un puissant facteur d'émission de gaz à effets de serre. On estime à 38% le taux de $CO_2$ émis provenant de l'exploitation industrielle du charbon. Il est bien difficile de faire la part des gaz émis par les phénomènes d'autocombustion, ne serait-ce que par le caractère anecdotique et parcellaire des informations fournies sur le sujet. De nombreux pays de par le monde sont pourtant concernés par ces problèmes, avec des conséquences parfois dramatiques sur les populations et l'écosystème local.

Chaque cas est unique, et les conséquences néfastes des mises en combustion spontanées, comme l'émission des gaz nocifs, $CO_2$, $CH_4$, $SO_2$, $NO_X$, $H_2S$, ne peuvent avoir qu'un caractère local. La mise a feu d'un matériau, ou d'un ensemble de matériaux, est soumise à l'interaction des trois éléments fondamentaux que sont le combustible, la source de chaleur et l'oxygène (représentés usuellement par le “triangle du feu”). Une action ciblée envers l'un quelconque de ces éléments arrêtera sûrement l'incendie, principe qui est mis en oeuvre dans tout protocole d'extinction de feu. Ci-dessous, une liste non exhaustive des actions à entreprendre pour lutter contre ces phénomènes, en agissant principalement sur leurs causes, pour éviter leur déclenchement, et leurs effets, s'ils n'ont pas pu être évités:

- repérer et étudier des sites “fossiles” ayant subi, par le passé, de tels phénomènes
- adapter des procédures de prévention de tels risques aux méthodes d'exploitation des sites miniers
- sensibiliser la population aux risques sanitaires et environnementaux encourus. Mettre en place des protocoles de protection à la personne, voire d'évacuation de la zone, en cas de risques majeurs

- surveiller les terrils en autocombustion avec matériels scientifiques adaptés (mesure in situ des gaz éjectés, des flux de chaleur, etc..).
- établir un réseau mondial d'échange d'informations par tous les supports possibles (publications dédiées, conférences...).
- développer une politique de recherche volontariste, suffisamment budgétisée, sur ces phénomènes.

Compte tenu des coûts engendrés par ces risques, les mesures préconisées ci-dessus ont commencé à être mise en place par une partie de la communauté internationale. La France reste en retard dans ce processus et nous espérons que ce travail contribuera à sensibiliser les autorités sur ces problèmes.

# INTRODUCTION

Expanding consumption of energy and the discovery of coal in northern France resulted in the increased activity in the coal mining industry in this region over 200 years. The underground mining of coal accompanied by creation of coal wastes which were disposed in areas near the coal mine, near by roads and in close vicinity to towns; and without specific care for the environment. Huge overburden dumps contain combustible and flammable materials and they are not compact to reduce the ingress of air. The materials of the coal waste heaps are subject to spontaneous combustion and they are also susceptible to other means of ignition such as heat from burning rubbish or bush fires. The fact that these types of waste materials are a fire hazard and cause air-water-soil pollution is either unrecognized or ignored in the Nord-Pas-de Calais region.

Coal fires are reported from nearly all over the world resulting in a global environmental catastrophe characterised by the emission of enormous quantities of noxious gases and particular matter into the atmosphere; perilous land subsidence; formation of baked and melted sediments; and condensation products responsible for water and soil pollution. Coal fires are responsible for human diseases and fatalities. They have displaced entire communities, turning cities into “ghost towns”, and they have destroyed floral and faunal habitats (e.g. China, India, the U.S.A. and South Africa). Coal mining around the world has facilitated the proliferation of these fires.

During the past five years, numerous articles about the environmental significances of coal fires and their threat to human health appeared internationally in newspaper and magazine articles, research journals, and on the internet. Studies of the relationship between coal seam and coal waste heap fires and health problems are rare and inconclusive; however, studies of residential coal use in China have caused widespread and sever health problems. Therefore, by analogy, we might expect that the health of people living near coal waste heaps may be at risk from the release of trace elements, emission of gases, and particulates. Uncontrolled emissions of greenhouse ($CH_4$ and $CO_2$) and acidic (NOx and $SO_2$) gases contribute to global warming of the earth’s atmosphere. Scientists from all over the world studying the phenomenon of the burning coal seams and coal waste heaps are asked to publish the results of their research because this can provide a valuable service to local communities by familiarizing themselves with clinical signs of exposure to potentially harmful emissions, especially the trace elements. This made the organisation of the first international coal fires research in Beijing, China by the U.N.E.S.C.O. in 2005, where the present author was invited to present some parts of her research work as well as France.

It is in this sense, and in absence of national or international scientific research in France, that the research exposed in this thesis started in the Nord-Pas-de-Calais region: "coal fires associated with the coal waste heaps in northern France: the environmental pollution and resulting by-products". The project was proposed to the Science and Technology University of Lille, Geology Department, laboratory of "Processus et Bilanes des Domaines Sédimentaires", and it was carried out during five years with no financial grant from private or public organisations. Two coal waste heaps in the Pas-de-Calais region were chosen for coal fire gas emission analyses and measurements. The principal research site is coal waste heap n°76 situated in Avion, the second coal waste heap n°83 is an abandon site situated in Fouquières les-Lens. In addition to these sites, some secondary minerals were collected and studied from the coal waste heap n°144 in the Nord region, the coal fire in this later site is man-made. Some identified minerals from coal waste heap n°144 are similar to those found at the coal waste heap n°76 this aimed to estimate the possible temperature formation of baking process and the temperatures of the formation of certain secondary by-products.

The porcellanites, the slags and the paralavas resulted from the coal seam fire in the North Island in New Zealand provided opportunities researching some unique mineral assemblages and brought evidences that coal fire provides insight for the recognition in the geological record of preserved mineral assemblages that are diagnostic of ancient fires.

Some results of present thesis were already presented as abstracts; posters and oral presentation during national and international conferences (see cited references). A part of articles in chapters 3 and 4 were combined and presented during the First International Conference on Coal Fire Research in Beijing, China 2005, the article is accepted for publication by the U.N.E.S.C.O. in the "ERSEC Ecological Book Series N°4". The article in Chapter 6 is also accepted for publication in the first "Coal Fires Book Special Edition by the "Geological Society of America". The entire article in Chapter 3 is under progress and was submitted to the Environmental Pollution Journal. The author is invited to present the article in Chapter 4 for the publication in the first "World Atlas of Coal Fires" by Elsevier. This latter article will be also submitted as to Mineralogical Magazine in near future.
The organisation of the present thesis is explained below:

**Chapter 1** gives a general review of the coal waste heaps in the Nord-Pas-de-Calais region; and describes coal fires and spontaneous combustion within the coal waste heaps the basic causes of spontaneous combustion associated with coal waste heaps are also explained. **Chapter 2** presents the results of laboratory simulations and shows the liability of coal waste heaps materials to heat spontaneously. **Chapter 3** provides the results of in situ gas measurements and analyses from two burning coal waste heaps in northern France. Secondary mineral occurrences and mineralization processes from coal fire gas will be given in **Chapter 4**. Analysis of fluid inclusions trapped in crystals of sodium sulphate mineral formed from coal fire gas is described in **Chapter 5**. An article in **Chapter 6** describes mineralogy and petrography of unique iron-rich paralavas and slags formed from spontaneous coal fire in the North Island in New Zealand. This will put an insight light to this present research work. Finally, conclusions, recommendations and preventions are presented in **Chapter 7**.

This present Ph.D thesis research is also a team interdisciplinary research work of expert scientists from French Universities, Engineering Schools and research organisations (e.g. Université de Lille 1; Université Littoral, Dunkerque; Université de Paris VI; Jeussieu; Ecole des Mines de Douai; and INERIS, St. Etienne); and from Universities and research organisations overseas (e.g. Auckland University, New- Zealand, University of Gant, Belgium; and CSIRO, Sydney Australia). It is hoped that the findings and methods present herein will provide some information and guides to those who may be interested to research about similar topic. The problems outlined in this thesis are not unique to the particular coal waste heaps in northern France. Similar problems are found in other coal waste heaps (e.g. in Alés and St. Etienne in central France) and elsewhere around the world. Gas exhaled from numerous surficial vents and solid combustion by-products associated with the gas have potential to serve as vectors for the transmission of toxins to humans by atmospheric pollution and food grown in soils that contain these solids. These problems necessitate a more-detailed study of the coal seam or coal waste heap fires to prevent and to predicate the cause of combustion; and assess their long-term environmental and health impacts. It is in this concept that I join colleagues (e.g. G.B.Stracher, R.B.Finkelman, D.J.Pone, A. Prakash, F.G.Bell etc) and continue researching about coal fire and its by-products.

# CHAPTER I
# PART 1: COAL WASTE HEAPS IN NORTHERN FRANCE

# 1. THE NORD-PAS-DE-CALAIS COALFIELD

## *1.1. Geological Context*

The coal basin of the North-Pas-de-Calais (Fig. 1) is part of the long band of productive coal deposits which extends from North of France to Belgium and on more than 100 km from East to West. Its average width varies from 12 km in the East of Pas-de-Calais, to 8 km in North until 5 km for its most Western part; its bases are found in the immediate vicinity of the sea, it is thus of paralic type (Bouroz, 1969). The surface of the exploitation is about 1150 km$^2$. It covers a surface of more than 1100 km$^2$ on a thickness of 1.2 km (Fig. 2).

The origin of the coal deposits in the North-Pas-de-Calais region goes back to the end of Dinantien. About 300 million years ago the phase “sudète” appeared in Europe by the uplift of the “varisque” assembly (Fig. 3). The North region escaped from these phenomena but the orogenic constraints show that the sea is withdrawn gradually to leave the place to the coal basin in the region. This basin received the erosion products of the “fluvial” of the uplift assembly, which accumulate in a vast swampy plain in functioning of paralic. This plain is crossed by channels in which accumulate sands resulting from dismantling alternation of mudstones, silts (carbonaceous shales) rich in carbon and conglomerates presenting meters of blocks of this order. In this series, coal beds are intercalated (Delattre et al. 1973).

Following the deformations “hercyniennes” of the phase “asturienne”, then the erosion assembly of the “varisque” formed an undulating territory where the Carboniferous sediments (“namuro-Westphalian”) were only reserved in basins of “Boulonnais”, of “Strouanne”, in the small basin of “Seclin” and in the small basins of “Picardie – Thiérache”.

After important deformations and a long period of erosion, the structured coal basin was covered by the marine transgression “cénomanienne” which yielded deposit of “cénomanienne – turonienne” chalk ("morts-terrains"). The transition enters Carboniferous coal measures and 20-250 m of "morts-terrains" is found by the intermediate of a littoral conglomerate basal named “Tourita” (Delattre et al. 1973).

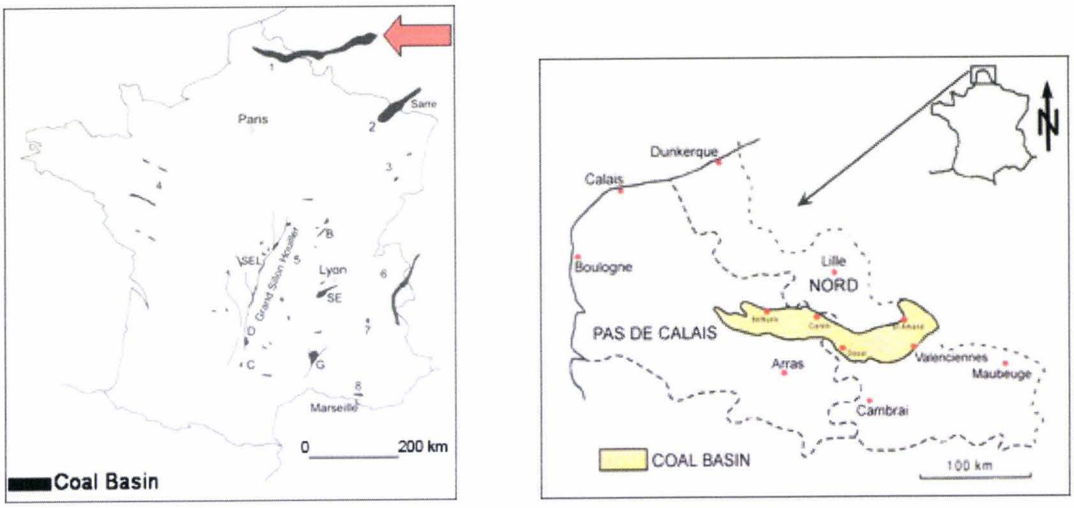

**Figure 1.** Geographical map of the Nord-Pas-de-Calais Coal Basin (Vetter, 198; Denimal, 2001).

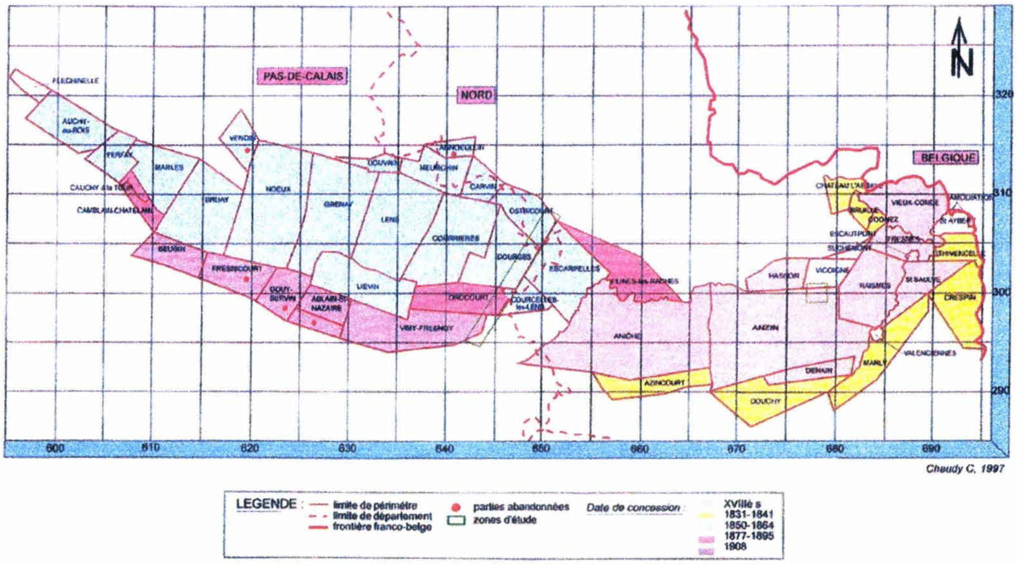

**Figure 2.** The coalfields in the Nord-Pas-de-Calais region (Chaudy, 1997).

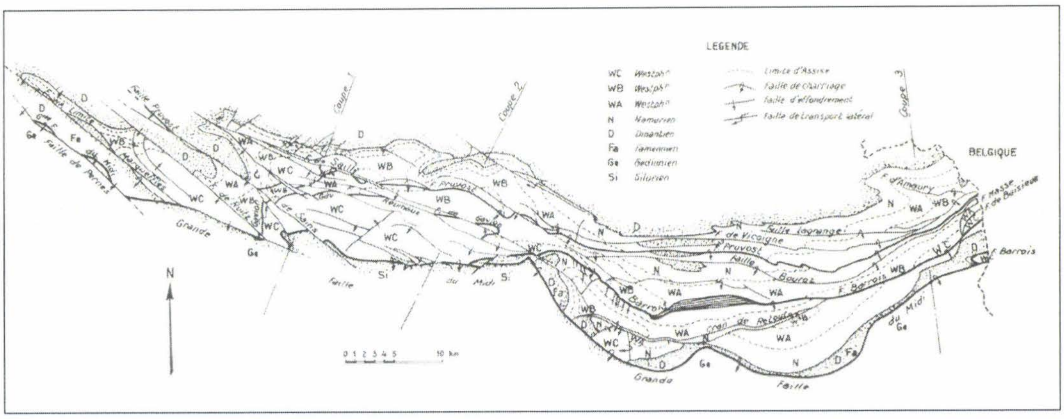

**Figure 3.** The coal basin of the Nord- Pas-de-Calais region (Bouroz, 1969).

### *1.2. Historical context*

The exploitation and the use of coal in Belgium and North of France had been well-known before year 1000 in “Liege, Mons and Charleroi” where the outcrops are frequent. In XVII century, a coal deposit was discovered in “Boulonnais”. In 1718, the coal mines of “Hardinghem and Rety entered in activity. Then later, the exploitation extended to what has become the coal mining basin of the North-Pas-de-Calais region. About 1735, some coal deposits in “Valenciennois” were found, but it was only in 1841 in Oignies and in 1847 in “Escarpelle” that the rich coal seams of the Nord-Pas-de-Calais region were discovered. Then, this huge coal basin became the most important productive coal basin in France. In 1984 its production exceeds 55% of the tonnage of coal extracted from underground coal beds in France (Dubois and Minot, 1991).

The last mining shaft “10 de Oignies” on December 25, 1990 followed up the dissolution of the “Houillères du North-Pas-de-Calais (H.B.N.P.C.)”. On December 31, 1992 this then put an end to the underground coal mining activities over 250 years in this region. It should be stressed that in the 1720-1842 tons of coal (nearly 2.500.000.000 tons) were extracted from underground in North-Pas-de-Calais region. In other words, nearly 100.000 km of galleries were mined in the ex-coal basin of the North-Pas-de-Calais In fact this figure represents approximately 10% of the potential contained in the total of Carboniferous coal measures: it thus remains more than $20.10^9$ tons of coal underground. In addition, one can consider that globally in the Nord-Pas-de-Calais region for 1 ton of coal extracted from underground, 3 tons remained underground for various reasons:

- protection of infrastructure and indispensable network to the exploitation
- faulty zones
- zone where the coal seam is altered , dichotomy, fault, etc.

In the exploited horizons, at least $7{,}5.10^9$ tons of coal thus remained underground in the Nord-Pas-de-Calais region. However, it should be stressed that since 1990 the G.I.E. Methamine and (50% Charbonnages de France and 50% GDF) extract $CH_4$ (firedamp) from underground by means of in-situ underground coal gasification method in Avion (near by coal waste heap n°76 and around pit n° 5 in Lens. Each year, approximately 100.000.000 $m^3$

of gas is thus extracted, corresponding to 600.000.000 kWh of energy value (Charbonnages de France, 2005).

### *1.3. Classification of coal in the B.H.N.P.C.*

In the Nord-pas-de-Calais coal basin (B.H.N.P.C.) the classification of coal was established according to their index of volatile matters and their swelling number, thus eight categories of combustible coal are distinguished. However, in this basin we note a correspondence between the technical structure and the distribution of the categories of coals. Figure 4 shows different coal classification in this basin.

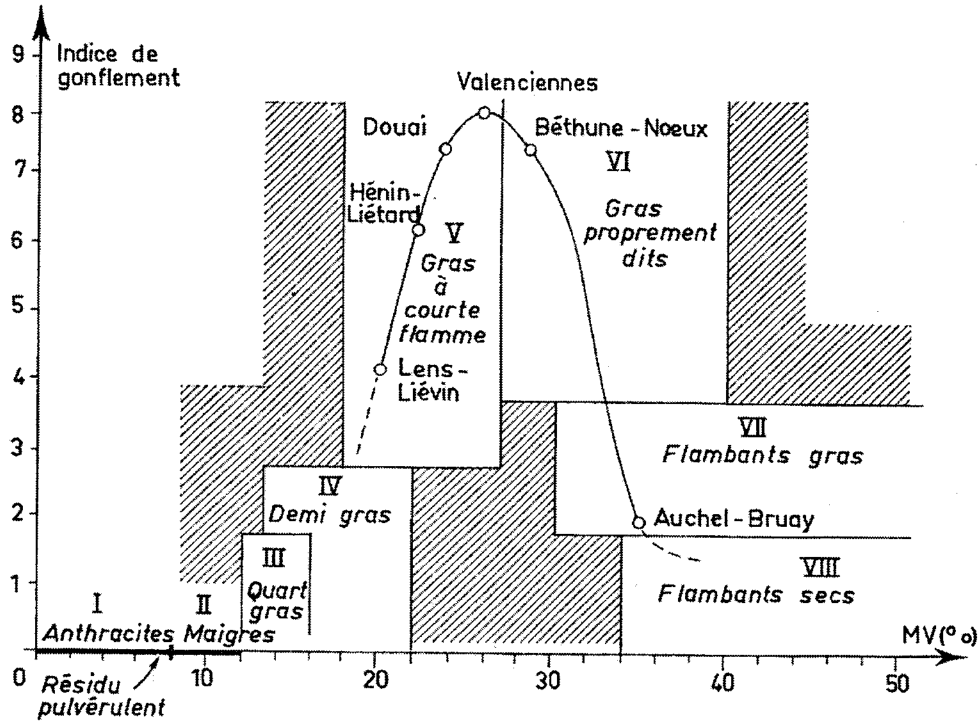

**Figure 4.** Classification of coal (AFNOR M 10 - 001, Delattre et al. 1973).

## 2. COAL WASTE HEAPS

### *2.1. Definition*

“Terri” or “terril”, two spellings exist in the region. The first word probably draws its origin from the regional deformation of the word "terre", it is also possible that it comes from "stérile". The latter spelling is based upon the description of miners to Parisian journalists who described how the explosion of $CH_4$ happened at underground mine of “Courrières” in 1960. The term “schiste”, in a strict sense, applies to an argillaceous rock, transformed by metamorphism. This term in the North region defines Carboniferous sedimentary coal measures which were extracted from underground the same time as coal. These rocks are argillaceous and hardened; have schistose cleavage, have laminated character; and are fragile and rich in carbon. In this same region the terms "schiste noir" and "schiste rouge" are locally used by the industry of exploitation of the coal waste heaps’ materials to differentiate and classify the rock debris. The term "schiste noir" indicates that carbonaceous shale debris has not undergone combustion; and the term "schist rouge" classifies carbonaceous shale debris which has undergone spontaneous combustion or the combustion was man-made by the exploiter himself at the coal waste heap.

### *2.2. Nature of material*

The principal material composing coal waste heaps are carbonaceous shale (70 to 80%) and some sandstone (a few percent). Coal waste heaps also contain some quantities (30 to 20%) of residual coal. The latter depends on the form (the age) of the coal waste heap, the oldest one contain sufficiently coal (see below) to consider the reworking of the site (for example the coal waste heap n°144 in Rieulay) (Masalehdani et al. 2005)

### *2.3. Types*

In the Nord-Pas-de-Calais region two types of coal waste heaps are distinguished:

- dormant coal waste heaps which have not undergone combustion (e.g. Sainte-Henriette in Hénin Beaumont). These types of coal waste heaps have entirely black to grey surface due to their carbonaceous shale component. Depending on the physicochemical conditions of coal waste heaps and thanks to their rich organic carbon content ($\geq$ 14%) some of these coal waste heaps are characterized by fauna and very particular flora (for example :coal waste heap of Pinchonvalles in Avion).

- the second type of coal waste heap is the research subject of this study and the results are written either in chapters or in forms of articles in this thesis. This type of coal waste heap has undergone either spontaneous combustion (e.g. coal waste heap n°76 in Avion) and/or the combustion is man-made where the aim is to bake and dehydrate artificially the carbonaceous shales debris into superior qualities called "schiste rouge" (Coal waste heap n°144 in Rieulay). As explained above, the coal waste heaps are composed of large quantities of combustible materials. In the Nord-Pas-de-Calais region 50% of the 300 coal waste heaps have undergone combustion (Parquette and Laversanne, 2004).The phenomenon of spontaneous combustion in general will be explained in part 2 in this chapter.

The geo-environmental hazards related to the combustion of two coal waste heaps in the Nord-Pas-de-Calais region are published in Masalehdani and Potdevin (2004). Paquette and Laversanne (2003 and 2004) also summarized risks and the preventive measures associated with the burning coal waste heaps.

**Figure 5.** The construction and composant of cone-shaped coal waste heaps about 1960, Loos-en-Gohelle, Pas-de-Calais, (Paquette et Laversanne, 2003).

### *2.4. Forms*

Depending on the technique used at the time of construction of the coal waste heaps, the coal waste heaps vary in size and in form. The form, the size and the method of construction of the coal waste heap influence its susceptibility to spontaneous combustion. Globally, in the Nord-Pas-de-Calais region the coal waste heaps are classified in three forms:

- flat coal waste heaps are the oldest coal waste heaps which were constructed around XIX century when the mining methods were not mechanised yet. They are thus flat, because the rock debris could not be transported high the slopes. They are about 10 to 20 meters in height containing approximately 1 million tons of mixed carbonaceous shale and coal.

- conical coal waste heaps resulted following the introduction of mechanical mining equipment. This led to large quantities of solid wastes being removed by various processes which included coal as well as coal measures. This solid material was transported to the surface and dumped in large cone-shaped coal waste heaps in average they contain 3 million tons of reject material. They are three times larger than latter ones and have an average height of 100 metres (Fig. 5). The cone-shaped coal wastes heaps are known to be prone to undergo spontaneous combustion than the others (see part 2).

- elongated coal waste heaps are the most recent coal waste heaps. The separation of coal and the rock debris were carried out in the washing processes where large quantities of raw materials extracted from different pits were treated. Gigantic, this type of coal waste heap however, are better integrated into the landscape.

# CHAPTER I

## PART 2: COAL FIRES SPONTANEOUS COMBUSTION AND COAL WASTE HEAPS

## 1. COAL FIRES: INTRODUCTION

Coal fires are reported from nearly all parts of the world (Fig. 1). The coal layers or seams are mined by both open pit and underground mining methods. Coal is an organic, highly carbonaceous, which when exposed to certain conditions (temperature, moisture, oxygen etc.) tends to ignite/combust spontaneously at rather low temperatures. This spontaneous combustion may occur naturally or the combustion process may be triggered by other causes (see below). However, once a coal seam catches fire and nothing is done to stop it at an early stage, the seam may continue burn for tens to hundreds of years, depending primarily on the availability of coal and oxygen. Such burning of naturally occurring coal is referred to in general as coal fires. In a broader sense, coal fires include surface coal seam fires, underground seam fires, fires in coal and carbonaceous coal waste heaps and stockpiles (Prakash, 2002) (Figs. 2 and 3). Additional categories include, Paleo coal fire, fire was burning in the paleo time. Recent coal fire, fire was burning in recent time. Extinct coal fire, now fire is extinct, incapable of further burning. Dormant coal fire, fire is not spreading, but is probably capable of re-ignition. Active coal fire, fire is burning and spreading.

## 2. IMPACTS

The burning of coal beds in the ground is not a new event, many fires having been started by nature, not by humans, over the last few million years (e.g. Powder River basin, the USA). What is new in the last few hundred years is the introduction of mining, which exposes large areas of fresh coal to oxidation in places particularly suited to the ignition and spread of fires. Coal mining has facilitated the proliferation of these fires, resulting in a global catastrophe characterised by the emission of enormous quantities of noxious gases and particular matter into the atmosphere, perilous land subsidence, and condensation products responsible for water and soil pollution (Stracher and Taylor, 2004). Coal fires are responsible for human diseases and fatalities (van Genderen and Haiyan, 1997; Finkelman and Gross, 1999, Finkelman, 2004). They have displaced entire communities, turning cities into “ghost towns”, and they have destroyed floral and faunal habitats (e.g. China, India and South Africa, Stracher and Taylor, 2004).

Gas exhaled from numerous surficial vents and solid combustion by-products associated with the gas have potential to serve as vectors for the transmission of toxins to humans by atmospheric pollution and food grown in soils that contain these solids. These problems necessitate a more-detailed study of the coal seam or coal waste heap fires to prevent and to predicate the cause of combustion; and assess their long-term environmental and health impacts. Coal fires present opportunities of discovering rare and new mineral occurrences (Masalehdani et al. 2004; Masalehdani et al. 2005; Pone et al. 2005; Stracher et al. 2005). Coal fires also provide insight for the recognition in the geological record of preserved mineral assemblages that are diagnostic of ancient fires (Masalehdani, 1985).

## 3. SELF-HEATING AND SPONTANEOUS COMBUSTION

Mining activities (underground and/or open pit) produces large quantities of coal waste heaps. Large quantities of material, removed during mining operations, are dumped to form coal waste heaps which, in general, are made up of broken sedimentary rocks including carbonaceous shales, sandstones etc. In addition reject coals, which are uneconomic to mine, as well as partings material which can contain appreciable amounts of carbonaceous material, can also be dumped.

Natural processes that trigger coal fires within coal waste heaps include lightning, forest fires (e.g. Alès, central France), and spontaneous combustion (e.g. coal waste heaps of Wingles, Fouquières-les-Lens, Calonne-Ricourt and Avion in northern France; Ronchamp and La Vaysse, Cransac in central France) (Flann and Lukaszewski, 1971; Maneval, 1976; Saraf et al. 1995; Paquette and Laversanne, 2003; Masalehdani and Potdevin, 2004; Stracher and Taylor, 2004; Zhang et al. 2004a). As a global issue, spontaneous combustion (sponcom) and/or spontaneous ignition is the principal cause of coal fires associated with coal waste heaps. Nevertheless, human interventions such as careless burning of trash on or near the coal waste and intentional ignition to create residue which may be used for road base materials (e.g. coal waste heap n°144 in Rieulay, northern France, Masalehdani and Potdevin, 2004) may also lead to ignition of a coal waste heap. However, once a coal waste heap catches fire and nothing is done to stop it at an early stage, it may continue burn for decades, depending primarily on the availability of coal and oxygen (Prakash, 2002).

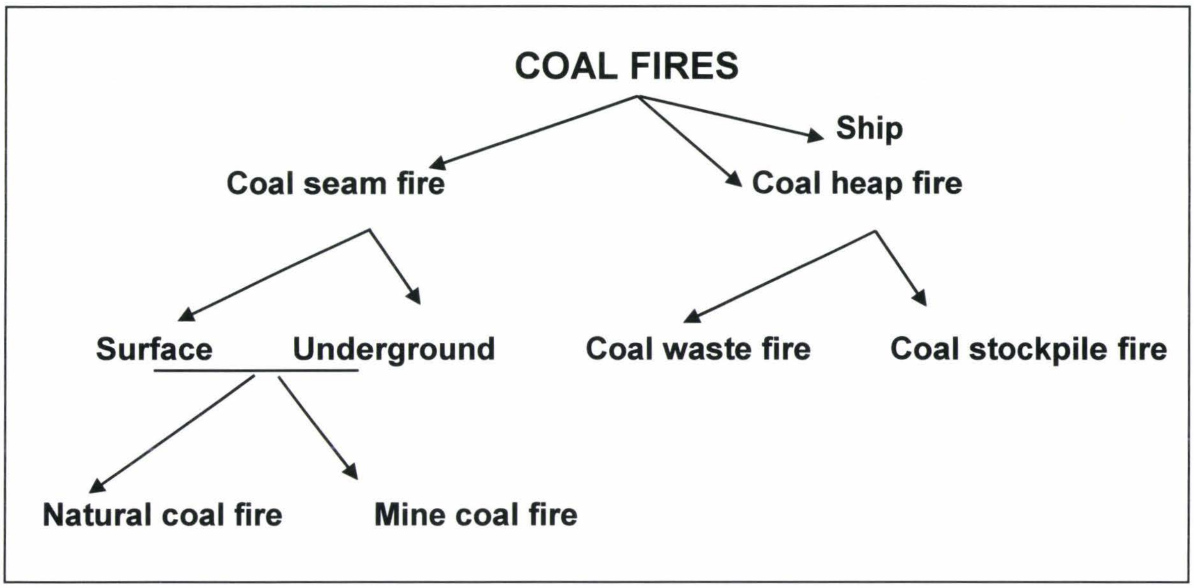

**Figure 1**. Coal fires types.

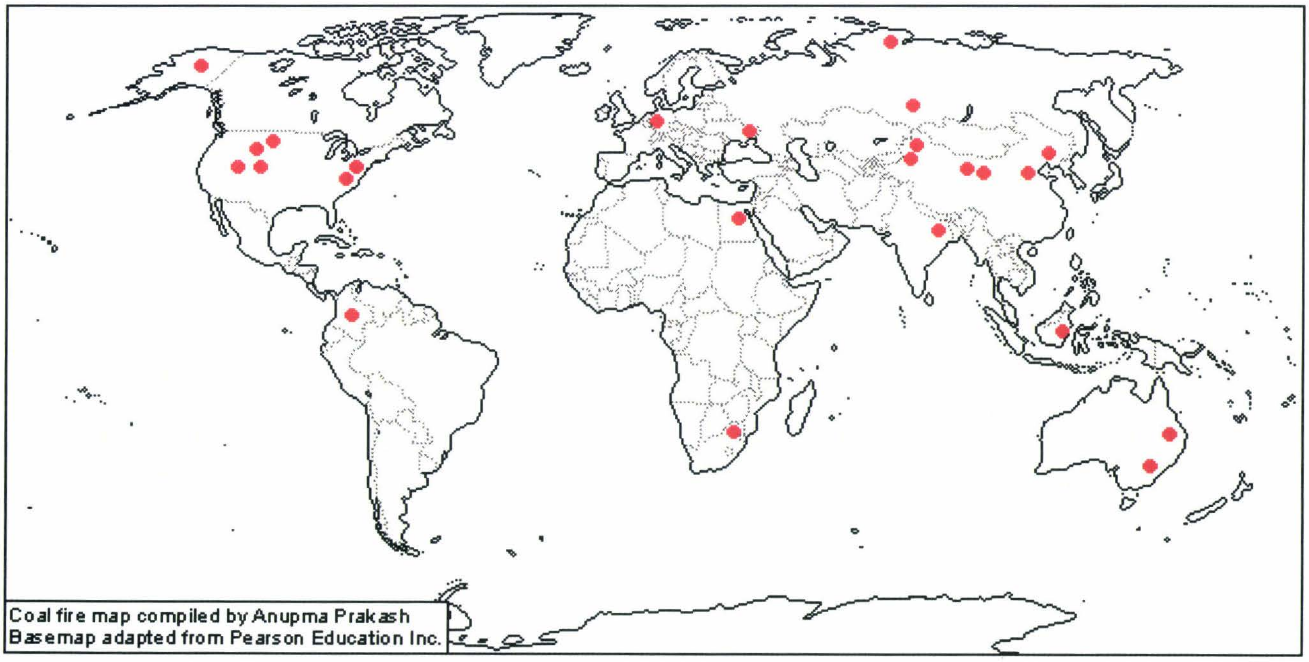

**Figure 2**: Coal fire world map (After A.Prakash, 2005).

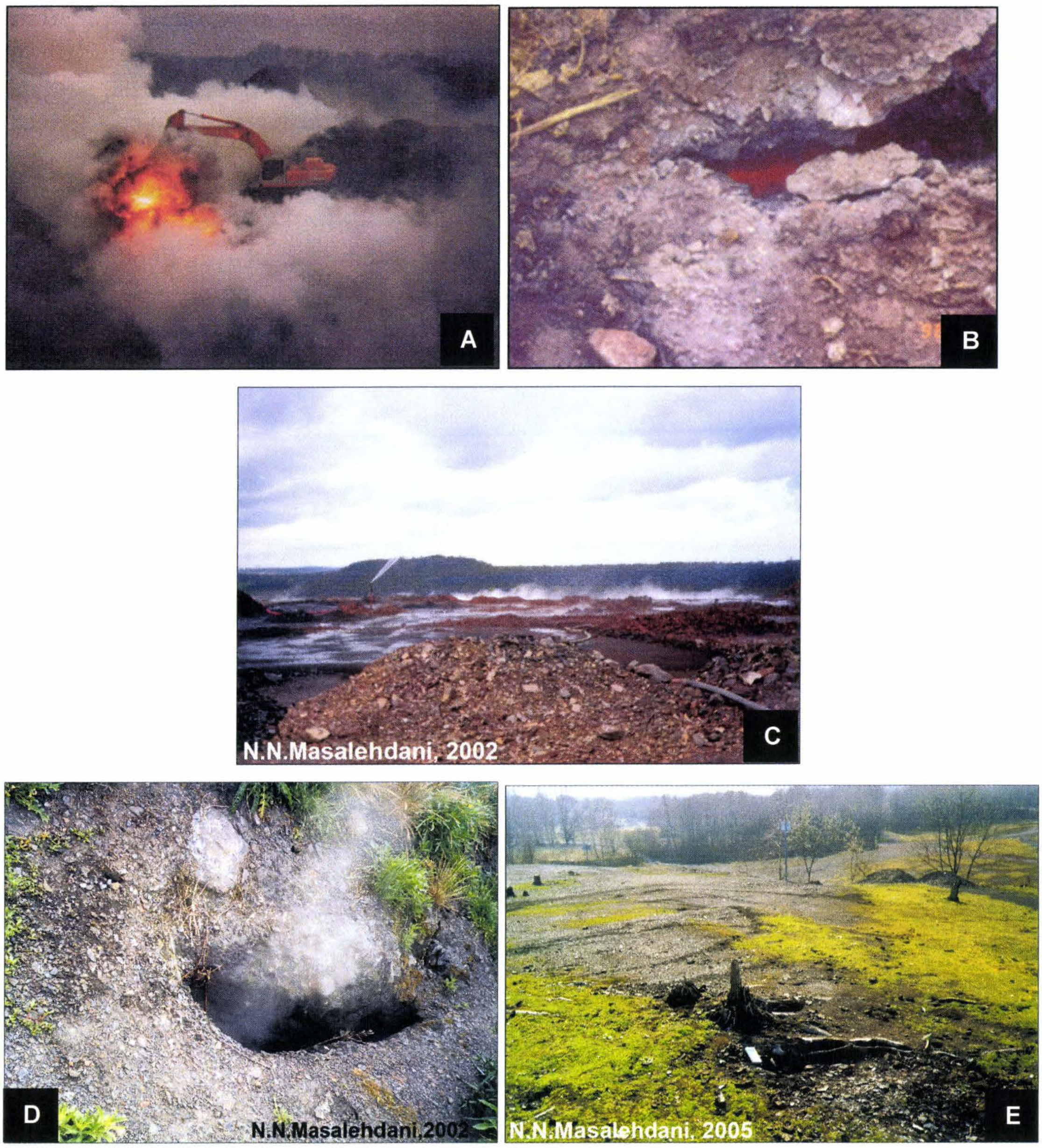

**Figure 3**: Subsurface spontaneous coal waste fires. **(A)** Ignition, extinguishing of fire in the coal waste heap n°70 Ronchamp, France (Paquette and Laversanne, 2003). **(B)** Incandescent fire (750°C) on a slope of coal waste n°12 La Vaysse, Cransac, France (Paquette and Laversanne, 2003). **(C)** Steam emitting vents coal waste heap n°76 Avion, northern France. Note water is used to put out the coal fire, the local population lives in vicinity to the site. **(D)** Gas vent and emission of noxious gases. After extraction of rock debris the site is simply abandoned with little regard to the environment, coal waste heap n°83, Fouquières-les-Lens, northern France. **(E)** Burned trees and vegetation dieback zones coal waste heap of Wingles, northern France.

The instances of burning coal wastes are increasing with the increase in the percentage of coal mined by mining methods. Wastes created in open pit or underground mining often contain coal. Spontaneous combustion of coal has long been a concern for mankind (see Introduction). Globally, spontaneous combustion occurs (in varying degree) whenever oxygen comes into contact with an organic material. Coal waste heap provides just an opportunity for this reaction on the surface. Spontaneous combustion associated with coal waste heaps is slow and can last for decades. Coal and carbonaceous shales react with oxygen in the atmosphere, producing heat (see section 3). The oxidation reaction is exothermic and if the heat produced cannot be dissipated at a rate equal to that at which it is generated, the oxidation rate will accelerate and spontaneous heating will result. The overall oxidation rate will depend upon both physical diffusion and chemical processes. (Cudmore and Sanders, 1984; Carras and Saghafi, 1998).

The propensity for natural oxidation and spontaneous combustion and the susceptibility to external heating vary in different coals and coal waste heap. Spontaneous combustion of coal starts due to susceptibility of coal to self-heating (Gentzis and Godarzi, 1989). The onset of spontaneous combustion depends on both intrinsic properties of the coal waste heap and external factors. The actual mechanisms involved in spontaneous combustion are still a matter of discussion and research, Table 1 presents some of the major factors conductive to ignition and propagation of fire in coal waste heaps (Flann and Lukaszewski, 1971; Chamberlin and Hall, 1973; Kim, 1977; Das and Hucka, 1986).

## 4. COMBUSTION OF COAL WASTE HEAP: EFFECTS OF VARIOUS FACTORS

Most of the key factors summarized in Table 1 contribute to self-heating in the coal waste. It is possible that some of these factors are associated with coal waste heap in Avion which have caused the spontaneous combustion. Some of the factors seem to play a more significant role in self-heating of the coal waste heap's materials. They are summarized below.

### *4.1. Rank of coal*

Coal rank has a dominating influence in self-heating of coal. The tendency of coal to self-heating decreases as of the rank increases with lignite and sub-bituminous coals being more susceptible to self-heating than bituminous coals and anthracite (Table 2) (Maneval, 1976;

Speight, 1994; Pis, 1996; Walters, 1996). It was demonstrated that as volatile matter (VM) and oxygen contents increased, the rate of self-heating also increased (Schmidt, 1945).

There are no published, or official records, or archives indicating the coal rank and its chemical properties from northern France and/or from Pits n°7 or 7bis of Liévin. The propensity of dumped coal from this location has never been investigated.

### *4.2. Coal composition and petrographic content*

Chemically, coals are made up of various proportions of carbon, nitrogen, hydrogen, oxygen, and impurities. As shown in Table 2 from lignite to anthracite there is a progressive elimination of water, oxygen, and hydrogen, and an increase in carbon. The carbon is present as fixed carbon (FC) and in volatile matter (VM). Nitrogen in coal the (coal-N) exists in the forms of pyridinic$^-$, pyrrolic$^-$ and quaternary $^-$N (Kelemen et al. 1994). Hydrogen in coal (C-H bonds) exists within the coal macromolecule (Grossman et al. 1992). Sulphur in coal occurs in organic and inorganic forms. The organic form generally occurs in the forms of thiols, sulphides, disulphides, thiophenes and cyclic sulphides. The inorganic sulphur is present mainly in two forms, as iron disulphides ($FeS_2$), cubic yellow pyrite and rhombic marcasite (Coward, 1957). The mineral pyrite has an exceptional position in the natural oxidation process of coal. The presence of sulphides in coal is known to accelerate spontaneous heating (see section 5.3). These minerals may swell upon heating, causing the coal to disintegrate and reducing the particle size involved in the reaction, generally pyrite must be present in concentrations $\geq 2$ % before it has a significant affect (Kim 1973).

The petrographic composition (vitrinite compounds) of coal from Pits n°7 or 7bis of Liévin was not previously determined. However, it is believed that at constant ranks, as the exinite content of a coal increase, its self-heating propensity increase too (Cudmore and Sanders, 1984; Walters, 1996).

### *4.3. Moisture*

Moisture is imperative for pyrite oxidation to take place. However, it is possible that moisture may have an influence, not only on pyrite but also on the organic part of coal. The effect of moisture on the oxidation of coal is not continues. At relatively low temperatures, an increase in free moisture increases the rate of spontaneous heating High internal moisture a feature of low rank coals, is indicative of a tendency to spontaneous heating (Maneva, 1976).

### *4.4. Particle size and surface area*

Particle size has an inverse relationship to spontaneous combustion in coal. The smaller the particle size the grater surface area is available on which oxidation can take place (Kim, 1973). The rate of oxidation of coal with oxygen of air is proportional with specific internal surface. The proportional coefficient at low temperatures is the cube root but analyses also show that both rate and extent of oxidation increase with the decrease in particle size, until a critical particle diameter is reached, below which the rate remains fairly constant (Bannerjee, 1985).

### *4.5. Construction method of the coal waste heap*

Apart from the high carbonaceous content of coal waste heaps, it is suggested that form of and construction of coal waste heap influences its self-heating. The large size and height of heap construction encourages the segregation of the larger pieces of run-of-mine materials to the toe of the coal waste heap (Maneval, 1976). In turn, this allows easy passage of air into the inner part of the coal waste heap. The rising bedding plans and the lack of consolidation may allow internal convection current to flow and steep faces encourages penetration by wind, therefore the oxidation of coal and carbonaceous shales (Flann and Lukaszewski, 1971).

The size, form, differences in material composition, large rock particle size and low packing densities during dumping results in considerable air space volumes (voids) which in turn let air and moisture (i.e. rain fall) penetration, making the coal waste heaps' materials susceptible to combustion. All the physical and structural factors which favour access of air and impede the loss of heat will promote self-heating and the spread of fire within the coal waste heap (Flann and Lukaszewski, 1971).

### *4.6. Rock debris*

The physical and chemical properties of rock debris play a significant role before and during spontaneous combustion. The bulk physical properties of coal waste heap vary considerably owing to differences in material composition. The angular fragment shapes and size distributions which yield low packing densities during dumping may result in considerable air spaces volumes. Subsequent weathering products changes in physical properties which may affect the strength of the bulk material and in poorly constructed coal waste heaps may result in subsidence and collapse in the coal waste heap body and sides.

**Tablel.** Some factors related to spontaneous combustion potential in coal waste heap.

| Chemical | Physical | Environmental |
|---|---|---|
| Rank of coal | Porosity | Ambient temperature |
| Petrographic composition | Permeability | Available air |
| Rock composition | Hardness | Atmospheric conditions |
| Pyrite content | Thermal conductivity | Wind direction |
| Amount of moisture | Specific heat | Time |
| | Partitioning of coal | Mining method |
| | Particle size | Construction method |

**Table 2.** Representative analyses for peat and various coal (Speight, 1994).

| Rank | % C | % H | % O | %N | % S |
|---|---|---|---|---|---|
| Peat | 55.0 | 6.0 | 30.0 | 1.0 | 1.3 [a] |
| Lignite | 72.7 | 4.2 | 21.3 | 1.2 | 0.6 |
| Subbituminous High-volatile B | 77.7 | 5.2 | 15.0 | 1.6 | 0.5 |
| High-volatile B Bituminous | 80.3 | 5.5 | 11.1 | 1.9 | 1.2 |
| High-volatile A Bittuminous | 84.5 | 5.6 | 7.0 | 1.6 | 1.3 |
| Medium-volatile Bituminous | 88.4 | 5.0 | 4.1 | 1.7 | 0.8 |
| Low-volatile Bituminous | 91.4 | 4.6 | 2.1 | 1.2 | 0.7 |
| Anthracite | 93.7 | 2.4 | 2.4 | 0.9 | 0.6 |

[a] Ash and moisture content remaining weight %

Such movements in turn increase air and moisture penetration, making the material more susceptible to combustion Rock debris (Flann and Lukaszewski, 1971). Laboratory tests (e.g. screen test etc) are necessary to determine the physical properties of coal waste heap materials.

The chemical composition and mineralogical contents of rock debris contributes to self-heating of coal waste heap (see Chapter II).

### *4.7. Atmospheric conditions*

Environmental parameters (e.g. ambient temperature, oxygen, Water (rain) and relative humidity and convention of air (wind)) play a major role on the self-heating of coal in coal waste heaps. The weather influences the induction or promotion of the combustion, since the natural process of oxidation is accelerated by high ambient temperatures and solar radiation. Fluctuations in ambient temperature and pressure also cause the movement of both air and moisture in heaped waste coal, including critical ventilation. Hot dray conditions (dry summers) may favour the retention of heat which can lead to self-heating and ignition (Maneval, 1976).

Moisture is imperative for pyrite oxidation to take place, as described earlier. Water is an oxidation agent, in the presence of pyrite (in coal and carbonaceous shales) and at ambient temperature; moisture accelerates oxidation and contributes to self-heating (Maneval, 1976, Chen and Scott, 1993; Carras and Saghafi, 1998).

The air flow rate provides both, oxygen for the oxidation process but also dissipates heat generated by oxidation. Sensögüt (1997) stated a very high flow rate provides almost unlimited oxygen but dissipates heat efficiently. Conversely, a low flow rate restricts the amount of oxygen available but allows heat to remain in the coal, so that there is an increasing rate of oxidation until the ignition takes place (Flann and Lukaszewski, 1971).

### *4.8. Time*

Time is an important factor controlling the self-heating within the coal waste heap. If the dumped coal in coal waste heap is weathered (i.e. saturated with oxygen over a long time and under near isothermal conditions) then it is relatively uncreative to oxygen compared to fresh coal (Cudmore and Sanders,1984).

Many workers performed many long term tests for which they derived a relationship between the rate of oxidation of coal and the oxidation period. They noted that the rate of oxidation decreases with time (Cudmore and Sanders, 1984).

## 5. PROCESS OF SPONTANEOUS COMBUSTION AND SOURCES OF HEAT

The process of spontaneous combustion associated with a coal waste heap could be divided into three stages (Haifeng, 1994): (1) oxidation, (2) spontaneous combustion, and (3) burning (see section 4). Heat is generated from four major sources. The most important is the direct oxidation of coal. Oxidation of carbonaceous shales also occurs. The third source is the oxidation of pyrite. In addition condensation of water vapour within porous structures, as described earlier, due to changes in relative humidity, releases considerable heat and self heating (Carras and Saghafi, 1998).

### *5.1. Coal oxidation*

The behaviour of coal towards molecular oxygen is a matter of practical importance. In contact with the atmosphere nearly all coals show sooner or later signs of weathering, which results in the decrease of the calorific value. As described earlier above, the hazard of spontaneous combustion arises if the amount of heat generated during coal oxidation exceeds the amount of heat dissipated. Due to this possible heat accumulation the temperature arises in the coal until the inflammation temperature is reached and spontaneously ignites (Carras et al. 1999).

The interaction of coal with oxygen is exothermic and has been studied for many years (e.g. Schmitd, 1945; Sondreall and Ellman, 1974; Nordon et al., 1979; Cudmore and Sanders, 1984; Nelson, 1989: Khan et al. 1990; Carras and Young, 1994; Krishnaswamy et al. 1996; Chen and Scott, 1997). Research has concluded that natural coal oxidation obeys an Arrhenius-type rate law (Walker, 1999). The relationship between reaction chemistry, rate of reaction constant and temperature determines the Arrhenius equation (Falbe, 1995):

$$In(K) = In(A) \frac{E_A}{R.T}$$

K: Rate of reaction constant
A: frequency factor
$E_A$: activation energy
R: Gas constant
T: absolute temperature

Three types of processes are involved in the coal-oxygen oxidation (Dividson, 1990), this is termed oxycoal (Havenga, 1993) or per-oxygen (Cudmore and Sanders, 1984). Oxygen is physically and chemically adsorbed by the coal. Physically sorbed oxygen ($E_A = 42$ kJmol$^{-1}$) diminishes in amount with temperature and becomes inappreciable beyond $T \leq 50°C$ (Wang, 2002). Chemical adsorption ($E_A = 139$ kJ mol$^{-1}$) leads to the formation of coal-oxygen (per-oxygen) complexes and oxygenated carbon compounds (i.e. carboxylo and carbonyl groups) at low temperature ≥80°C (reaction 1, Wang, 2002). The formation of carbon compounds proceeds selectively. The benzylic positions, being the most reactive, are first oxidised to produce carbonyll groups and carboxylic acids. The aliphatic groups of coals are first oxidised to form aldehdes, and these are oxidised further to form carboxylic groups and esters (Worasuwannarak, 2002). Finally the formation ($E_A = 105$ kJ mol$^{-1}$) and release of gaseous products, typically CO, $CO_2$ and $H_2O$ (water vapour) (2) (Dividson, 1990; Walker, 1999).

$$\text{coal} + \text{oxygen} \rightarrow \text{coal-oxygen complex} + \text{heat} \qquad (1)$$
$$\text{coal-oxygen complex} \rightarrow CO + CO_2 + H_2O + \text{heat} \qquad (2)$$

The decomposition of the chemisorption intermediates mainly generates CO while the liberation of $CO_2$ comes from the decomposition of the carboxyl. Three simultaneous reactions proceed in the thermal decomposition process. The carbonyl groups are supposed to be generated via dehydroxylation process. The decarboxylation and decarbonylation both result in gaseous products, including CO, $CO_2$ and $H_2O$ (water vapour) (Walker, 1999). At temperature ≥150°C decomposition of carboxyl and carbonyl groups occurs, leading to the production of $CO_2$ and CO along two independent reaction pathways (Fig. 4, Wang, 2002).

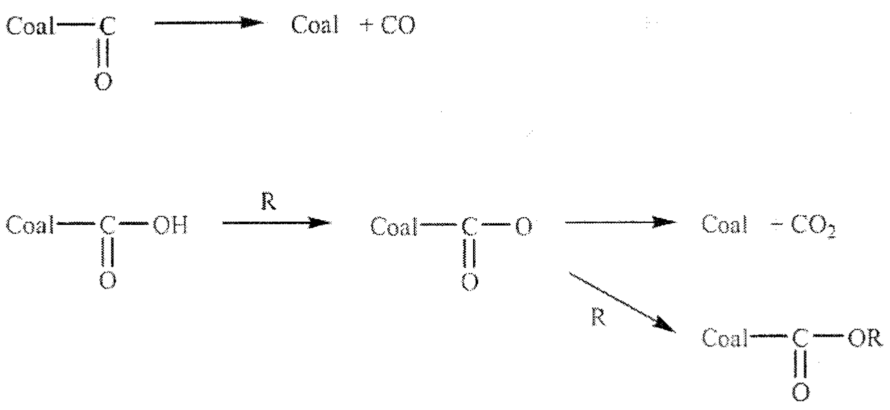

Figure 4. Decomposition of carboxyl and carbonyl groups.

The complete oxidation of carbon to carbon dioxide and to carbon monoxide is an exothermic reaction (reactions 3 and 4). Reaction 3 leads to heat generation and in normal circumstances, this heat will be lost to the atmosphere (as pollutant), and in such condition the ignition temperature for coal lies between 420°C and 480°C. These temperature ranges of coal oxidation are in agreement with our laboratory testing on coal oxidation samples (see Chapter II). However, it should be noted that in adiabatic conditions, where all of the heat is retained rather than being emitted, the minimum temperature at which coal can ignite falls dramatically to between 35°C and 140°C depending on the coal being considered (Sujanti, 1999).

$$C + O_2 \rightarrow CO_2\uparrow + 394 \text{ kJ mol}^{-1} \tag{3}$$

$$2C + O_2 \rightarrow 2CO\uparrow + 170 \text{ kJ mol}^{-1} \tag{4}$$

While there is continuing debate as to the details of the exothermic reactions of coal with oxygen and the relative importance of different mechanism, at ≈35°C the rate of initial oxidation for coal is ≈ 0.1 to ≈ 8 x $10^{-9}$ ($gO_2$/g coal/s), for a particle size range of -3 to +1.7mm depended on coal type (Carras and Young, 1994). Further, measurements based on isothermal calorimetry, Nordon et al. (1985) have shown values of the heat of reaction ≈250 to 400 kJ $mol^{-1}$ $O_2$. Such rates of reaction and heat generation give rise to thermal outputs of ≈ $10^{-6}$ to $10^{-4}$ W/g coal for coal oxidising without oxygen limitation at ≈35°C (Carras and Saghafi, 1998). In addition to coal carbon processes, the reactions involved in the oxidation of coal hydrogen to form water are also exothermic. This is a particular importance for low rank coals (e.g. lignite) that have high inherent hydrogen content (Walker, 1999).

### *5.2. Carbonaceous shale oxidation*

It is common that overburden strata in underground or open pit coal mining contain carbonaceous horizons other than coal. These materials extracted and dumped in coal waste heaps are generally less reactive, contain less carbon than coal (see Chapter II, Table 1a) but there is often vastly greater quantities of these materials in the coal waste heap than coal (≈ 75 % vs 25% respectively). Also, should combustion begin, these materials can provide a major fuel source for subsequent combustion. According to (Carras and Saghafi, 1998) at constant temperature of 75°C the heat of reaction of carbonaceous shale has a value between ≈ 13 to 16 J/cc$O_2$. This gives a range of ≈ 290 to 360 kJ/g mole $O_2$ which is similar to the range measured for coal, as described earlier.

### *5.3. Pyrite oxidation*

As described earlier, pyrite occurs in coal and in carbonaceous shales. The third source in coal waste heap is the oxidation of pyrite. There has been considerable work on pyrite oxidation, particularly as it affects acid generation (Harries and Ritchie, 1981; Jaynes et al. 1983; Carras and Saghafi, 1998).

It is supposed that pyrite may assist the oxidation of the carbonaceous content because of the volume increase of $Fe_2O_3$ compared to $FeS_2$ by breaking down the coal into smaller fragments and exposing larger surface area to the air or developing cracks in the coal whereby the surface area for air exposure is increased (Gaschnitz et al. 2005). However, this supposition, in addition to elevating the temperature due to heat liberated from pyrite oxidation has not been scientifically established yet. The low-temperature oxidation of pyrite might prove these facts though (5) and (6) (Bannerjee, 1985; Speight, 1994):

$$2FeS_2 + 7O_2 + 16H_2O \rightarrow 2H_2SO_4 + 2FeSO_4.7H_2O + 1324\ \text{kJ mol}^{-1} \qquad (5)$$

or

$$2FeS_2 + 7O_2 + 2H_2O \rightarrow 2H_2SO_4 + 2FeSO_4 + 260\ \text{kJ mol}^{-1} \qquad (6)$$

The reactions are exothermic and are catalysed by the presence of thiobacillus ferrooxidans (Harries and Ritchie, 1981). The reaction products have a greater volume than the original pyrite, with the result that it would break open any coal in which they are embedded and thus exposing a grater surface of coal to the air. These reaction equations indicate that the oxidation stage release considerable amount of heat. Since there is a poor heat advection condition at the deep layers of a coal waste heap, the heat produced during the oxidation stage accumulates. When the temperature reaches the ignition point of carbon or sulphurous iron ore, spontaneous combustion occurs (Chunli, 1997).

As described earlier, spontaneous combustion is enhanced by the relatively large size of the waste heap, airflow into the waste dump through voids existing within the tip, and fractures produced by heat advection. This stage (spontaneous combustion) produces larger quantity of heat as well as pollutant gases (7) (Chunli, 1997):

$$4FeS_2 + 11O_2 \rightarrow 2Fe_2O_3 + SO_2 \uparrow + 3412 \text{ kJ mol}^{-1} \qquad (7)$$

Although, as demonstrated above, during oxidation of pyrite more heat is generated, the oxidation of the carbon is the main cause for the spontaneous combustion within the coal waste heaps in Avion because the content of pyrite (sulphur) is relatively low (see Chapter II Tables 1a). The rate of oxidation of pyrite is dependent upon the accessible surface area and the state of subdivision of the pyrites which helps to promote spontaneous combustion only when it is present in a finely divided state (Cudmore and Sanders, 1984) and when its concentrations is $\geq 2$ % (Kim 1973; Bannerjee, 1985).

In some spoil heaps, heat evolved from aerial oxidation of pyrite may be a significant contributing factor of spontaneous heating of coal and further work is required for the relative importance of pyrite, coal and carbonaceous materials in coal waste heaps to be quantified from their self-heating perspective.

### *5.4. Heat of wetting*

The process of wetting generates heat:

$$\text{dry coal} + \text{moisture} \rightarrow \text{wet coal} + \text{heat} \qquad (8)$$

The mechanism of heating is not fully understood, it is thought to be chemisorption and heat of condensation. Liquid water will cause heating if it comes in contact with dray coal (chemisorption), that heating will not be as great as that which occurs when the coal is in contact with humid air (head of condensation). The heat of condensation is thought to be much more than the heat of chemisorptions. The heat of condensation of water amounts 2441 J/g, provided that coal is dray (reaction 8). When water vapour condenses into water without a change in temperature, this energy is given off as heat (Carras and Saghafi, 1998; Davidson, 1990; Lohrer et al. 2005).

However, the equilibrium moisture contents for coal waste materials are usually quiet small and generally less than a few percent (see Chapter II, Tables 1a, 2a). Consequently, the energy generated from heat of wetting may not be significant heat source for most coal waste heap materials.

## 6. SUMMARY

The process of self-heating is shown in Figure 5. The phenomenon of spontaneous combustion is a three stage process. The oxidation of coal is the initial step. This reaction is exothermic and heat is not dissipated (second stage), Heat is generated during the initial surface oxidation with coal. If the heat is not removed, oxidation accelerates until the reaction becomes self-sustaining. The second stage then proceeds until temperature reaches the combustion point (Walker, 1999), self-heating occurs which may lead to self-ignition (third stage) of the coal. Spontaneous combustion is thus the final stage of a three-stage process. These reactions are affected by several coal properties and external factors:

- rank
- petrographic composition
- volatile matter
- methane content
- available air
- temperature
- time
- particle size
- moisture
- pyrite
- physical properties
- others (lightning, forest fires, human intervention etc)

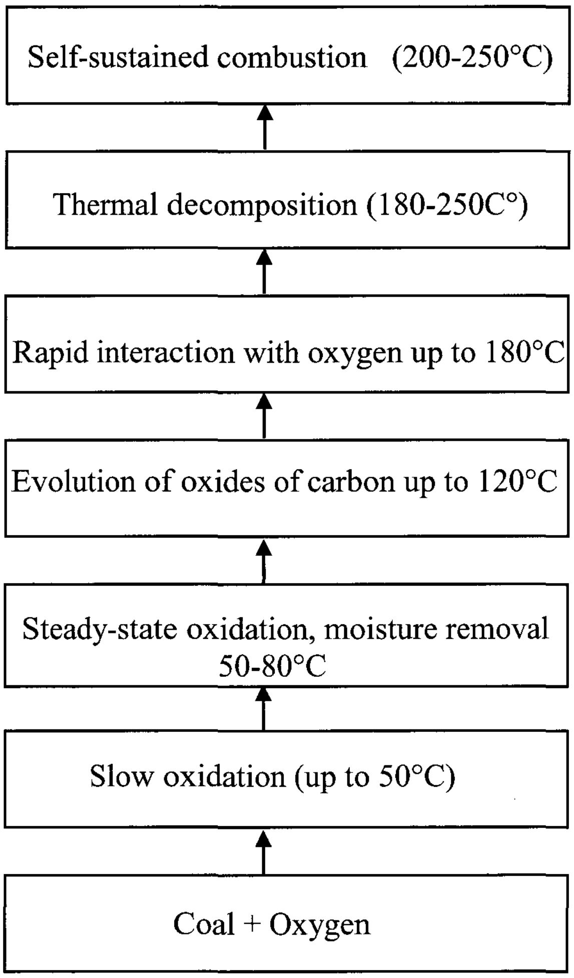

**Figure 5**. Sequential stages in the spontaneous combustion of coal.

# REFERENCES

Bannerjee, S.C. (1985). Spontaneous combustion of coal and mine fires, A.A.Balkema, Rotterdam. www.coafire.caf.dlr.de/media/download/studywP2410a6.pdf/

Bouroz, A. (1969). Le carbonifère du nord de la France. ANN.Soc.Géol.Nord, **LXXXIX**, 47-65.

Carras, J.N., Day, S. and Saghafi, A. (1998). Predicting spontaneous combustion in spoil piles from open cut coal mines. Proceeding of the 1st Australian Coal Operators Conference Coal'98, Wollongong 18-20, 617-625.

Carras, J.N., Day, S., Saghafi, A. and Williams, D.J. (1999). Spontaneouse combustion in spoil piles from open cut coal mines and the emission of greenhouse gases. In: 2nd International Symposium on the Operationalization of Remote Sensing, ITC, Enschede, 16-20 August, The Netherlands.

Carras, J.N. and Young, B.C. (1994). Self-heating of coal and related materials: models, applications and test methods. Prog. Energy Combustion Science, 20, 1-15.

Chamberlain, E.A.C. and Hall, D.A. (1973). The ambient temperature oxidation of coal in relation to the early detection of spontaneous heating: Part 2, the Mining Engineer, **132**, 387-397.

Charbonnages de France (2005).Le charbon: ses utilisations, 28p.

Chaudy, C. (1997). Méthodologie de reconstitution 3D de la structur géologique du basin minier Nord-Pas-de-Calais. DSR, Université de Lille1,141p.

Chen, X.D. and Scott, J.B. (1993). Oxidation rates of coal as measured from one-dimensional spontaneous heating. Combustion and flame, **109**, 578-586.

Chunli, L., Shusshen, L., Qingdang, Q., Jingshu, W. and Ziqiang, P. (1997). Management of spontaneous combustion in coal mine waste tips in China. Water, Air and Soil Pollution, **103**, 441-444.

Coward, M.F. and Jones, G.W.(1952). Limits of flammability of gases and vapours. U.S.B.M. Bulletin **503**.

Cudmore, J.F.and Sanders, R.H. (1984). Spontaneous combustion of coal, mine fires and interpretation of analyses of mine gases, a literature review. Australian coal industry research laboratories Ltd. (ACIRL), report n°**10**, ISBN n° 0 86772 049 2,60p.

Das, B. and Hucka, V.J. (1986). Control of spontaneous combustion of coal through an analysis of its mechanism and the affecting factors. In: Preprint, AIME Annual Meeting, New Orleans, March 2-6.

Denimal, S. (2001). Impact des terrils houillers du basin minier Nord-Pas-de-Calais sur la qualité des eaux de la nappe de la Craie. PhD. Thesis, Université des sciences et technologies de Lille, U.F.R. des Sciences de la Terre, France, 237p.

Delattre, C., Meriaux, E. and Waterlot, M. (1973). Guides géologiques régionaux, Région du Nord, Bassin de Mons, 176p.

Dividson, R.M. (1990). Natural oxidation of coals, IEA Coal Research – The Clean Coal Centre, London.

Dubois, G. and Minot, J.M. (1991). Histoire des mines du Nord et du Pas-de-Calais. Tome 1, 176p.

Flann, R.C. and Lukaszewski, G. M.(1971). The prevention and control of burning in waste coal dumps. Proc. Australian Inst. Min. Met. No. **238**, 11-29.

Finkelman, R.B. and Gross, P.M.K. (1999). The types of data needed for assessing the environmental and human health impacts of coal. International Journal of Coal Geology, **40**, 91-101.

Finkelman, R.B. (2004). Potential health impacts of burning coal beds and waste banks. International Journal of Coal Geology, **59**, Iss. 1-2, 19-24.

Gaschnitz, R., Aeckersberg, R., Wirtgen, C., Verhoeven, M. and Rüter, H. (2005). Burning waste dumps a potential source of energy. In: Proceeding conference book, International conference on coal fire research, 187-189.

Gentzis, T. and Goodarzi, F. (1989). Organic petrology of a self-burning coal wastepile from Coleman, Alberta, Canada. International Journal of Coal Geology, **11**, 257-271.

Grossman, S.L., Davidi, S. and Cohen, H. (1994). Emission of toxic and hazardous gases from open air coal stockpiles. Fuel, **73**, No. 7, 1184-1188.

Harries, J.R. and Ritchie, A.I.M. (1981). The use of temperature profiles to estimate the pyretic oxidation role in a waste rock dump from an open cut mine. Water, Air and Soil Pollution, **15**, 405-423.

Havenga, W.J. (1993). Rapid gas analyses for the investigation of spontaneous combustion using capillary gas chromatography. Talanta, **40**, No. 2, 213-219.

Jaynes, D.A., Rogowski, A.S., Pionke, H.B. and Jacoby, E.L. (1983). Atmosphere and temperature changes within a reclaimed coal strip mine. Soil Science, **136**, 164

Kelemen, S.R., Gorbaty, M.L. and Kwiatek, P, J.(1994). Quantification of nitrogen forms in Argonne premium coals. Energy Fuels Vol. **8**, 896-906.

Khan, R.M., Everitt, C.E. and Lui, A.P. (1990). Modelling of oxygen chemisorption on coal char. Combustion and Flame, **80**, 83-93.

Finkelman, R.B. (2004). Potential health impacts of burning coal beds and waste banks. International Journal of Coal Geology, Vol. **59**, 19-24.

Finkelman R.B., Gross P.M.K. (1999). The type of data needed for assessing the environmental and human health impacts of coal. International Journal of Coal Geology, Vol. **40**, 91-101.

Gangopadhyay P.K., van der Meer F., van Dijk P. (2005). Monitoring coal fires using dynamic remote sensing. In: International conference on coal fire research, Beijing, China, 136-140.

Grossman, S.L., Davidi, S., Cohen, H. (1994). Emission of toxic and hazardous gases from open air coal stockpiles. Fuel Vol.**73**, No. 7, 1184-1188.

Harries, J.R. and Ritchie, A.I.M. (1981). The use of temperature profiles to estimate the pyretic oxidation role in a waste rock dump from an open cut mine. Water, Air and Soil Pollution, **15**, 405-423.

Havenga, W.J. (1993). Rapid gas analyses for the investigation of spontaneous combustion using capillary gas chromatography. Talanta, Vol. **40**, No. 2, 213-219.

Hookham, M. (2004). Novel Power Generation Technology. Queensland Government Mining Journal, Vol.**103**, No. 1217, December, 40-41.

International Energy Agency (IEA) World Energy Outlook (2000), 66p.

Kambara, S., Takarada, T., Yamamoto, Y., Kato, K.(1993). Relation between function forms of coal nitrogen and formation of NO. Energy Fuels, 7, 1013.

Keating, M. (2001). Cradle to the grave. The environmental impacts from coal. www.catf.us/publications/reports/Cradle to Grave.pdf, viewed 9/12/04.

Kelemen, S.R., Gorbaty, M.L. and Kwiatek, P, J.(1994). Quantification of nitrogen forms in Argonne premium coals. Energy Fuels Vol. **8**, 896-906.

Khan, R.M., Everitt, C.E. and Lui, A.P. (1990). Modelling of oxygen chemisorption on coal char. Combustion and Flame, **80**, 83-93.

Kim, A. (1973). The composition of coalbed gas. U.S. Bureau of Mines report of Investigations, 7762, U.S. Department of the interior, Bureau of Mines and Safety Research Center, Pittsburgh, PA, 9p.

Krishnaswamy, S., Bhaat, S., Gunn, R.D. and Agarwal, P. (1996). Low-temperature oxidation of coal . Part I. A single particle reaction-diffusion model. Fuel, **75**, 333-343.

Lefohn, A.S., Husar, J.D., Hasar , R.B. (1999). Estimating historical anthropogenic global sulfur emission patterns for the period 1850-1990. Atmospheric Environmental, Vol.**33**, 3435-3444.

Panov, B.S., Dudik, A.M., Shevchenko, O.A. and Matlak, E.S. (1999). On pollution of the biosphere in industrial areas: the example of the Donets Coal Basin. International Journal of Coal Geology, **40**, 199-210.

Saraf, A.K., Prakash, A., Sengupta, S. and Gupta, R.P. (1995). Landsat TM data for estimating ground temperature and depth of subsurface coal fire in Jharia Coal Field, India. International Journal of Remote Sensing, **16**, 2111-2124.

Schmidt, L.D. (1945). Chemistry of coal utilisation, **1**, chapter 18.

Sensögüt, C. (1997). A general outlook on spontaneous combustion in underground coal mines, research report, Aachen.

Sondreal, E.A. and Ellman, R.C. (1974). Laboratory determination of factors affecting storage of North Dakota lignite. U.S. Bur. Mines Rep. Invest. **7887**, 83p.

Speight, J.C. (1994). The chemistry and technology of coal, Dekker, New York.

Stracher, G.B. and Taylor, T.P. (2004). Coal fires burning out of control around the World: thermodynamic recipe for environmental catastrophe. International Journal of Coal Geology, **59**, 7-17.

Stracher, G.B., Pone, J.D.N., Finkelman, R.B., Annegarn, H.J., Mccormack, J., Blake, D.R., Rowland Hall, I. and Schroeder, P.(2005). Gas vent mineralogy and geochemistry: the burning culm banks of South Africa. Geological Society of America, Abstracts with Programs, **37**, n°. 7, 453.

Sujanti, W.(1999). A laboratory study of spontaneous combustion of: the influence of inorganic matter and reactor size. Fuel, 78, 549-556.

Vetter, P. (1981). In: Klingebiel, A. (1981). La géologie des charbons, des schistes bitumineux et des kérogènes, 717p.

Walters, A.D. (1996). Joseph Conard and the spontaneous combustion of coal – Part 1, coal preparation, **17**, issue 3-4, 147-166.

Wang, H., Dlugogorski, B.Z. and Kennedy, E.M. (2002). Thermal decomposition of solid oxygenated complexes formed by coal oxidation at low temperatures. Fuel, **81**, 1913-1923.

Worasuwannarak, N. (2002). Effect of pre-oxidation at low temperature on the carbonisation behaviour of coal, Fuel, **81**, 1477-1484.

# CHAPTER II

# FIELD AND LABORATORY INVESTIGATIONS

## 1. INTRODUCTION

In this chapter the results of the subsequent temperature monitoring in coal waste heap n°76 and the results of the laboratory experimental studies are explained. The aims were to:

- determine the heat distributions at the study area,
- identify the active combustion zones,
- determine the effect of temperature on coal oxidation,
- determine the effect of combustion on carbonaceous shales under various temperatures,
- evaluate the sources of heat and gases especially the greenhouse gases (GHS).

## 2. SURFACE TEMPERATURE DISTRIBUTIONS: FIELD MEASUREMENTS

Surface temperature measurements within the coal waste heap n°76 were measured around selected hot spots at the top surface of the site at about 1m interval (Fig. 1), using a 15cm long temperature thermometer Comark C9001 and an infra-red temperature gun AGA thermopoint 80. The measurements were seasonal it started in the beginning of January 2002 and lasted for one year.

The maximum temperature near the NE in front A is 255.7°C (Fig. 2). In the front B (SW zone) temperatures measurements also show evidence of active sub-surface heating but the peak temperature is only 99.7°C. Both fronts C and D show little, if any, sign of sub-surface heating. The temperature gradient shows that heat is conducted towards fronts A and B.

Near gas vents, temperatures were measured higher this is probably because heat is transferred from the fire zone by conduction and hot gases. In front A temperatures is high as 255.7°C was measured. The location was secluded from air movement.

The trend of progressive in temperature measurements falls within the dump is attained during cold autumn and winter months. The near-surface temperature measurements show more variability because they are not only influenced by the zone of combustion, but also are subject to variations in insolation, cloud cover, air temperature and rainfall. According to (Harries and Ritchie, 1980) diurnal temperature changes should not have significant effect at depths beyond 2m on the temperature, but weekly and monthly (i.e. seasonal) weather changes should have an effect on temperature distribution. Further, the amplitude of the temperature changes should generally be reduced deeper within the coal waste (Lefebvre et al.1993). Flann and Lukaszewski (1971) confirmed that the weather can play a major role in determining the progression of combustion in coal waste heap. They contend that high ambient air temperatures, solar radiation and hot dry conditions favour self-heating, ignition promotion and temperature increase in coal waste heaps in eastern Australia. Contrary to the findings of the latter authors, Nichol and Tovey (1998) noted that resurgence of the combustion within the coal waste tip at Brymbo in northeast Wales appear to be associated with winter weather.

In spite of numerous investigations around coal waste combustion, the relative contribution of those factors remains uncertain. We could not use drilling technique (i.e. probe holes) to indicate the sub-surface combustion temperature at depth about 5 m below the dump. This could have determin if the combustion and the heat generated deeper within the coal waste heap. However, temperature readings at the coal waste heap n°76 in Avion continue in order to identify the eventual end of spontaneous combustion activity within this dump.

## 3. OXIDATION-COMBUSTION: LABORATORY TESTS

As stated earlier in Chapter I part 2, we could not document any recorded or published papers which show the coal rank or coal analyses belonging to the Pits 7 and 7bis of Liévin. Coal mining activities in northern France stopped in 1990 (see Chapter I part 1), therefore it is almost impossible to get some fresh coal in this region. The selected coal sample (AVC123) was collected from the non burning zone (from the base of coal waste heap) at the coal waste heap n°76 in Avion. Prior to oxidation tests, coal sample was analysed using methods explained in ASTM (1997) for C, O, N, H, Fe, S contents as well as for major and trace elements (Table 1). The fixed carbon content of the sample determined its rank: medium-volatile bituminus (see Chapter I part 2 Table 2).

Numerous measures were carried out on a Thermobalance of mark NETZSCH STA 409 allowing simultaneous measurements of thermogravimetry analysis (TGA) and differential thermic analysis (DTA) between the ambient temperature and 1000°C with a different temperature rise for each analysis (5°/min, 1°/min and 0,5°/min). The analysis involved in grinding 65 mg of coal sample (AVC123) then it was placed inside of an alumine crucible (volume of 0.2mL). The grinded sample was then placed inside of the balanc, which was crossed by flux of dry air (75 mL/min). The aim was to asses the effect of temperature increase on combustion of coal. Moreover, the analysis led to follow the evolution of solid with temperature rise. Figures 3a, 3b and 3c illustrate graphically the laboratory results obtained by DTA-TGA analyses. Following observations were obtained:

- analysis at 5°/min (Fig. 3a) oxidation starts at 50°C, loss of mass 0.67% between 50-170°C, mass gain 0.16% between 250-305°C, 93% mass loss at 565°C and ignition temperature appears at 565°C.
- analysis at 1°/min (Fig. 3b), oxidation starts at 30°C, 1.24% mass loss between 120-175°C, 0.91% mass gain between 175-284°C, at 465°C the mass loss is 95% and the ignition temperature occurs at 520°C
- analysis at 0,5°/min (Fig. 3c), oxidation starts at 30°C, loss of mass between 30-140°C is 1.40%, mass gain 2.20% between 150-272°C, 95% of mass loss at 430°C and ignition temperature occurs at 515°C.

**Table 1**: Analysis of coal (sample AVC123) from coal waste heap n°76.

|  | wt% | Major elements | wt% | Trace elements | ppm |
|---|---|---|---|---|---|
| C | 87.76 | $SiO_2$ | 24.28 | As | 0.984 |
| H | 3.40 | $Al_2O_3$ | 19.67 | Be | 5,55 |
| N | 1.07 | $Fe_2O_3$** | 1.84 | V | 141,93 |
| St* | 0.71 | MNO | 0.00 | Co | 98,43 |
| O | 2.17 | MgO | 0.39 | Ni | 143,52 |
| Fe | 0.13 | CaO | 9.59 | Cu | 247,8 |
|  |  | $Na_2O$ | 0.40 | Zn | 102,51 |
|  |  | $K_2O$ | 0.23 | Ga | 11,15 |
|  |  | $TiO_2$ | 0.11 | Y | 116,58 |
|  |  | $P_2O_5$ | 8.09 | Zr | 2,55 |
|  |  | LOI | 37.12 | Mo | 15,14 |
|  |  | Total | 100.74 | Cd | 0,27 |
|  |  |  |  | In | 0,045 |
|  |  |  |  | Sn | 0,98 |
|  |  |  |  | La | 8,92 |
|  |  |  |  | W | 2,53 |
|  |  |  |  | Pb | 101,55 |
|  |  |  |  | Th | 7,09 |
|  |  |  |  | U | 4,25 |
|  |  |  |  | Cr | 59,41 |
|  |  |  |  | Sr | 241,08 |
|  |  |  |  | Ba | 184,44 |

* St: total sulphur ** $Fe_2O_3$ : refers to total iron

As can clearly be seen, all of the curves in Figures 3a, 3b, and 3c show the same general shape. A rapid rise in oxygen consumption followed by mass loss, steady rise, mass gain and complete ignition. The results indicate that decreasing the temperature during analyses makes it possible to move the maximum of coal oxidation towards the lower temperatures of 100°C depending on the temperature rise of 5°/min, then programmed with 1°/min. Measurement at 0,5°/min allows to move the coal oxidation to 35°C. The temperature values obtained for these oxidations are slightly influenced, they are moved between 320-280°C respectively. It should be due to the heat generated during oxidation which is retained and not lost into atmosphere this in turn can influence the coal ignition temperature (Chapter I, section 5.1).

The temperature rise during analyses was slow but it is noted that the mass gain is all the more important (Figs. 4a, 4b). In fact, the choice of slow temperature rise favours the separation of the measurement phenomena during oxidation of coal analyses (i.e. mass loss or mass gain). According to our analyses, at 0.5°/min, mass gain is +2.20% and the mass loss reach -95.1%. On the other hand, the measures of mass gain indicate only +0.16% at 5°/min, this can probably be due to the superposition of the two phenomena which prevents particularly a clear distinction of the first phenomenon. This superposition is confirmed, in this case the mass loss for the coal combustion reaches 93.7%. In other words, the phenomenon of mass gain intervenes in exothermic form (i.e. during oxygen-coal reaction).

The phenomenon of mass loss and mass gain observed during analyses might be due to oxidation process of coal-oxygen following formation of sulphates, formation of different gases and complete ignition of coal (Chapter I part 2, section 5.1). According to Cudmore and Sanders (1984) the change of slope (i.e. loss or gain of mass) can occur during oxidation processes and it is highly depended on oxidation rate, temperature, particle surface size and coal type. However, the study of the propensity of self-heating associated within coal waste heaps merits and requires further isotherm analyses of several coal samples of the same rank from the site (e.g. coal oxidation rate, rate of heat generation and heat of reaction) at constant temperatures (≤35°C and ≤75°C); and under longer period of time (e.g. 96 hours).

## 4. EFFECT OF COMBUSTION ON CARBONACEOUS SHALES: BAKING AND DEHYDRATION TESTS

Selected carbonaceous shale (sample AV2410E) collected from the base of the coal waste heap n°76 (non combustion zone) were subjected to heating and dehydration analyses by processes of baking at various times and under different temperature ranges (Appendix 1). As analysed by XRD, kaolinite, illite, muscovite, quartz ± calcite ± pyrite are the main minerals in this sample.

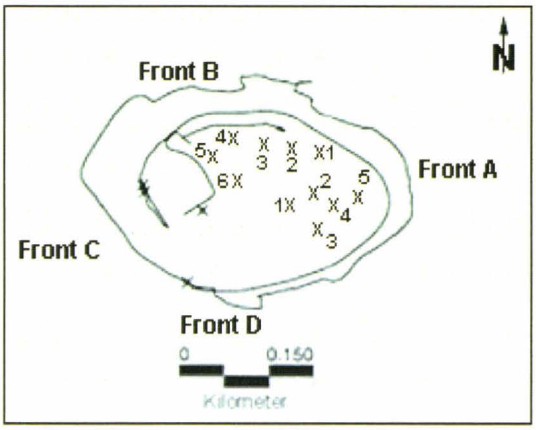

**Figure 1**. Temperature measurements locations at the coal waste heap n°76.

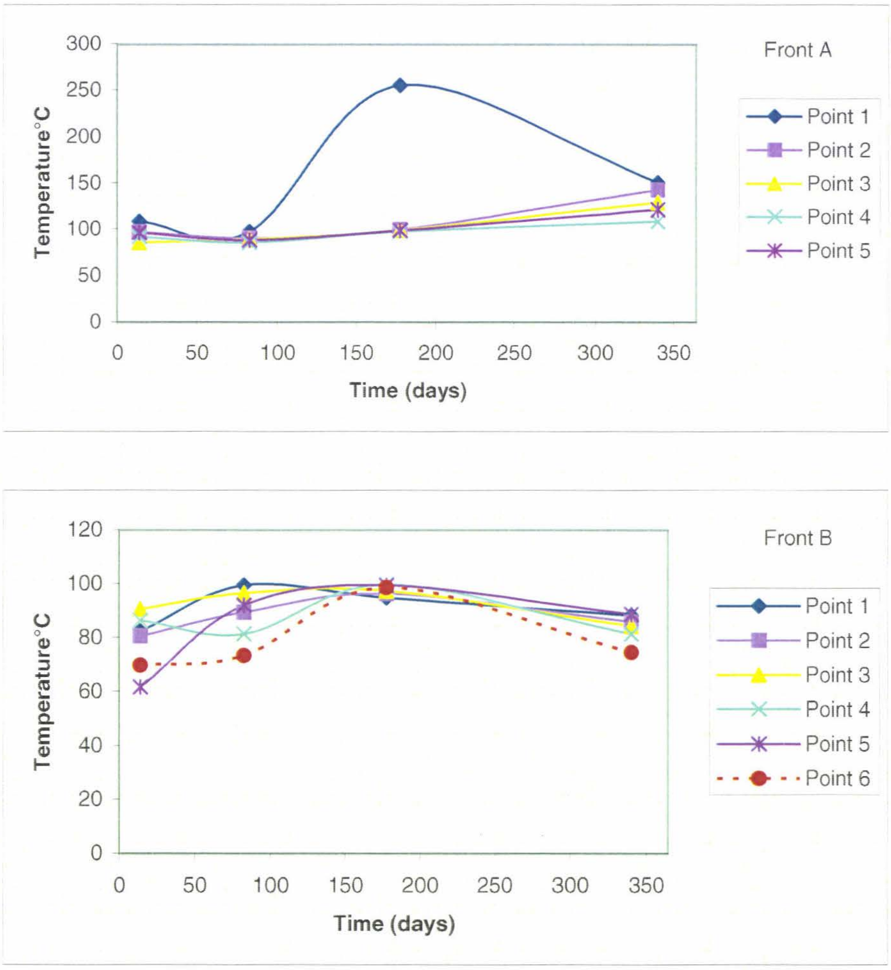

**Figure 2**. Surface temperature measurements at the burning coal waste heap n°76, 2002.

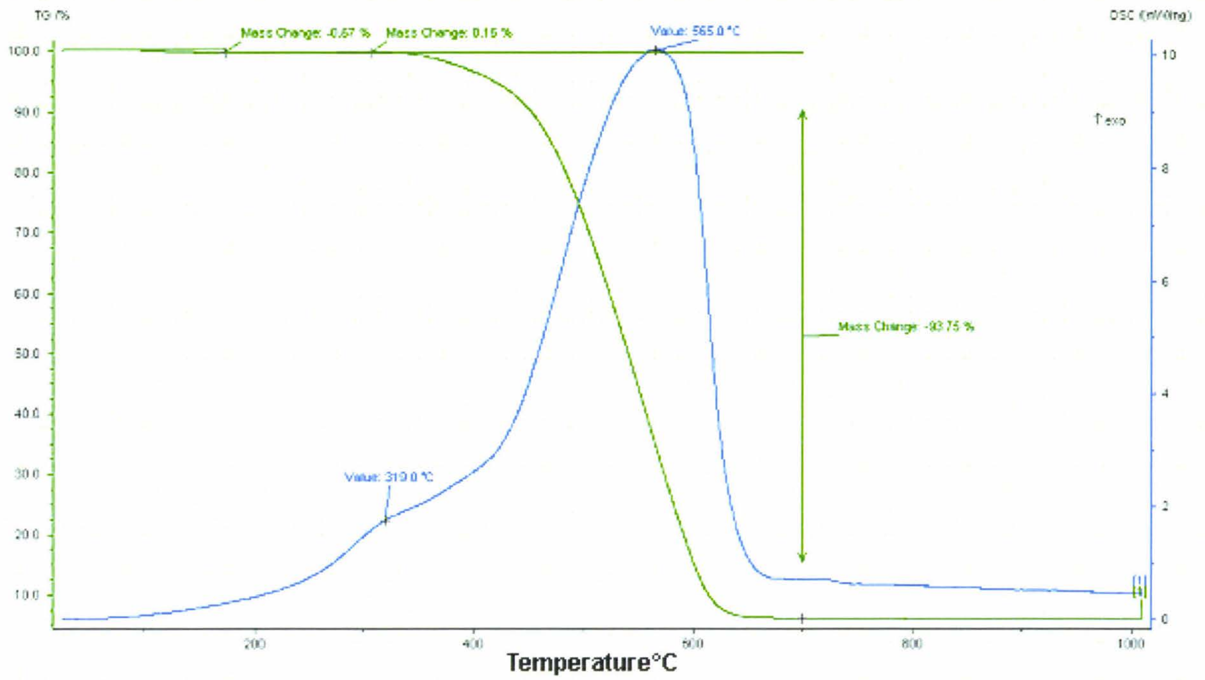

**Figure 3a**. Coal oxidation analysis at 5°/min.

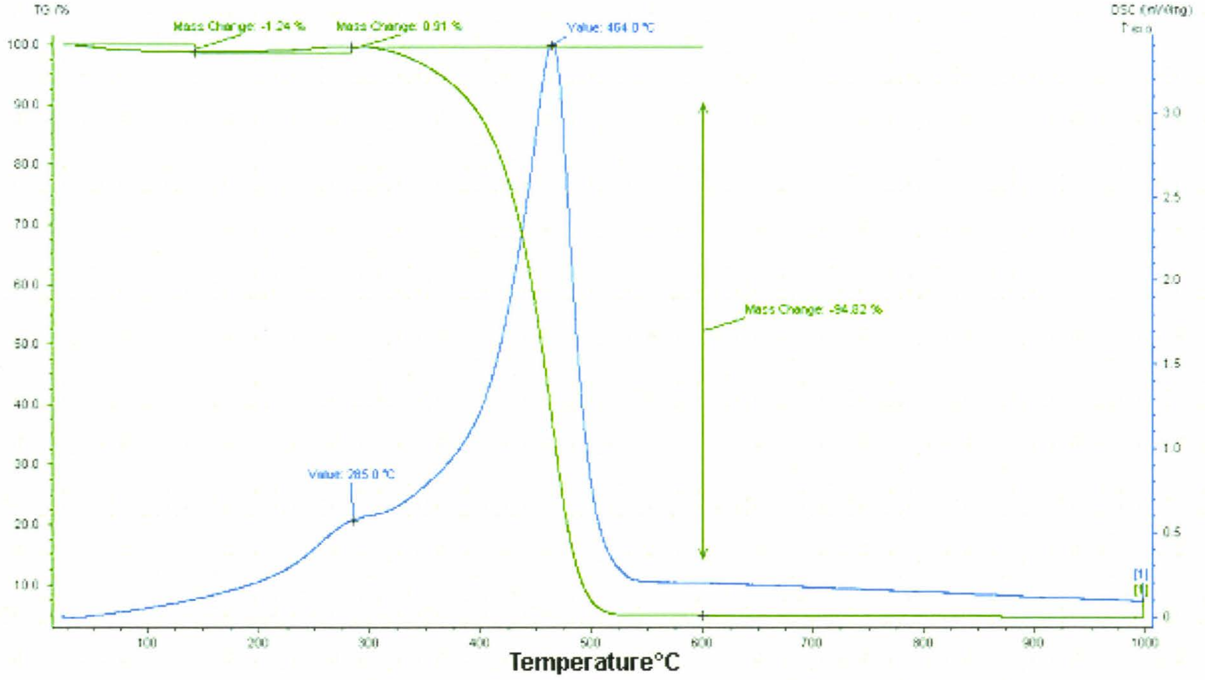

**Figure 3b**. Coal oxidation analysis at 1°/min.

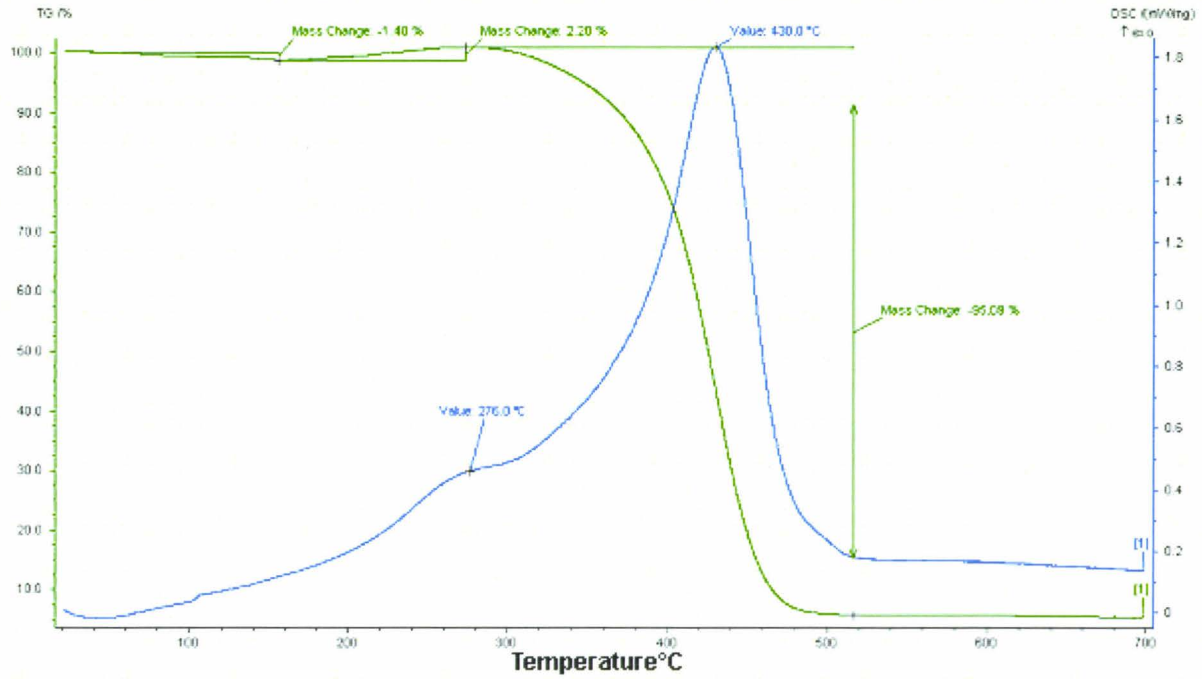

**Figure 3c**. Coal oxidation analysis at 0.5°/min.

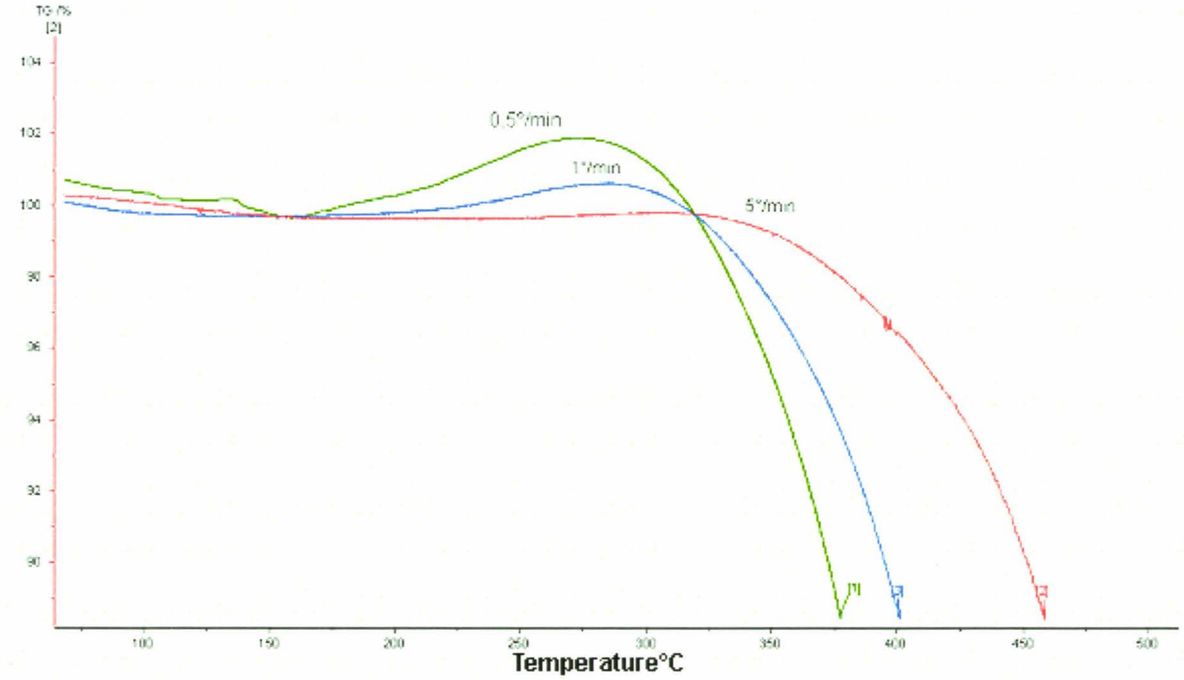

**Figure 4a**. Zoom on the phenomenon of the mass gain following the temperature rise.

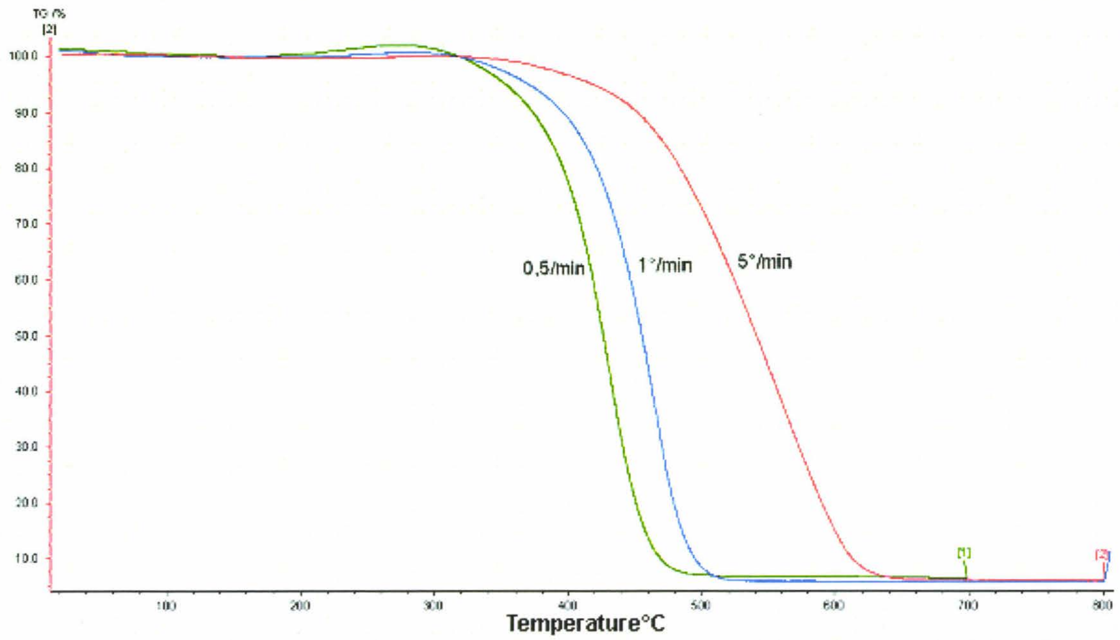

**Figure 4b**. Comparison of the thermogravimetry and effect of the temperature rise .

The results obtained from the experimental data and XRD analyses of heated samples show that dehydration of clay minerals appears at 500°C. At this temperature all water molecules and (OH) ions in kolinite are driven off and it disappears from the XRD patterns (sample AV2411E). Illite, muscovite and calcite persist until temperatures 700°C, sample is highly oxidized ad has reddish colour (decolouration, oxidation and formation of hematite). Above temperatures 900°C the latter minerals are completely decomposed. As baking temperature increases, at 1200°C XRD patterns reveal the presence of new phases, such as mullite,

Further, all heated samples were chemically analysed in order to with draw a comparison between the chemical composition of the original sample and those baked experimentally (Table 2a). As shown in this table there is a heterogeneous increase or decrease in element contents following the temperature rise during baking. The most significant changes brought about temperatures from 500 to 1200°C are: slight increases in Si, Al, Fe, Mg, Na and P. Large increase appears in K content. Ca, Ti and Mn content decrease with temperature increases. Na or K-bearing phases were not revealed in XRD patterns of the baked samples, these cations are probably concentrated in the matrix.

XRD patterns of baked reddish rock debris (the porcellanites) or locally called "schiste rouge" have not shown presence of kaolinite but illite and muscovite were detected. This clearly indicates that the temperatures of ≥650°C are a common place at the burning coal waste heap n°76. The thermal transformation of illite to spinel would have acquired temperatures ≥900°C (Deer et al. 1977; Bauluz et al. 2004).

The chemical and mineralogical composition of the coal waste heap's rock debris play significant role before and during spontaneous combustion. These rocks originally rich in clay minerals contain organic carbon (13.7-8.50 wt%) and sulphur (0.36-0.20 wt%). Sulphur is found in very fine pyrite and also in gypsum in the form of sulphate (second sulphur-bearing mineral). The loss-on-ignition (LOI) of oven-dried varies from 17.4 to 3.93 wt% this loss can be attributed to the dehydration of clay minerals, the loss of carbon dioxide from carbonate materials and the oxidation of sulphides (e.g. pyrite, see Chapter I part 2) (Table 2 and Table 3 below).

**Table 2a**. Chemical analyses of original carbonaceous shale (AV 2410E) and experimentally baked samples.

| | | **T°C 500** | **T°C 700** | **T°C 900** | **T°C 1200** |
|---|---|---|---|---|---|
| **Elements** | **AV 2410E** | **AV 2411E** | **AV 2412E** | **AV2413E** | **AV2414F** |
| $SiO_2$ | 63.70 | 79.44 | 65.46 | 83.79 | 67.31 |
| $Al_2O_3$ | 18.84 | 13.30 | 20.79 | 12.69 | 20.46 |
| $Fe_2O_3$* | 3.67 | 0.84 | 4.60 | 0.84 | 4.22 |
| MnO | 0.05 | 0.00 | 0.05 | 0.00 | 0.04 |
| MgO | 1.67 | 0.55 | 1.99 | 0.52 | 1.82 |
| CaO | 0.22 | 0.00 | 0.31 | 0.00 | 0.16 |
| $Na_2O$ | 0.33 | 0.23 | 0.39 | 0.22 | 0.66 |
| $K_2O$ | 2.98 | 1.98 | 3.59 | 1.79 | 4.09 |
| $TiO_2$ | 1.04 | 0.85 | 1.05 | 0.83 | 0.91 |
| $P_2O_5$ | 0.09 | 0.037 | 0.13 | 0.041 | 0.12 |
| LOI | 7.71 | 2.50 | 2.50 | 0.62 | 0.41 |
| Total | 100.30 | 99.72 | 99.72 | 100.10 | 99.37 |

*$Fe_2O_3$: total Fe

**Table 2b**. Loss on weight during baking experiments (sample AV 2410E).

| **Time/h** | **T°C** | **Wt/g before heating** | **Wt/g after heating** | **Wt/g loss** |
|---|---|---|---|---|
| 5 | 500 | 20.93 | 18.69 | 2.24 |
| 5 | 700 | 12.10 | 9.40 | 2.70 |
| 5 | 900 | 17.60 | 12.50 | 5.10 |
| 5 | 1200 | 187.45 | 58 | 129.45 |

**Table 3**. Chemical composition of the carbonaceous shales and the baked debris "porcellanites" from the coal waste heap n°76, Avion.

| **Wt %** | **Shales** | | **Porcellanites** | |
|---|---|---|---|---|
| **Elements** | **AV1** | **AV33** | **AV9** | **AV25** |
| $SiO_2$ | 54.50 | 50.90 | 59.40 | 62.40 |
| $Al_2O_3$ | 18.30 | 19.30 | 19.60 | 16.80 |
| $Fe_2O_3$* | 3.50 | 4.30 | 9.20 | 8.60 |
| MnO | 0.03 | 0.053 | 0.137 | 0.191 |
| MgO | 1.50 | 1.60 | 1.90 | 2.0 |
| CaO | 0.10 | 3.80 | 0.50 | 0.40 |
| $Na_2O$ | 0.32 | 0.54 | 0.33 | 0.59 |
| $K_2O$ | 2.74 | 3.53 | 2.98 | 2.99 |
| $TiO_2$ | 1.17 | 0.84 | 1.06 | 0.96 |
| $P_2O_5$ | 0.06 | 0.13 | 0.17 | 0.14 |
| H20 | 1.77 | 2.12 | 1.19 | 0.63 |
| LOI | 17.74 | 14.73 | 4.99 | 3.93 |
| Total | 99.91 | 99.64 | 100.29 | 99.05 |
| %C | 13.7 | 8.50 | 0.06 | 0.05 |
| %St** | 0.36 | 0.20 | 0.08 | 0.09 |

*$Fe_2O_3$: refers total Fe    ** St: total sulphur

Subsequently, during combustion the strength, composition and coherence of the rock debris become affected by heating, as a result of shrinkage following dehydration during baking process and decrease in volume brought about by consumption of coal waste heap's materials (Table 3). This is in good agreement with the heating laboratory tests described above, thermal investigations have shown that dehydration of these materials occurs at 500C° and loss on weight appears at all temperatures due to brake down of clay minerals (Table 2b ). According to Nichol and Tovey (1998) the rate of propagation varies greatly depending on the physical and chemical characteristics of the dump, density packing and oxygen access. In general during combustion a 40-60% reduction in volume takes place as the material is baked or reduced to ash. The volume reduction, in turn, leads to development of surface cracking or vents in the wake of the active burning zone. Such surfacial fissures control the paths of the hot gases, relieve internal pressures and increase more air and moisture penetration at the base of the coal waste heap (Masalehdani, 1985; Masalehdani and Potdevin, 2004).

One such example of the combustion and development of numerous surfacial fissures, cracks and gas vents are reported by Masalehdani and Potdevin (2004) in association with the burning coal waste heap n°83 in Fouquières les-Lens in Pas-de-Calais (see Chapter III).

## 5. SOURCES OF HEAT AND GASES: OXIDATION TESTS

There are almost no published data stating that carbonaceous shales (of coal waste heaps) are sources of heat and pollution. As described in Chapter I part 2 these materials can provide a major fuel source for subsequent combustion in the coal waste heap therefore, they contribute to gas emissions.

Selected carbonaceous shale (sample AV1) and coal (sample AV123C) from coal waste heap n°76 in Avion were subjected to laboratory gas analyses at various temperatures for about 2 hours and under dry air (see also Chapter III). The objectives centred on determining:

- the nature and concentration of gases produced during the combustion from carbonaceous shales (e.g. the pollution potential of carbonaceous shale) and from the coal,
- the temperature of emitted gases.

Results of the laboratory analyses of carbonaceous shale and coal are shown in Figures 5 and 6 respectively. Significant amounts of carbon monoxide (CO) were detected during analyses. Carbon monoxide emission starts at about 110°C, at temperatures $\geq 600°C$ the CO content in carbonaceous shale is between 1600-2000 ppm (i.e. 48.99- 49.11 g/Kg of sample, averaging 49.05 g/Kg of sample) (Fig. 5a); and 3500 ppm (461.07 g/Kg) in coal (Fig. 5b). The analyses show that the concentration of CO in both samples is a function of temperature. The temperature dependency of carbon monoxide is clearly observed in these Figures. In other words, the higher the temperature of the combustion the higher the CO content in the emission gas. It is also observed during in-situ gas analysis, the low temperatures ($\leq 99.7°C$) of combustion influences the concentration of CO ($\leq 110$ppm) but it is in favour of $CO_2$ emission (see Chapter III). Sulphur dioxide ($SO_2$) is given off above 200°C from the carbonaceous shale and about 180°C from the coal. The concentrations of this gas is between 30-35 ppm (0.48-0.54 g/Kg of sample, averaging 0.51 g/Kg of sample) in carbonaceous shale and 50ppm in coal (Figs. 5b and 6b) respectively. As shown in these Figures the concentrations of $SO_2$ from experimental analyses measured slightly higher than that obtained $SO_2$ during in-situ gas analysis (Chapter III, Table 2).

Hydrocarbons were not detected in carbonaceous shale whereas in coal sample they were (Figs. 6a). Methane ($CH_4$) emissions occurs about 120°C, at 450°C methane concentration is recorded 700. Non methanic hydrocarbon (NMHC) 500ppm occurs at 450°C.

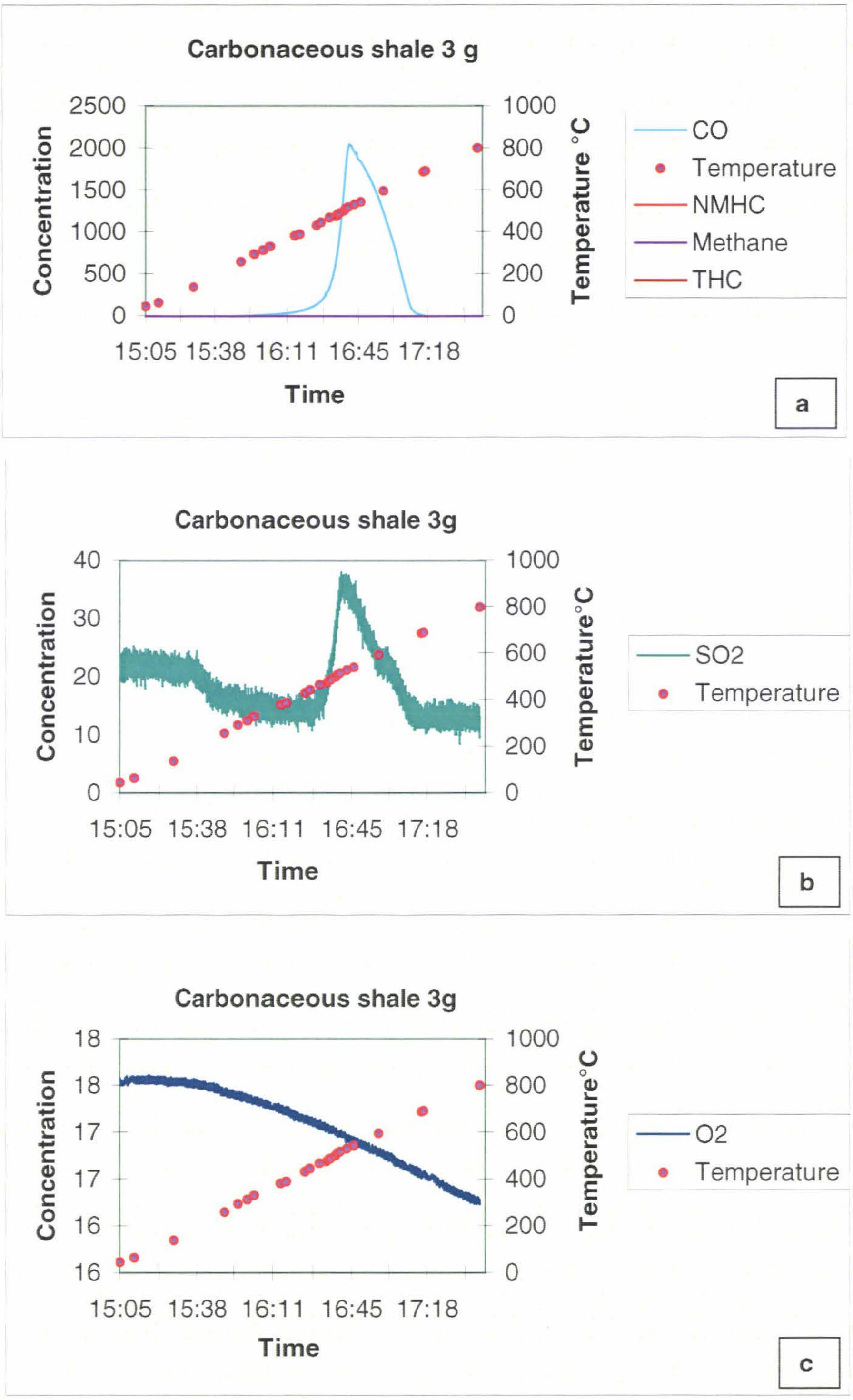

**Figure 5**. Results of laboratory gas analyses on carbonaceous shale.

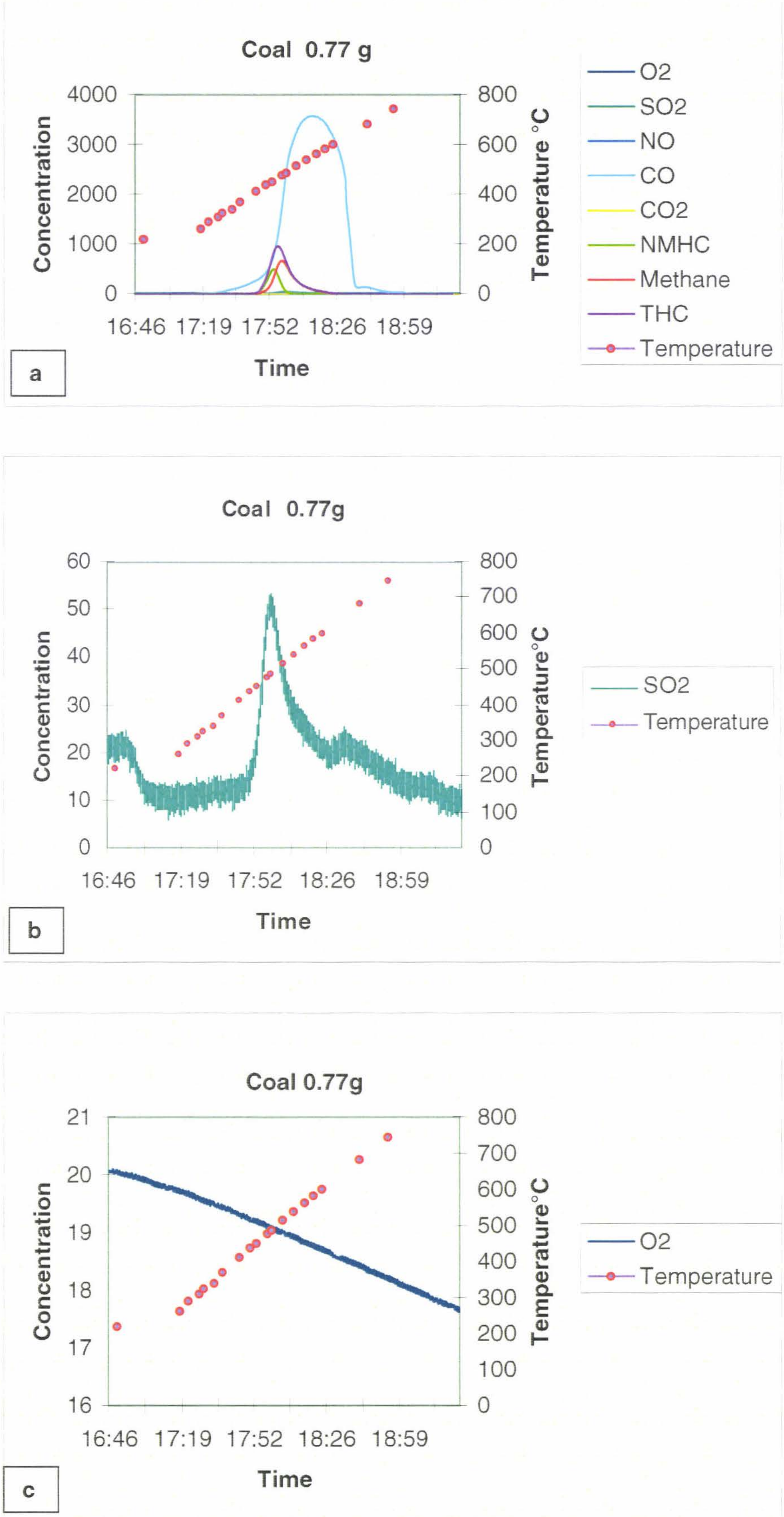

**Figure 6**. Results of laboratory gas analyses on coal.

Based on the results of experimental studies it can be concluded that emission of hydrocarbon gases from coal sample is a function of temperature, in other words, the composition of the gas is not constant with temperature. At higher temperatures the gas in coal sample contained a larger proportion of hydrocarbons. Methane, greenhouse gas was detected experimentally as well as during field gas analyses (see Chapter III).

During oxidation tests, oxygen ($O_2$) concentrations at 300°C measured 18% in carbonaceous shale. At 250°C it was 20% in coal sample (Figs. 5c and 6c respectively). Other gases such as $CO_2$, $NO_x$ detected in very low concentrations in both samples.

The results of laboratory investigations indicate that the carbonaceous shales fuel the combustion in the coal waste heap and they are also source of pollutant atmospheric gases such as $SO_2$. Further investigations at lower temperatures are necessary to determine the possible amount of $CO_2$ production from the carbonaceous rock debris in order to model the heat equivalent discharge of this gas from these rock debris. However, emission of various gases from coal and carbonaceous shales oxidation follow clearly defined patterns and temperatures. An example of so called "fire ladder" of gas emissions, depended on coal rank, that can be used to indicate the progress and temperature dependent of various gases in self-heating of coal is shown in Figure 7 (Walker 1999; Chamberlain, 1971; Chamberlain and Hall, 1973).

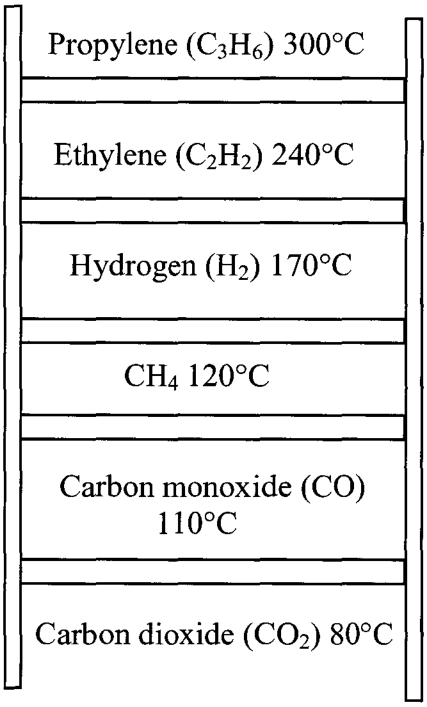

**Figure 7**. "Fire ladder", showing the different products of combustion emitted with increase in fire temperature.

## REFERENCES

ASTM (American Society for Testing and Materials) (1997). Annual book of ASTM Standards, Volume. **05.05**: Gaseous Fuels: Coal, and Coke: ASTM, Philadelphia, P.A., 207-523.

Bauluz, B., Mayayo, A., Fernandez-Nieto, C. and Gonzalez Lopez, J.M. (2004). TEM study of mineral transformations in fired carbonated clays: relevance to brick making. Clay Minerals, **39**, 333-344.

Chamberlain, E.A.C. (1971). The ambient temperature oxidation of coal. Natinal Coal Board, Hobart House, London.

Chamberlain, E.A. and Hall, D.A.(1973). The ambient temperature oxidation of coal in relation to the early detection of spontaneous heating: Part 2. The Mining Engineer, **132**, (152), 387p.

Cudmore, J.F. and Sanders, R.H. (1984). Spontaneous combustion of coal, mine fires and interpretation of analyses of mine gases, a literature review. Australian coal industry research laboratories Ltd. (ACIRL), report n°**10**, ISBN n° 0 86772 049 2, p.60.

Deer, W.A., Howie R.A. and Zussman, J. (1977). An introduction to the rock-forming minerals, 528p.

Flann R.C. and Lukaszewski G.M.(1971). The prevention and control of burning in waste coal dumps. In: Proceedings of the Australian Institute of Mining and Metallurgy, **238**, 11-29.

Harries, J. and Ritchie A.I.M. (1980). The use of temperature profiles to estimate the pyritic oxidation and Soil Pollution rate in waste rock dump from an open cut mine. Water, Air, **15**, 405-423.

Lefebvre R., Gélinas P. and Isabel D. (1993). Heat transfer during acid mine drainage production in a waste rock dump, la mine Doyon Québec. Final report May, 48 p.

Nichol D. and Tovey N.P. (1998) Remediation and monitoring of a burning coal refuse bank affecting the Southsea Looproad at Brymbo, North Walse. Engineering Geology **50**, 309-318.

Masalehdani M.N. (1985). Thermal metamorphism associated with burnt coal seams, Rotowaro Coalfield, Huntly, New Zealand. (Unpublished MSc Thesis, Auckland University, 102 p.

Masalehdani, M.N.N. and Potdevin, J.L. (2004). Problèmes Géo-Environnentaux lies à la combustion des Terrils dans les Zones Miniers de la Région Nord-Pas-de-Calais, France. In: Conference proceeding book, Journées nationales de géotechnique et de géologie de l'ingénieur géotechnique et aménagement, 28-30 June , Lille, France, 209-218.

Walker, S. (1999). Uncontrolled fires in coal and coal wastes, IEA Coal Research-The Clean Coal Centre, London.

# CHAPTER III

# IN-SITU GAS MEASUREMENTS AND ANALYSES: BURNING COAL WASTE HEAPS, NORTHERN FRANCE

# In-situ gas measurements and analyses: Burning coal waste heaps, northern France.

M.Naze-Nancy Masalehdani. University of Lille1, Department of Geology, UMR CNRS 8110, Bâtiment SN5, 59655 Villeneuve d'Ascq CEDEX, France
**MN.Masalehdani@ed.univ-lille1.fr**

Jean-Luc Potdevin. University of Lille1, Department of Geology, UMR CNRS 8110, Bâtiment SN5, 59655 Villeneuve d'Ascq CEDEX, France

Fabrice Cazier .Université du Littoral, Laboratoire de Catalyse et Environnement Côte d'Opale 145, Avenue Maurice Schumann 59140 Dunkerque, France.

Habiba Nouali. Université du Littoral, Laboratoire de Catalyse et Environnement Côte d'Opale 145, Avenue Maurice Schumann 59140 Dunkerque, France.

Part of this article was combined with the one in Chapter IV and it was orally presented during "The First International Conference on Coal Fire Research in Beijing, China 2005", which is accepted for publication by the U.N.E.S.C.O. in the "ERSEC Ecological Book Series N°4".

## ABSTRACT

Two coal waste heaps located in urban areas in the Pas-de-Calais region in northern France have undergone combustion. Continuous emissions of noxious gases, fumaroles, formation of secondary by-products and development of large cavities at the sites have required detailed geological investigations and direct field gas measurements. Field investigations and aerial infrared thermographic survey were combined to detect gas spots, open surface fissures and vegetation dieback zones. In-situ gas measurements and analyses around selected gas spots were performed using the chamber method. Gas measurements were carried out three times at the coal waste heap n°76 in Avion and twice at the coal waste heap n°83 in Foquières-les-Lens. Gas temperature measurements and the quantification of concentrations of emitted gases such as $H_2S$, $SO_2$, $NO_x$, CO, $CO_2$, hydrocarbons, $O_2$ and $H_2O$ were determined. The concentrations of the various gases were compared to each other and to TLV (Threshold Limit Value) in order to determine the negative impacts of such gases on the human health and on the environment. Field measured surface temperatures around active events (56-255.5°C) showed heterogeneity of combustion at both sites. $H_2S$ was absent, the most important finding was the concentration of $CO_2$ (7%) much higher than TLV; the concentrations of $SO_2$ (<5 to 25 ppmv) and $NO_x$ (8 to 25 ppmv) are also above TLV. CO concentration is in order of 20-110 ppmv therefore, either below and/or above TLV. $CH_4$ is the main emitted hydrocarbon; methane concentrations were measured (47 to 260 ppmv) outside the explosion limits. Further, the level of $O_2$ (<1%-19%) around the gas vents is below the atmospheric level it requires that access to the sites must be limited to authorised people only. Smouldering fires on mining coal waste heaps contribute with their carbon dioxide emission to the greenhouse effect considerably. Uncontrolled release of gas from burning coal waste heaps is an environmental risk; inhalation of very small amounts of some of these gases is extremely dangerous to human health.

**Keywords**: Coal waste heap; combustion; risks; toxic gas measurements; pollution

## 1. INTRODUCTION

Today, the world anthropogenic $CO_2$ emissions represent roughly twice the total uptake (ocean plus continental ecosystem). The world must divide its $CO_2$ emission by 2, or bring the $CO_2$ emissions down to 3 billion tons of carbon per year (Gangopadhyay, 2005). Coal fires (coal seams and coal waste heaps) are known from different coalfields around the world, China, India, the U.S.A., Australia, Indonesia and South Africa are the main countries affected by coal fires (Fig.2, Chapter I). The fires are a severe threat to valuable resources and the local, regional and global environment. Geo-natural hazards such as spontaneous combustion of coal discharge not only a large amount of toxic gases, e.g. CO, but also climate active greenhouse gases like $CO_2$, $CH_4$ and acidic gases $SO_2$ and $NO_x$ which contribute to the heating of the atmosphere and air-water-soil pollutions.

Coal wastes are by-products of coal mining operations they are usually generated in huge quantities and must be disposed of. During beneficiation of coal in northern France around 300 coal waste heaps with considerable amounts of coal and carbonaceous shale were produced. Depended on their shape and age these coal wastes may contain 15-35% reject coal (Paquette and Laversanne, 2004). The waste material is subject to spontaneous combustion and is highly susceptible to other means of ignition such as heat from burning rubbish or bush fires (Flann and Lukaszewski, 1971). According to Stracher and Taylor (2004) the coal fires are a global catastrophe and are responsible for a lot of human illnesses. Coal contains numerous persistent, bioaccumulative trace elements (e.g. mercury, dioxins, arsenic, radionucleotides, cadmium and lead) that are released during combustion and end up in the atmosphere, water bodies and soil (Finkelman and Gross, 1999; Keating, 2001). Many of the health and environmental problems (e.g. in China) are attributed to these toxic elements (Finkelman, 2004). By contrast, coal is not toxic to the environment in the sense that it or its constituents are not directly absorbed into organic systems to any major degree. Coal that is mined or exposed during mining but not utilised can give toxic products where it is subjected to slow and air-starved combustion (Clarke, 2003).

On a coal waste heap containing combustible materials and which has undergone spontaneous combustion the most obvious indicator of the subsurface combustion are discharge of fumaroles along the surface cracks in early mornings and or during wet and snowy seasons. Formation of secondary new minerals (by-products) around the gas vents; alteration of parent rock debris; and vegetation dieback areas are also indicator of subsurface combustion of colliery wastes. These phenomena were detected at two coal waste heaps in the Nord-Pas-de-Calais region, in northern France. The main objective of this study was focused on investigations of gas spots and direct field gas measurements and analyses at both sites. Field investigations were carried out along with aerial infrared thermographic survey to detect gas spots, open surface fissures and vegetation dieback zones. A special technique was designed to measure, analysis and quantify in-situ the concentration of emitted gases such as $H_2S$, $SO_2$, $NO_x$, CO, $CO_2$, hydrocarbons, $O_2$ and $H_2O$ from coal waste heaps n°76 and n°83 in Avion and in Fouquières-les-Lens respectively. Near surface temperature at which the above gases emit into the atmosphere were monitored. In this paper the results of field gas measurements are presented. The measurements of different gases are correlated with each other and compared with Threshold Limit Value (TLV) in order to explain the differences in gas contents at the study sites; to determine negative impacts of such noxious gases on the human health (people living in vicinity of burning coal waste heaps) and on the environment.

## 2. SITE LOCATIONS AND DESCRIPTIONS

### *2.1. Coal waste heap n°76, Avion*

The coal waste heap n°76 of "Liévin" lies in the Nord-Pas-de-Calais Coalfield 1.3 km south of Avion within the Pas-de-Calais (Fig. 2a). The development of the coal waste heap spanned about 60 years (1921-1987). During this period the site was used for indiscriminate disposal of reject coal, carbonaceous shaley waste and sweepings from wagon cleaning operations of pits n°7 and 7bis of Liévin. The site has undergone spontaneous combustion since about 1987. It used to be cone like in shape, standing 85m above natural ground level and covers an area of 96 000 $m^2$ (Fig. 2 b). It was estimated to contain 5 million tonnes of mixed waste materials of a heterogeneous accumulation of fine to coarse loose debris of baked and unbaked carbonaceous shales and minor amounts of sandstone. At the top of that, it also contains varying amounts of rejected coal (Cogema, 1992).

The thermal metamorphism associated with the coal waste heap n°76 comprises red baked rock debris (the "porcellanites"), emission of noxious gases, vent deposition of secondary by-products and open surface fissures (Fig. 2c). The burning zones and the top surface of this heap are not covered by any vegetation.

Drill hole records and data provided by Cogema, 1992 revealed crucial information on the combustion of this coal waste heap. These boreholes were drilled 30m deep to the centre of the coal waste heap. Figure 3a, shows varying thickness of the thermally baked red rock debris (the porcellanites) therefore the active combustion zones within this site. It also clearly shows that these debris occupy superficially the NW and SW of the coal waste heap and it makes a complete tour of the site from its base passing by the apex down until mi-slope to SE. The morphological information obtained from the boreholes data as well as field observations were used along to locate the gas spots for gas measurements at this site (Fig. 3b).

### *2.2. Coal waste heap n° 83, Fouquières-les-Lens*

The coal waste heap n° 83 (7/19 Marais) borders on motorway A21 and lies within the NE of Fouquières-les-Lens, it is situated in the Pas-de-Calais region too (Fig. 4a). It is tabular in shape, slopes +/- 30 % on circumference, ranges up to about 10m above the natural ground, and is traceable discontinuously for about 6.82 ha (Fig. 4b). The development of this heap took place between 1882-1960. During this period a wide variety of rejected coaly materials, originated from underground coal mining activities of pit 7 of Courrières, were loaded onto wagons for dispatch along Fouquières-les-Lens. This gave rise to the formation of the actual site. The total volume of the carbonaceous waste materials, which was dumped in this coal waste heap, is unknown. But, its primary product (mixed fine to coarse heterogeneous baked and unbaked carbonaceous shales) in 1972 and 1998 was 470.000 $m^3$ and 88 000 $m^3$ respectively (Paquette, 2001). The site was exploited for its both black and red baked carbonaceous shales for civil work from 1992 to 1999, thereafter it was abandoned. The subsurface combustion of this coal waste heap was identified during our field investigations in 2002. However, it should be stressed that this coal heap presents environmental hazards and a serious danger to public. The site has several large gas vents and surficial cracks through which noxious gases emit into the atmosphere (Fig. 4c). It had already experienced sub-surface explosion and as a consequence a man was seriously injured (oral confirmation). This coal waste heap was declared as a dangerous site and it was fenced around with the billboards in 2002. Despite, the declaration of burning and other dangers, the fence lines have been broken and removed and the site remains accessible to public.

**Figure 2**. Coal waste heap n°76 Avion. **(a)** Location map 1/60000 (S.A.Terrils, 1993). **(b)** Aerial photo of the site during combustion, 1987. **(c)** Emission of heat and noxious gases, 2002.

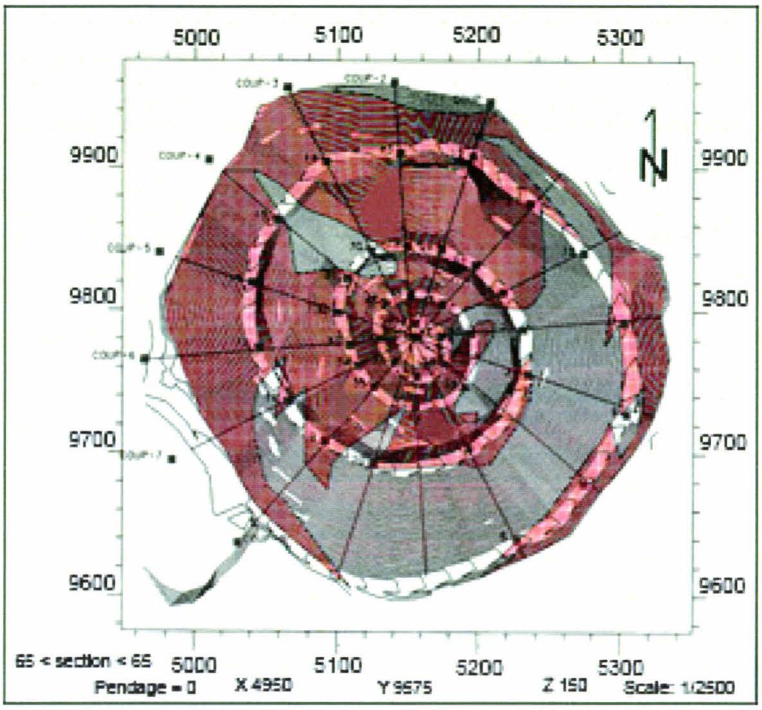

**Figure 3a.** Plan of the cutting and position of the "porcellanites" red debris, coal waste heap n°76 Avion (after Cogema, 1992).

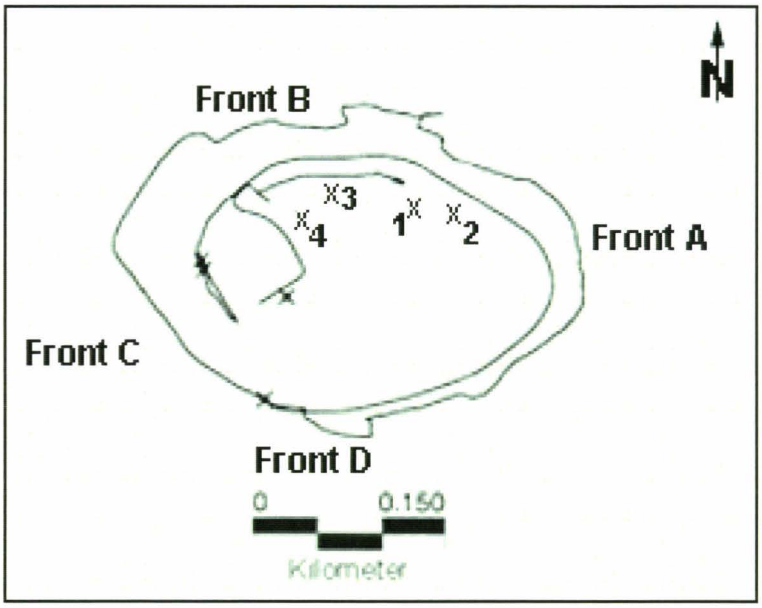

**Figure 3b.** Locations of the gas measurements, (S1, S2, S3 and S4) at the coal waste heap n°76, Avion.

Detection of gas spots for gas measurements at the site n°83 was based on field investigations and on the results of the aerial infrared thermography survey which were provided by the Charbonnage de France. The use of the latter method revealed the thermic radiation in the surface of the site, therefore, indicating notably the combustion more in depth and as well as the vegetation zones at this coal waste heap. Figure 5a clearly shows the presence of numerous combustion zones (gas spots) at the different flanks within the coal waste heap n°83. The combustion is located principally on top of the slope, particularly, along the east flanks, near by the purification station, along the west flank of the Marais de Lengles sector; and at the southwest flank of Le Tierce sector (Figs. 5b, 5c).

## 2. IN SITU GAS MEASUREMENTS: METHODS

Since the site conditions at the coal waste heap n°83 were not optimum (it is covered by vegetation and small trees; and it contains numerous dangerous gas vents) gas measurements at this site were carried out twice and from a single gas spot, along the east flank near by the purification station (Fig. 5a). Whereas gas measurements at the coal waste heap n°76 were done at four selective gas spots (Figs. 3a, 3b). However, it should be noted that during the first gas measurements the authors were not able to measure the $CO_2$ and CO concentrations in either site due to some technical problems.

In situ gas measurements involved the use of a purpose built stainless steel chamber placed on the surface of the gas spot at the coal waste heap. The chamber contained an orifice which enabled the pumping of the gas from the ground. The presence of water vapour in the gases disturbs infra-red measurements and is detrimental to the analyser. Therefore, in order to eliminate the moisture content of the sampled gases a tangential condenser filled up with dry ice as cooling agent was placed right after the chamber and before the analyser respectively. The use of a tangential condenser is studied, to limit to the maximum time of contact between sampled gases and water vapour, water being trapped in ice form. Then the gases were directed towards an analyser bay (Fig.7). Before the trap, a fraction of the gases was directed towards the bubblers which allowed the trapping of H2S, water vapour being not a hazard in this case.

**Figure 4**. Coal waste heap n°83 Fouquières-les-Lens (Paquette, 2001). **(a)** Location of the study area 1/25000. **(b)** Aerial photo of the site, 1/5000° (Paquette, 2001). **(c)** Surface horizontal fissure and gas vent (35cm wide and 3m long) emission of heat and fumaroles, 2005.

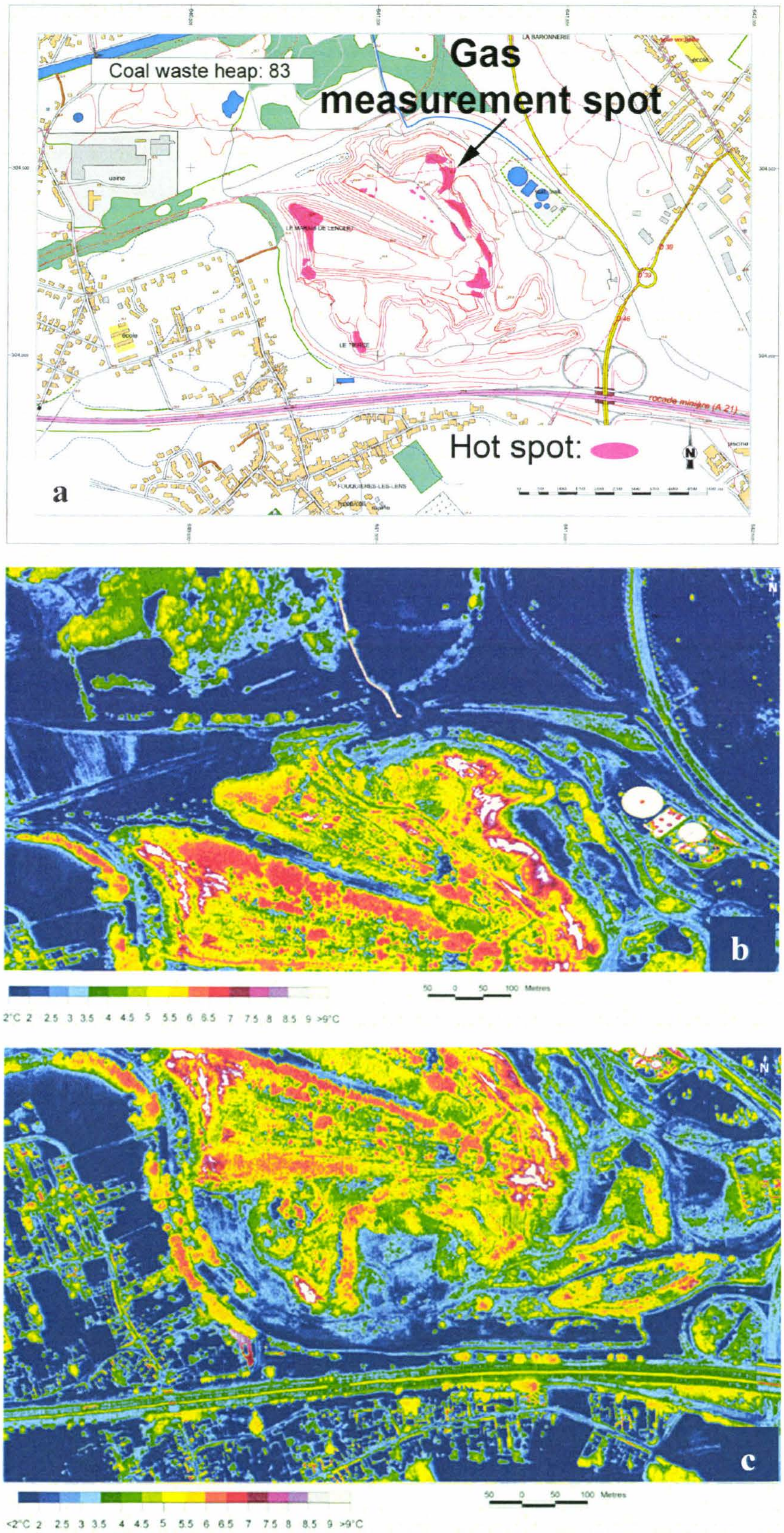

**Figure 5**. Aerial infrared thermography analysis, coal waste heap n°83 (after Paquette, 2001). **(a)** A plane of the site (1/5000°), map of the gas spots and location of gas measurements. Analysis thermography (1/5000°), **(b)** north sector, **(c)** south sector.

At the exit of the trap with the help of a cold transfer line in one hand gases were directly transferred to the analyser bay placed in a specially equipped vehicle (a mobile laboratory) which yielded analysis of $CO_2$, CO, hydrocarbons, $SO_2$, $NO_x$ and $O_2$. On the other hand they were directed towards the bubblers which enabled the trapping of the $H_2S$ (Figs. 6a, 6b).

### *3.1. Hydrogen sulphide ($H_2S$) analysis*

Hydrogen sulphide analysis involved in $H_2S$ trapping by bubbling through the 0.5 N sodium hydroxide solutions (NaOH 0.5 mol/L). Afterwards the solution was reacted with N,N-dimethyl-p-phenylendiammonium ion to form the blue of methylene. Subsequently, in order to measure and verify the presence and the concentration of hydrogen sulphides ($H_2S$), the analysis was examined by UV spectrum of a standard sulphide solution ($Na_2S$ to 0.114 mg/L or 47ppb in sulphide; and absorbance to 665nm). The intensity of the blue colour developed during the reaction is proportional to the concentration of $S^{2-}$.

### *3.2. Other gas analysis*

Other gases such a $CO_2$, CO, $SO_2$, $NO_X$, $O_2$, and hydrocarbons measured with the help of an analyser bay which was composed of the following elements (Fig. 7):

- A membrane pump with heated head.
- A heated dust filters in order to eliminate the particles.
- A group of cooling apparatus trapping residual moisture.
- A methane and non-methane hydrocarbon analyser (FID-model Cosma Graphite 355).
- A non-dispersive infra-red analyser (Hartmann and Braun, Model URAS 100) for CO / $CO_2$, NO / $NO_2$ and $SO_2$.
- An oxygen analyser (using the paramagnetic detection properties of the oxygen).

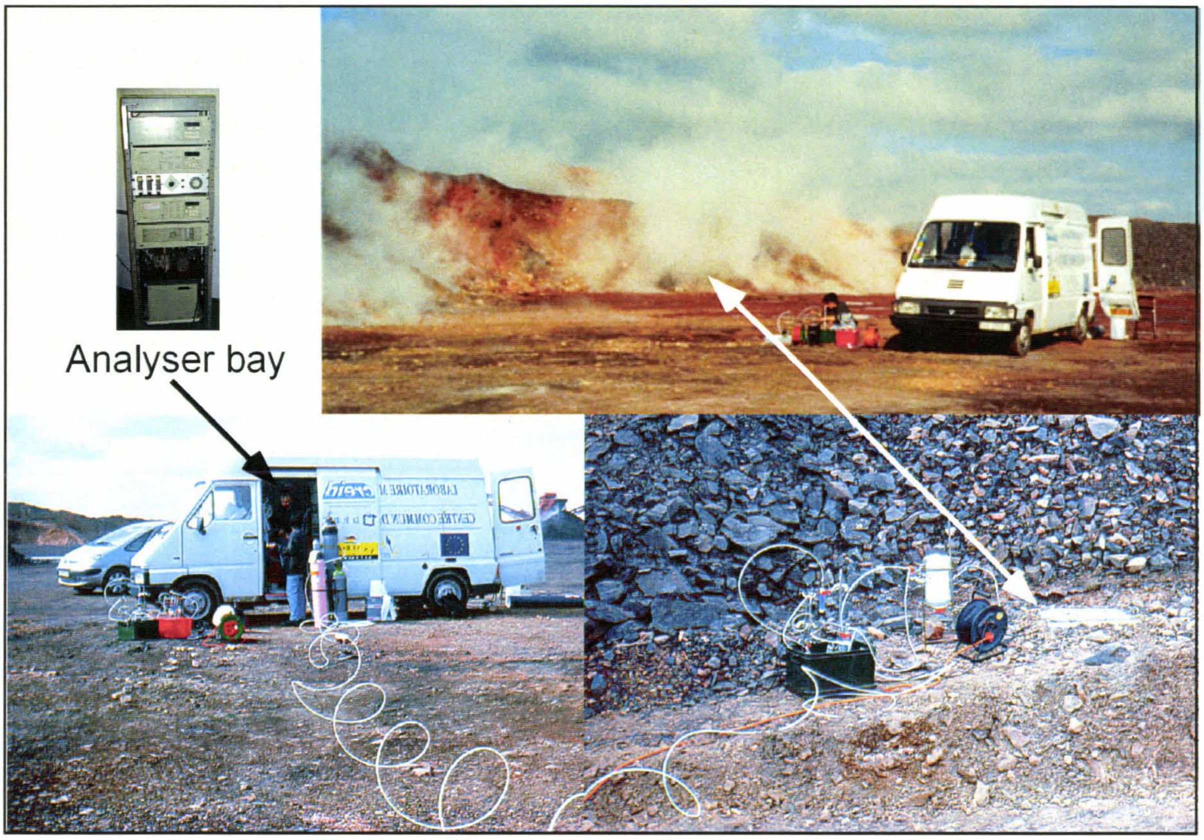

**Figure 6a**. In-situ gas measurements coal waste heap n°76 Avion, 2002

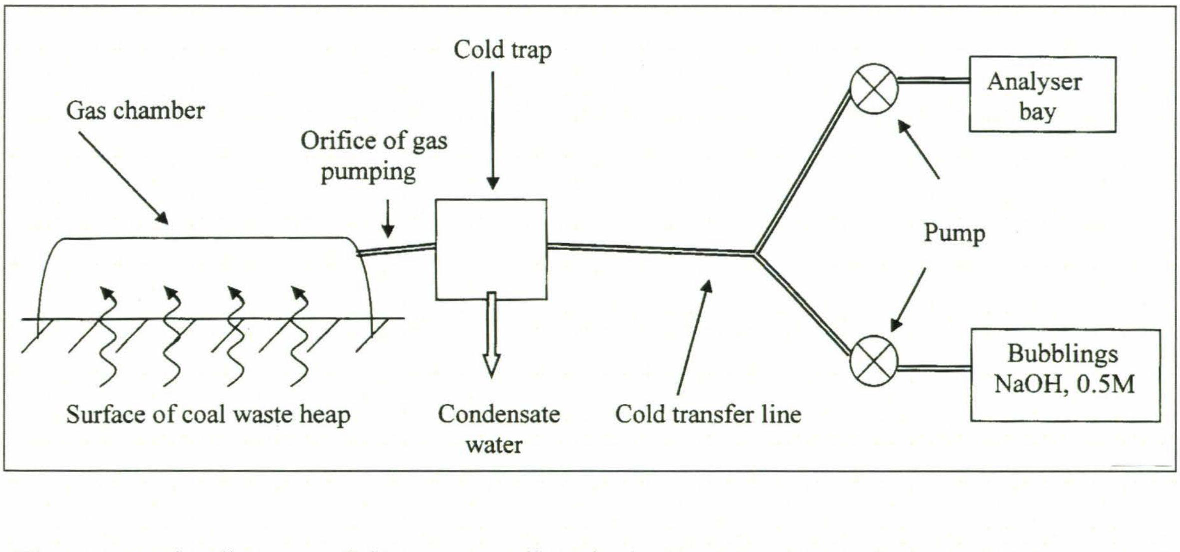

**Figure 6b**.The diagram of the gas sampling device.

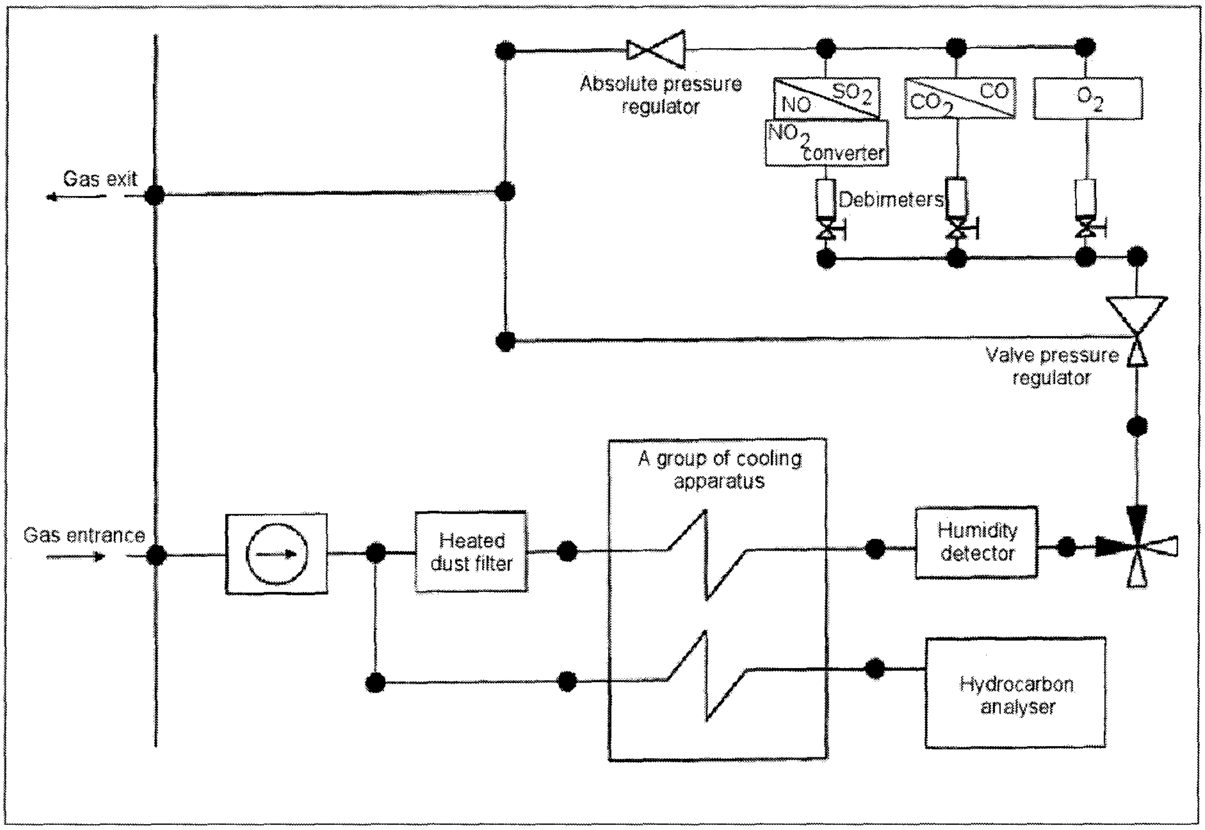

**Figure 7.** Scheme of the analytical system of gas analysis.

## 3. RESULTS

The results of the measurements for $H_2S$, $SO_2$, $NO_x$, CO, $CO_2$, $CH_4$, $O_2$, $H_2O$ and the gas temperatures are presented in Table 1 and in Figures 9 and 10.

### *4.1. $H_2S$*

The solutions of bubbling (NaOH 0.5 N) obtained during the gas measurements from gas spots S3 at coal waste heap n°76 and E1 at coal waste heap n°83 were analysed by UV/Visible spectrum according to the method described in section 3.1. The layout of standard solution of sulphide ($S^{2-}$) shows a peak of absorption at 665nm characteristic of sulphides whereas the other two layouts from study sites do not show any peak on the same wavelength (Fig. 8).This confirms that hydrogen sulphide is absent in our solutions. In addition to this process, condensate waters collected from the cold traps were also analysed. The latter measurements were carried out in order to verify if the hydrogen sulphide was not trapped in the condensates before its arrival in the bubbling. Likewise, analysis of condensates did not show any trapped hydrogen sulphide in the bubbling solutions.

Hydrogen sulphide ($H_2S$) also known as stink damp was not detected during the gas measurements. It should be stressed that, on several occasions during the field investigations at both burning coal waste heaps "rotten egg smells" known to be indicator of $H_2S$, was smelt around some gas spots. Thus, it is likely that any $H_2S$ present in the emission gases has precipitated out and or oxidised at higher temperatures than we were able to measure, or it may be lost from gas rising through vents. However, $H_2S$ is known to be produced by the reaction of elemental sulphur present in coal at high temperatures, usually at temperatures above the massive decomposition caused by the pyrolysis (Mondragón et al, 2002), provided there is not enough air for complete oxidation (Bell et al., 2001).

### *4.2. Other gas emissions*

Novel measurement is the detection of $CO_2$ (7%), which points out the presence of relatively high amounts of greenhouse gas from both coal waste heaps (Figs. 9d, 9f, 10c). As shown in Table 1 depended on the location of measurement concentrations of CO, $SO_2$,, $NO_x$, $CH_4$ and $O_2$ varied. When the gas temperature in measured location is high, the data show high concentrations of CO in sampled gas, for example in gas spot S3 at the coal waste heap n°76 (Fig. 9e). At this location the gas temperature was measured 99.7°C and the CO content measured 110 ppmv.

As described earlier, during the second gas measurements condensate waters collected from the cold traps (gas spots S3 and S1) were analysed for $H_2S$ detection. In addition, analyses have also enabled us to reveal that part of $NO_x$ and $SO_2$ were trapped in the forms of nitrate ($NO^-_3$), nitrite ($NO^-_2$) and sulphate $(SO_4)^{2-}$ respectively. In other words, at gas spot S3 at the coal waste heap n°76, 25 ppmv $NO_x$ and 13.4 ppmv $SO_2$ were directly measured by the analyser, and 1 ppmv ($NO^-_3$) and 0.61 ppmv $(SO_4)^{2-}$ were trapped in the condensates. Likewise, at the site n°83 (S1), equivalents of 0.91 ppmv ($NO^-_3$ and $NO^-_2$); and 0.05 ppmv $(SO_4)^{2-}$ were trapped in the condensates.

Furthermore, the $O_2$ concentration in gas emission varies widely. Oxygen concentrations around gas measured locations were detected $\leq$ 19%, being as low as <1% at the coal waste heap n° 83 (gas spot E1). In other words there was 99% oxygen deficiency at this location (Fig.10a).

**Table 1:** Results of gas measurements and gas temperatures from burning coal waste heaps n°76 and n°83.

| Site, Spot | Gas T°C | $SO_2$ | CO | $CO_2$% | $CH_4$ | NOx* | $O_2$% | $H_2O$**ml |
|---|---|---|---|---|---|---|---|---|
| 76, S1 | 100.5 | <5 | N.D | N.D | 80 | 15-26 | N.D | 100 |
| 76, S2 | 225.7 | 11 | N.D | N.D | 47 | 15-26 | 18-19 | N.D |
| 76, S3 | 99.7 | 9.6 | 110 | 7 | N.D | 26 | 15-18 | 3550 |
| 76, S4 | 56 | 19.8 | 22 | 6.13 | 191 | 7.87 | 14-15 | 30 |
| 83, E1 | 74.3 | 20 | N.D | N.D | 96 | 25 | <1 | N.D |
| 83, E1*** | 77.8 | 15-25 | 20-25 | 3 7 | 100-260 | 15-25 | 13-18 | 68 |

* NO + $NO_2$ ** $H_2O$ (h/min) emitted from the gas vent, $SO_2$, CO, NOx and $CH_4$ in ppm
*** second measurement, N.D. (no data)

Methane ($CH_4$) is the principal hydrocarbon in sampled gas from both coal waste heaps (Table1). The superposition of profiles of total hydrocarbon (THC) and Methane ($CH_4$) also allowed determining the presence of $CH_4$ as the major hydrocarbon gas (Figs.9a, 9b, 9c, 9f, 10a and 10b). Although methane is detected in the gas analyses from both sites but a significant variation is observed in the concentration of this gas. At the coal waste heap n°76 the methane concentrations vary depended on the location, being in order of 80 - 47 - 191% (gas spots S1, S2 and S4 respectively). Whereas at the coal waste heap n°83 from the same gas measurement location concentration of $CH_4$ increases when $O_2$ and gas temperatures are high (Table1). Indeed, emission of $CH_4$ from the latter site measured to be higher than the former site.

## 5. DISCUSSION

The most obvious indicator of the subsurface combustion within the two selected coal waste heaps in northern France is emission of mixed noxious gases. Results of gas measurements and analyses from two sites show, the variations in the concentration of emitted gases. These emissions, measured and analysed in-situ consist of the combustion gases such as CO, $CH_4$, $CO_2$, $SO_2$, NO, $NO_2$ and $H_2O$ (water vapour) (Table1). However, during gas measurements temporal variations in gas composition on the scale of minutes and seconds were recognized at the coal waste heap n°83 (gas spot E1). During an hour and 45 minutes period of gas measurements at this location, the $SO_2$, CO, $CO_2$, $CH_4$, $NO_x$ and $O_2$ were found to vary from 15 to 25 ppm; 20 to 25 ppm; 3% to 7%; 110 to 260 ppm; 15 to 25 ppm; and 13% to 18% respectively. Thus, locally at this site, there is a pulsation in gas emission, through, or by passing the zone of combustion and gasification. A general observation at both coal waste heaps is that the temperature around the gas vents and measurement locations is quite heterogonous.

The temperatures at which the different gases first appear is unknown but at the active gas spots the near surface temperatures in order of 56-255.7°C and 74.3-77.8C° were measured at the coal waste heaps n°76 and n°83 respectively (Table1). The above gases could not have been generated at such temperatures and thus undoubtedly they came from the hotter internal zone of the coal waste heaps.

### *5.1. Carbon monoxide (CO)*

Carbon monoxide (CO) or white damp is a colourless and an odourless dangerous toxic gas since it cannot be detected by taste, smell or irritation (Bell, 1996). By contrast, CO is a good coal-fire detector gas because it is released sequentially as temperature increases during heating (Stracher and Taylor, 2004).

The interaction of coal with oxygen is an exothermic reaction which leads the formation of a "coal-oxygen" complex and it has been studied for many years (e.g. Schmitd, 1945; Sondreall and Ellman, 1974; Nordon et al., 1979; Cudmore and Sanders, 1984; Nelson, 1989: Khan et al., 1990; Carras and Young, 1994; Krishnaswamy et al., 1996; Chen and Scott, 1997). Carbon monoxide is known to be a result of incomplete combustion of carbon contained in the coal (Kim, 1973). The results of our experimental tests revealed that CO is released from coal and also from carbonaceous shale oxidation and at relatively high temperatures (≥ 100°C). However, as it can be seen in Table 1, the concentration of CO in the emitted gas is a function of temperature. In other words, the higher the temperature of the combustion the higher the CO content in the emission gas (Wang et al., 2002).

Concentrations of CO from gas spot S3 at the coal waste heap n°76 were measured as high as 110 ppmv, thus, above the Threshold limit value (TLV). On the other measurement locations the content of CO was below the TLV (Tables 1 and 2).Even though carbon monoxide in the other gas measured locations is produced in smaller concentrations, yet the emission of this gas should be considered dangerous because it readily binds to haemoglobin in red blood cells, even at low concentrations.

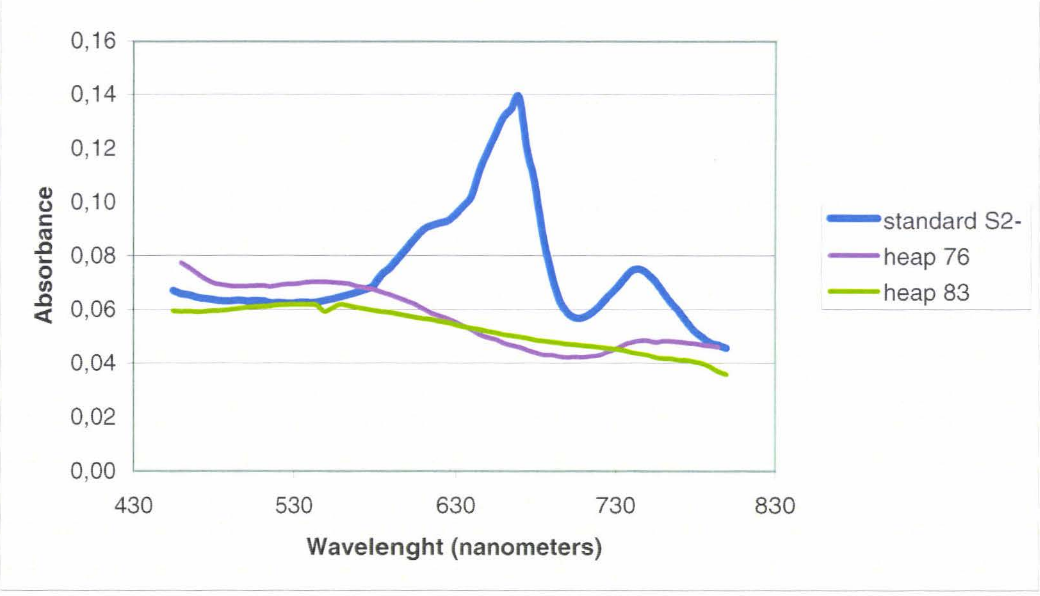

**Figure 8**. Sulphur (hydrogen sulphide) verification: the comparison of the UV/V spectrum of standard solution ($S_2^-$) with the bubbling solution of gas emissions.

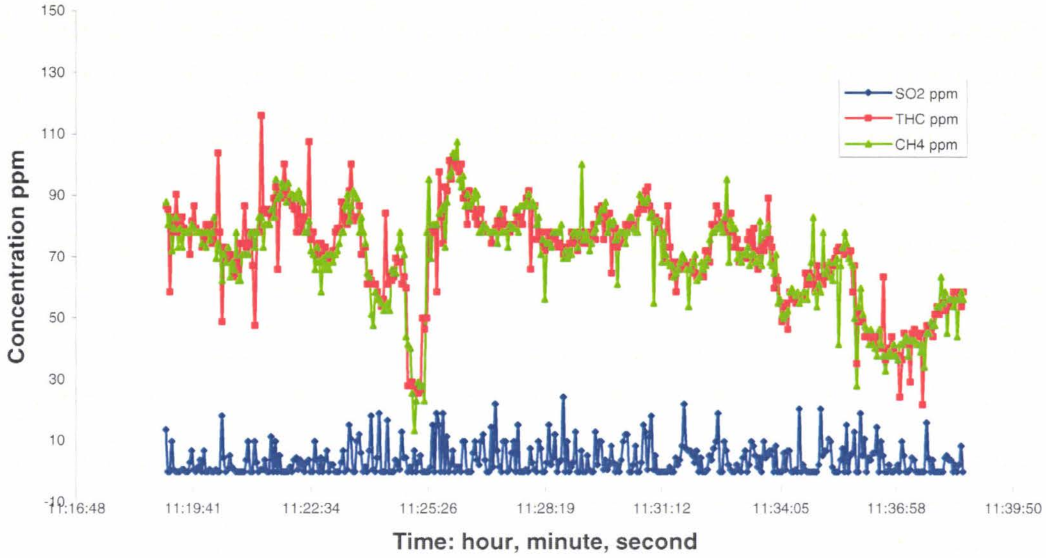

**Figure 9a**. Gas analysis at gas spot S1 coal waste heap n°76, Avion.

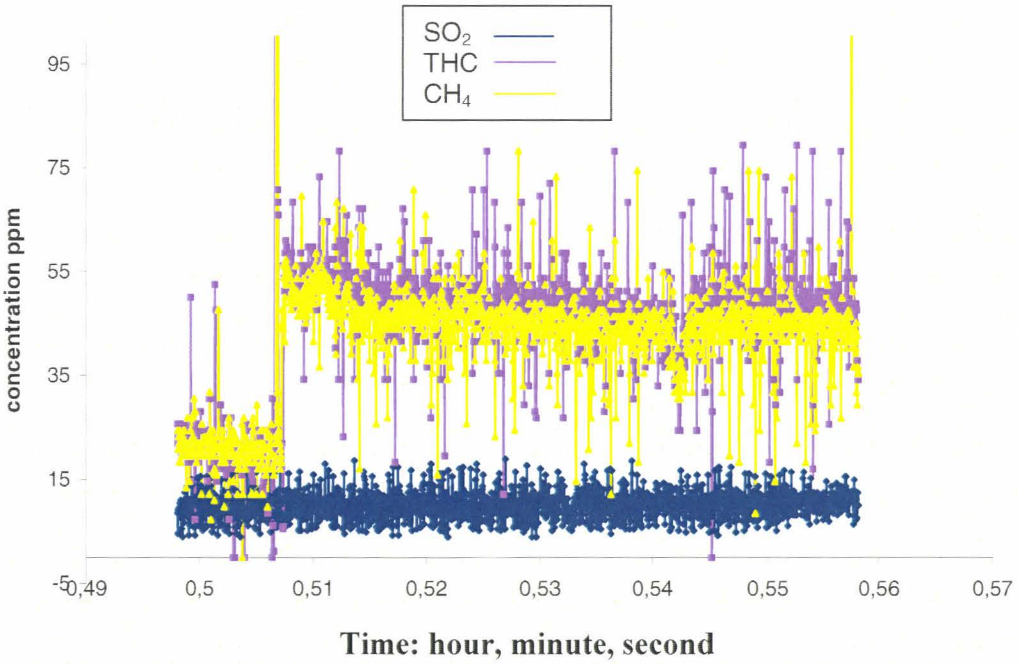

**Figure 9b**. Gas analysis at gas spot S2 coal waste heap n°76, Avion.

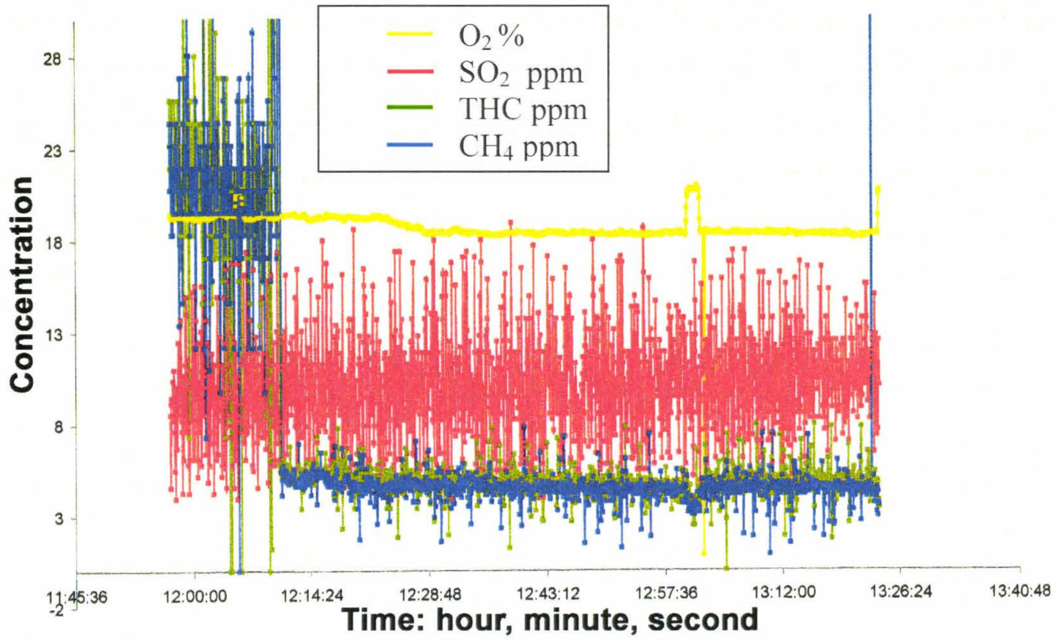

**Figure 9c**. Gas analysis at gas spot S2 coal waste heap n°76, Avion.

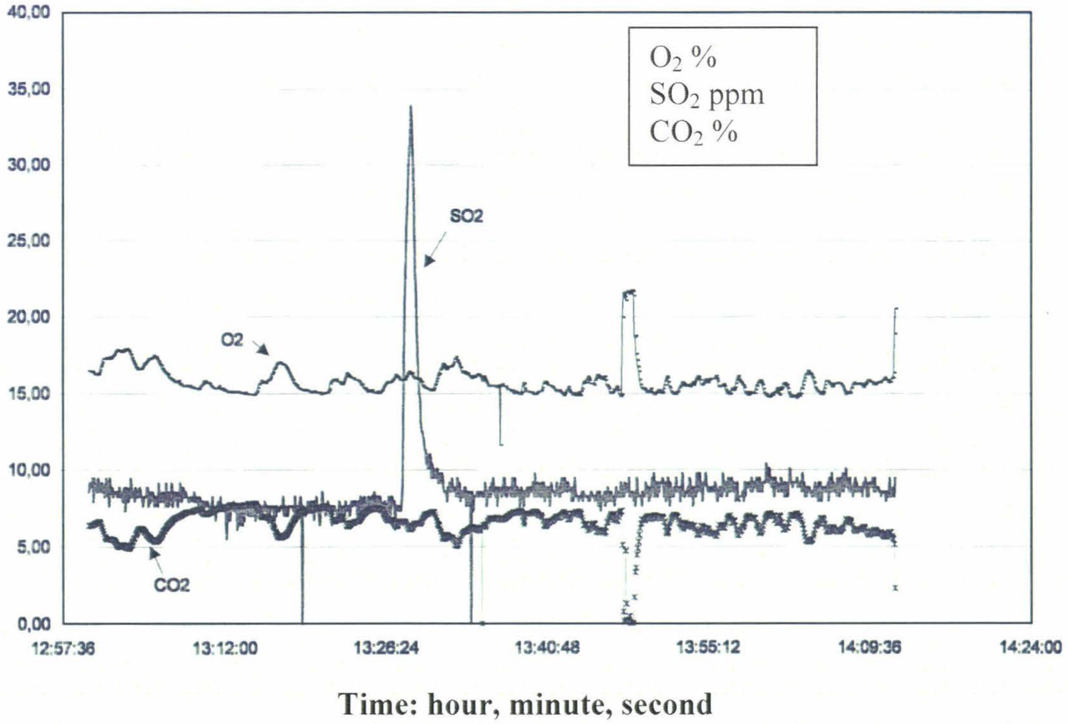

**Figure 9d**. Gas analysis at gas spot S3 coal waste heap n°76, Avion.

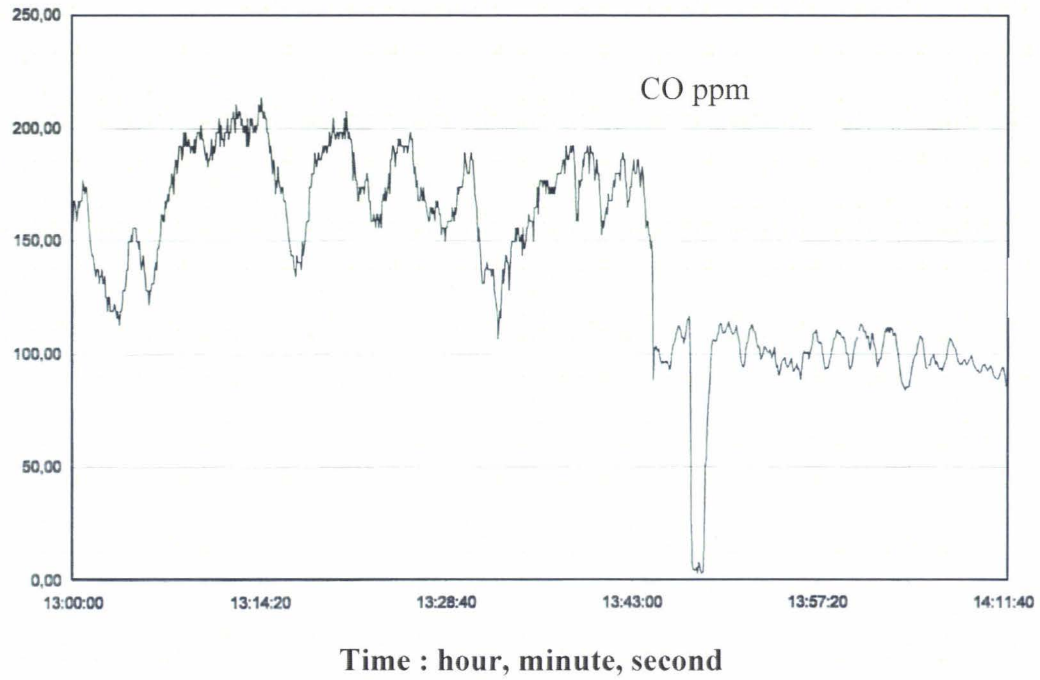

**Figure 9e**. Gas analysis at gas spot S3 coal waste heap n°76, Avion.

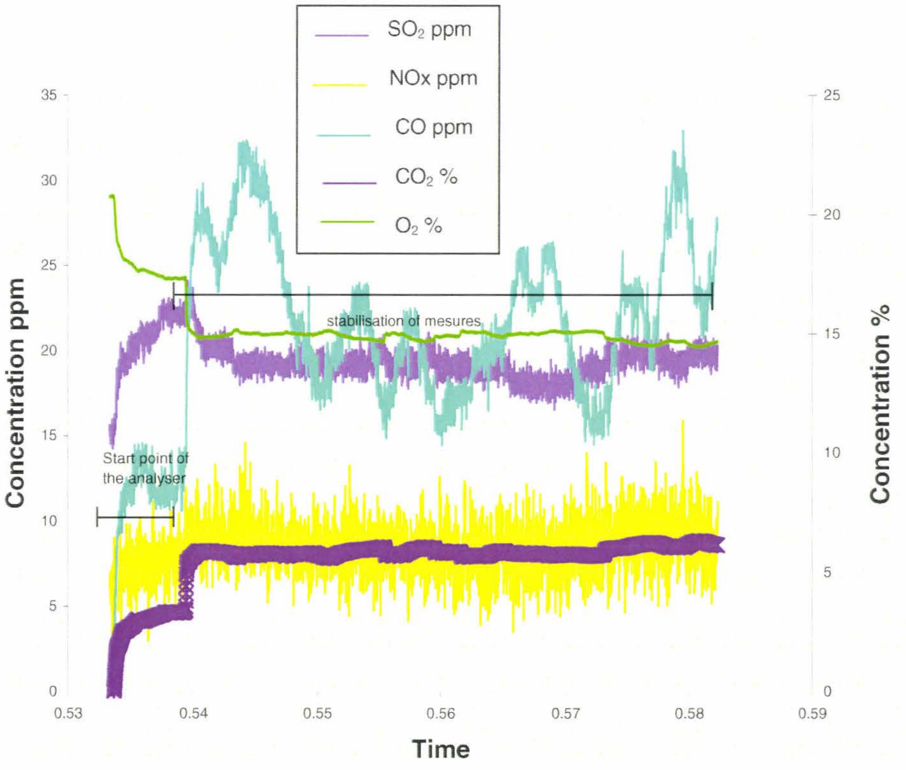

**Figure 9f**. Gas analysis at gas spot S4 coal waste heap n°76, Avion.

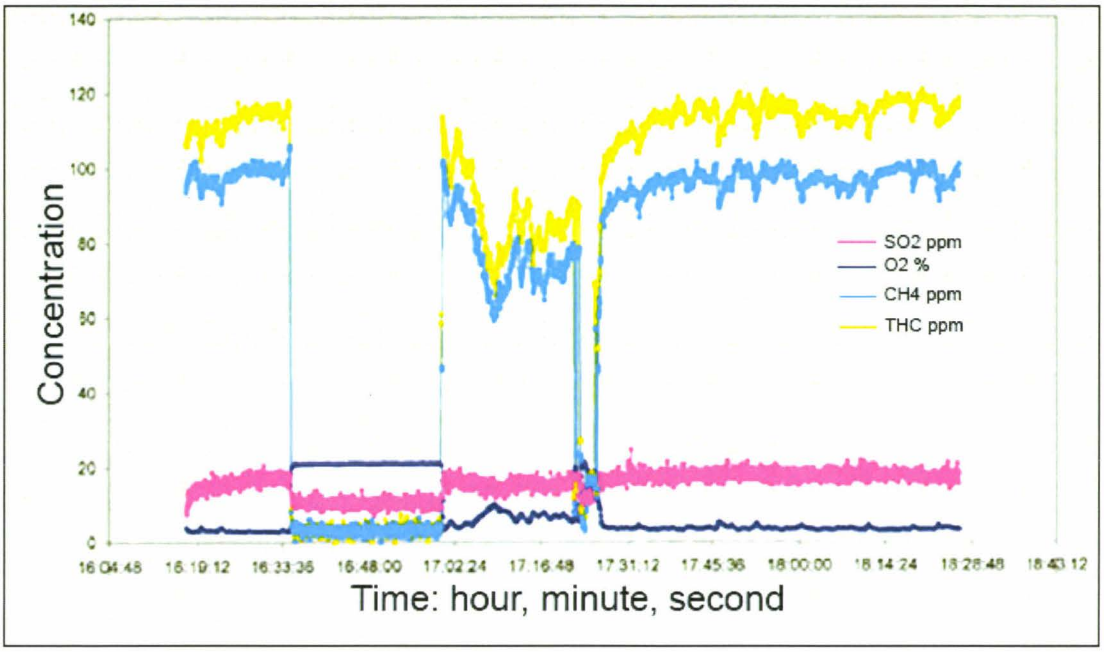

**Figure 10a**. Gas analyses at gas spot E1 coal waste heap n°83, Fouquières les-Lens.

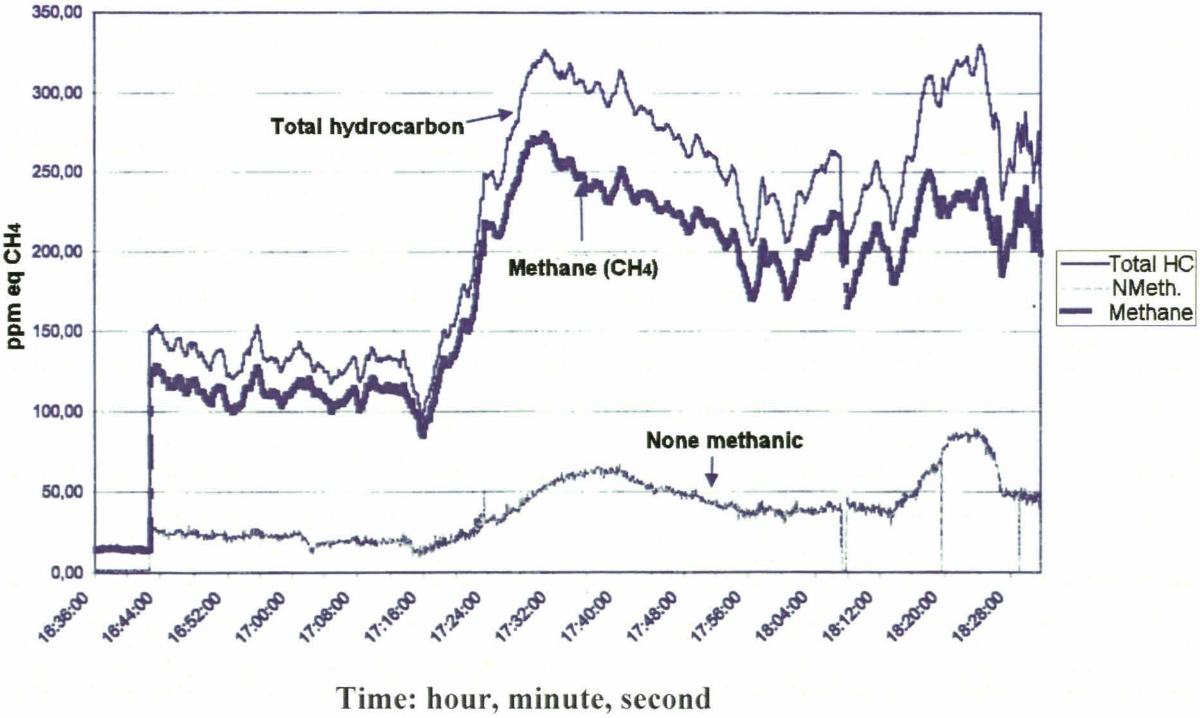

**Figure 10b**. Gas analyses at gas spot E1*** coal waste heap n°83, Fouquières les-Lens.

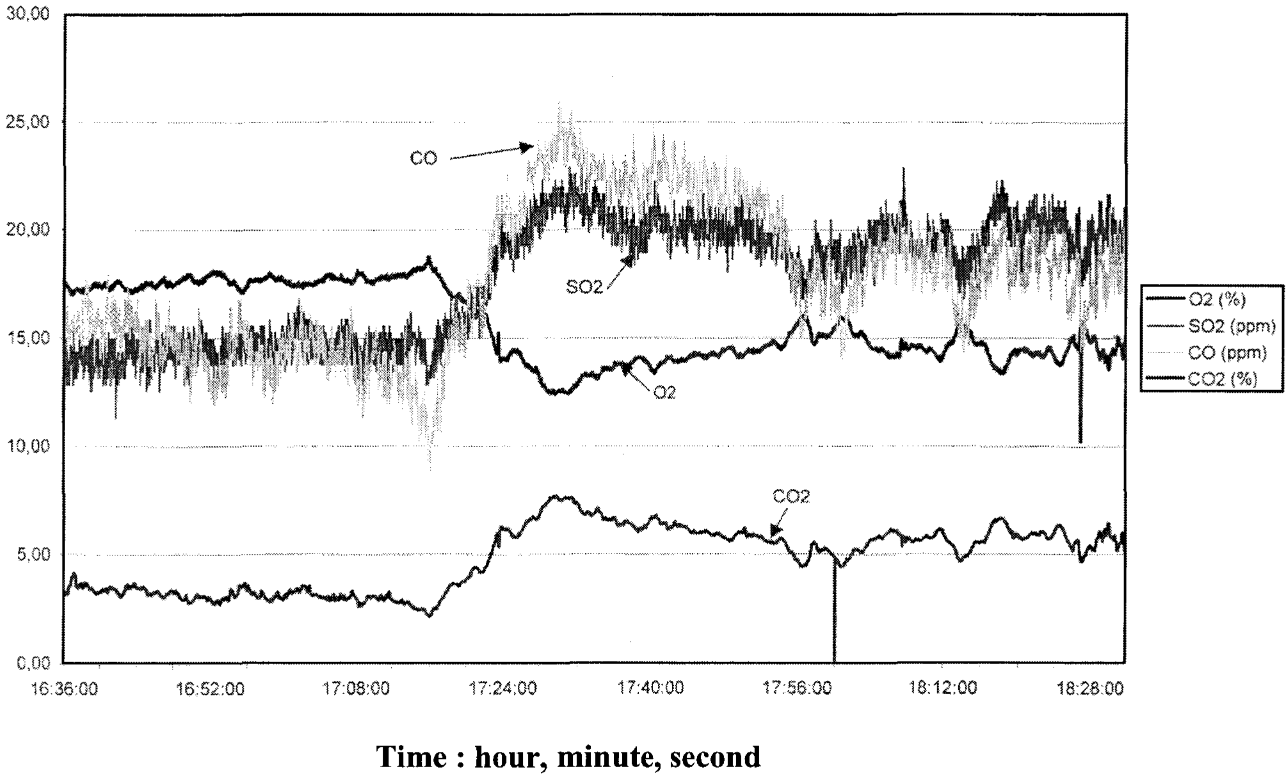

**Figure 10c**. Gas analyses at gas spot E1$^{***}$ coal waste heap n°83, Fouquières les-Lens.

As shown in Table 2 the highest concentration of CO to which man may be exposed day after day without adverse effect is 50 ppm (TLV). Above this level, if breathed, symptoms such as headache, fatigue and dizziness appear in healthy individuals (Grossman et al., 1994). Moreover, higher concentrations of this gas could contribute to combustion hazards (Pennsylvania Department of environment Protection, 2001a).

### ***5.2. Carbon dioxide ($CO_2$) and methane ($CH_4$)***

Carbon dioxide is also produced due to exothermic interaction of coal with oxygen as described above. The liberation of $CO_2$ comes from the decomposition of the carboxyl. The carbonyl groups are supposed to be generated via dehydroxylation process (Walker, 1999). The complete oxidation of carbon to carbon dioxide is an exothermic reaction (1). This reaction leads to heat generation and in normal circumstances, this heat will be lost to the atmosphere (as pollutant), and in such condition the ignition temperature for coal lies between 420°C and 480°C. These temperature ranges of coal oxidation are in agreement with our laboratory testing on coal oxidation samples. However, it should be noted that in adiabatic conditions, where all of the heat released from $CO_2$ is retained rather than being emitted, the minimum temperature at which coal can ignite falls dramatically to between 35°C and 140°C depending on the coal being considered (Sujanti, 1999).

$$C + O_2 \rightarrow CO_2\uparrow + 394\ \mathrm{kJ\ mol^{-1}} \qquad (1)$$

Carbon dioxide and methane are greenhouse gases (GHGs). The global $CO_2$ emission is expected to increase to 29.575 and 36.102 million tones in 2010 and 2020 respectively. Geo-natural hazards such as spontaneous combustion of coal beds and or coal waste heaps around the world discharge not only a large amount of toxic gases, e.g. CO, but also climate active greenhouse gases like $CO_2$ and $CH_4$ which contribute to the heating of the atmosphere and air pollution. $CO_2$ is a product of the organic carbon in coal. Unfortunately, it cannot be eliminated from the combustion, but it can be significantly reduced (International Energy Agency (IEA) in World Energy Outlook, 2000).

In deed, the results of gas measurements from both coal waste show that $CO_2$ is produced in high quantity and is being the most predominant among the emitted gas. $CO_2$ concentrations as high as 70,000 ppmv (7%) were detected during gas measurements from both study sites therefore, much higher than TLV 5,000 ppmv (0.5%) (Table 1 and Figs. 9d, 9f and 10c). Apart from having negative environmental impacts, higher $CO_2$ concentrations if breathed may have negative health impacts to people living in vicinity of burning coal waste heaps. Inhalation of carbon dioxide stimulates respiration and this in turn increases inhalation of both oxygen and possible toxic gases and vapours produced by the combustion. Stimulation is pronounced at 5% (50,000 ppm) concentration, and 30-minute exposure produces signs of intoxication; above 70,000 ppm unconsciousness results in a few minutes (Documentation of the Threshold Limit Values, 1971). Onargan et al. (2003) indicated that exposures to concentrations of $CO_2$ at 3-9% for 5-60 minute might cause serious health problems. Moreover, the combustion is incomplete at study coal waste heaps this produces a portion of $CH_4$ and thus causing a substantially higher emission of $CO_2$ equivalent. According to Havenga (1993), $CO_2$ concentration in burning heaps may increase to approximately 20%.

Methane ($CH_4$) is the principal hydrocarbon gas emitted at varied concentrations at the study sites. Our experimental oxidation tests revealed that this gas is not emitted from carbonaceous shales but rather from the coal samples and at temperatures $\geq$ 120°C. Therefore, all the emitted $CH_4$ in the in-situ gas measurements and analyses result from coal combustion. The concentration of $CH_4$, at the moment, is outside the explosion limits ($\leq 260$ ppmv) and it is controlled by $O_2$ content and gas temperature (Table 1). It should be pointed out that at the coal waste heap N° 83 there was a gas explosion 10 years ago (oral confirmation) and an explosion may develop around gas vents in the presence of a sufficient concentration of $O_2$ and $CH_4$ and other factors (e.g. human activities). $CH_4$ is the most combustible gas associated with the coal waste heaps n°76 and n°83. The explosion of $CH_4$ is possible when this gas is present in the atmosphere at a concentration of 5-15% (Yaclin and Gurgen, 1995; Pennsylvania Department of Environmental Protection 2001a). This concentration is called Lower Explosion Limit (LEL), and it can be affected by the presence of $O_2$ and the ambient temperature (Onargana et al., 2003). The latter authors underlined that an explosion due to the presence of $CH_4$ may take place at 5.5% at 100°C, 5% at 175°C, 4.5% at 250°C and 3% at 600°C. Whereas, if the $CH_4$ concentration is less than 5% there will be burning gas but no explosion below 100°C (US EPA, 1993). And if the $CH_4$ concentration is >14% and the $O_2$ deficiency <12% explosion is not possible due to the high specific heat of methane ($C_p$ =2.254kJ / Kg) (Solid Waste Landfill Guidance, 1999).

Since the international meeting on greenhouse gas emission held in Kyoto 1997, there has been increased attention given to quantify greenhouse gas emissions from a variety of sources. Included among these have been the emissions associated with coal mining. Moreover, scientists note that if coal-producing countries could tackle the infernos, it might be a cost-effective way to meet their targets under the Kyoto protocol, drawn up to cut the emission of greenhouse gases. Methane gas (mine methane gas) is of greater concern as a greenhouse gas since its global warming potential is some 21 times greater than that of $CO_2$ (Carras et al., 1999; Yoshimura, 1999). It should be stressed that burning methane reduces the carbon dioxide equivalent by a factor of six (Hookham, 2004).

**Table 2:** Effect of noxious gases (Sumi and Tsuchiya, 1971; Anonymous, 1973).

| | **Concentration by Volume in Air** | | |
|---|---|---|---|
| **Gas** | **%** | **ppm** | **Effect** |
| **$NO_2$** | 0.005 | 5 | **Threshold Limit Value***. |
| | 0.062 | 62 | Least amount causing immediate irritation to the throat. |
| | 0.077 | 775 | Rapidly fatal for short exposure. |
| **CO** | 05 | 50 | **Threshold Limit Value**. |
| | 0.02 | 200 | Headache after about 7 hours if resting or after 2 hours if working. |
| | 0.04 | 400 | Headache and discomfort with possibility of collapse, after 2 hours at rest or 45 minutes exertion. |
| | 0.12 | 1200 | Palpitation after 30 minutes at rest or 10 minutes exertion. |
| | 0.20 | 2000 | Unconsciousness after 30 minutes at rest or 10 minutes exertion. |
| **$CO_2$** | 0.5 | 5000 | **Threshold Limit Value**. Lung ventilation slightly increased. |
| | 5.0 | | Breathing is laboured. |
| | 9.0 | | Depression of breathing commences. |
| **$SO_2$** | 0.0001/ 0.0005 | 1- 5 | Can be detected by taste at the lower level and by smell at the upper level. |
| | 0.0005 | 5 | **Threshold Limit Value**. Onset of irritation to the nose and throat. |
| | 0.002 | 20 | Irritation to the eyes. |
| | 0.04 | 400 | Immediately dangerous to life. |

* The Threshold Limit Value is the value below which it is believed nearly all workers may be repeatedly exposed day after day without adverse effect.

Notes: (1) Some gases have a synergic effect, that is, they augment the effect of others and cause a lowering of the concentration at which the symptoms shown in the above table occur. Further, a gas which is not itself toxic may increase the toxicity of one of the toxic gases, for example, by increasing the rate of respiration; strenuous work will have a similar effect.

(2) Of the gases listed, carbon monoxide is the only one likely to prove a danger to life, as it is the commonest and the others become intolerably unpleasant at concentrations far below the danger level.

### *5.3. Sulphur dioxide ($SO_2$)*

Sulphur dioxide is a colourless, water soluble toxic gas. It can be detected by taste at concentrations of 0.35-1.05 ppm and it has an immediate pungent irritating odour at a concentration of 3.5 ppm (Rabinovitch et al., 1989).

X-ray diffraction patterns; petrography, energy dispersive spectrometry (EDS); and scanning electron microscope (SEM) observations of images revealed the presence of pyrite ($FeS_2$) in carbonaceous shale samples. This mineral is also found in coal. Our experimental oxidation tests results revealed the emission of $SO_2$ from the coal as well as from the carbonaceous samples. This clearly indicates the low-temperature oxidation of pyrite reactions 2 and 3. The reactions are exothermic and are catalysed by the presence of thiobacillus ferrooxidans (Harries and Ritchie, 1981; Bannerjee, 1985; Speight, 1994). Further, emission of $SO_2$ gas (4) produces larger quantity of heat as well as pollutant gases (Chunli, 1997):

$$2FeS_2 + 7O_2 + 16H_2O \rightarrow 2H_2SO_4 + 2FeSO_4.7H_2O + 1324\ kJ\ mol^{-1} \quad (2)$$

or

$$2FeS_2 + 7O_2 + 2H_2O \rightarrow 2H_2SO_4 + 2FeSO_4 + 260\ kJ\ mol^{-1} \quad (3)$$

$$4FeS_2 + 11O_2 \rightarrow 2Fe_2O_3 + SO_2 \uparrow + 3412\ kJ\ mol^{-1} \quad (4)$$

During in-situ gas measurements depending on the location of measurement, varying concentrations were obtained for $SO_2$, being in order of detection limit (<5 ppmv) to 19.8 at coal waste heap n°76, and 15-25 ppmv at coal waste heap n°83 (Table 1 and Figs. 9 and 10). In deed, the concentration of $SO_2$ from the gas spot S1 at the former site was detected very low and secondary soluble sulphate minerals were observed forming on the rock debris at this location (Masalehdani et al. 2004). This may be due to the emission of vapour which yields the oxidation of this gas (Table 1 and Fig. 6a). In other words, part of $SO_2$ might have been dissolved in water vapour to produce acid aqueous solution (e.g. $H_2SO_4$). Further reaction of acid-rich solution with clay minerals of the rock debris resulted the formation of secondary sulphate bearing minerals (Masalehdani et al., 2005).

According to Rabinovitch et al., (1989) at ambient temperature sulphur dioxide can react with oxygen to form sulphur trioxide (5), which then reacts with water (on moist surfaces) to produce sulphuric acid (6).

$$SO_2\,(g) + 1/2\ O_2\,(g) \leftrightarrow SO_3\,(g) \tag{5}$$

$$SO_3\,(g) + H_2O(g) \leftrightarrow H_2SO^-_4\,(g) \tag{6}$$

Low concentration of $SO_2$ at gas spot S1 may also be related to the inhibition of $NO_X$ in the gas emission which significantly reduced the $SO_2$ content at this location.

However, as described above sulphur dioxide is a toxic gas and the exposure to concentration of 15-25 ppmv $SO_2$ has negative effects on human health (Table2). This may cause distress to person with respiratory ailments (Bell, 1996) and such concentrations may create sulphuric acid when comes in contact with mucous membranes and respiratory tract, causing pulmonary oedema (Documentation of the Threshold Limit Values, 1971).

In addition, sulphur dioxide is an atmospheric pollutant, which has a profound impact on environment being the major cause of acid rains. When deposited, $SO_2$ can contribute to acidification of soils and surface waters (de Kluizenaar et al., 2001). Consequently, recent increases in global sulphur emissions are also linked to the coal seam fires around the world for example from China (Lefohn et al., 1999). Emission of uncontrolled $SO_2$ from burning coal waste heaps may also contribute to global increase of $SO_x$ in the atmosphere.

### *5.4. Nitrogen oxides ($NO_x$)*

The emission of $NO_X$ (or fuel-$NO_X$) at the coal waste heaps originates from nitrogen in coal (coal-N), and this depends on the course of coal pyrolysis. The coal-N exists in the forms of pyridinic-, pyrrolic- and quaternary-N and it is released only during coal pyrolysis (Kelemen, et al., 1994). Xu and Kumagai (2002) showed that during hydropyrolysis of coal the dominant nitrogen gaseous species is ammonia ($NH_3$) which evolves from slow heating pyrolysis, together with a little amount of HCN (released from decomposition of N-containing rings in coal tar). Further, most HCN is concerted to $NH_3$ through secondary reactions. The cited authors indicated that the nitrogen evolution during pyrolysis depends on coal type and the nitrogen content in coal. Bassilakis et al.(1993) suggested three possible pathways for NH3 formation observed in the TG experiments:

$$(C, H, N) \text{ in coal} \rightarrow HCN + NH_3 \tag{7}$$

$$HCN + H \text{ in coal} \rightarrow HCN + NH_3 \tag{8}$$

$$2HCN + H_2 \rightarrow HCN + NH_3 + C \tag{9}$$

Further, Kambara et al. (1993) demonstrated that $NH_3$ comes from the decomposition of quaternary-N, whereas HCN is released from pyridinic- and pyrrolic-N in coal.

The results of in-situ gas measurements and analyses revealed the presence of nitrogen oxides ($NO_X$) in the emitted gas which occur in the forms of nitrogen dioxide ($NO_2$) and nitric oxide (NO). Whereas studies of some secondary minerals formed around gas vents on rock debris at the surface of the coal waste heap in Avion are $NH_4$-bearing efflorescent salt minerals (salammoniac, mascagnite, lecontite and tschermigite) (Masalehdani, et al., 2004 and 2005). It is believed that interaction of $NH_3$-gas with atmospheric oxygen yields the formation of $NO_X$ gases. Further, solution of the $NH_4$-bearing minerals and interaction of gas with oxygenated atmospheric precipitation results in formation of nitrate ($NO^-_3$) and nitrite ($NO^-_2$) which were found trapped in the condensate waters. The migration of nitrate and nitrite into the subsurface water may cause environmental pollution (Panov et al., 1999).

During gas measurements $NO_x$ emission was obtained in varied concentrations at both coal waste heaps being in order of 7.8 to 26 ppmv (Table 1), therefore above the TLV (5 ppm). Nitrogen dioxide ($NO_2$) is a toxic gas and it is produced from the combustion of cellulose nitrate. Nitric oxide (NO) does not exist in atmospheric air because it is converted into dioxide in the presence of oxygen. These compounds are strong irritants, particularly to mucous membranes and thus when inhaled will damage tissues in the respiratory tract by reacting with moisture to produce nitrous ($HNO_2$) and nitric ($HNO_3$) acids (Sumi and Tsuchiya, 1971).

Further, the nitrogen oxides have been considered worldwide as one of the major causes of acid rain also known as GHGs; needs to be acknowledged both their phytotoxic effect and their role in the ozone formation process in the stratosphere. Some studies indicate that the nitrogen oxides increase the susceptibility for lung bacterial infections. Long period exposures to concentrations of 1ppm cause pulmonary alveoli soaring with symptoms; which are similar to those of pulmonary emphysema. The principal effect of the NO is to be the precursor of the nitrogen peroxide $NO_2$, which is insoluble and penetrates the depths of the respiratory system. The $NO_2$ acts on the pulmonary alveoli, and it can even cause emphysema, it inhabits the pulmonary defences and has a phytotoxic effect (Teixeira and Lora, 2004).

## 6. CONCLUSION

The gaseous products liberated from two free burning coal waste heaps in northern France are, in broad terms, similar to those from large scale coal seam combustion. The main emission is $CO_2$ (7%) with smaller concentrations of $NO_x$ and $SO_2$. In addition the products of incomplete combustion of CO and $CH_4$ are also present. Other hydrocarbons were not detected.

Carbonaceous shales are the main component of coal waste heaps. They contain pyrite and organic carbon which in turn during oxidation followed by spontaneous combustion contribute to $SO_2$ and CO emissions. These rock debris are therefore sources of pollutant gases need to determine their $CO_2$ (heat source) content.

The release of $NH_3$ gas and its interaction with oxygen yields the formation of $NO_x$ (NO and $NO_2$) gases and further precipitation of nitrate ($NO^-_3$) and nitrite ($NO^-_2$). Resulting secondary minerals such as $SO_4$-bearing, $NH_4$-bearing and $NH_4$-$SO_4$-bearing phases should be studied and could be considered as environmental (air, water and soil) pollutants.

Oxygen concentrations were measured in the range between <1% to19%. This is not in agreement with mining law (19.5 % minimum amount of oxygen required by law) (Sumi, and Tsuchiya, 1971). The air on or around some gas spots could be classified as contaminated and/or poisonous. The perimeters of such burning coal waste heaps should be fenced with notice boards. Also, emissions of various gases may pose negative health impacts to the public living in vicinity of burning coal waste heaps, which must be considered as an urgent task.

The total amount of GHGs in the atmosphere accumulates and the average temperature of the whole planet is increasing. Where a coal fire (i.e. coal seam or waste coal heap) has occurred, direct and regular field gas measurements are required to identify the gas composition, quantify the rate of emission gases, especially greenhouse gases; and indicate the extent and location of active burning zones.

Precaution must be taken for those who are employed on the exploitation of burning coal waste heaps to prevent accident, poisoning and to provide suitable working conditions (e.g. gas mask).

Further research work is required to measure the heat flux of $CO_2$ discharges from burning coal waste heap n°83 in Fouquières-les-Lens. Under the Geneva Convention on Long-Range Transboundary Air pollution (LRTAP), the parties of the United Nations Economic Commissions for Europe (UNECE) are required to report emission data annually to the Executive Body (EB) of the CO-operative Programme for monitoring and Evaluation of Long-Range Transmission of Air Pollutants in Europe (EPEP). Concordantly, the authors, through presenting this article, have undertaken the responsibility to report the release of noxious pollutant gases from two burning coal waste heaps in northern France.

## ACKNOWLEDGEMENTS

The authors wish to gratefully acknowledge Mr Yves Paquette of Institut. National de l'Environnement Indusriel et des Risques (INERIS), Saint Etienne for providing the thermography report and photos. Dr Valérie Nollet of Ecole Superior Chimie of the University of Lille is acknowledged for advising on various gas measurement techniques. We would like to thank the laboratory staff of the University of Littoral Côte d'Opale-CCM, Dunkerque Mrs D.Dewaele and Ms. A.Vasseur; and Pascale Ciurlik of Geology Department of the University of Lille who provided assistance during the gas measurements and the preparations of data. Finally the authors extend their thanks to Mr Jean Maurice Planchenault, Charbonnages de France service des sites arrêtés et de l'environnement du Nord-Pas- de- Calais who supplied data of the coal waste heap n°83.

## REFERENCES

Anonymous (1973). Spoil heaps and lagoons. Technical handbook: National Coal Board, London, England, 232 p.

Bannerjee, S.C. (1985). Spontaneous combustion of coal and mine fires, A.A.Balkema, Rotterdam. www.coafire.caf.dlr.de/media/download/studywP2410a6.pdf/

Bassilakis, R., Zhao, Y., Solomon, P.R., and Serio, M.A. (1993). Sulfur and nitrogen evolution in the Argonne coals: experiment and modeling. Energy and Fuels 7, 710.

Bell, F.G. (1996). Dereliction: Colliery spoil heaps and their rehabilitation. Environmental and Engineering Geosciences, Vol. **II**, No.1, Spring, 85-96.

Bell, F.G., Bullock, S.E.T., Hälbich, T.F.J., Lindsay, P. (2001). Environmental impacts associated with an abandoned mine in the Witbank Coalfield, South Africa.International Journal of Coal Geology, Vol. **45**, 195-216.

Carras, J.N. and Young, B.C. (1994). Self-heating of coal and related materials: models, applications and test methods. Prog. Energy Combustion Science, **20**, 1-15.

Carras, J.N., Day, S., Saghafi, A., Williams, D.J. (1999). Spontaneouse combustion in spoil piles from open cut coal mines and the emission of greenhouse gases. In: 2nd International Symposium on the Operationalization of Remote Sensing, ITC, Enschede, 16-20 August, The Netherlands.

Chen, X.D. and Scott, J.B. (1993). Oxidation rates of coal as measured from one-dimensional spontaneous heating. Combustion and flame, **109**, 578-586.

Chunli, L., Shusshen, L., Qingdang, Q., Jingshu, W. and Ziqiang, P. (1997). Management of spontaneous combustion in coal mine waste tips in China. Water, Air and Soil Pollution, **103**, 441-444.

Clarke, M. (2003). The missing link in clean coal technology; the proper use of waste coal as an environmental measure. http://www.metts.com.au/clean-coal html

Cogema (1992). Evaluation du terril 76, rapport par Dupuis, J.C., pour Surchiste, 8p.

Cudmore, J.F.and Sanders, R.H. (1984). Spontaneous combustion of coal, mine fires and Interpretation of analyses of mine gases, a literature review. Australian coal industry research laboratories Ltd. (ACIRL), report n°**10**, ISBN n° 0 86772 049 2,60p.

de Kluizenaar, Y., Aherne, J., Farrell, E.P. ( 2001). Modelling the spatial distribution of $SO_2$ and $NO_x$ emissions in Ireland. Environmental Pollution, Vol.**112**, 171-182.

Documentation of the Threshold Limit Values. American Conference of Governmental Industrial Hygienists. Third Edition, 1971, 286 p.

Flann, R.C., Lukaszewski, G. M. (1971). The prevention and control of burning in waste coal dumps. Proc. Australian Inst. Min. Met. No. **238**, 11-29.

Finkelman, R.B. (2004). Potential health impacts of burning coal beds and waste banks. International Journal of Coal Geology, Vol. **59**, 19-24.

Finkelman R.B., Gross P.M.K. (1999). The type of data needed for assessing the environmental and human health impacts of coal. International Journal of Coal Geology, Vol. **40**, 91-101.

Gangopadhyay P.K., van der Meer F., van Dijk P. (2005). Monitoring coal fires using dynamic remote sensing. In: International conference on coal fire research, Beijing, China, 136-140.

Grossman, S.L., Davidi, S., Cohen, H. (1994). Emission of toxic and hazardous gases from open air coal stockpiles. Fuel Vol.**73**, No. 7, 1184-1188.

Harries, J.R. and Ritchie, A.I.M. (1981). The use of temperature profiles to estimate the pyretic oxidation role in a waste rock dump from an open cut mine. Water, Air and Soil Pollution, **15**, 405-423.

Havenga, W.J. (1993). Rapid gas analyses for the investigation of spontaneous combustion using capillary gas chromatography. Talanta, Vol. **40**, No. 2, 213-219.

Hookham, M. (2004). Novel Power Generation Technology. Queensland Government Mining Journal, Vol.**103**, No. 1217, December, 40-41.

International Energy Agency (IEA) World Energy Outlook (2000), 66p.

Kambara, S., Takarada, T., Yamamoto, Y., Kato, K.(1993). Relation between function forms of coal nitrogen and formation of NO. Energy Fuels, **7**, 1013.

Keating, M. (2001). Cradle to the grave. The environmental impacts from coal. www.catf.us/publications/reports/Cradle to Grave.pdf, viewed 9/12/04.

Kelemen, S.R., Gorbaty, M.L. and Kwiatek, P, J.(1994). Quantification of nitrogen forms in Argonne premium coals. Energy Fuels Vol. **8**, 896-906.

Khan, R.M., Everitt, C.E. and Lui, A.P. (1990). Modelling of oxygen chemisorption on coal char. Combustion and Flame, **80**, 83-93.

Kim, A. (1973). The composition of coalbed gas. U.S. Bureau of Mines report of Investigations, 7762, U.S. Department of the interior, Bureau of Mines and Safety Research Center, Pittsburgh, PA, 9p.

Krishnaswamy, S., Bhaat, S., Gunn, R.D. and Agarwal, P. (1996). Low-temperature oxidation of coal . Part I. A single particle reaction-diffusion model. Fuel, **75**, 333-343.

Lefohn, A.S., Husar, J.D., Hasar , R.B. (1999). Estimating historical anthropogenic global sulfur emission patterns for the period 1850-1990. Atmospheric Environmental, Vol.**33**, 3435-3444.

Masalehdani, M.N.N., Potdevin, J.L., Récourt, P., Fialin, M. (2004). Products of oxidation and combustion within the burning coal waste heaps in the Nord-Pas-de-Calais northern France. In: Joint Earth Sciences Meeting, 20-25 September Coalfield, 2004, Strasbourg, France.

Masalehdani, M.N.N., Potdevin, J.L., Cazier, F. and Courcot D. (2005). Coal waste heap fire: emission of toxic gases and condensation minerals, northern Franc: Measurements and analyses. In: Proceeding conference book, International conference on coal fire research, 101-103.

Mine gases Threshold Limit Values (2006). www.usmra.com/download/minegases.htm

Mondragón, F., Ruíz, W., Santamaría, A. (2002). Effect of early stages of coal oxidation on its reaction with elemental sulphur. Fuel Vol. **81**, 381-388.

Nelson, C.R. (1989). Coal weathering : chemical processes and pathways. In: Chemistry of Coal weathering. ED C.R. Nelson, Elsevier, 1-32.

Nordon, P., Bainbridge, N.W., Szemes, F. and Myers, C.J. (1985). A low temperature reaction calorimeter of the Calvet type for the measurement of the heat of oxidation of coal. Phys. E. Sci. Inst., **18**, 338.

Onargan, T., Kucuk, K., Polat, M. (2003). An Investigation of the presence of methane and other gases at the Uzundere-Izmir solid waste disposal site, Izmir, Turkey. Waste Management **23**, 741-747.

Orica (1999).Chemical fact sheet, sulphur dioxide. ww.pacia.org.au/_upoaditems:docs/3. suphar_dioxide.pdf

Panov, B.S., Dudik, A.M., Shevchenko, O.A., Matlak, E.S. (1999). On pollution of the biosphere in industrial areas: the example of the Donets Coal Basin. International Journal of Coal Geology Vol. **40**, 199-210.

Paqutte, Y. (2001). In: Concession de Courrières, Terrils No. **83**, 100 et 230, Pas-de-Calais, 3p. et annexes.

Paquette Y., Laversanne J. (2004). Présentation du guide du détenteur de terrils et autresdépôts miniers issus de l'activité charbonnière. In : Journées nationales de géotechnique et de géologie de l'ingénieur, géotechnique et aménagement, 235-242.

Pennsylvania Department of Environmental Protection (2001a). Questions and answers on mine rescue and recovery operations following coal mine fires and explosions. Pottsville district mining office, Pottsville, PA. http://www.dep.state.pa.us (August 2001).

Rabinovitch, P, S., Greyson, N.D., Weiser, W., Hoffstein, V. (1989). Clinical and laboratory features of acute sulfur dioxide inhalation poisoning: two-years follow-up (case report). American Review of Respiratory Disease. Vol. **139**, n°.2, 556-558.

Schmidt, L.D. (1945). Chemistry of coal utilisation, 1, chapter 18.

Sondreal, E.A. and Ellman, R.C. (1974). Laboratory determination of factors affecting storage of North Dakota lignite. U.S. Bur. Mines Rep. Invest. **7887**, 83p.

Solid waste landfill guidance (1999). Landfill gas monitoring and mitigation, technical section, division of solid waste management, solid waste management program, Tennessee division of solid waste management, 3 March.

Speight, J.C. (1994). The chemistry and technology of coal, Dekker, New York.

Stracher, G.B., Taylor, T.P., 2004. Coal fires burning out of control around the World: Thermodynamic recipe for environmental catastrophe. International Journal of Coal Geology, Vol. **59**, 7-17.

Sujanti, W.(1999). A laboratory study of spontaneous combustion of: the influence of inorganic matter and reactor size. Fuel, 78, 549-556.

Sumi, K., and Tsuchiya, Y. (1971). Toxic Gases and vapours produced at fires. National Research Council of Canada, division of building research, BRN 76.

Teixeira, F.N., Lora, E.S. (2004). Experimental and analytical evaluation of $NO_x$ emissions in bagasse boilers. Biomass and Bioenergy **26**, 571-577.

US EPA (1993). Solid waste disposal facility criteria: Technical manual (EPA 530-R-93-017). US EPA office of solid waste and emergency response, Washington, DC. (NTIS PB 94-100-450).

Walters, A.D. (1996). Joseph Conard and the spontaneous combustion of coal – Part 1, coal preparation, **17**, issue 3-4, 147-166.

Wang, H., Dlugogorski, B.Z., Kennedy, E.M. (2002). Thermal decomposition of solid oxygenated complexes formed by coal oxidation at low temperatures. Fuel Vol. **81**, 1913-1923.

Xu, W.C., Kumagai, M. (2002). Nitrogen evolution during rapid hydropyrolysis of coal. Fuel, **81**, 2325-23334.

Yalcin, E., Gurgen, S. (1995). Mine ventilation (in Turkish), Dokuz Eylul University Faculty of Engineering. Publication No. **251**, Izmir.

Yoshimura,Y.(1999). Energy policy and support for overseas resource development. In: Coal and safety journal No.**15**, September 1999, 1-4.

# CHAPTER IV
# OCCURRENCES OF SALT MINERALS ON A BURNING COAL WASTE HEAP AVION, FRANCE

# Occurrences of salt minerals on a burning coal waste heap Avion, France

M.Naze-Nancy Masalehdani and others
University of Lille1, Department of Geology, UMR CNRS
8110, Bâtiment SN5, 59655 Villeneuve d'Ascq CEDEX, France

**MN.Masalehdani@ed.univ-lille1.fr**

In this chapter we describe the occurrence and processes of formation of secondary salt minerals formed on a burning coal waste heap n°76, Avion, Pas-de-Calais, northern France. Some of these mineral assemblages are the first to be described for a coal-fire context, and two sulphate phases are possible new minerals. The salt minerals are crystallized around different hot spots (gas vents), at different temperature ranges and they vary in composition. Various analyses were carried out in order to determine constituents of rock debris, secondary minerals, condensate water and drinking water. The aim was to assess possible negative impacts of burning coal heap products on the environment and on human health. Part of the present article was presented during the Joint Earth Sciences Meeting (Strasbourg, 2004), and as oral presentation and article* during the First International Conference on Coal Fire Research (Beijing, 2005). The entire article will be published in the forthcoming journal as well as in the first "Coal Fires Elsevier Atlas**" in near future.

*Accepted for publication in ERSEC Ecological Book Series N°4 by UNESCO.

** Invited author.

# ABSTRACT

Secondary salt efflorescence composed of single minerals or mineral assemblages formed on carbonaceous shale debris around gas vents, associated with a subsurface burning coal waste heap in Avion, Pas-de-Calais, northern France. Much of the minerals were deposited at temperatures of less than 300°C as encrustations on rock debris around fumarole vents. They include various sulphates (thenardite, bloedite, konyaite, glauberite, aphthitalite, langbeinite, arcanite, gypsum, epsomite, hexahydrite, alunogen, kalinite, pickeringite, halotrichite, tschermigite, mascagnite, lecontite, and two possible new minerals), as well as halides (salammmoniac and halite) and native sulphur. Most of the sulphate minerals, and the presence of fluid inclusions in thenardite crystals, are documented for first time from coal-fire gas. The major chemical components making up the fumarole-related deposits are $SO_4$, $NH_4$, $H_2O$, Cl, Mg, K, Na, Al, Ca, Fe, Mn and S. Field observations, in-situ gas analyses, optical microscopic examinations, X-ray diffraction (XRD), scanning electron microscope observations, EDS (energy-dispersive spectrometry), WDS (wavelength-dispersive spectroscopy) and total chemical analyses (ICP-MS) were combined to study the occurrences of the secondary minerals. It appears likely that the mineralization occurred from a complex solution chemistry (acid-rich aqueous solution) and sequence of processes. Minerals begin to crystallize during cooling and dehydrate immediately after deposition. Salammoniac formed by direct gas sublimation. Thenardite, bloedite, aphthitalite, langbeinite, arcanite, glauberite, halite, gypsum, epsomite, pickeringite, halotrichite, alunogen, tschermigite, mascagnite and native sulphur formed from a cooling gas-liquid system (condensation). Konyaite and hexahydrite formed from partial alteration (hydration of bloedite, dehydration of epsomite), at the vent or after sampling. Kalinite can be a dehydration product of K-alum, and lecontite may be an alteration (hydration) product of pre-existing ammonium aphthitalite. Variation in the mineral assemblages between locations at the study site indicate: variations in coal content within the waste; influence of continuous gas-rock interaction on the chemistry of gas escaping to the surface; variations in temperature and cooling rate of the gas; influence of atmospheric conditions (i.e. seasons, meteoric water etc); and variable composition of the aqueous solution. The salt occurrences may represent potential environmental and health hazards. The study of chemical nature and mutual interactions of the phases carrying harmful elements should be investigated.

**Keywords**: burning coal waste, mineral formation, coal-fire gas, sublimation, condensation

## 1. INTRODUCTION

Coal mining produces surficial west deposits that can have a high organic carbon as well as sulphide content and are therefore prone to combustion and a potential source of pollution. Burning coal waste heaps associated with active or non active coal producer countries are reported from Czeck Republic (Rost, 1937 and 1942; Žáček and Ondruš, 1997; Sejkora and Kotrly, 1998); the U.S.A (Finkelman and Mrose, 1977); Canada (Gentzis and Goodarzi, 1989); Germany (Witzke,1990; Thalheim et al. 1991; Gaschnitz et al. 2005); Walse (Nichol and Tovey, 1998); Australia (Carras et al. 1999); Ukraine (Panov et al. 1999); China (Chunliliu, 1997); South Africa (Bell et al. 2001; Pone et al. 2005, Stracher et al. 2005); and France (Masalehdani et al. 2004 and 2005). Very few studies reported the occurrence of secondary minerals forming around vents created by escaping gases from burning coal waste heaps (e.g. Finkelman and Mrose 1977; Žáček and Ondruš 1997; Panov et al. 1999; Masalehdani et al. 2004 and 2005; Pone et al. 2005 ). Research involving the mode of mineralization of efflorescence salts on burning coal waste heaps and the possible chemical reactions that occur during the mineralization of the minerals is almost non-existent with exception of Stracher et al. (2005) who have reported the occurrence of some mineral assemblages and their possible mineralization processes from coal-fire gas (underground coal seam fires, China).

The primary objectives of our study were to investigate the nature and genesis of secondary salt mineral assemblages from a burning coal waste in Avion, northern France, studied by means of X-ray diffraction (XRD), optical microscopy (OM), scanning electron microscopy (SEM), energy-dispersive spectrometry (EDS), wavelength-dispersive spectroscopy (WDS) and total chemical analyses (ICP-MS). In addition, the results of in-situ gas analyses and collected condensate waters are discussed. The identified minerals were deposited on rock debris around gas vents related to subsurface burning of the coal waste heap (Fig. 1). Some of the mineral assemblages are for the first time documented for a coal-fire context (i.e. burning coal waste heaps or coal seam).

One would argue that minerals formed by coal fire gas at the coal waste heaps should not generally be considered as minerals, because the origin of a particular fire is often difficult to determine (i.e. natural processes or human interventions). As discussed below the combustion at the coal waste heap in Avion started spontaneously, therefore human activities were not involved. Spontaneous combustion is a natural process that tigers the coal waste heaps or coal seams (Masalehdani, 1985; Stracher and Taylor, 2004). The fact that natural processes are sometimes defined to include those not occurring by simulation in the laboratory (Klein 2002, p.4), the mineral phases that we identified are considered as minerals.

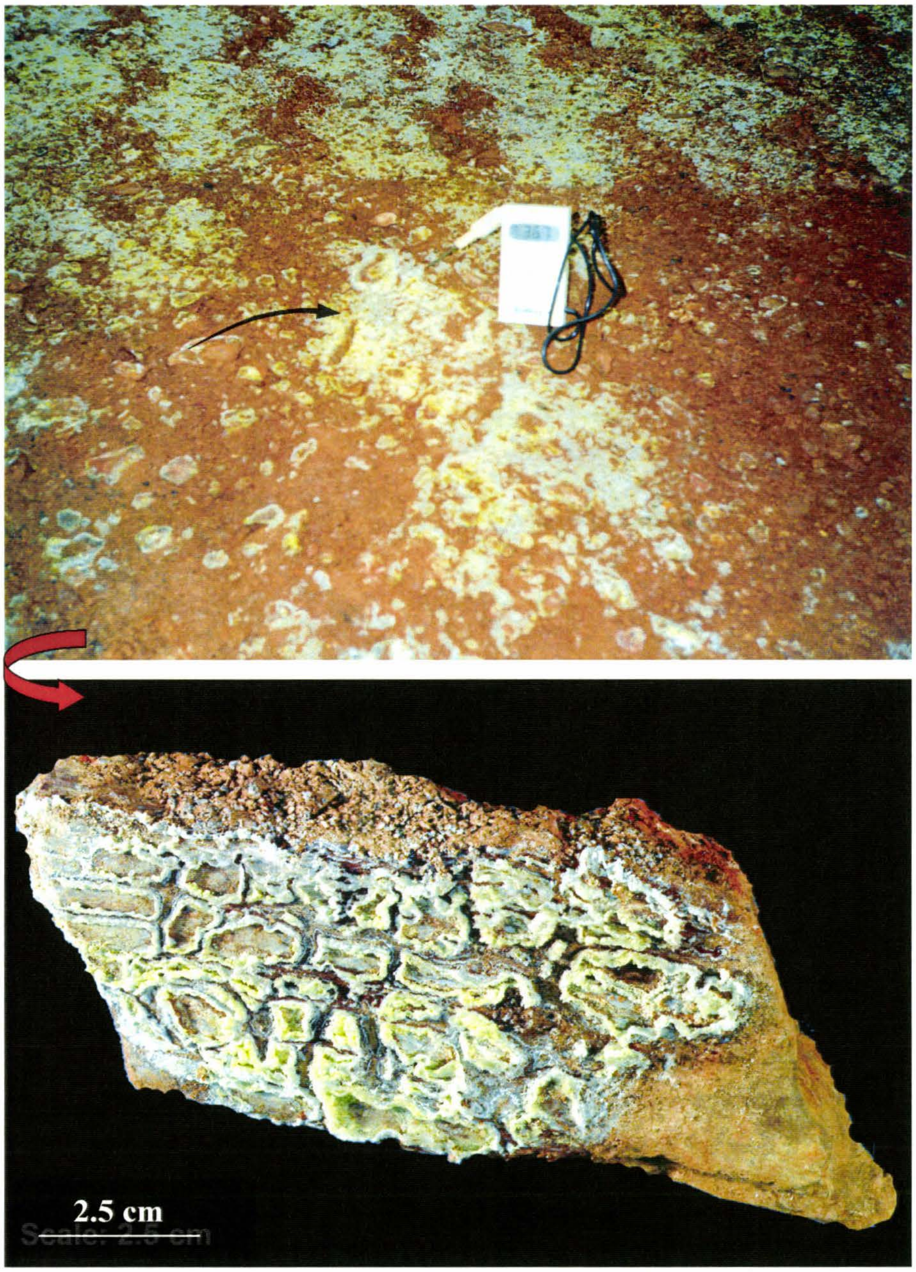

**Figure 1**. Field occurrences of salt minerals (whitish yellow) crystallised on the red porcellanites at the surface of the coal waste heap in Avion. Scale: temperature recorder 15cm.

The mineralization processes associated with coal-fire gas initially involve the exhalation of the gas from vents or fissures (Lapham et al. 1980, Stracher, 1995). The process is rather analogous to the exhalation-condensation of minerals which form in solfataric or other fumarolic environments (Stoiber and Rose, 1974).

## 2. SITE LOCATION AND DESCRIPTION

The coal waste heap n°76 of "Liévin" lies in the Nord-Pas-de-Calais coalfield, 1.3 km south of Avion (Fig. 2a). To the NW at the base of the coal waste, coal is still exploited by in-situ underground gasification. The coal waste is the result of the exploitation of a subsurface coal mine (pits n°7 and 7bis of Liévin). The mine was in operation from 1921 to 1987 and produced low-sulphur (average 0.7 wt %) medium-volatile bituminous coal. Mining was at a depth of 423m. The local bedrock comprises coal measures of Carboniferous age, intercalated with a cyclic repetition of marine black carbonaceous shale and sandstone.

The heap is cone like in shape, standing 85m above natural ground level and covers an area of 96 000 $m^2$ (Fig. 2b). It consists of a chaotic mixture of variably fragmented carbonaceous shale (75-80 wt%), minor sandstone and coal (25-20 wt%) (Cogema, 1992). This assemblage of lithologies reflects the composition of the overlying marine Carboniferous bedrock that was excavated to provide ventilation and access to the mine workings. The coal waste heap is devoid of vegetation.

Subsurface spontaneous combustion at the site started around 1987. The thermal metamorphism associated with the coal waste heap n°76 comprises baked red to pinkish-red rock debris (the porcellanites), surficial fissures, fumarole activity (Masalehdani and Potdevin 2004; Masalehdani et al. 2005) and vent deposition of secondary by-products. White to yellowish-white efflorescent sulphate salts crystallize on the surface of the coal waste heap and they are easy to identify against the dark grey-to red-coloured rocks (Fig. 1)

## 3. METHODS

### *3.1. Sample collections*

A total of 30 effloresce salt samples encrusted or crystallized on rock debris were carefully taken from different active combustion zones (Fronts A and B) around the fumarole discharge

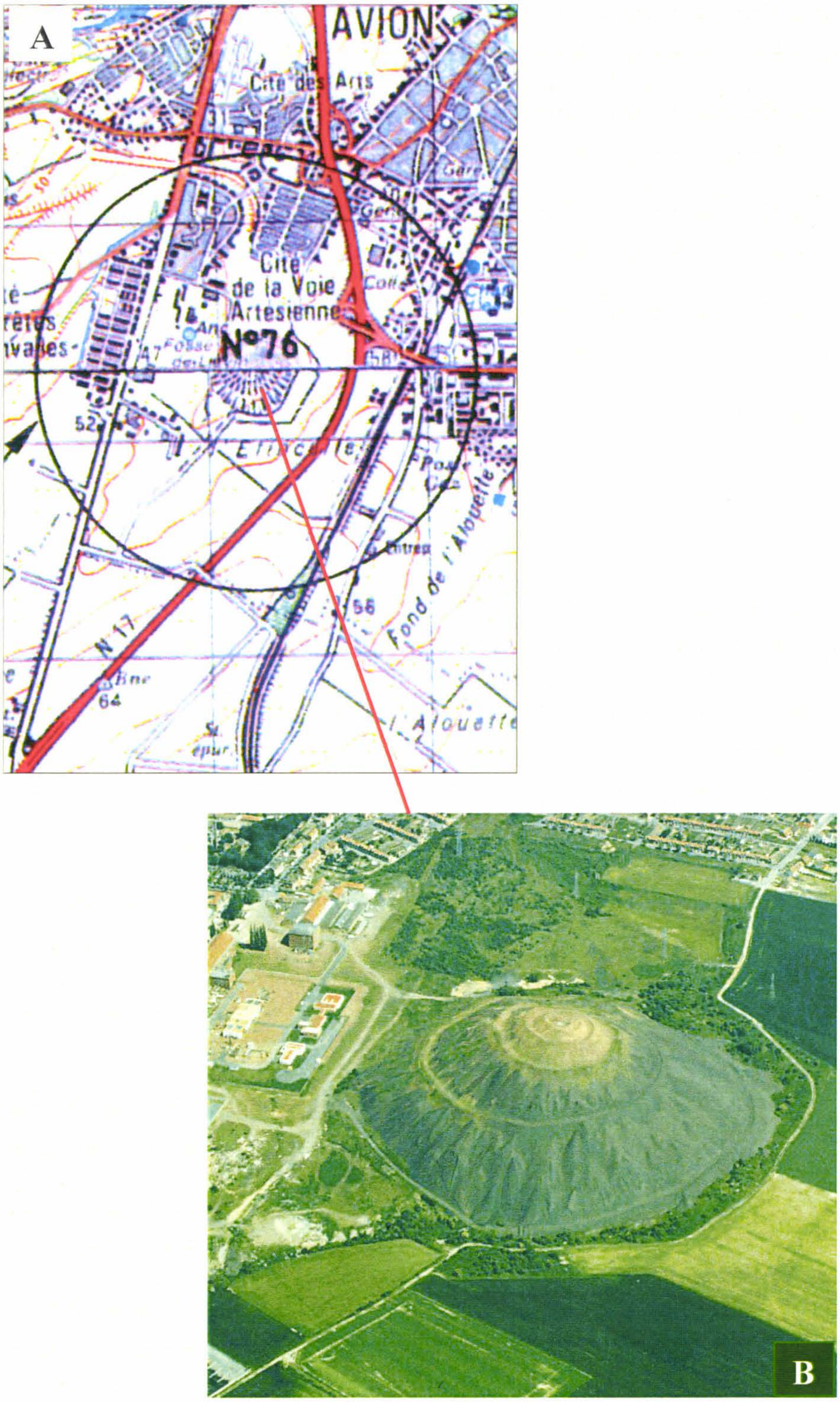

**Figure 2**. Coal waste heap n°76 Avion. **(A)** Location map 1/60000 (S.A.Terrils, 1993). **(B)** Aerial photo of the site during combustion, 1987.

at the top surface of the coal waste heap during field work (Fig. 3), locations are indicated as "gas spot (S)". After cooling in fresh air for about 5 minutes, specimens were placed into containers that were sealed and transported to the laboratory for analyses. The ephemeral nature of these salts and their sensitivity to temporal variations in temperature and humidity rendered the preparation of samples difficult for various studies. Prior to analyses all samples were kept at ambient temperature in a shelter at the laboratory. A first series of analyses for all samples was done within a week of collection. A short morphological description of selected samples is given in Table 1.

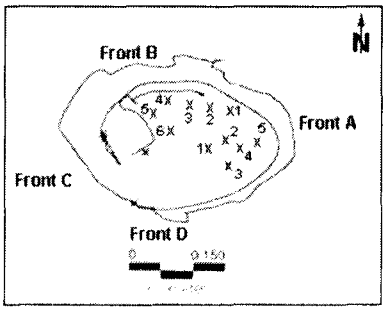

**Figure 3**. Locations of sample collection (gas spots (S)) at the coal waste heap n°76.

**Table 1**. Morphological description of selected salt samples from coal waste heap n°76, Avion

| Sample | Location | T°C* | Description |
|---|---|---|---|
| AV1443 | Gas spot S1 | 90 | Opaque snow white botryodal crust 1cm thick. |
| AV1443b | Gas spot S1 | 90° | Opaque snow white, brownish coating botryodal crust 1cm thick. |
| AV2503 | Gas spot S2 | 62 | Opaque fine-grained granular crust, chalky white in colour. |
| AV1955 | Gas spot S3 | 75 | Very fine, brittle, opaque white crust with yellow coating. |
| AV1443d | Gas spot S4 | 75 | Milky white crystals, contains opaque snow white to pale yellow granules. |
| AV1443e | Gas spot S4 | 78 | Transparent to translucent, vitreous concave crystals about 1cm long, pearly-white in colour, contains snow white fine-grained granules. |
| AV1443f | Gas spot S4 | 79 | Opaque snow white crust with pale yellow fine-grained granules, 1mm thick |
| AV1443g | Gas spot S4 | 80 | Opaque snow white crust, contains pale yellow granules, 4mm thick. |
| AV1443h | Gas sopt S4 | 80 | Transparent to translucent milky white, vitreous concave crystals 1cm long. |
| AV1443i | Hot spot S4 | 90 | Transparent to translucent milky white, vitreous crystals 1cm long. |
| AV8111 | Gas spot S4 | 79 | Pearly-white transparent to translucent, vitreous crystals <1cm long. |
| AV17204 | Gas spot S4 | 89 | Fibrous cotton-like white masses formed on unbaked rock debris. |
| AV2344w | Gas spot S4 | 57 | Vertical coral-like crystal growth <1cm, opaque creamy-white in colour. |
| AV2344a | Gas spot S5 | 169-256 | Brittle brownish-orange or white cubic crystals 2mm in size. |
| AV2504 | Gas spot S6 | 68 | Yellowish microcrystalline botryodal crust. |
| AV2703 | Gas spot S6 | 40 | Whitish microcrystalline botryodal crust |
| AV2502w | Gas spot S6 | 92 | Opaque snow white in colour, botryodal crust 1cm thick. |
| AV5204a | Gas spot S6 | 52 | Very fine, brittle, opaque white crust with yellow coating. |

* Temperature of the escaping gas

### *3.2. Analytical techniques*

All samples examined by different methods were derived from the same specimen. X-ray powder diffraction was used to identify the dominant minerals present. Samples were analyzed using CuKα radiation from a Phillips 1710 diffractometer, the accelerating voltage was 40kV and current was 25 mA. Diffraction patterns were collected over 3-60°2θ using CuKα radiation at 1°2 $\theta \mathrm{min}^{-1}$. The peak search for minerals within each X-ray pattern was performed using MACDIFF version 4.2.2a software.
Polished uncovered thin sections were prepared for selected samples that were amenable to examination of minerals by optical microscope and the scanning electron microscope. Optical observations of minerals were done using an Olympus BX60 transmitted and reflected light with a digital camera.

The scanning electron microscope (SEM) equipped with energy dispersive spectrometry (EDS) was used to determine surface morphology and major element compositions of selected samples. Specimens were solid fragments mounted on thick pyrolytic graphite substrates using conducting carbon paint, and carbon-coated uncovered polished thin sections. They were examined at 15kV using a Quanta 200 and a Jeol-JSM 840A at the Department of Geology, University of Lille and University of Paris VI Jussieu respectively. The aim was to confirm XRD mineral identification as well as identify the minerals that were present in minor concentrations and/or they were cryptocrystallized and could not be detect by XRD or observed under optical microscope.

Quantitative electron microprobe WDS (wavelength-dispersive spectroscopy) determination of the chemical composition of selected specimens was performed using a Cameca SX50 and SX100 at the CAMPARIS, University of Paris VI Jussieu. Because of instability and fragility of minerals, beam power was minimized to 15 kV, intensity was 5-10nA and spot size was 10μm. Specimens for analyses were all carbon coated uncovered polished thin sections.

### *3.3. Analyses*

In-situ gas analyses from selected locations and around sample collections were carried out according to method described in Masalehdani and Potdevin (2004) and Masalehdani et al. (2005). Chemical analyses (ICP-MS) of selected samples were carried out to determine the major and trace elements of the coal, unaltered rock debris (carbonaceous shales and sandstones), and the baked debris, as well as the salt efflorescences. Additional chemical analysis (ICP-MS and ICP-OES) includes that of condensate water collected during the in-situ gas measurements. The aim was to make a comparison and to verify the elements in these materials. We know of no published coal-fire gas studies reporting the analyses of condensate water after gas chromatographic analysis (e.g., Chamberlain and Hall 1973; Kim 1973; Carras et al. 1999, Stracher et al. 2005). Therefore, it is still unclear if the coal gas (water vapour included) can transport cations in the volatile form to the surface upon escaping from the depth.

## 4. RESULTS

### 4.1. *Mineralogy at gas spots*

Table 2 lists all the minerals identified, their locations and methods of identifications in our study from burning coal waste heap at Avion. Figure 4 shows hand specimens of selected samples. Of the 21 minerals found, 18 are sulphates (hydrated and anhydrous), two are halides and one is a native element. A common characteristic of all the samples is their fragile nature which made manipulations extremely difficult. The cryptocrystalline nature of some efflorescences also hindered their study by optical microscopy.

**Table 2**. Analytical methods and identified secondary minerals, coal waste heap n°76, Avion.

| Minerals | Gas spot | XRD* | Microscope | SEM/EDS** | EMP/WDS*** |
|---|---|---|---|---|---|
| Thenardite | S1 & S2 | X | X | X | X |
| Bloedite | S2 & S4 | X | X | X | X |
| Konyaite | S2 | X | X | X | |
| Langbeinite | S4 | X | | X | X |
| Glauberite | S4 | X | X | X | X |
| Aphthitalite | S4 | X | X | X | X |
| Halite | S4 | X | X | X | X |
| Epsomite | S2 & S3 | X | | X | |
| Hexahydrite | S2 & S6 | X | X | X | |
| Arcanite | S4 | X | | X | |
| KNaMg-sulphate | S4 | X | X | X | X |
| MgMnFe-sulphate | S1 | X | | X | X |
| Gypsum | S3 & S6 | X | X | X | X |
| Lecontite | S1 | X | | X | |
| Mascagnite | S1 & S6 | X | X | X | X |
| Salammoniac | S5 | X | | X | |
| Tschermigite | S6 | X | | X | |
| Alunogen | S3 & S6 | X | X | X | X |
| Pickeringite | S3 & S6 | X | X | X | X |
| Kalinite | S3 | X | | X | |
| Sulphur | S6 | X | X | | |

*X-Ray diffraction **Scanning electron microscope and energy dispersive spectrometry
***Electron microprobe and wavelength-dispersive spectroscopy

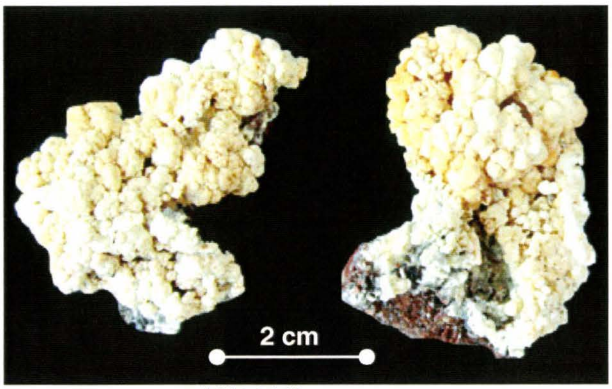

AV1443b

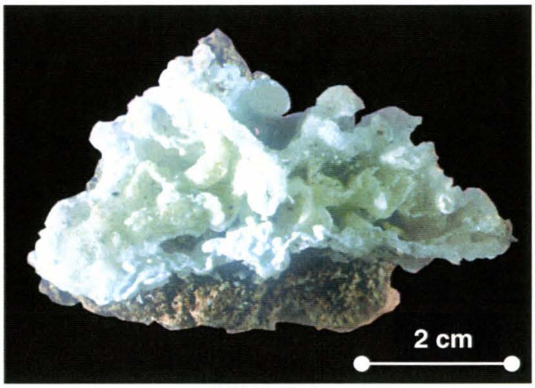

AV1443d

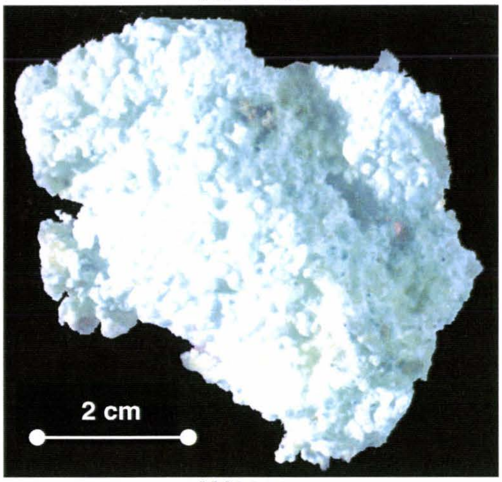

AV1443e

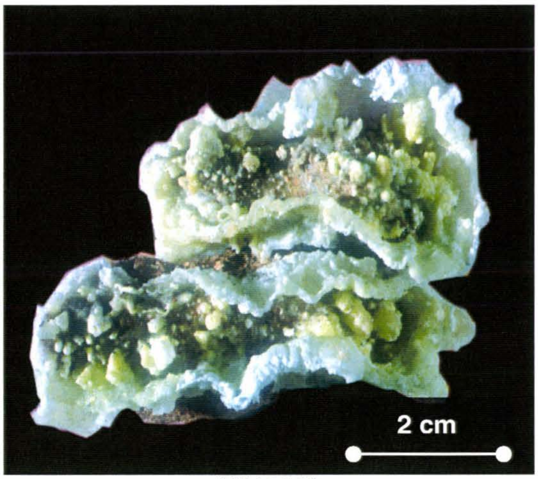

AV1443f

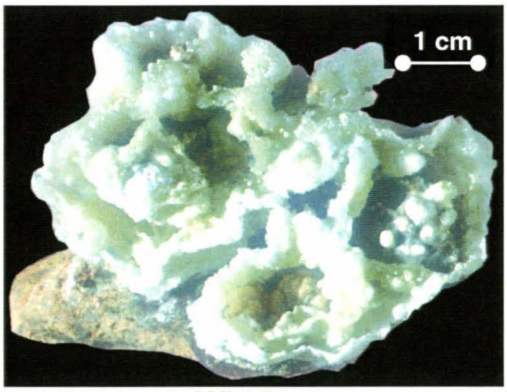

AV1443g

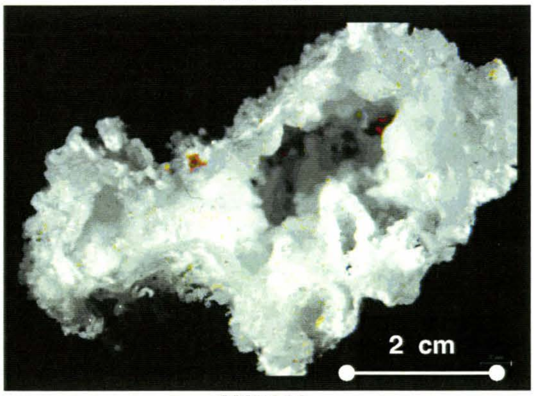

AV8111

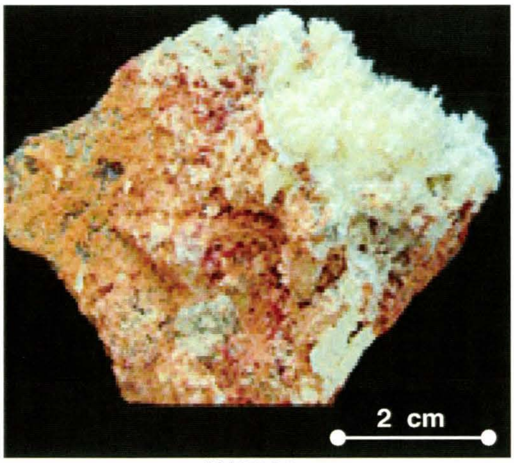

AV2344w

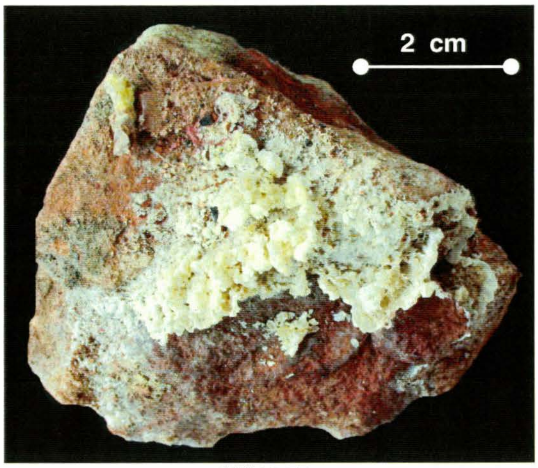

AV1955

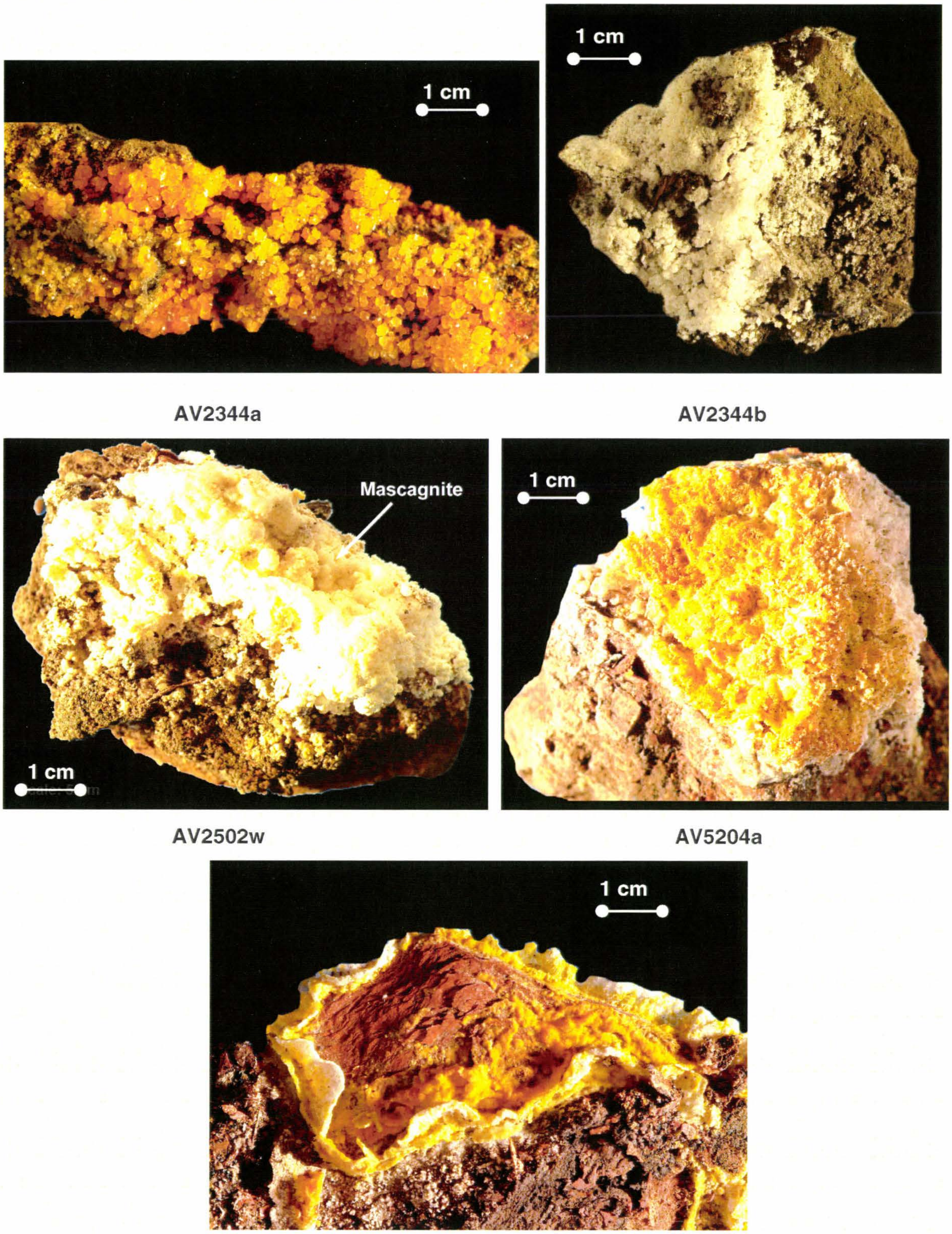

AV2344a

AV2344b

AV2502w

AV5204a

AV5204b

**Figure 4.** Hand specimens of selected salt samples collected from coal waste heap n°76, Avion (see also Table 1).

#### *4.1.1. Gas spot S1*

Mineral assemblages from this location are: (i) mascagnite-thenardite-lecontite (sample AV1443a) and (ii) mascagnite-thenardite-lecontite-glauberite-gypsum-MgMnFe-Sulphate-quartz (Figure 4, sample AV1443b).

Mascagnite in these samples and assemblages is the dominant mineral. In thin sections it shows an acicular or skeletal crystal habit, with a fan-like arrangement of the elongated crystals (Figs. 5a, 5b and 5c). The crystals show prominent cleavage perpendicular to the long axis (Fig. 5d). In cross-polarised light, they have first order grey interference colour. Thenardite in these samples occurs as fine-grained aggregates or as lozenge-shaped crystals occupying the spaces between mascagnite crystals and/or as euhedral lath-shaped crystals with pointed edges (Fig. 5e).

SEM images of solid fragments of samples AV1443a and AV1443b show lath-shaped crystals of mascagnite and fine-grained thenardite that formed between mascagnite crystals. In BSE (back-scattered electron) images, thenardite has lighter colour than mascagnite (Fig. 6a, 6b and 6c). Lecontite was identified in X-ray diffractograms, SEM/EDS images, zone mapping and element analyses of solid fragment of sample AV1443a are shown in Figure 6a. This mineral occurs along the margins of mascagnite and/or thenardite crystals indicating late crystallization in these assemblages. Glauberite and gypsum are the accessory minerals in sample AV1443b. They were identified by XRD and SEM/EDS analysis. SEM images show groups of parallel elongated glauberite crystals filling spaces between mascagnite crystals (Figs. 6b, 6C and 6e). Gypsum appears as rosettes (Fig. 6g, greyish-white in BSE images). White angular small quartz grains occur in this sample as an impurity (Fig. 6h)

In addition to the minerals described above, a previously unreported MgMnFe-sulphate occurs in sample AV1443b. SEM images of this sample observed in BSE mode show whitish grey aggregates (Figs. 6b-6h). EDS element analysis and zone mapping of solid fragment and thin section of sample AV1443b clearly show the occurrences of this new sulphate in the specimen studied (Figs.6e-6h ), but XRD patterns of sample AV1443b (Fig. 4) do not include peaks which can be attributed to this mineral. Results of electron microprobe analyses (WDS: wavelength-dispersive spectroscopy) of this phase are given in Table 3. Because no mineral with the same composition exists, this phase may be a new mineral.

**Table 3.** Electron microprobe (WDS) analyses of MgMnFe-sulphate in sample AV1443b.

| Elements | $Na_2O$ | $K_2O$ | MgO | MnO | FeO* | $Al_2O_3$ | CaO | Cl | $SO_4$ | Total |
|---|---|---|---|---|---|---|---|---|---|---|
| | 0.828 | 0.082 | 11.257 | 1.466 | 2.309 | 0.658 | 0.056 | 0.120 | 72.64 | 89.40 |
| | 0.37 | 0.014 | 6.73 | 3.13 | 3.86 | 0.88 | 0.00 | 0.202 | 74.01 | 89.19 |
| | 0.570 | 0.144 | 7.529 | 1.138 | 1.88 | 0.77 | 0.00 | 0.424 | 60.195 | 72.704 |

*FeO: Refers to total iron

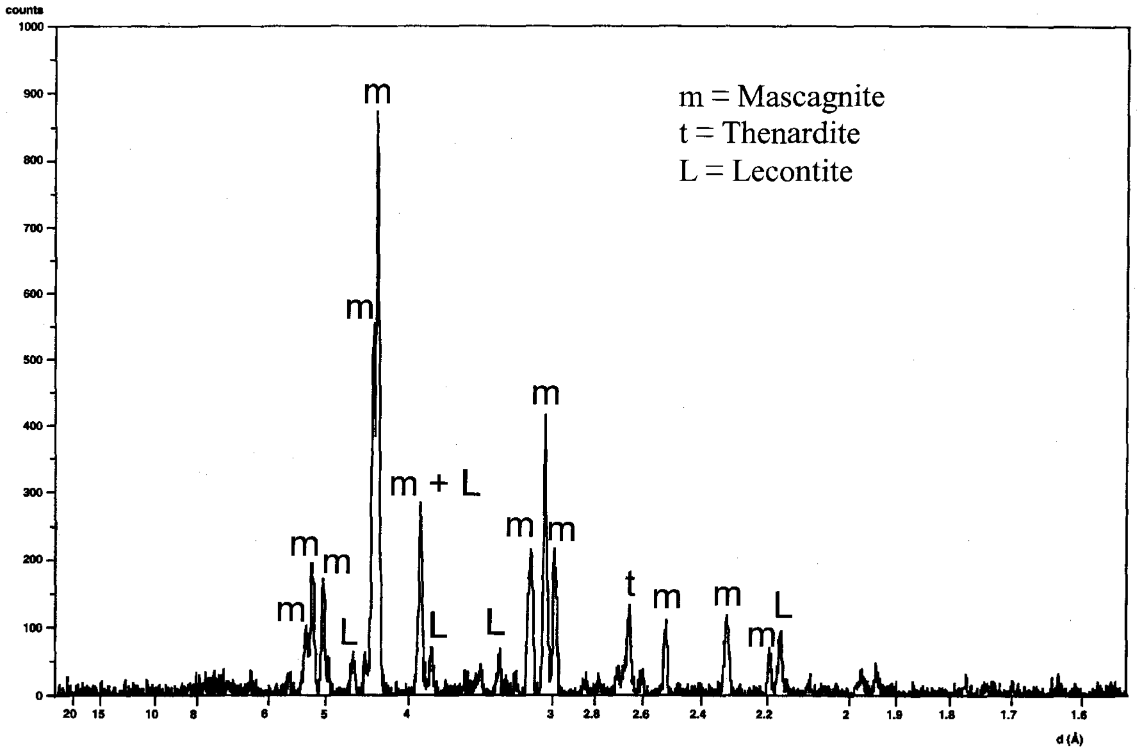

**Figure 4.** X-ray patterns of sample 1443b.

### *4.1.2. Gas spot S2*

The mineral assemblage from this location is bloedite-hexahydrite-konyaite-epsomite thenardite (Table 2, sample AV2503). In this assemblage bloedite occurs as the main phase followed by hexahydrite, konyaite, epsomite and thenardite.

In thin sections, this mineral assemblage shows an acicular habit and cryptocrystalline fabric (Fig. 7). As observed in SEM images, bloedite and konyaite both occur as acicular crystals, which cover hexahydrite crystals (Figs. 7a, 7d). Bloedite is also observed to occur as fan-like intergrowths, containing fine-grained aggregates of hexahydrite. Hexahydrite occurs as aggregates grown on konyaite (Figs. 7a, 7d). Epsomite, which is less abundant appears, as aggregates having smoothly curved outlines and occupies spaces between the bloedite and/or konyaite crystals (Fig. 7c). Minor amounts of fine granular crystals of thenardite occurs concentrated around bloedite and/or konyaite in the matrix (Fig. 7c). Quartz, angular in shape, occurs as an impurity (Fig. 7b).

EDS analysis of mineral phases in sample 2503 show that sulphur, sodium, and magnesium are the most abundant elements.

### *4.1.3. Gas spot S3*

Figure 8 shows the field occurrence of efflorescent minerals at this location. XRD and SEM investigations of minerals in sample AV1955 revealed the assemblage: pickeringite-kalinite-alunogen-epsomite-gypsum (Table 2).

In thin section, the minerals in this sample are fine-grained and they have similar crystal morphologies. Acicular and/or dendritic habits are the most common (Fig. 9).

SEM images of minerals in sample AV1955 (thin sections) are given in Figure 10. Acicular crystals of pickeringite occur in the matrix. Clusters of parallel elongated crystals covering kalinite crystals are also observed (Figs. 10 and 10a). Kalinite occurs as aggregates of acicular crystals (Figs. 10b and 10c). Needle-like crystals of alunogen are observed crystallizing in cavities (Fig. 10e). Gypsum (white) is crystallized around or on the pickeringite-kalinite crystals (Fig. 10b). Minor amounts of epsomite were observed crystallized between pickeringite-kalinite needles.

Pickeringite is the principal mineral in mineral assemblage in sample AV1955, followed by kalinite. Alunogen, epsomite and gypsum are all minor phases. EDS element maps show that sulphur, magnesium, aluminium and potassium are the most aboundant elements, with a lesser amount of iron and manganese (Fig. 10e).

### *4.1.4. Gas spot S4*

Hand specimens of selected samples from this location are shown in Figure 4. The following sulphate minerals and mineral assemblages were found:

- ***Thenardite***

This mineral occurs as the sole component in samples AV8111, AV17204 and AV2344w (Table 2). In transmitted light, thenardite crystals are characteristically elongated lozenge-shaped or hexagonal (<1mm long). Twinned crystals and fan-like aggregates are also observed (Fig. 11a).

- ***Thenardite -Bloedite***

These two minerals are the most abundant phases crystallized at gas spot S4 (Table 2). In thin sections of samples AV1443h and AV1443g, thenardite exhibits similar habits as described earlier. Bloedite characteristically occurs as radial aggregates and/or flattened brownish-grey needles (2-5mm) (sample AV1443g, Figs. 11b and 11c).

- ***Thenardite - Bloedite - Aphthitalite***

This assemblage occurs in samples AV1443d and AV1443f (Table 2). In these samples thenardite and bloedite are the most abundant minerals with a lesser amount of aphthitalite (Fig. 11d). This assemblage is particularly interesting in that the thenardite crystals in sample AV1443d contain fluid inclusions. They are monophase vapour, biphase vapour-liquid (variable ratios) and monophase liquid. Microthermometric analysis of fluid inclusions revealed that trapped inclusions in thenardite crystals are Na-$SO_4$-Cl dominated (see chapter VI). In thin sections of both samples, thenardite and bloedite show similar occurrences as described earlier. Aphthitalite, when observed, appears as tabular dull grey to nearly opaque crystals (Fig. 11e).

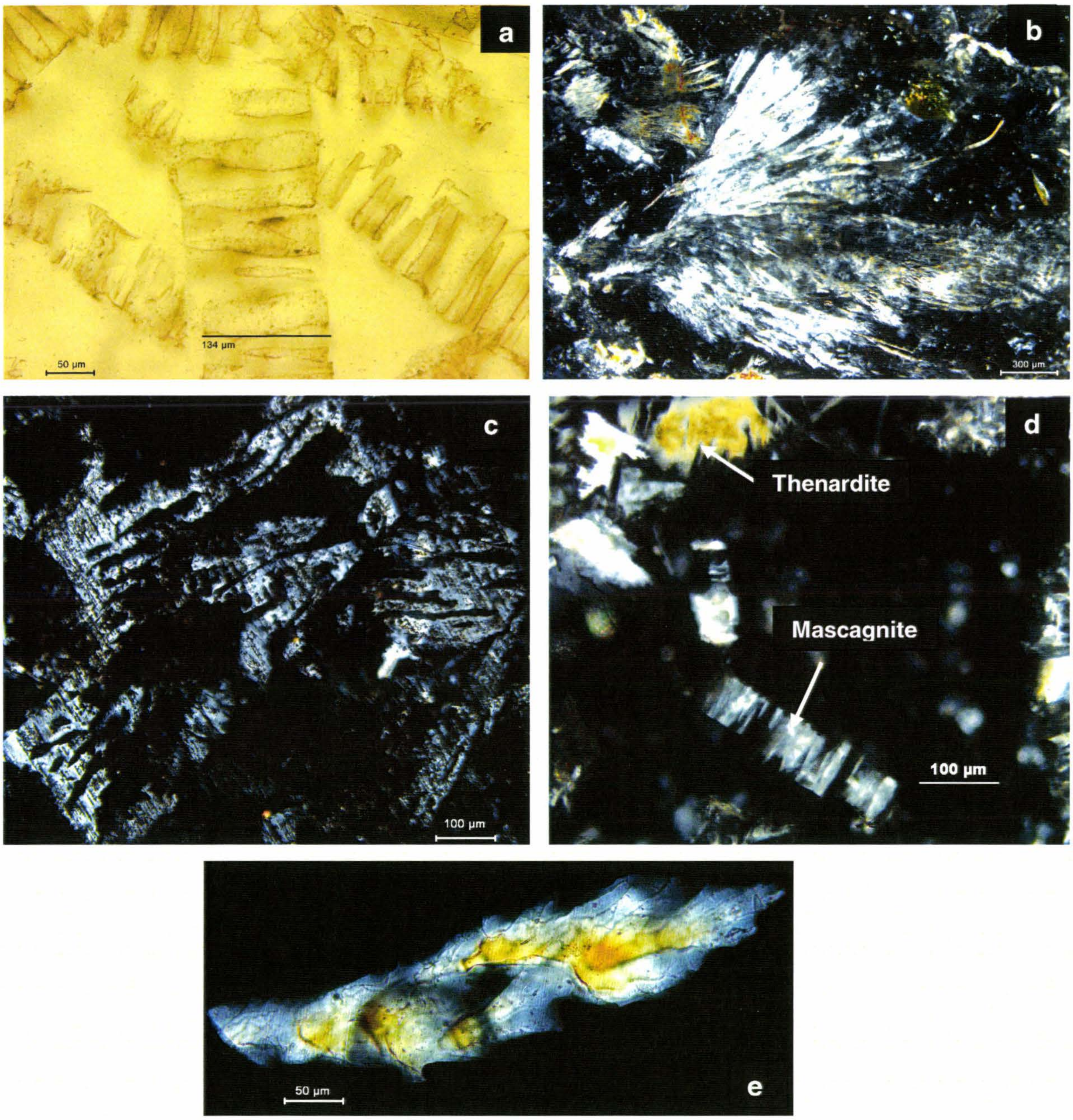

**Figure 5**. Transmitted light micrograph, sample AV1443b. **(a)** Tabular crystals of mascagnite, PPL. **(b)** and **(c)** Mascagnite crystals showing an acicular and skeletal crystal habit, CPL. **(d)** Arrangement of mascagnite crystals showing cleavage perpendicular to the long axis, CPL. **(e)** Euhedral lath-shaped crystal of thenardite, CPL.

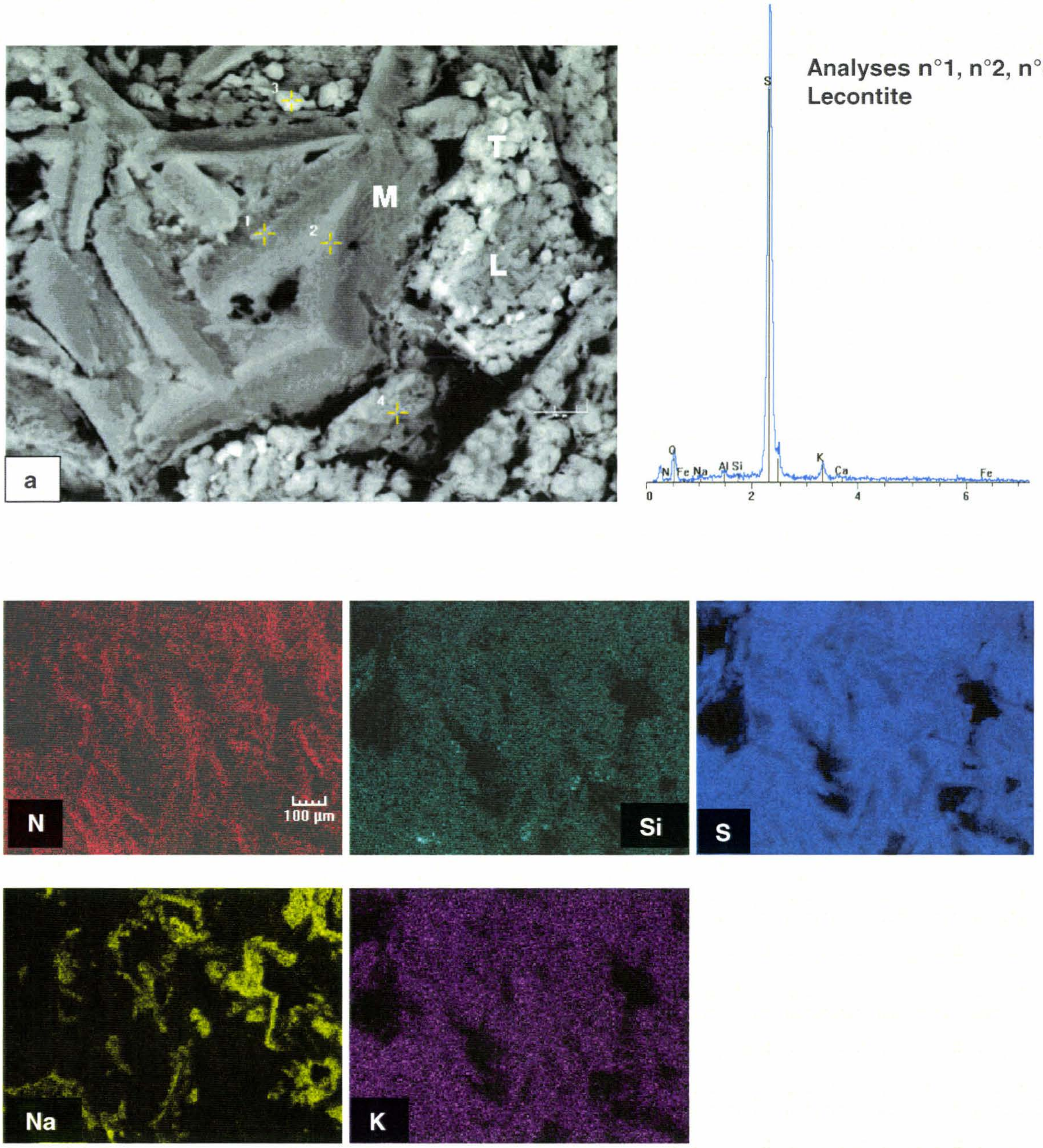

**Figure 6a**. SEM image of mascagnite assemblage, EDS analysis of minerals and zone map of solid fragment in sample AV1443a. Analyses n°1, n°2 and n° 4 are lecontite, crystallized on margins of mascagnite (grey) and thenardite (white). Analysis n°3 is thenardite Scale bar: image 10µm, zone maps 100µm.

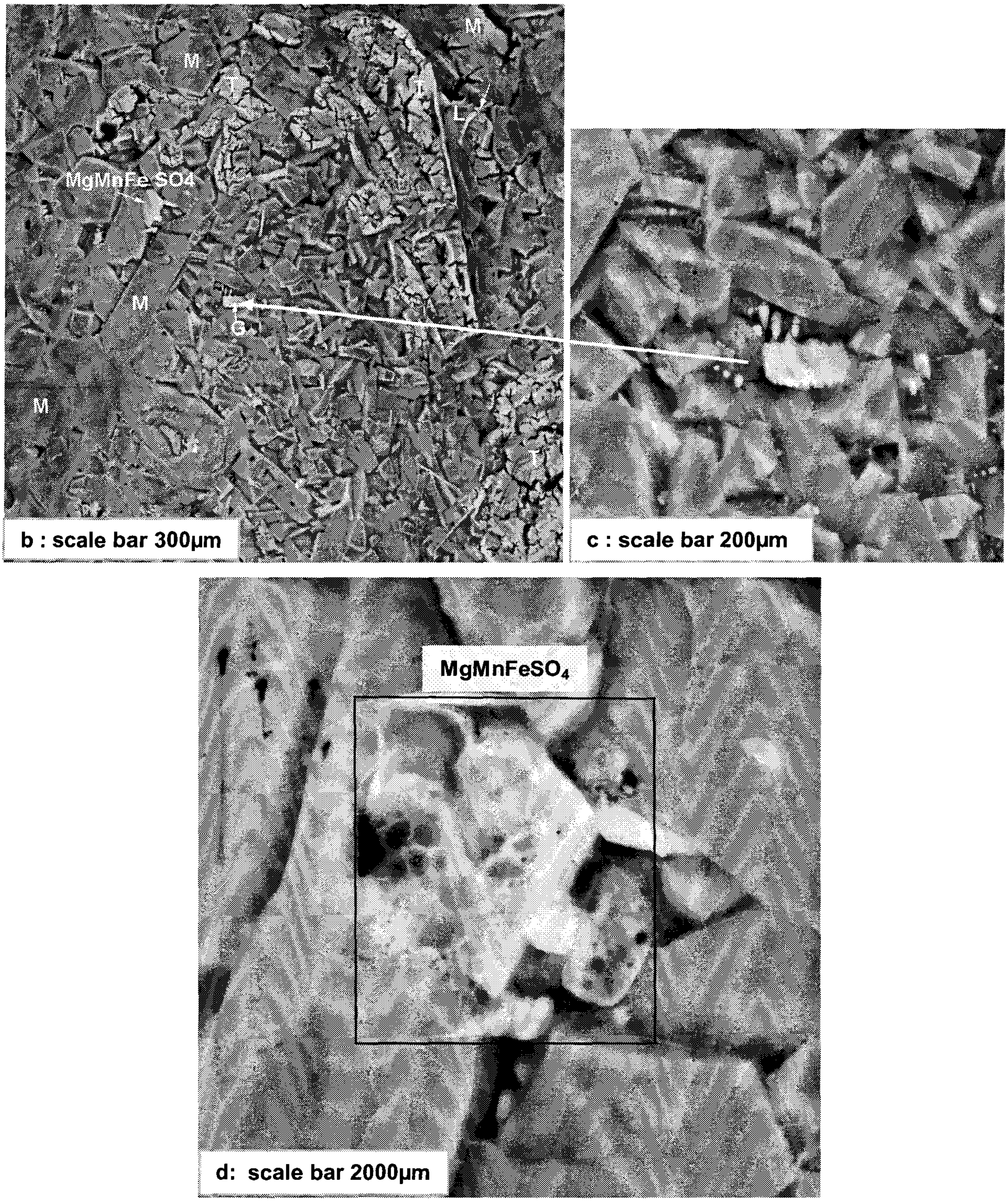

**Figure 6b, c and d**. SEM/BES images of soild fragment of sample AV14433b. Mascagnite (M) dark grey show lath-like crystals. **(b)** Note lecontite (L) occurs on the margins mascagnite. Thenardite (T) whitish- grey appears as fine-grained aggregates. MgMnFeSO$_4$ (new sulphate) is crystallized on or between mascagnite crystals. **(c)** Glauberite (white) filling spaces between crystals of mascagnite. **(d)** MgMnFe-sulphate (whitish- grey) in is crystallized on euhedral mascagnite (grey) laths or it occurrs filling spaces.

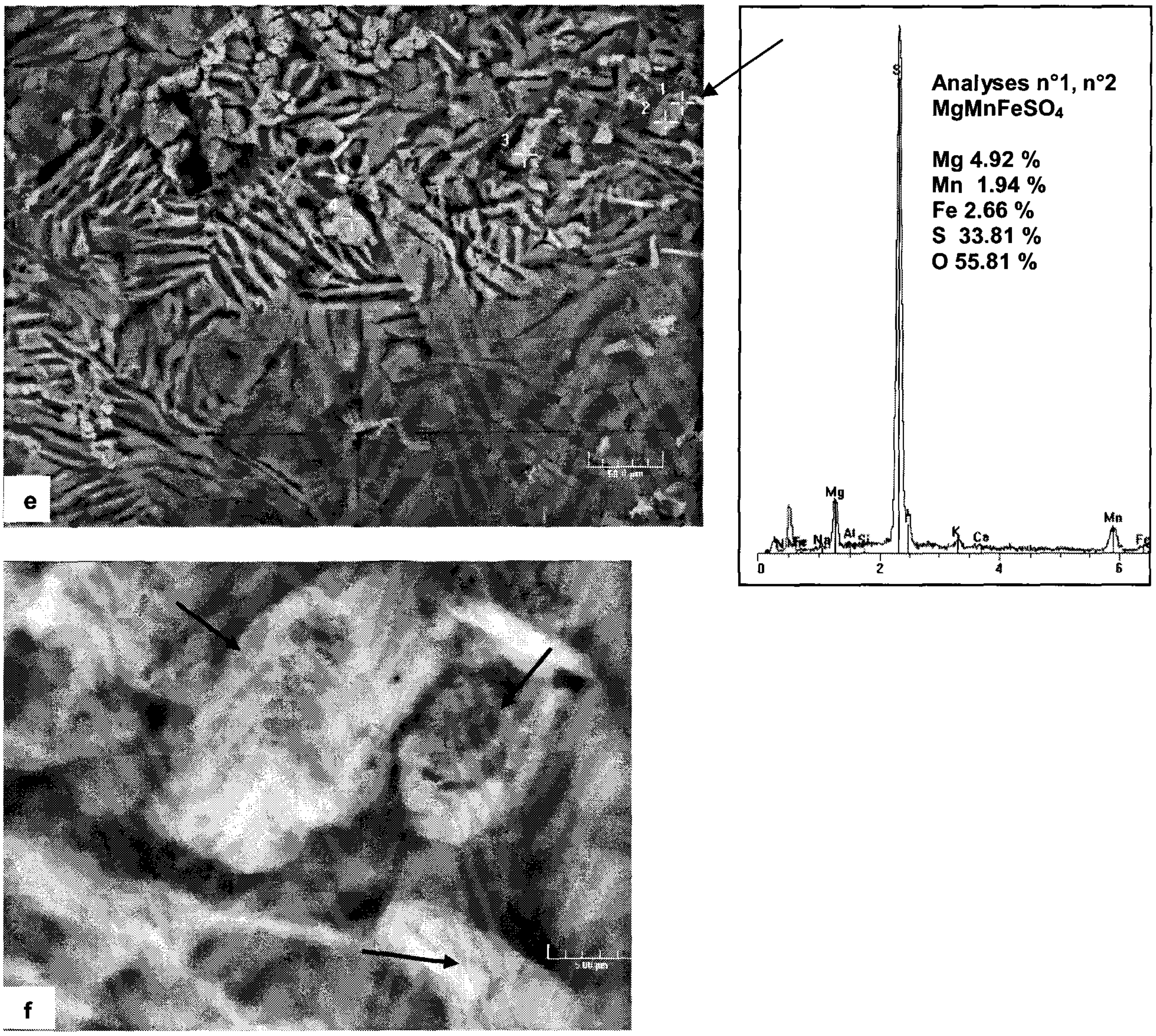

**Figure 6e and 6f.** (**e**) EDS/BSE analysis of minerals of solid fragment of sample AV1443b. Analysis n°1 and n°2 are MgMnFe-sulphate, analysis n°3 is glauberite, and analysis n° 4 is thenardite (white). Dark grey mineral is mascagnite. (**f**) SEM/BSE image of MgMnFe-sulphate (arrows), scale bar 500μm.

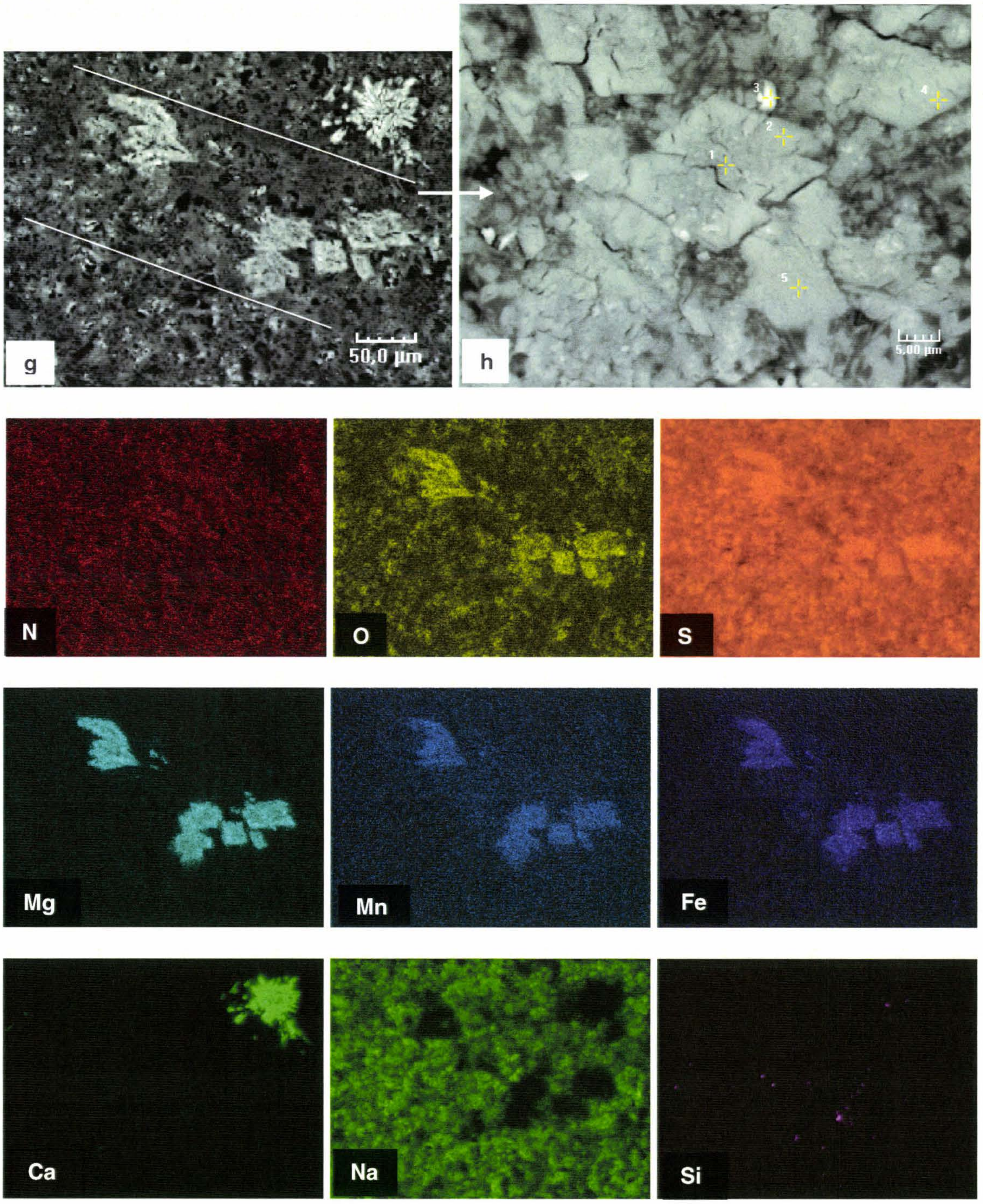

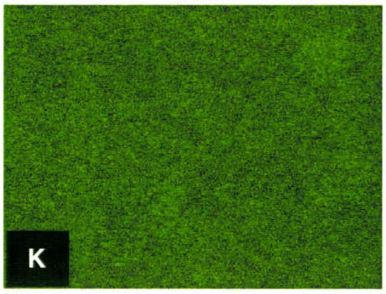

**Figure 6g and 6h .** SEM/ BSE images of sample AV1443b (thin section ). **(g)** EDS zone map of MgMnFe-sulphate, note rosettes of gypsum on the right corner. **(h)** SEM image and EDS analysis of MgMnFe-sulphate (analyses 1, 2 and 4), analysis 3 is quartz.

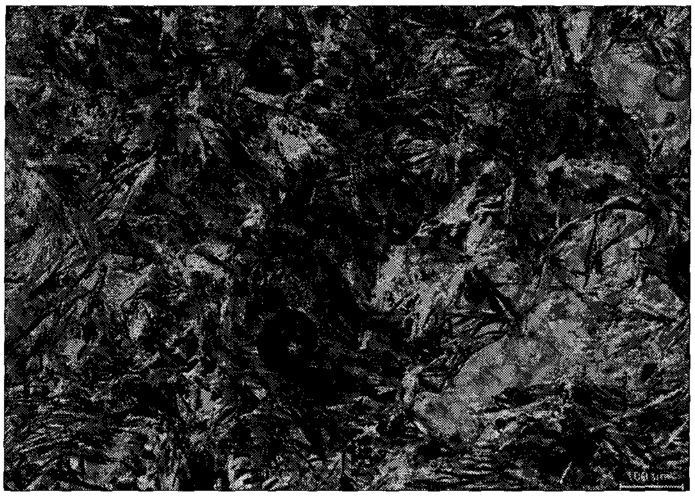

**Figure 7**. Transmitted light micrograph of needle-like mineral assemblage showing cryptocrystalline fabric in sample AV2503, CPL x 100. Round black spots are cavities.

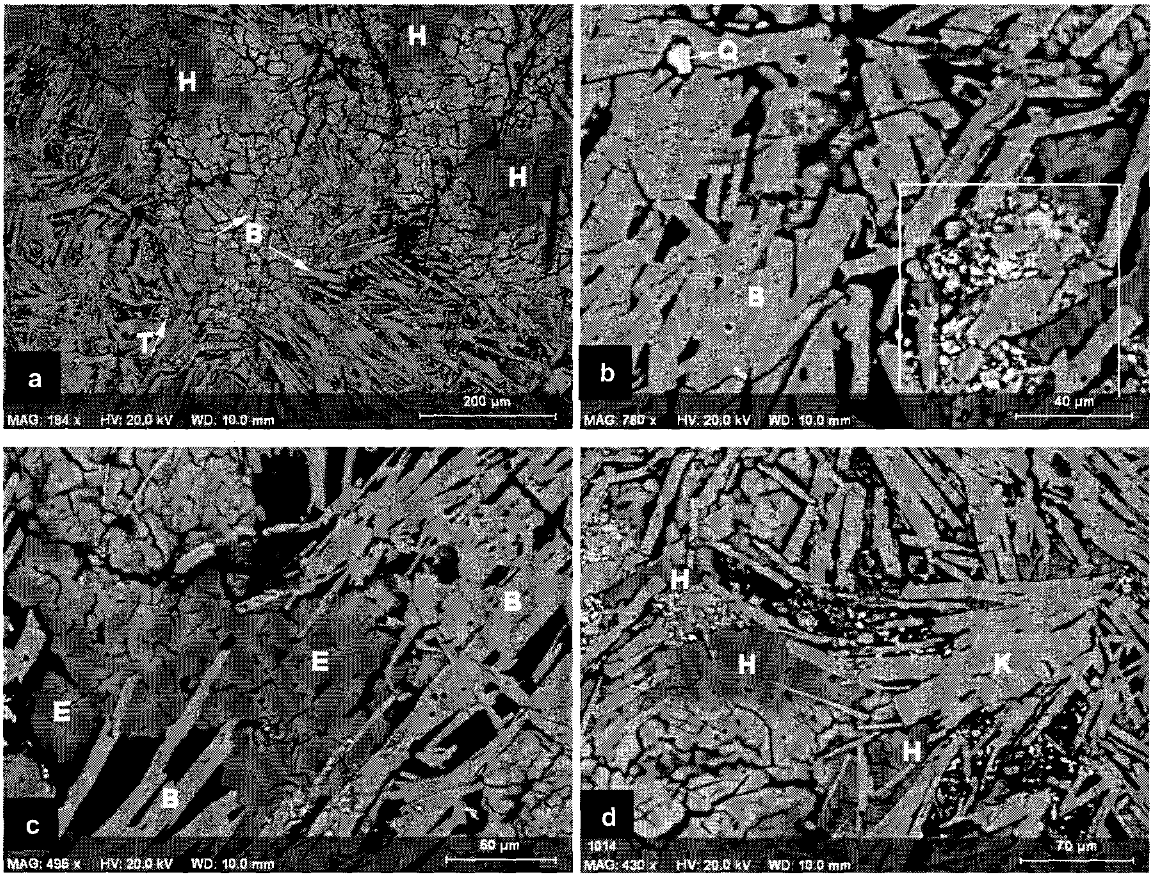

**Figure 8**. SEM images of mineral assemblage in sample AV2503 (thin section). **(a)** Acicular habit shown by mineral assemblage.**(b)** White fine-grained granular of thenardite (T) filling spaces between acicular light grey laths of bloedite (B). **(c)** Aggregates of epsomite (E) dark grey grown between laths of bloedite. **(d)** Aggregates of hexahydrite (H) grey grown on laths of konyaite (K) light grey. Granular white crystals are thenardite. Quartz (Q), cavities are black.

**Figure 8**. Field occurrence of efflorecent minerals on the porcellanites at gas spot S3, see also Figure 4 for an example of a selected hand specimen. Nipper for scale bar 8cm.

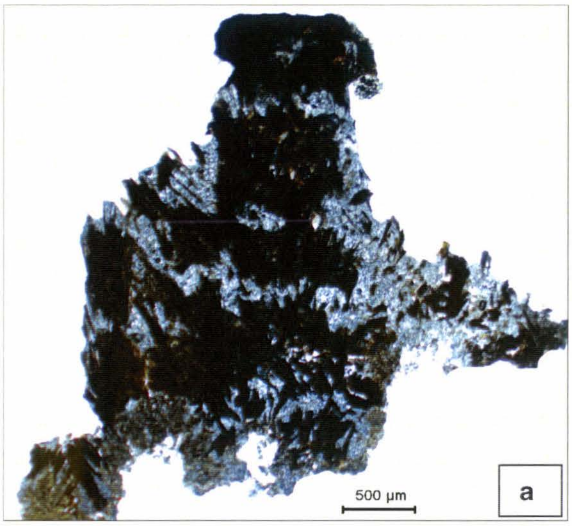

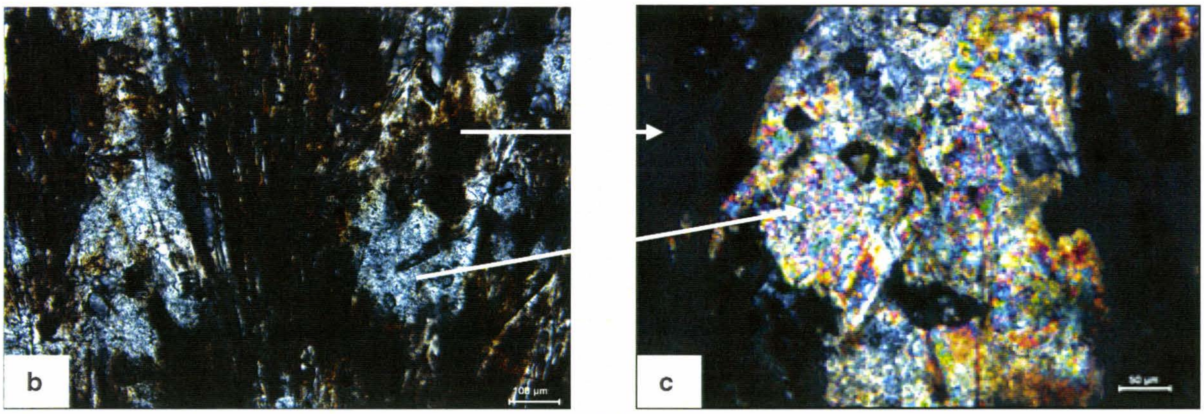

**Figure 9**. Transmitted light micrographs of minerals in sample AV1955. **(a)** Acicular habit shown by mineral assemblage, PPL. **(b)** Acicular pickeringite-alunogen (brown) assemblage, colourless crystals (white) are aggregates of kalinite-pickeringite-halotrichite-gypsum assemblage, PPL. **(c)** Nearly opaque pickeringite-alunogen (brown) and second order pinkish-blue kalinite-pickeringite-halotrichite-gypsum assemblage, CPL.

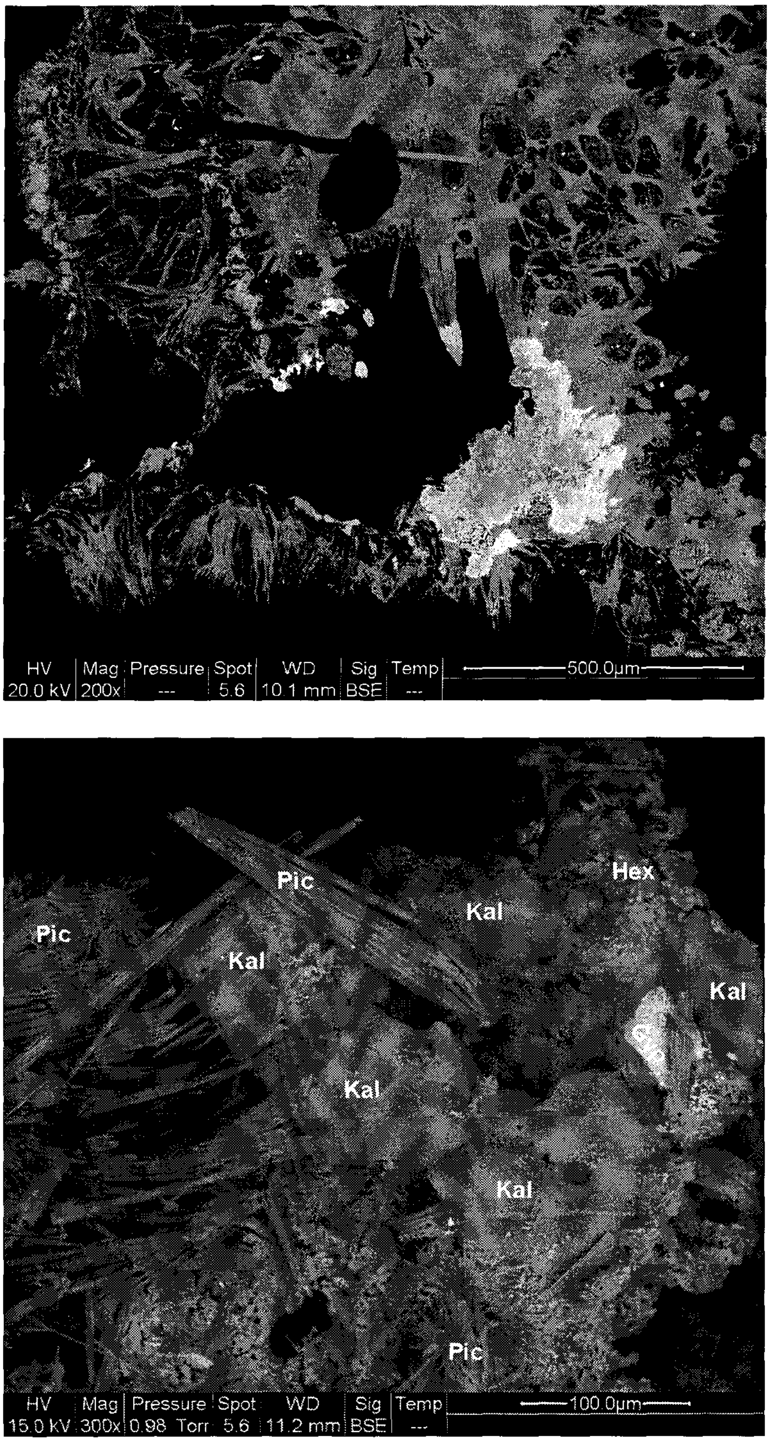

**Figure 10**. SEM/BES images of mineral assemblage observed in thin section (first image above) and in solid fragment (second image blow) in sample AV1955. Images of minerals in thin section are shown in the following figures. Pic: pickeringite, Kal: kalinite, Hex: hexahtdrite, Gyp: Gypsum

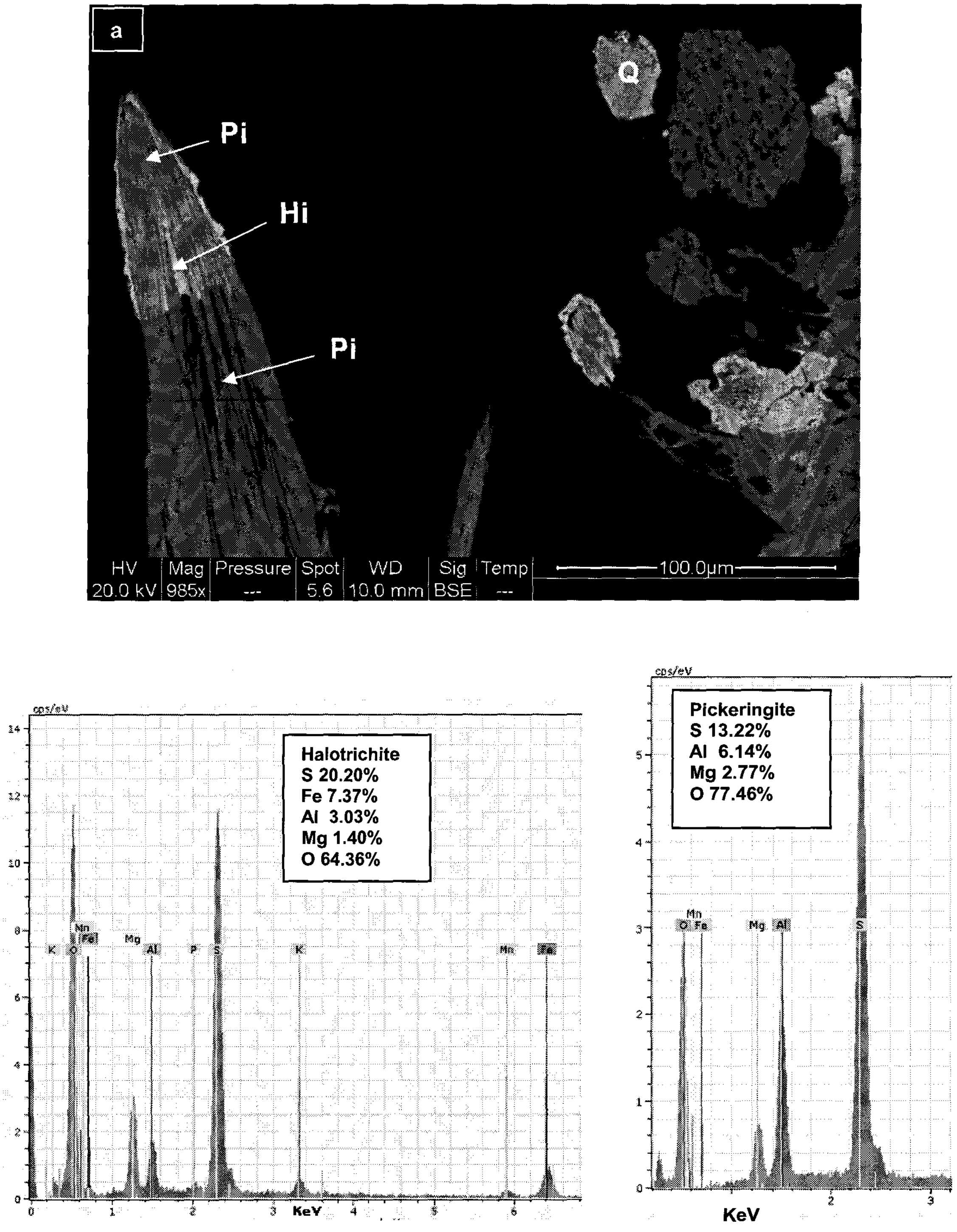

**Figure 10a**. SEM/BSE image of fibrous pickeringite (Pi) grey and halotrichite (Hi) white mineral assemblage in sample AV1955. Q: quartz. EDS element analyses in these two minerals are shown below.

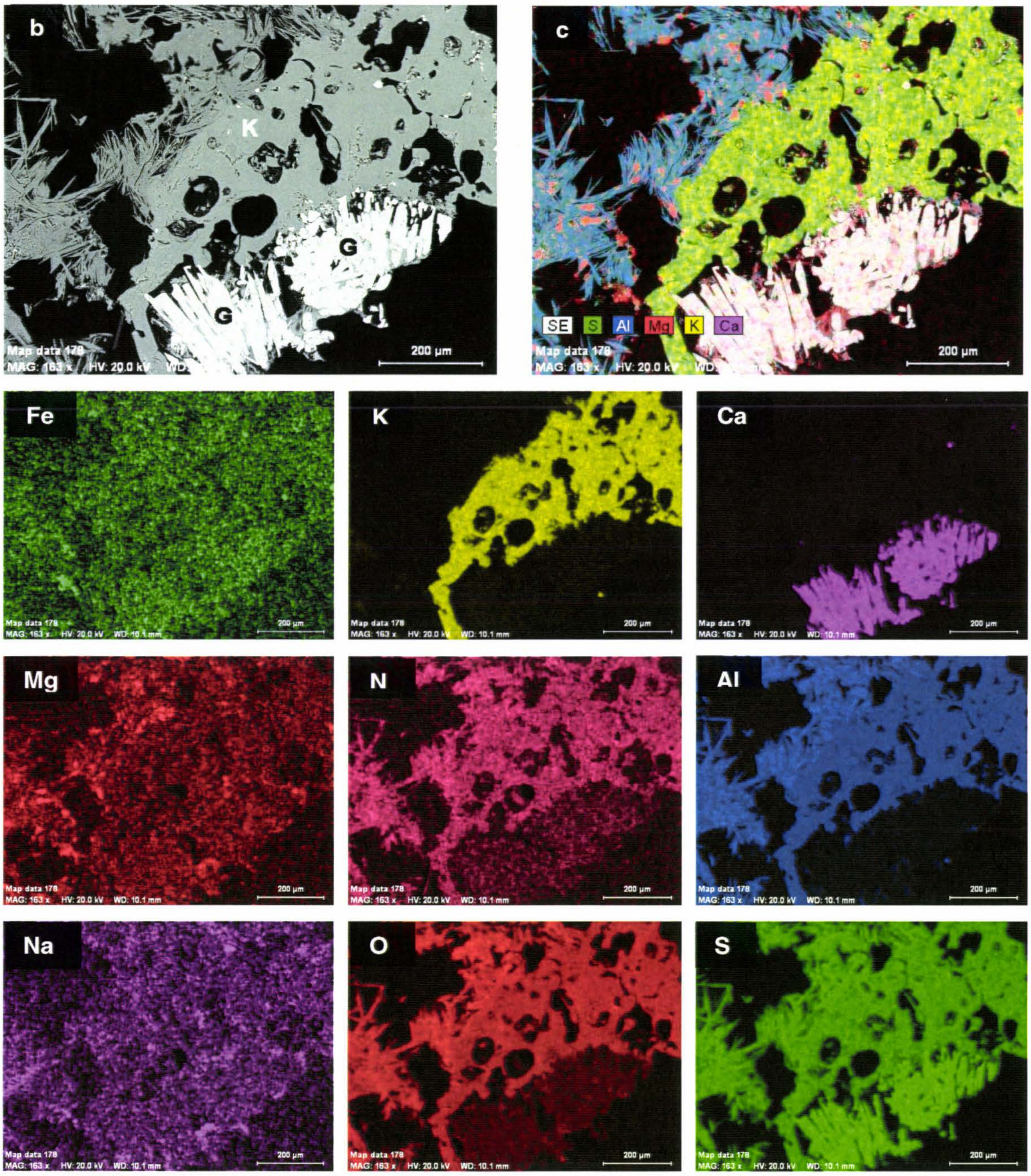

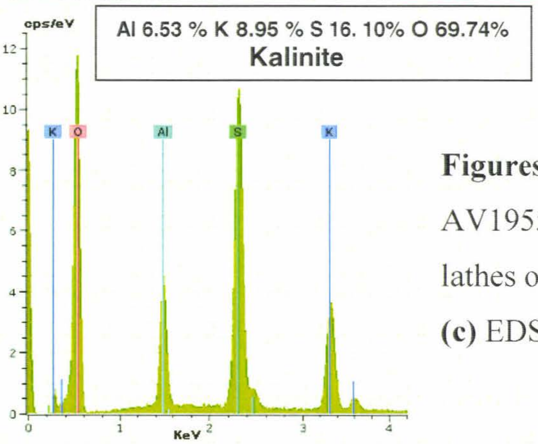

**Figures 10**. **(b)** SEM/BSE image of minerals in sample AV1955. Aggregates of kalinite (K) grey, and group of lathes of gypsum (G) white covering kalinite aggregates. **(c)** EDS zone mapping of elements in sample AV1955.

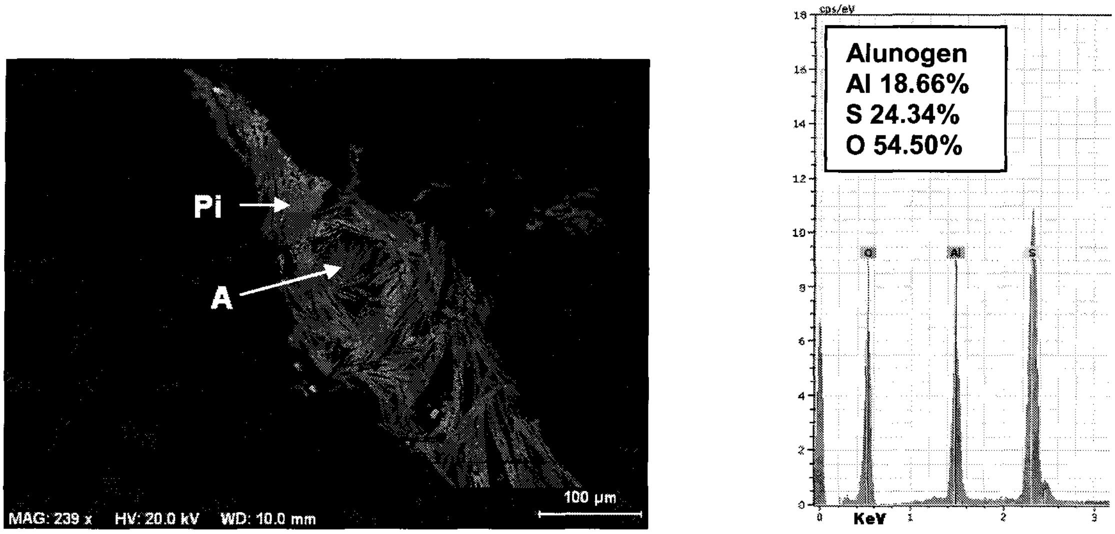

**Figure 10d**. SEM/BSE image of needle-like crystals of alunogen (A) formed in the cavities, and EDS element analysis in sample AV1955. Pi = pickeringite.

SEM images and EDS analyses of this assemblage in thin sections are given in Figure 12. Bloedite (dark grey in BSE mode) occurs as matrix overgrown or penetrated by thenardite Aggregates of thenardite (light grey) are principally concentrated along the sides and are rarely crystallized within the bloedite matrix. Aphthitalite (white) appears as inclusions in bloedite or as crystals between the bloedite-thenardite aggregates (Figs. 12a and 12b). Element mapping and EDS analysis of sample AV1443f have shown that sulphur, magnesium, sodium and potassium are the most abundant elements (Fig. 12c).

SEM images of solid fragments show long laths of bloedite (dark grey) grown on the fine-grained granular aphthitalite aggregates (white) in sample AV1443d (Fig. 12d), whereas in sample AV1443f, aphthitalite occurs on bloedite or thenardite aggregates (Fig. 12e). X-ray diffractogram of this assemblage in sample AV1443d is given in Figure 13.

- ***Bloedite- Thenardite -Langbeinite -Halite-Aphthitalite-KNaMg-sulphate***

Figure 14 shows X-ray diffraction patterns of sample AV1443e. The only reflections for this sample can be attributed to bloedite, thenardite and halite. Using optical transmitted light microscopy, langbeinite (which is optically isotropic) and aphthitalite were not observed. Bloedite shows brownish tabular or fine lath-like crystals with deformed or pointed outlines. Skeletal and hollow crystals are also observed (Figs. 15a and 15b). Thenardite shows greyish-

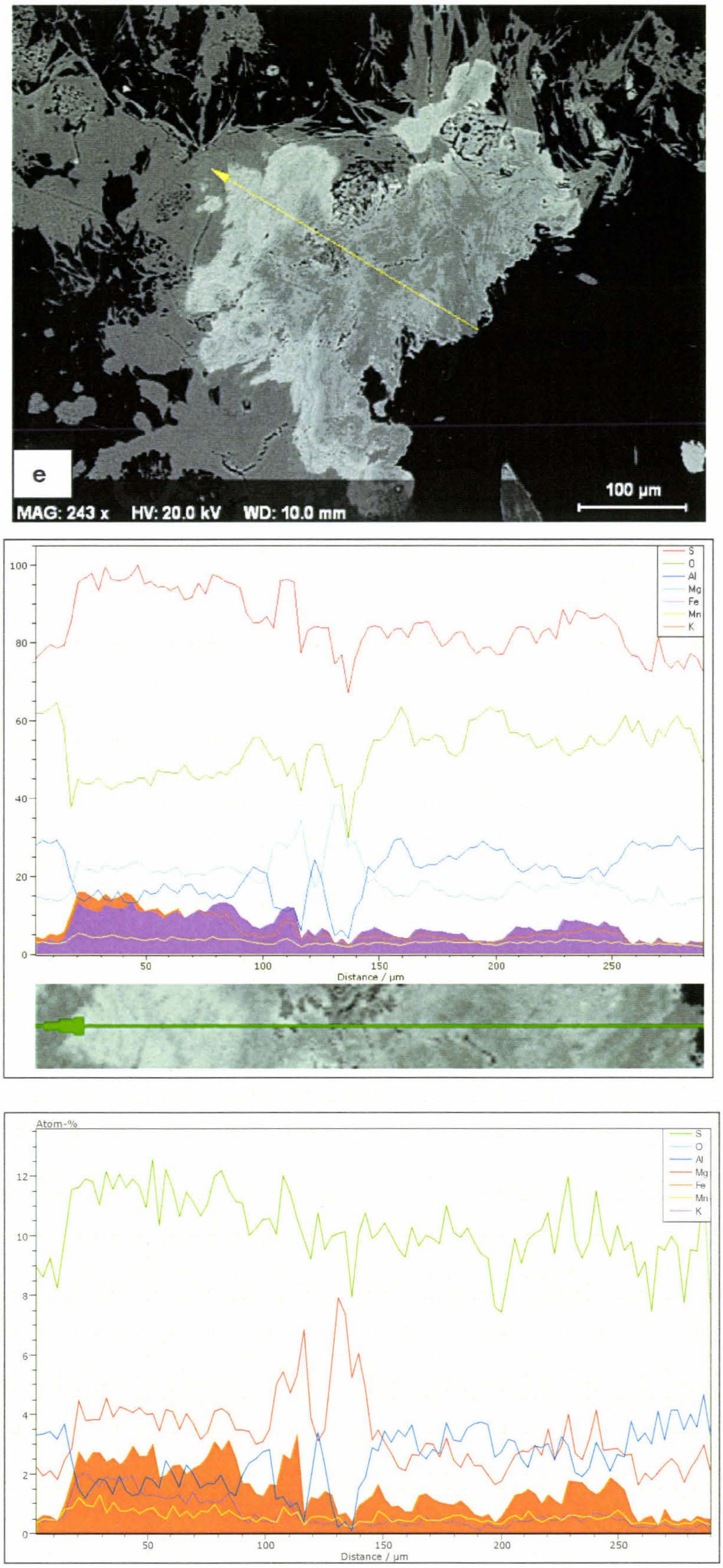

**Figure 10e** . SEM/BSE image and EDS zone element map (arrow) showing that S, O, Mg, Al, K and Fe as the most abundant elements.

blue or yellowish crystals and occurs as aggregates with pointed outlines in the matrix (15c). Halite occurs as aggregates and inclusions in bloedite and/or thenardite crystals, or it occurs along the sides of these two phases. KNaMg-sulphate occurs as clusters enclosed by bloedite and thenardite. Crystals of this mineral have angular or hexagonal or cubic shapes. In plain-polarized light, they are colourless; interferererence colors are up to second order bluish-pink (thin section thickness 30 µm) (Fig. 16). EDS analyses revealed that sulphur, potassium, sodium and magnesium are the most abundant elements (Fig. 17). Quantitative analysis of this mineral by WDS analysis confirmed the composition of this new sulphate (Table 4).

SEM images and analyses of minerals in sample AV1443e revealed the occurrence of aphthitalite (in thin section) and langbeinite (in thin section and in solid fragment). These minerals were not observed by optical microscopy. These two sulphate minerals are accessory phases in sample AV1443e (Fig. 18) Aphthitalite (light grey) occurs as an aggregate in bloedite (dark grey) matrix. Langbeinite (grey) is tabular in shape and often contains inclusions of halite (white) (Fig. 18a). Minor amounts of arcanite and halite were also observed in sample AV1443e (Figs. 18 b, 18c).

**Table 4.** Electron microprobe (WDS) analyses of KNaMg-Sulphate in sample AV1443e.

| Elements | $Na_2O$ | $K_2O$ | MgO | MnO | FeO* | $Al_2O_3$ | CaO | Cl | $SO_4$ | Total |
|---|---|---|---|---|---|---|---|---|---|---|
| | 12.027 | 16.141 | 8.303 | 0.110 | 0.049 | 0.016 | 0.205 | 0.00 | 54.75 | 91.612 |
| | 10.973 | 19.573 | 11.469 | 0.00 | 0.00 | 0.00 | 0.059 | 0.061 | 50.365 | 92.532 |
| | 11.967 | 17.940 | 10.343 | 0.00 | 0.00 | 0.035 | 0.516 | 0.020 | 50.561 | 91.382 |

*FeO: Refers to total iron

### *4.1.5. Gas spot S5*

Salammoniac crystallizes in the absence of sulphate minerals at this location. Field occurrences of this mineral are given in Figure 19. It is the least common mineral formed at the studied coal waste heap. Natural crystals of salammoniac when pure are white in colour and when impure (e.g. mixed with $FeCl_3$,) the colour is yellowish, orange to brown (Fig. 4). Salammoniac was determined using XRD analysis. SEM images of solid fragments of sample AV2344a shows cubic crystals of this mineral with almost straight crystal faces (Fig. 19a).

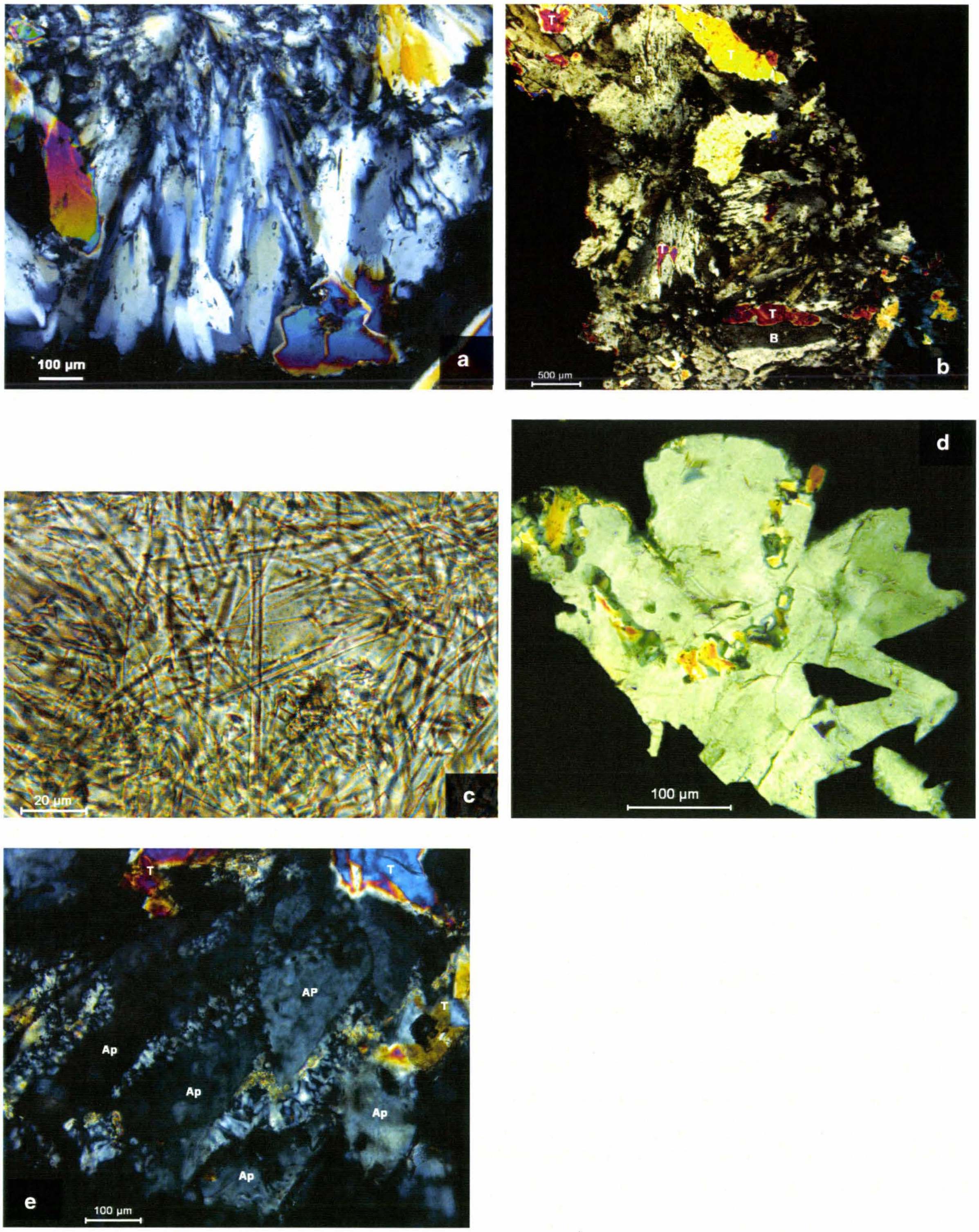

**Figure 11**. Transmitted light micrographs CPL. **(a)** Elongated lozenge-shaped thenardite crystals, sample AV2344w. **(b)** Aggregates of thenardite grown on bloedite crystals (grey), sample AV1443h. **(c)** Needle-like habit shown in crystals of bloedite, sample AV1443h. **(d)** Aggregates of bloedite (grey) with overgrown thenardite crystals (yellow), sample AV1443g. **(e)** Tabular dull grey crystals of aphthitalite in sample AV1443d. Bluish crystals in this sample are thenardite. A = aphthitalite, B = bloedite, T = thenardite

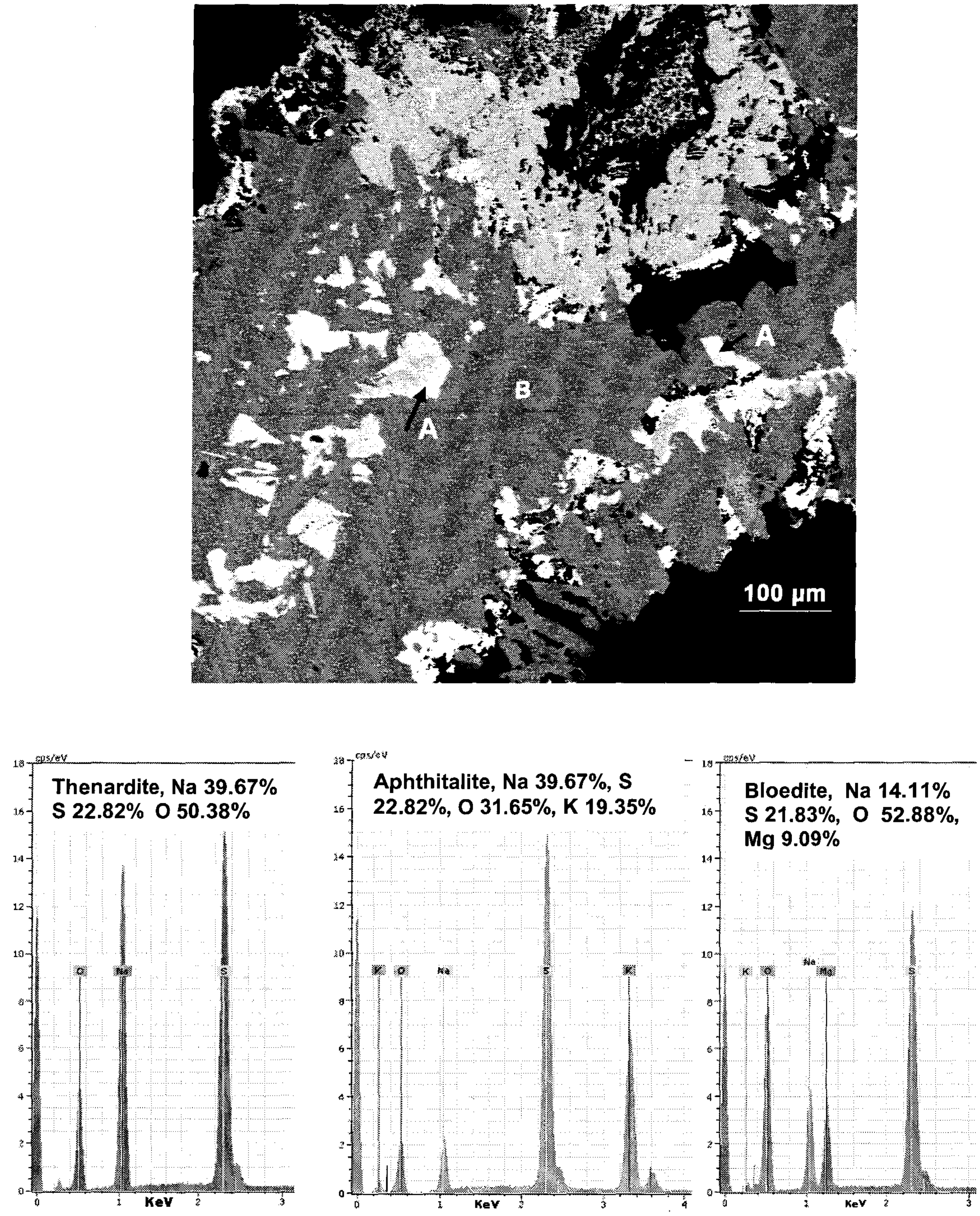

**Figure 12a**. SEM/BSE image and EDS element analysis in sample AV1443d. Mineral assemblage thenardite (T) light grey crystallized around the cavities (black) or in the matrix, bloedite (B) dark grey occurs as matrix, aphthitalite (A) white appears as inclusions in bloedite or is crystallized between the thenardite-bloedite aggregates.

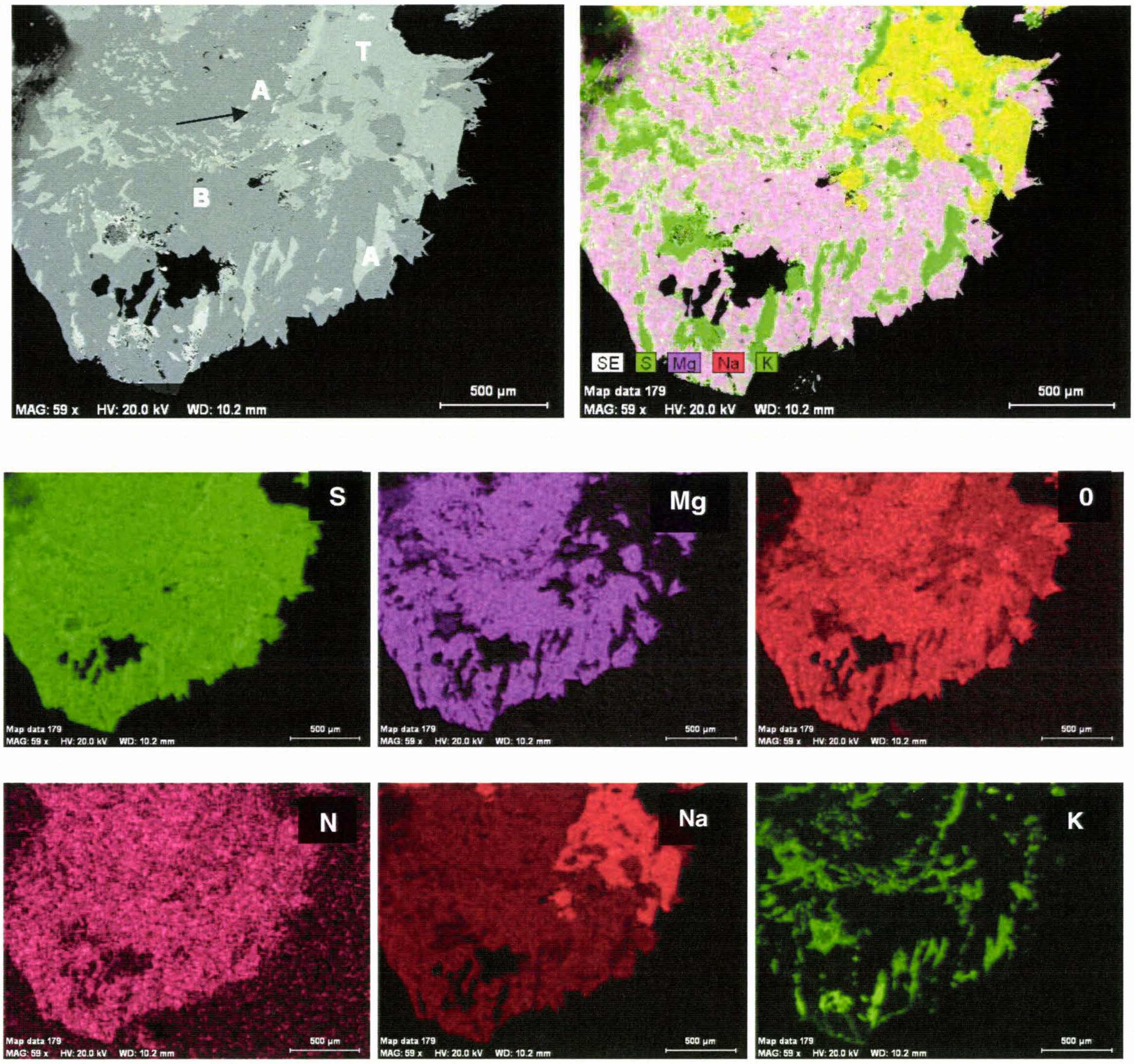

**Figure 12b**. SEM/BSE image and EDS element analysis in sample AV1443f (thin section). Mineral assemblage thenardite (T) light grey crystallized in the matrix, bloedite (B) dark grey occurs as matrix, aphthitalite (A) whitish grey appears as inclusions in bloedite aggregates in the matrix.

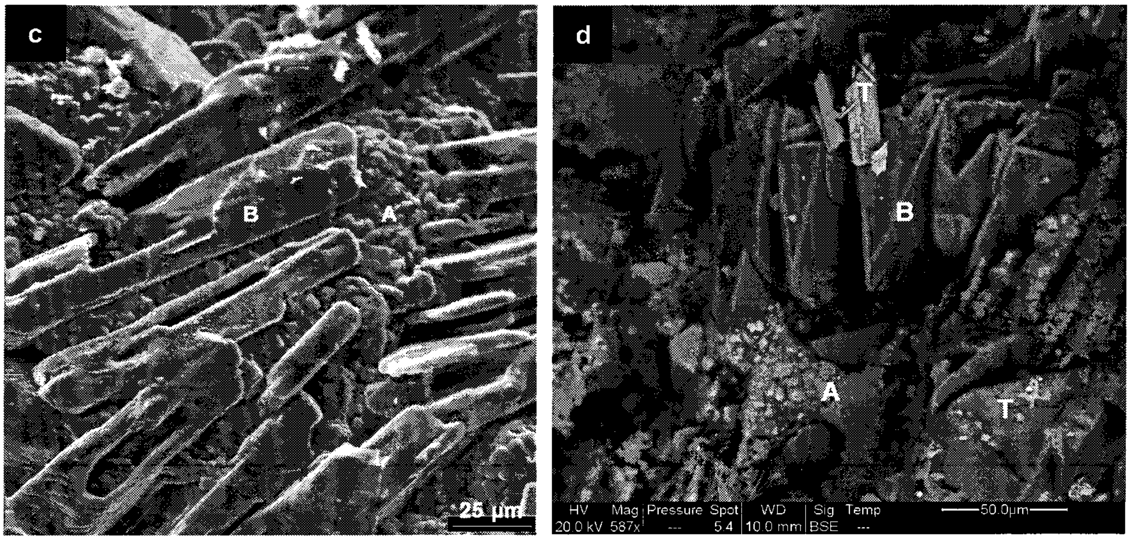

**Figure 12 c and 12d**. SEM/BSE images of solid fragments. **(c)** sample AV1443d showing skeletal laths of bloedite grown on granular aphthitalite. **(d)** sample AV1443f granular aphthitalite occurs on bloedite or on thenardite. A: aphthitalite, B: bloedite, T: thenardite

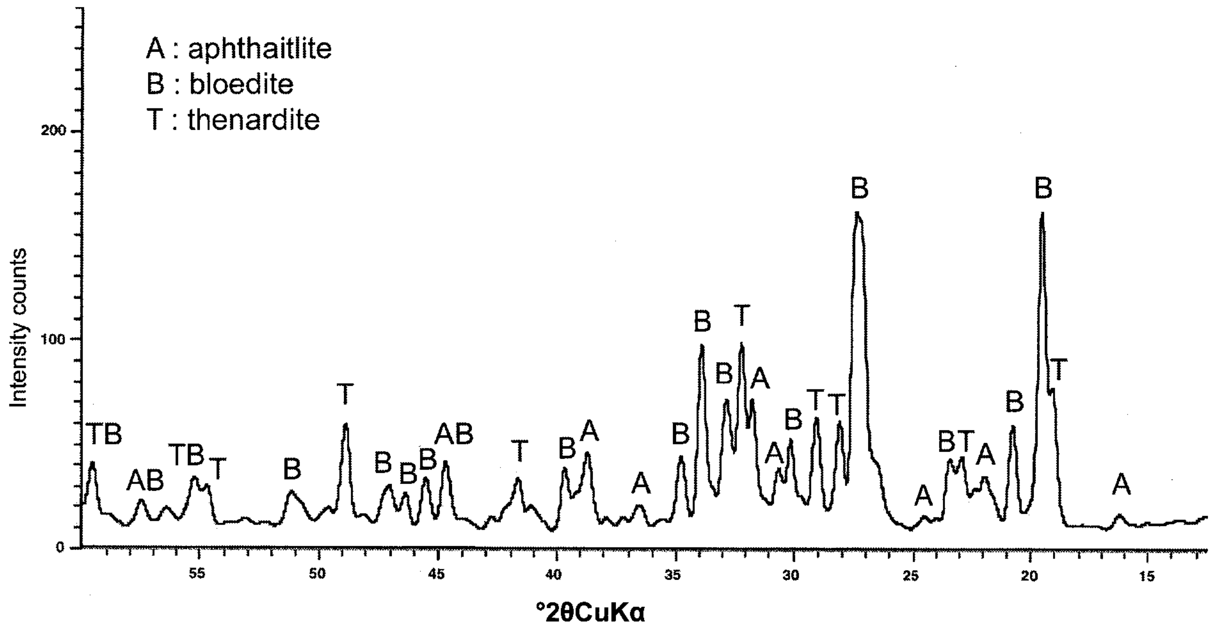

**Figure 13**. X-ray diffraction pattern of sample AV1443d.

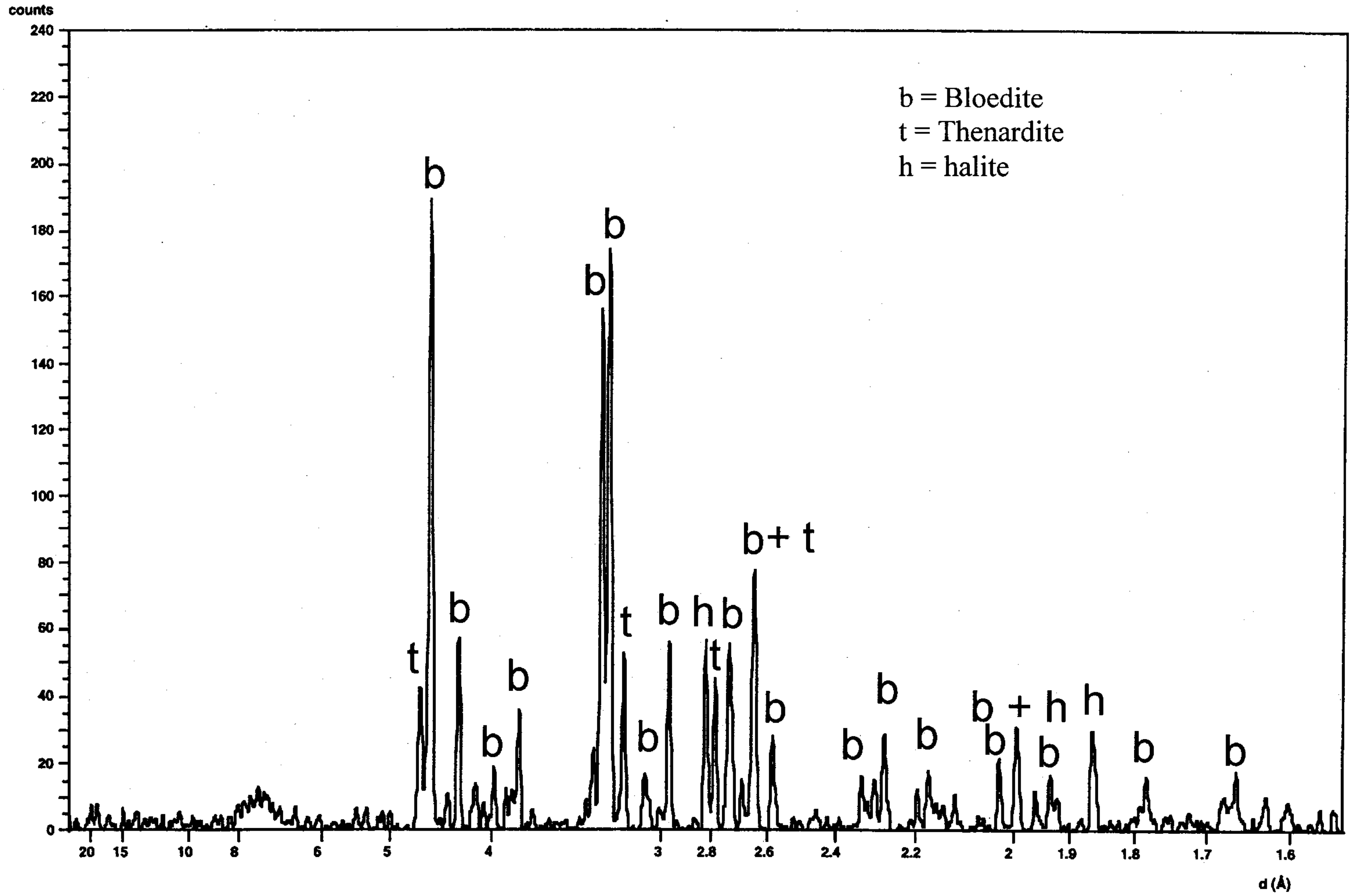

**Figure 14**. X-ray diffraction pattern of sample AV1443e.

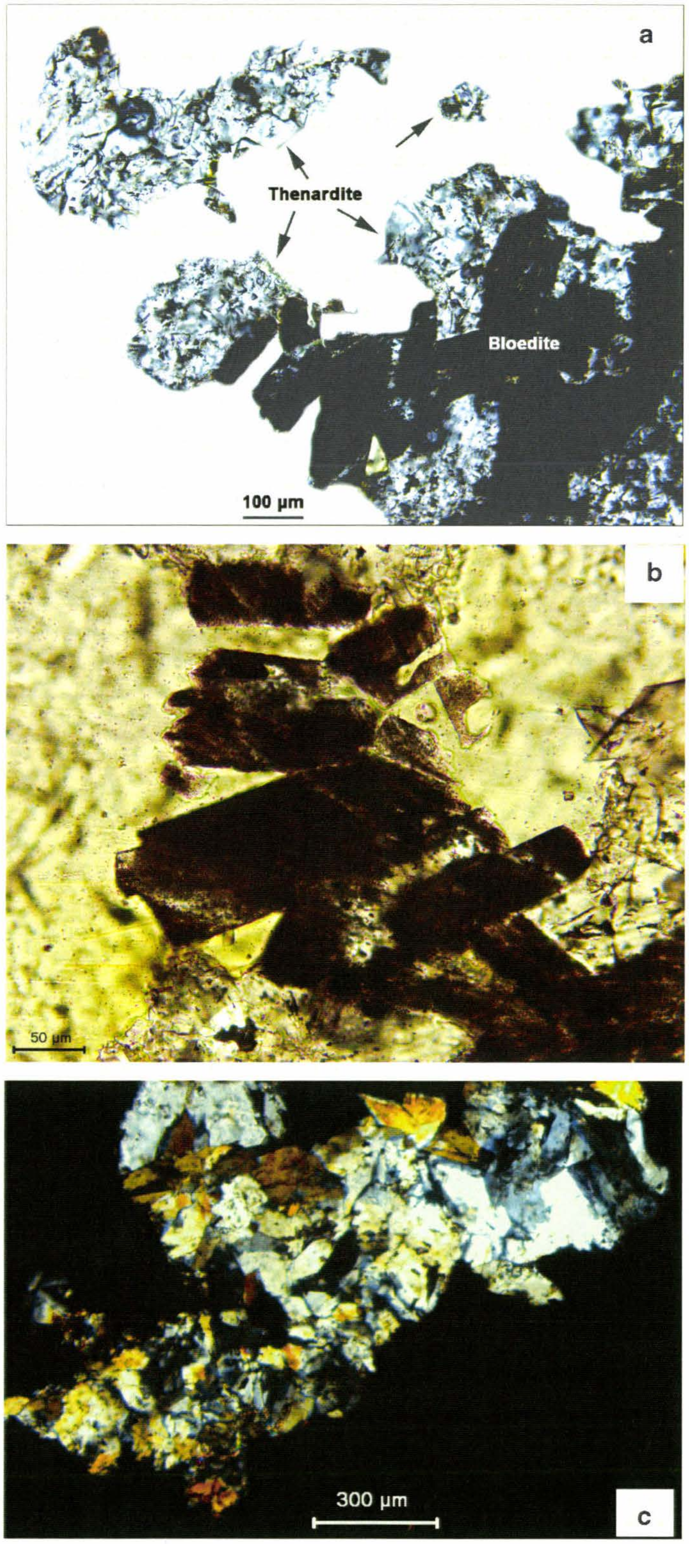

**Figure 15**. Transmitted light micrographs of minerals in sample AV1443e. **(a)** and **(b)** Brownish tabular or skeletal crystals of bloedite and colourless aggregates of thenardite, PPL. **(c)** Greyish-yellow crystals of thenardite with pointed outlines, CPL.

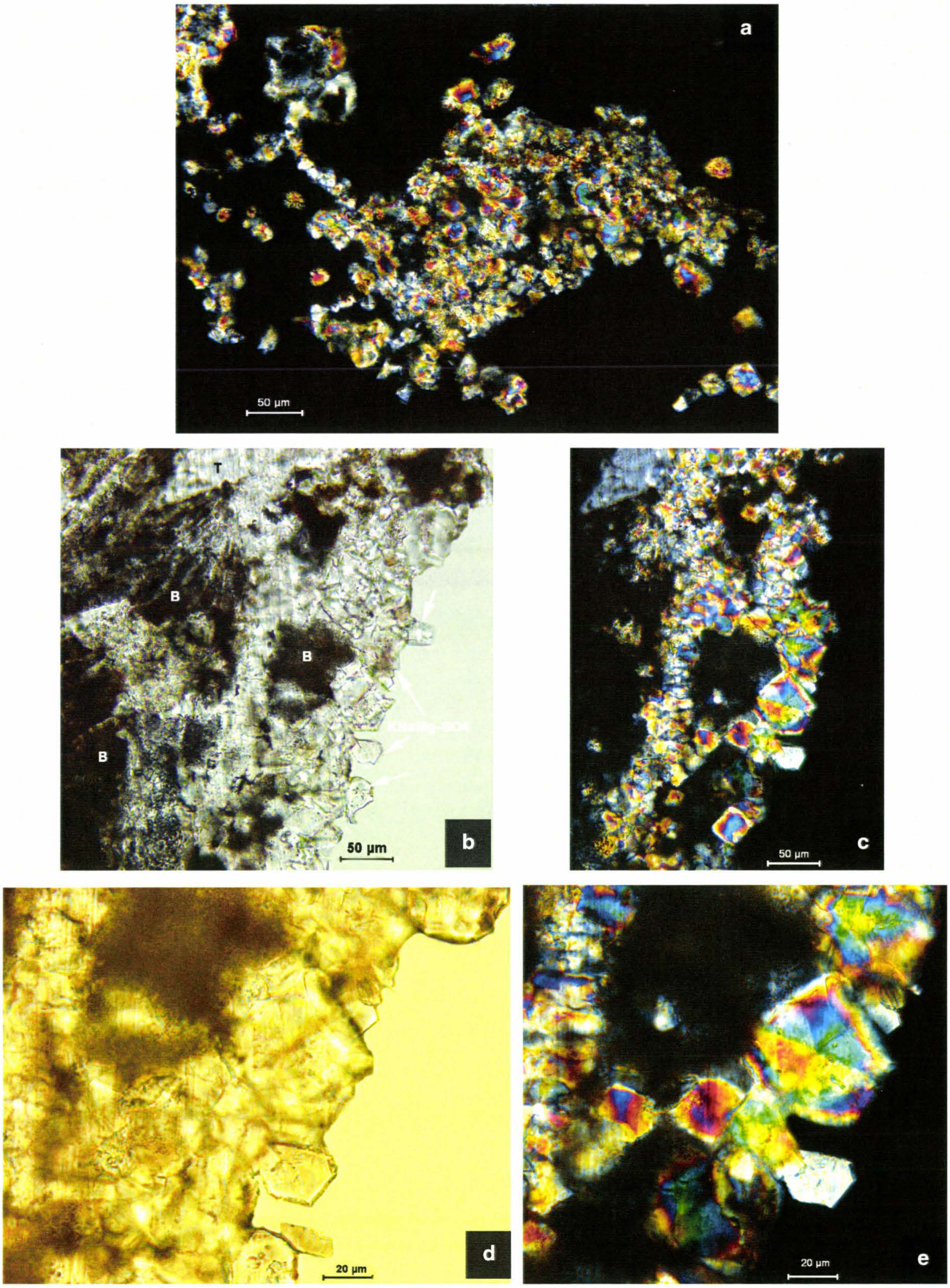

**Figure 16**. Transmitted light micrographs of KNaMg-sulphate in sample AV1433d. Figures (**a**), (**c**) and (**e**) are CPL and Figures (**c**) and (**d**) are PPL. Crystals of this new sulphate have angular, cubic or hexagonal shapes. Brownish aggregates (opaque in CPL) grown on crystals of this phase are bloedite (B). T: thenardite

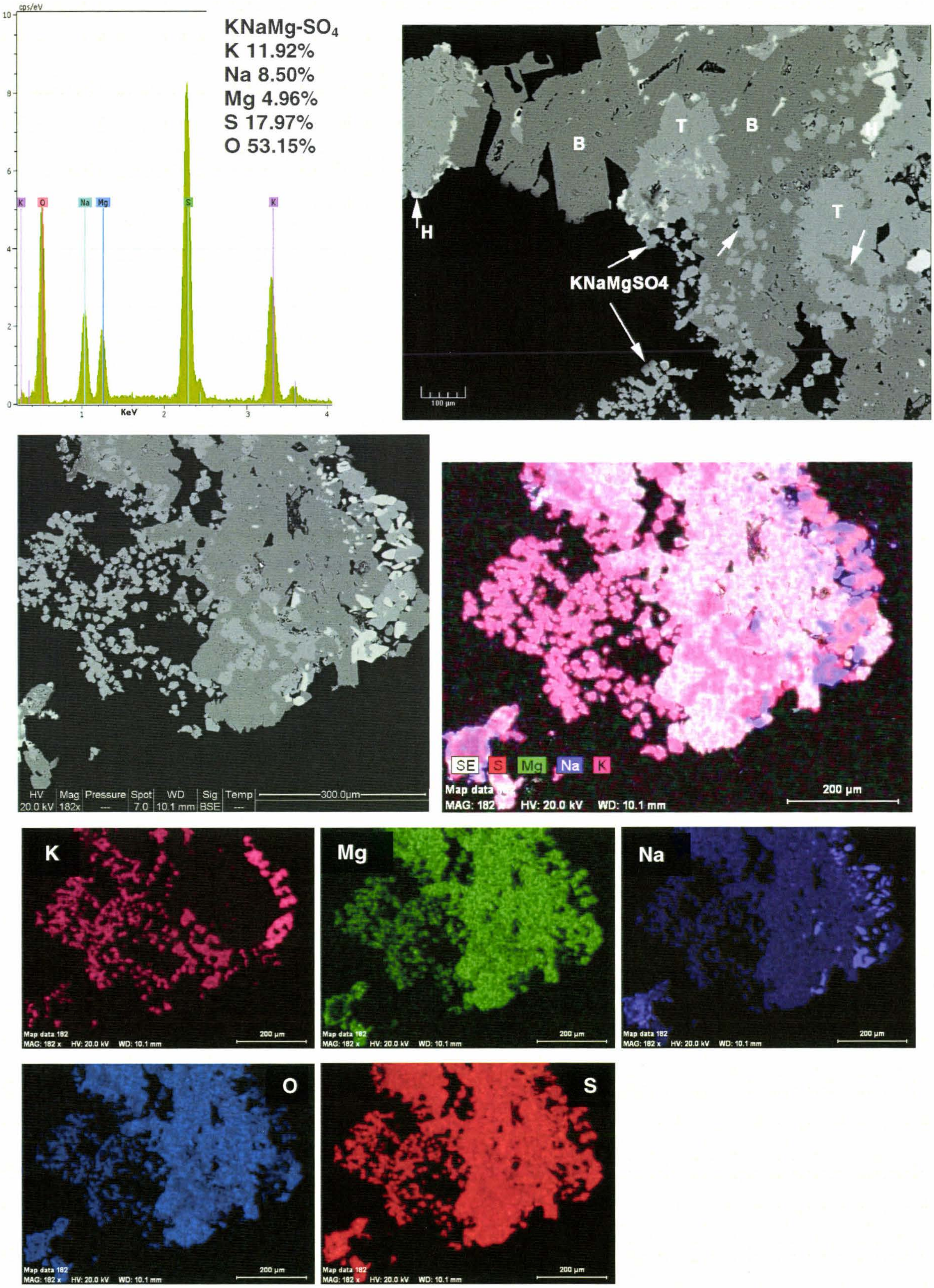

**Figure 17**. SEM/BSE images and EDS analysis of KNaMg-sulphate in sample AV1443e. Bloedite (dark gry) is the matrix and light grey minerals are new KNaMg-sulphate.

H: halite ; B: Bloedite; T: thenardite; arrows: KNaMg-sulphate

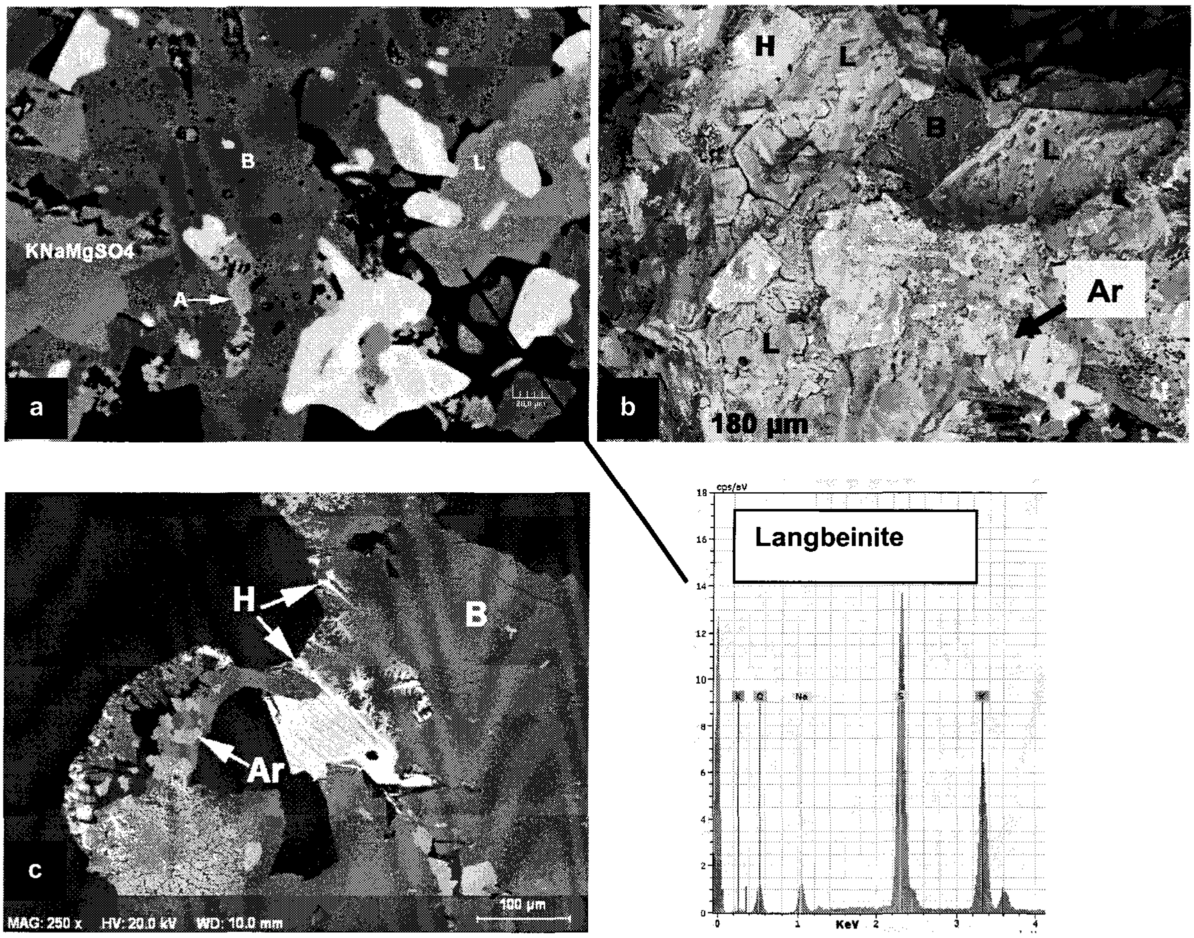

**Figure 18**. SEM images and EDS analyses of mineral assemblages in sample AV1443e.

**(a)** KNaMg-sulphate crystallized in bloedite matrix. Euhedral crystal of langbeinite (grey) with inclusion of halite (white), aphthitalite overgrown in bloedite matrix, white crystals are halite (thin section). **(b)** SEM/BSE image of mineral assemblages seen in solid fragment, euhedral crystals of langbeinite and fine aggregates of arcanite. **(c)** Overgrown arcanite (light grey) in bloedite. Large and fine skeletal white crystals in the bloedite matrix are halaite (thin section). L: langbeinite; B: bloedite, H: halite; A: aphthitalite; Ar : arcanite.

### *4.1.6. Gas spot S6*

Figure 20 shows field occurrence of efflorescence minerals at spot S6. Minerals occurring at this location are:

- ***Native sulphur, gypsum and mascagnite***

Native sulphur (sample AV2504) forms bright yellow microcrystalline botryoidal crusts (Table 1), it was determined by XRD. Gypsum occurs as monomineralic aggregates in sample AV2703. Thin section images show euhedral tabular crystals (Fig. 21a). Mascagnite occurs as white microcrystalline botryoidal monomineralic aggregates in hand specimens (Table 1, Fig. 4, sample 2502w). SEM images show groups of tabular crystals (Fig. 21b).

- ***Tschermgite-Alunogen-Pickeringite-Hexahydrite-Gypsum***

This assemblage occurs in sample AV5204 (Table 1, Fig. 4). XRD patterns for this sample show strong reflections for tschermigite, alunogen and pickeringite. Hexahydrite, gypsum, and sulphur were detected by WDS analysis.

SEM/EDS images show tschermigite occurring as groundmass constituents. The individual crystals of this mineral were not observed. Alunogen occurs as aggregates in the matrix. Pickeringite forms acicular crystals often as overgrowths on alunogen (Fig. 22a). Granular hexahydrite occurs as overgrowths on alunogen or acicular pickeringite crystals. Gypsum occurs as aggregates grown on alunogen (Fig. 22b). Figure 23 shows EDS results for sample AV5204a. Sulphur, nitrogen, aluminium and magnesium are the most abundant elements in this sample with a lesser amount of silicon (quartz impurities).

### *4.2. Gas, condensate and substrate chemistry*

Table 5 lists the in-situ gas analysis from selected gas spots where sulphate minerals were collected. The compounds S, H, N and O are all found in sulphate mineral assemblages. Although Cl, which occurs in salammoniac and halite, was not quantified in gas analysis, this element is known to occur in coal fire gas (e.g. $CH_3Cl$, Stracher, et al., 2005). None of the metallic cations in the stoichiometric formulae presented for the mineral assemblages at gas spots 1-4 and 6 occur in the in situ gas analyses. However, in addition to $SO_4^{2-}$, $NO_3^-$ and $NO_2^-$ they all occur in the collected condensate water (Table 6) (Masalehdani et al., 2005).

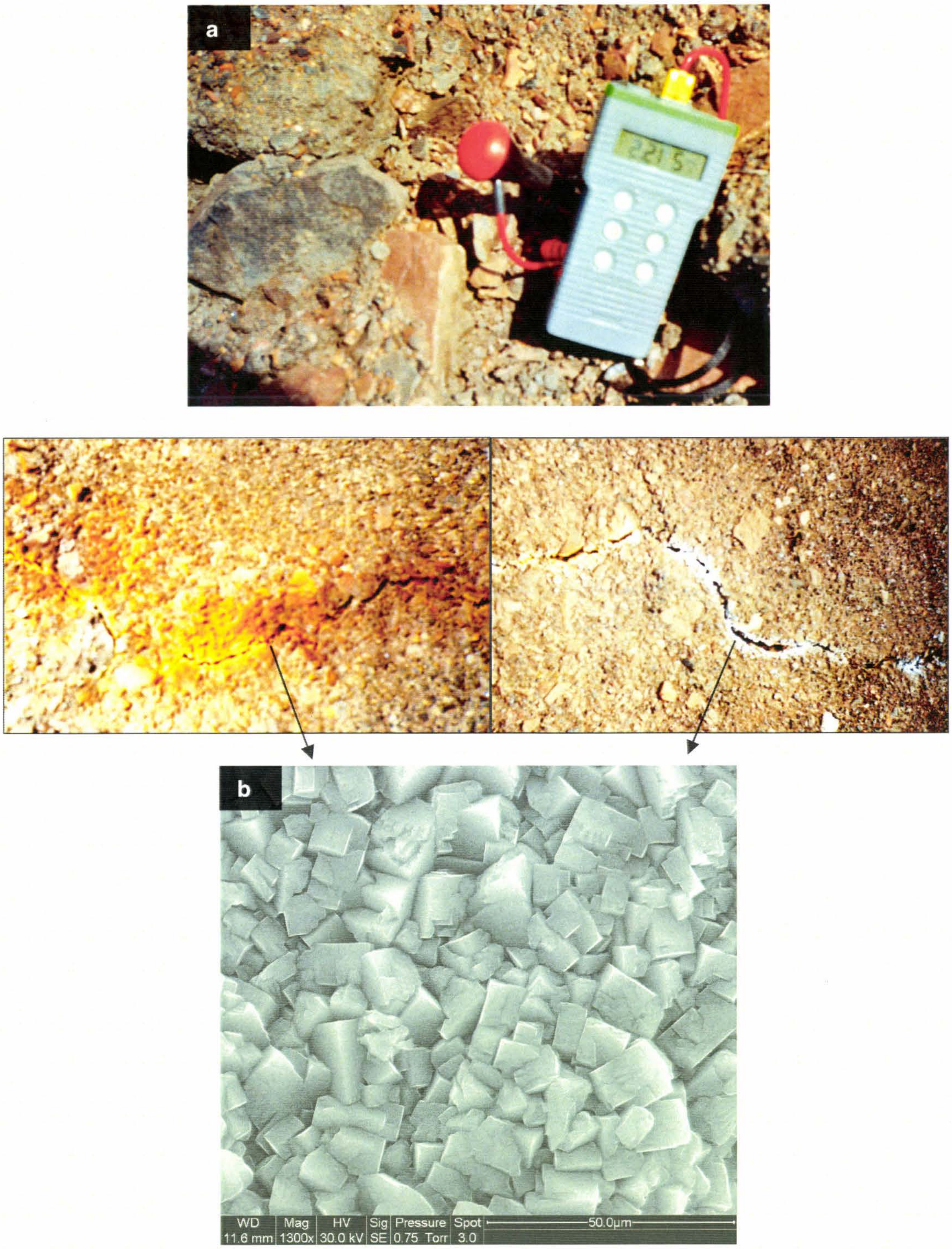

**Figure 19**. **(a)** Field occurrence of salammoniac along the surficial crack (T°C 221.5) at gas spot S5 coal waste heap n°76, Avion. **(b)** SEM/SE image of solid fragment of cubic salammoniac crystals (sample AV 23344a).

**Figure 20**. Field occurrences of mineral assemblages at gas spot S6 coal waste heap n°76, Avion.

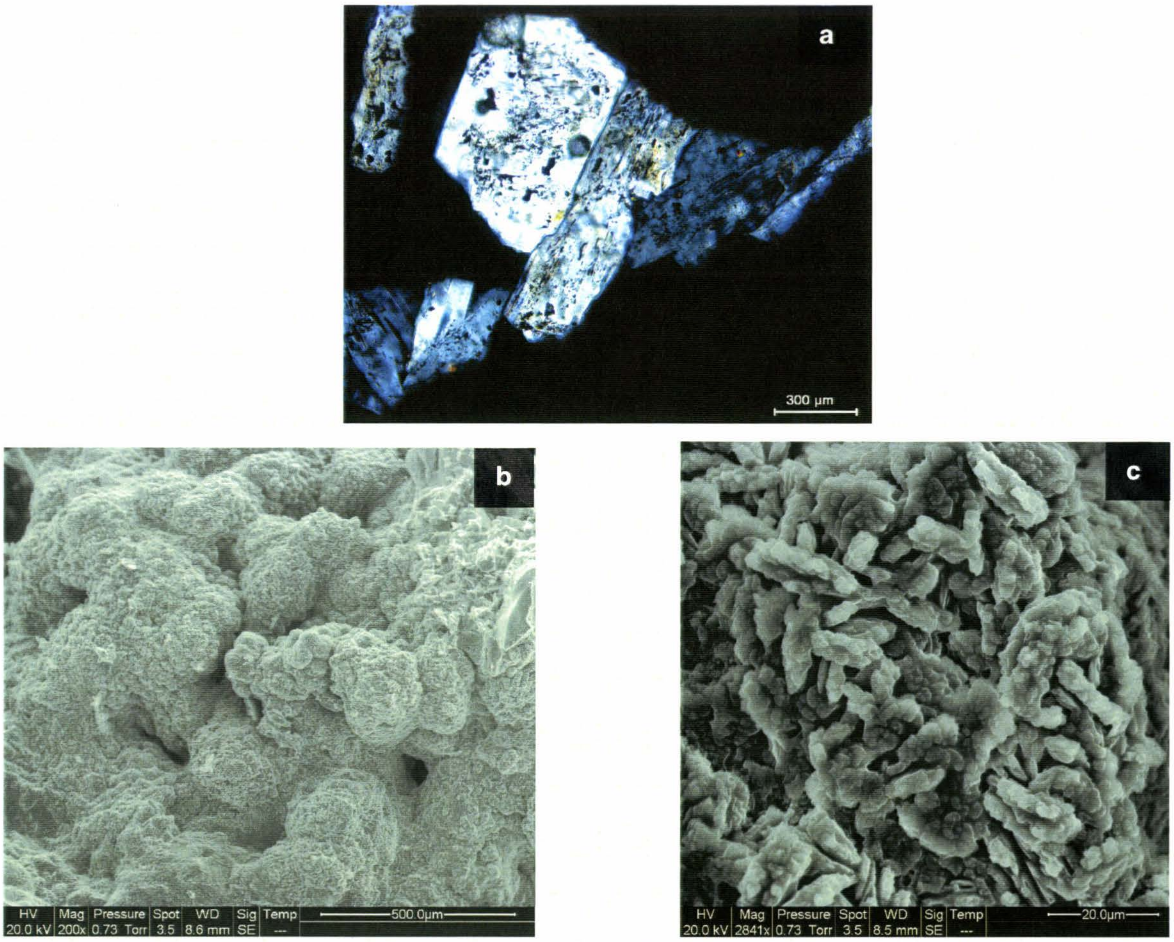

**Figure 21**. **(a)** Transmitted light micrograph of euhedral tabular crystals of gypsum (sample AV2703), CPL. **(b)** and **(c)** SEM/SE images of mascagnite showing fine-grained aggregates (sample AV2502w).

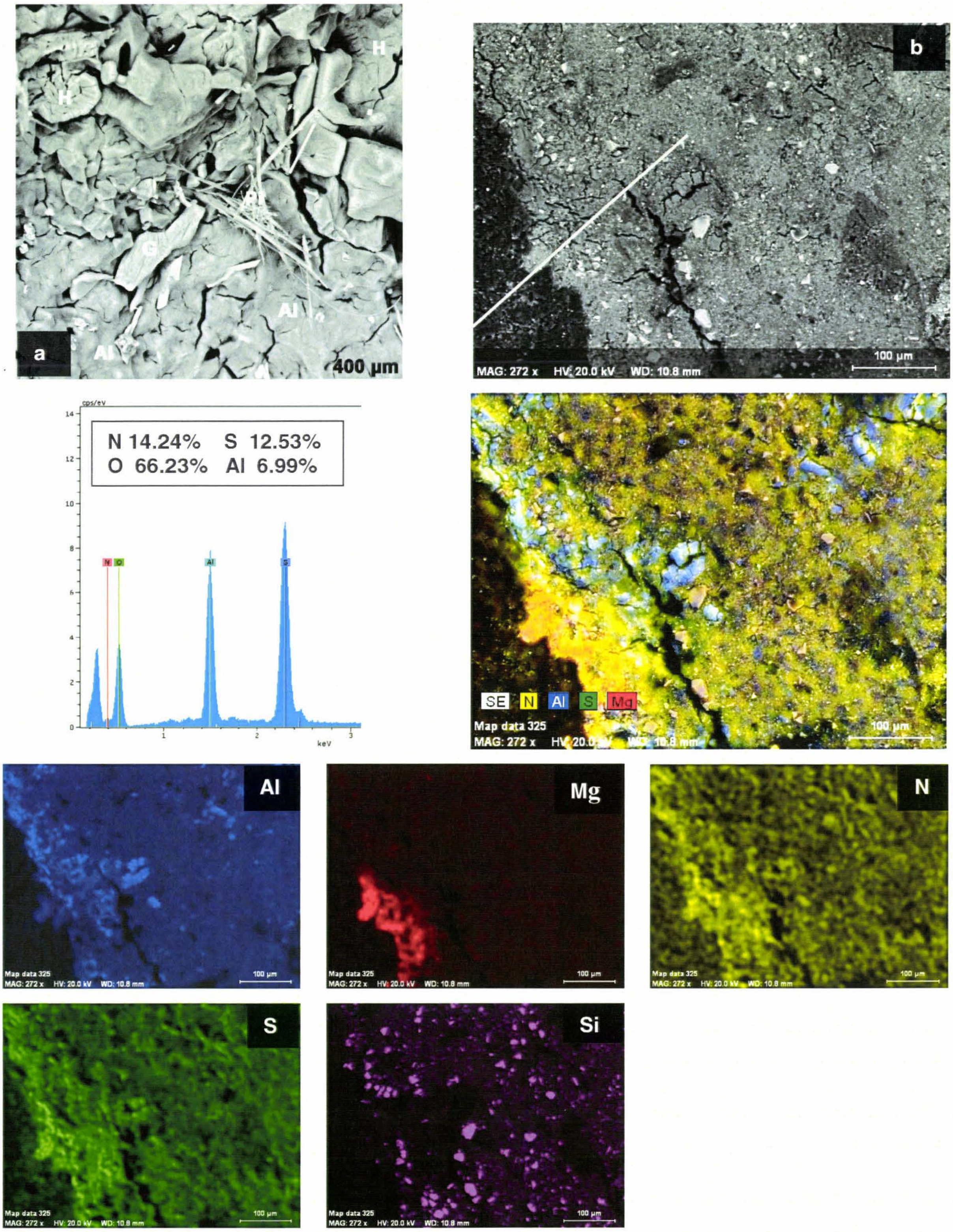

**Figure 22**. SEM images of mineral assemblage in sample AV5204. **(a)** Solid fragment BSE image. Alunagen (Al) aggregates with overgrown acicular crystals of pickeringite (Pi), minor amounts of hexahydrite (H) and gypsum (G) occur in the matrix. (b) BSE/EDS element analyses.

Lausen (1982) stated that metallic cations which gave rise to the formation of hydrous sulphates along surficial fissures associated with the United Verde mine fire in the U.S.A. were transported to the surface as gaseous oxides or molecules of the sulphates. Stracher et al. (2005) argued that those cations do not occur in the gas analyses reported by cited author. Furthermore, they pointed out that there are no published coal-fire gas studies which report that the coal fire gas may transport metal-bearing phases (e.g. Chamberlain and Hall, 1973; Kim, 1973, Giardino, 1999). These authors added that with exception of Hg, As and Se, the ambient heat energy necessary to keep metal-bearing phases volatilized would require temperatures exceeding those of any known coal fire.

The mineralogical and chemical composition of selected unaltered carbonaceous shales and sandstones and the altered baked debris are given in Table 7. The identified efflorescent sulphate minerals contain cations (Na, K, Mg, Al, Ca, Fe, Mn; see Table 6) which are found in the rock debris and in the collected condensate water. The secondary mineral assemblages that crystallized on rock debris contain metallic cations that were most likely derived from these sources.

## 5. DISCUSSION

As described above, the secondary mineral assemblages are crystallized on rock debris they contain metallic cations likely acquired from the substrate. This suggests that gas originally containing water vapour condensed as a liquid (i.e. as thin film) on the rock debris around each gas spot. If so, the resulting aqueous solution was acid-rich, containing N, S, and C compounds and water vapour originally in the gas, in addition to cations derived from hydrothermal alteration of the rock debris such as Na, Mg, K, Ca, Mn, Fe and Al. Gas cooled and ultimately resulted in crystallisation. Field observations, the direct in-situ gas analyses and analyses of collected condensate water support this process of formation of secondary minerals (Fig. 23). This is also in agreement with Stracher et al. (2005) who studied occurrences of coal fire-gas vent minerals of Inner Mongolia in China.

The process of mineralization which has given rise to the occurrences of various salt minerals at the coal waste heap in Avion is believed to be an isochemical mineralization processes. This refers to a process in which the bulk composition of a mineral is equivalent to that of the original (primary) gas phase from which it formed at a coal-fires vent.

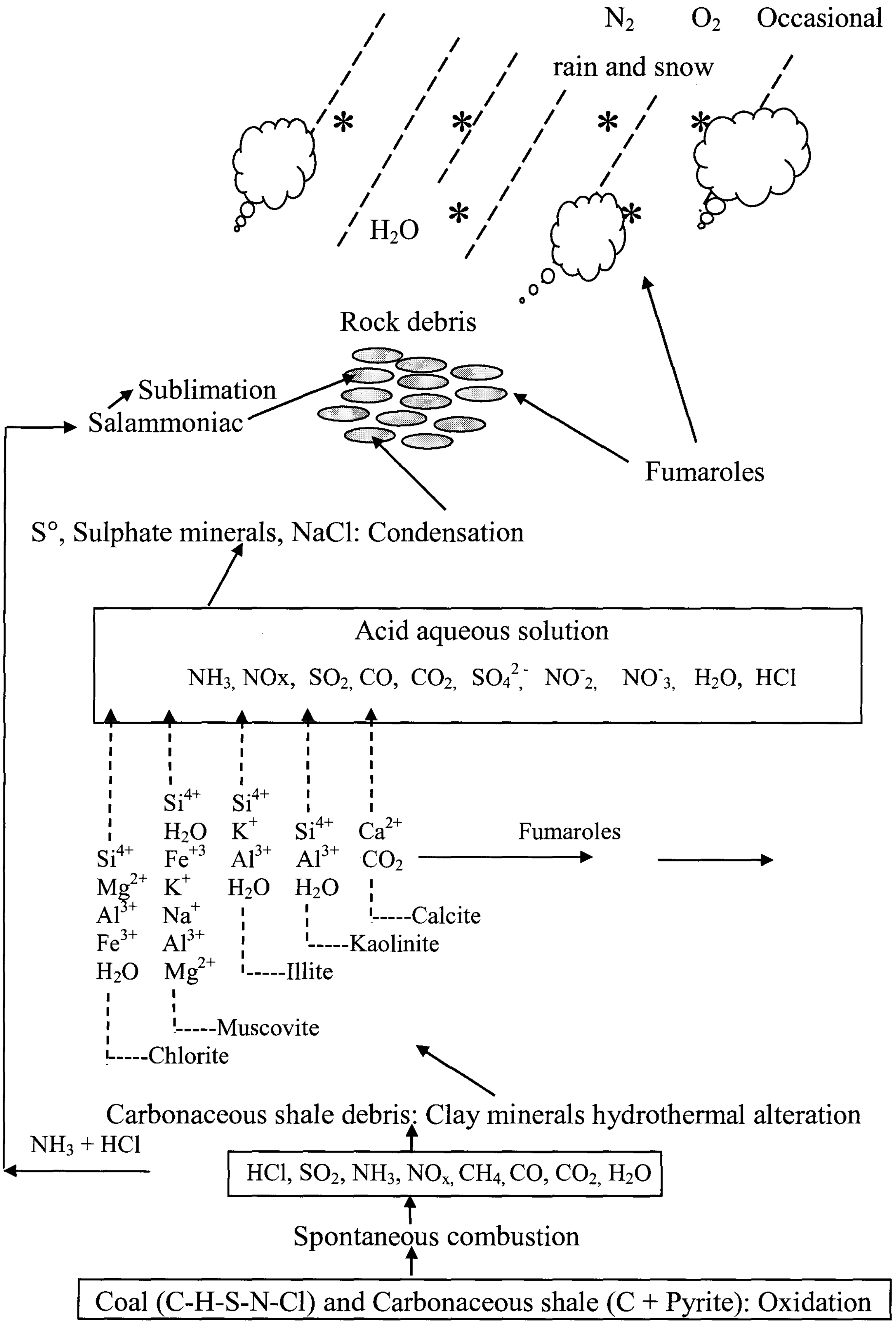

**Figure 23**. Schematic diagram illustrating the possible pathway of mineralization processes.

According to Hawley (1971, p. 231) the isochemical process is one whereby a gas undergoes a change in state during cooling and transforms directly into a liquid or a solid. Two isochemical-related processes, discussed below, may have occurred during the crystallization of minerals derived from coal-fire gas at the coal waste heap in Avion.

**(1)** the first process of mineralization, **sublimation** occurs when a gas component exhaled from a gas vent rapidly cools below the liquid to solid transformation temperature (supercools) and subsequently condenses to a solid without an intervening liquid state (Hawley, 1971, p. 832). Supercooling can occur in response to a temperature difference between the gas and the substrate (heat sink) encountered by the gas at the surface. Heat sinks include rock, sediment, vegetation, the atmosphere, etc. (Stracher, 1995; Stracher and Prakash, 2006). During sublimation, the gas condenses to a mineral substrate encountered by the gas during exhalation at the surface (Stracher, 1995; Stracher et al., 2005). Evidence for sublimation at the coal waste heap in Avion is crystallization of salammoniac on unaltered rock debris whose elements are contained in the gas. The processes of sublimation at the coal waste heap in Avion can be represented by:

$$\text{Element in the gas} \xrightarrow[\text{Supercools}]{\text{Sublimates}} \text{Elements in solid states} \qquad (1)$$

**(2)** the second process of mineral crystallization at the coal waste heap in Avion involved condensation to a liquid followed by precipitation. This process (**Gas-Liquid-Solid-sequence**) starts when a gas component (containing water vapour) first condenses to a liquid and then, as cooling continues, minerals crystallise within the liquid. The minerals form one after another according the cooling stages, temperature and relative humidity. This process has given rise to crystallization of numerous sulphate minerals and NaCl on altered baked red rock debris at the study site. Evidence for the involvement of a liquid phase includes the presence of trapped fluid inclusions in thenardite crystals (Masalehdani et al., 2005). This process can be represented by:

$$\text{Element in the gas} \xrightarrow{\text{Condenses}} \text{Element in the liquid state} \xrightarrow{\text{Precipitates}} \text{Element in solid state} \qquad (2)$$

### *5.1. Minerals originated by sublimation*

Salammoniac (isometric, $NH_4Cl$) occurs as monomineralic crusts on unaltered carbonaceous shale debris around gas spot S5. Deposition of a sublimate film from fumaroles along the surficial cracks began at temperature about 265°C. Rapid cooling of the almost colourless vapour produces a pale-yellowish-brown stain on crack walls. This stain material (sal ammoniac) is soluble in water and is removed after the first rain following its formation (Figs. 4 and 19). This mineral contains no metallic cations, and all its components are present in the analyzed gas (Table 5). The chemical composition of this mineral is not dependent on any liquid or gas reacting with the depositional materials (Stracher et al., 2005). This indicates that this mineral crystallized in a non-limited environment by sublimation as described earlier.

Sal ammoniac may be the solid-reaction product of N-, H-, and Cl-bearing coal gas components. If so, the genesis of salammoniac at $\leq 300°C$ and atmospheric pressure is due to the following reaction :

$$NH_{3\,(g)} + HCl_{\,(g)} \rightarrow NH_4Cl_{\,(s)} \qquad (3)$$

Salammoniac is chiefly found as a sublimation product on volcanic rocks near vents releasing fumes, e.g. at active Central American Volcanoes and Mount Vesuvius, Italy (Stoiber and Rose, 1974; Gaines et al., 1997). Its occurrence associated with underground burning coal seams at Tadzhikistan was found by Alexander the Great (Amethyst Galleries, Inc. 2006). It has been reported from burning coal waste heaps in eastern Bohemia, Czech Republic (Žáček and Ondruš, 1997), Donets coal Basin, and Ukraine (Panov et al., 1999). It is found in association with burning coal seams at New Castle, England (Amethyst Galleries, Inc. 2006), Mount Pyramide, Norway (Oftedal, 1922), and the Kehley's Run anthracite mines, eastern Pennsylvania (Lapham et al., 1980). This mineral has been identified as a condensation product associated with burning oil shale at Kimmeridge Bay on the Dorset Coast, Great Britain (Coal 1975; West 2001), and as a sublimate mineral from subsurface peat combustion in Mali (Svensen et al., 2003). Salammoniac was observed to sublimate in less than 24 hours at the Kehley's Run anthracite mines, eastern Pennsylvania (Lapham et al., 1980).

**Table 5.** Results of gas analyses from selected gas spots at coal waste heap n°76, Avion.

| **Gas spot** | **Gas T°C** | **$SO_2$*** | **CO*** | **$CO_2$**** | **$CH_4$*** | **$NO_X$***** | **$O_2$**** | **$H_2O$****** |
|---|---|---|---|---|---|---|---|---|
| S1 | 100.5 | <5 | N.D | N.D | 80 | 15-26 | N.D | 100 |
| S2 | 225.7 | 11 | N.D | N.D | 47 | 15-26 | 18-19 | N.D |
| S3 | 99.7 | 9.6 | 110 | 7 | N.D | 26 | 15-18 | 3550 |
| S4 | 56 | 19.8 | 22 | 6.13 | 191 | 7.87 | 14-15 | 30 |

N.D: No data * ppm ** % *** $NO_2 + NO_3$ ppm **** ml emitted in <2 hours

**Table 6**. ICP-OES and ICP-MS analyses of condensate water* from in-situ gas analyses, Coal waste heap n°76, Avion.

| **Elements** | | **Locations** | |
|---|---|---|---|
| **ppm** | **n° 76 S1** | **n° 76 S3** | **n° 76 S4** |
| Si | 0.460 | 0.110 | 0.348 |
| Ca | 1.250 | 0.470 | 4.300 |
| Fe | 0.004 | 0.004 | 0.046 |
| K | 0.860 | 0.450 | 2.041 |
| Na | 0.180 | 0.055 | 1.589 |
| Mg | 0.096 | 0.031 | 0.543 |
| Mn | 0.013 | 0.005 | 0.057 |
| Al | 1.300 | 0.500 | 0.120 |
| As | < 0.003 | < 0.003 | 0.008 |
| Ba | 0.005 | 0.003 | 0.022 |
| Cu | 0.065 | 0.009 | 0.108 |
| Pb | 0.110 | < 0.003 | < 0.003 |
| Zn | 0.190 | 0.066 | 0.212 |
| **Ions mg/L** | | | |
| $Cl^-$ | 3.3 | 0.6 | N.D. |
| $NO^{3-}$ | 2.7 | 0.5 | N.D. |
| $SO_4^{2-}$ | 2 | 0.6 | N.D. |

N.D: No data *pH = 4-5.6

**Table 7.** Chemical analyses of major and trace elements, carbon and sulphur contents in coal waste heap's rock debris, Avion.

| **Wt %** | **Shales** | | **Porcellanites** | | **Sandstone** |
|---|---|---|---|---|---|
| **Major elements** | **AV1** | **AV33** | **AV9** | **AV25** | **AV20** |
| $SiO_2$ | 54.50 | 50.90 | 59.40 | 62.40 | 68.60 |
| $Al_2O_3$ | 18.30 | 19.30 | 19.60 | 16.80 | 9.0 |
| $Fe_2O_3$** | 3.50 | 4.30 | 9.20 | 8.60 | 9.80 |
| MnO | 0.03 | 0.05 | 0.13 | 0.19 | 0.13 |
| MgO | 1.50 | 1.60 | 1.90 | 2.0 | 1.60 |
| CaO | 0.10 | 3.80 | 0.50 | 0.40 | 0.80 |
| $Na_2O$ | 0.32 | 0.54 | 0.33 | 0.59 | 0.92 |
| $K_2O$ | 2.74 | 3.53 | 2.98 | 2.99 | 1.33 |
| $TiO_2$ | 1.17 | 0.84 | 1.06 | 0.96 | 0.51 |
| $P_2O_5$ | 0.06 | 0.13 | 0.17 | 0.14 | 0.19 |
| H20 | 1.77 | 2.12 | 1.19 | 0.63 | 0.65 |
| LOI | 17.74 | 14.73 | 4.99 | 3.93 | 7.32 |
| Total | 99.91 | 99.64 | 100.29 | 99.05 | 100.24 |
| %C*** | 13.7 | 8.50 | 0.06 | 0.05 | 1.64 |
| %St**** | 0.36 | 0.20 | 0.08 | 0.09 | 0.06 |
| **ppm** | | | | | |
| **Trace elements** | | | | | |
| Ba | 454 | 506 | 468 | 455 | 223 |
| Co | 17 | 15 | 13 | 13 | 14 |
| Cr | 152 | 117 | 128 | 130 | 91 |
| Cu | 57 | 56 | 64 | 54 | 32 |
| Mo | 0.61 | 1.01 | 0.55 | 0.54 | 0.94 |
| Ni | 65 | 52 | 50 | 61 | 44 |
| Pb | 29.17 | 29.17 | 24.14 | 19.84 | 12.12 |
| Th | 12.39 | 11.98 | 12.09 | 11.62 | 5.13 |
| U | 3.01 | 3.12 | 3.59 | 3.10 | 12.12 |
| V | 156 | 134 | 143 | 133 | 76 |
| Zn | 145 | 89 | 116 | 99 | 74 |
| Zr | 200 | 140 | 172 | 201 | 119 |

** Total iron *** Total carbon **** Total sulphur

### *5.2. Minerals originated by condensation: Gas-Liquid-Solid-Sequence*

The mineralization processes at gas spots S1- S4 and S6 are complex. The minerals formed there contain metallic cations (with exception of mascagnite) which are found in the rock debris they crystallized on. Globally, as described earlier, mineralization at these locations involved condensation of cooling gas as an acid liquid followed by crystallisation on the altered rock debris (gas-liquid-solid-sequence, GLS).

All minerals described below are considered to be crystallized by a GLS condensation process but some minerals, after their crystallization, have undergone hydration and/or dehydration processes (see sections below).

### *5.2.1. Na- alkali-metal and $NH_4$-sulphat assemblage*

Mascagnite [orthorhombic, $(NH_4)_2SO_4$] occurs as a monomineralic condensate at gas spot S6 (sample AV2502w), as a dominate phase in association with lecontite and thenardite (sample 1443), and together with thenardite, glauberite, gypsum and an unknown MgMnFe-sulphate at gas spot 1 (sampleAV1443b) (Table 1).

Mascagnite was found as a sublimation product around gas vents on volcanic rocks of Mount Somma, Italy; Nymuragira, Congo and the Kamchatka Peninsula, Russia (Palache et al. 1957). It has been reported from burning coal waste heaps in eastern Bohemia, Czech Republic (Žáček and Ondruš, 1997), Donets coal Basin, Ukraine (Panov et al., 1999). Other unrelated occurrences of mascagnite are reported from geothermal field at Te Kopia in New Zealand (Martin et al., 1999).

The temperature at which mascagnite crystallizes around volcanic or coal fire gas vents is unknown. It was found forming as whitish-yellow crusts on unaltered carbonaceous shale at a burning coal waste heap in Rieulay, northern France. At this location the field crystallization temperature of this mineral was measured to be ≥400°C (in fall season and T 22°C air temperature) (Masalehdani et al., 2004, 2005).

At the present study site, mascagnite was found crystallizing in the temperature range 80-110°C (in winter season and T-10°C air temperature). This temperature range of mascagnite crystallization is too low compared to the one described above. It is assumed that it was influenced by the atmospheric conditions (rapid temperature decrease). Therefore, this temperature range may not be the actual temperature at which mascagnite crystallized at gas spots 1 and 6. Based on the direct field temperature measurements (at coal waste heap in Rieulay) we suggest that the crystallization of mascagnite around the coal fire gas vents may take place at ≥400°C.

Mascagnite does not contain metallic cations and all elements required for its formation occur in the in-situ analyzed gas sample (Table 5).The crystallization of mascagnite at gas spots S1 and S6 required high concentrations of ammonia and sulphate, the components that come directly from the combustion gas. The crystallization reaction which produced mascagnite at these gas spots upon cooling of the gas may be as follow (Sharp, 1990):

$$H_2SO_4 + 2NH_3 \rightarrow (NH_4)_2SO_4 \qquad (4)$$

As observed in SEM images, mascagnite is associated with thenardite and lecontite (samples AV1443 and AV1443a (Figs. 5 and 6). Mascagnite and thenardite are anhydrous sulphates whereas lecontite is a hydrous mineral. The anhydrous equivalent of lecontite is ammonium aphtithalite. It can be assumed that lecontite was originally ammonium aphtithalite. If so; ammonium aphtithalite crystallized following the formation of mascagnite because the aqueous solution was $NH_3$-rich and contained high concentrations of $Na^+$ and $K^+$ cations (ultimately supplied by the rock debris). Then, as a result of temperature decrease or atmospheric condition changes, as described above, it became hydrated. In this case the hydration reaction formula may be presented as follow:

$$\underset{\text{ammonium aphtithalite}}{(NH_4,K)Na(SO_4)} + 2H_2O \rightarrow \underset{\text{lecontite}}{(NH_4,K)Na(SO_4).\ 2H_2O} \qquad (5)$$

The occurrence of thenardite in the studied samples required a supply of $Na^+$ and $SO_4^{2-}$. The coexistence of thenardite and mascagnite may be a result of contemporaneous crystallization from the aqueous solution. Textural relationships support this hypothesis (Figs. 5 and 6).

The assemblage mascagnite-thenardite-lecontite is known from coal fire gas, indicating that their coexistence is not impossible. However, apart from this study, the authors could only document the occurrence of ammonium aphthitalite and lecontite as a product of bat guano from Las Piedras Cave, Honduras (Winchell and Benoit, 1951).

In sample AV1443b mascagnite and thenardite are associated with minor amounts of glauberite, gypsum and an unknown MgFeMn-sulphate (Fig. 6). Association of thenardite with glauberite and/or gypsum is a common occurrence in salt lakes and volcanic environments, but crystallization of glauberite in a mascagnite matrix (Figs. 6b, 6c ) is uncommon. Glauberite crystallized directly from the remaining of $SO_4^{2-}$, $Ca^+$ and $Na^+$ in the aqueous solution after the formation of gypsum and thenardite.

Although unrelated, glauberite occurs in some settings as a reaction product of interstitial brines rich in $SO_4^{2-}$ and $Na^+$ and pre-existing gypsum (Orti et al., 2002):

$$2CaSO_4.2H_2O_{(s)} + 2Na^+_{(aq)} \leftrightarrow CaSO_4.Na_2SO_{4(s)} + Ca^{++}_{(aq)} + 4H_2O_{(aq)} \tag{6}$$

An unknown MgFeMn-sulphate occurs in this specimen (Figs. 6b-h). The Mg:Fe:Mn ratio determined by WDS analysis is 8:3:2 (Table 3). $Mg^{2+}$, $Fe^{3+}/Fe^{2+}$and $^+$ $Mn^{2+}$ are present in minerals of the original substrate. Concentration of Mn in the carbonaceous shale and in the baked debris is ≤2 wt% (Table 7). It is likely that Mg and Fe are substituted by Mn. The MgFeMn-sulphate could be a new mineral. The crystals of this mineral as observed by SEM images do not have acicular, fibrous habits like those observed for pickeringite, for example. It is highly unlikely that this unknown sulphate belongs to mixed divalent-trivalent metal sulphate salts of halotrichte group. From electron microprobe analysis (Table 3) it seems like that it is a hydrated Mg-bearing mineral with $Mg_xFe_yMn_{1-x-y}SO_4.nH_2O$ as chemical formula. The mineralization processes at gas spots S1- S4 and S6 are complex. The minerals formed there contain metallic cations (with exception of mascagnite) which likely find in the rock debris they crystallized on. Globally, as described earlier, mineralization at these locations involved condensation of cooling acidic rich gas (aqueous solution) as a liquid followed by solidification (GLS-sequence) on the altered rock debris.

Although, generally all the minerals described below are considered to be crystallized by GLS-sequence condensation process but some minerals, after their crystallization, at gas spots S1, S3 and S6 have undergone further hydration and/or dehydration processes (see section below).

### *5.2.2. Mg-Na- alkali-metal-sulphate assemblage*

The mineral assemblages discussed in this section are principally sulphates of Mg and Na, with minor amounts of K and Ca. The mixed hydrous, anhydrous and double sulphate minerals found at gas spots S2 and S4 are particularly interesting and unique. As described earlier, the mineralization processes associated with coal-fire gas is rather analogous to the exhalation-condensation of minerals which form in solfataric or other fumarolic environments. The minerals, discussed in this section, globally occur as incrustations around fumaroles of volcanoes and/or are known as marine or non-marine evaporite minerals.

Prediction of formation sequences of Na-K-Mg bearing minerals herein is very difficult because of the number of identified salts with similar solubility and the complex solution chemistry.

### *5.2.3. Mg-bearing sulphate mineral assemblage*

The occurrence of bloedite, konyaite, epsomite and hexahydrite with minor amounts of thenardite at gas spot S2 (sample AV2503) indicates $Mg^{2+}$ and $Na^{+}$ rich aqueous solutions.

The mineral assemblage in sample AV2503 contains bloedite-konyaite and epsomite-hexahydrite. The coexistence of these phases indicates transformation processes. Thus, it is possible to assume that following the formation of the mineral assemblage due to momentary slight temperature and relative humidity (RH) increase and/or decrease minerals have undergone hydration or dehydration processes. The transformation of these minerals may have also occurred following sample collections from the gas spots. This has yielded the hydration of bloedite to konyaite (7) and dehydration of epsomite to hexahydrite (8). Such hydration and dehydration reactions may be presented as follows:

$$Na_2Mg\,(SO_4)_2.4H_2O + H_2O \rightarrow Na_2Mg\,(SO_4)_2.5H_2O \qquad (7)$$

$$Mg\,SO_4.7H_2O \rightarrow Mg\,SO_4.6H_2O + H_2O \qquad (8)$$

According to (Jambor et al. 2000; Chipera (2004) epsomite and hexahydrite will hydrate or dehydrate in response to local conditions i.e. temperature or relative humidity (RH) about 48°C.

SEM/EDS analyses show minor amounts of thenardite in sample AV2503 (Figs. 7b and 7e). From textural relationships shown by this mineral assemblage it appears likely that thenardite has crystallized after the formation of bloedite and epsomite when $Mg^{2+}$ was depleted from the solution.

### *5.2.4. Na-Mg-K-Cl- bearing mineral assemblage*

At gas spot S4 thenardite occurs as a single phase and/or in association with bloedite, K-bearing sulphates and halite.

**(1)** Thenardite occurring as a single phase (samples AV8111 and 2344W, Fig. 4). For these occurrences, it is likely that other cations were removed from the aqueous solution (i.e. poor in $Mg^+$ and $K^+$) and the solution was high in $Na^+$. Crystallization of thenardite also suggests that this mineral has reached to its stability line at temperatures >30°C and it was preserved.

Thenardite ($Na_2SO_4$), orthorhombic, occurs in non-marine evaporite deposits e.g. in arid climates in Great Konya basin, Turkey and in Aran Playa, Kashan, Central Iran (Driessen et al., 1973; Khalili and Torabi, 2003), on soils of the Jequetepeque Valley, northern Peru and the Otjomonogwa pan, Namibia (Mees and Stoops, 1991; Mees, 2003); in saline lakes of Taoudenni-Agorgott basin, northern Mali, Searles Lakes, California, and Sambhar Salt Lake in Rajasthan, India (Mees 1999; Amethyst Galleries, Inc. 2004; Sinha, Raymahashy, 2004). It also occurs around fumaroles in Central American volcanoes (Stoiber and Rose, 1974).

In the system $Na_2SO_4$-$H_2O$, thenardite is reported to precipitate directly from solution at temperatures ≥32.4°C and at relative humidity (RH) ≤71%. Below this temperature, the stable phase is mirabilite ($Na_2SO_4.10H_2O$) (Linke, 1965; Knacke and Von erdberg, 1975; Arnold, 1976). Note that mirabilite was not identified in none of the specimens studied and the field temperature of incrustation at spot S4 was ≥100°C (Table 1).

Thenardite has unusual solubility characteristics in water, its solubility increases between 0 and 32.4°C, where it reaches a maximum of 49.7g/100g water (Fig. 24). At this point the solubility curve changes slope and the solubility becomes almost independent of temperature. In the presence of NaCl, the solubility of thenardite is markedly diminished (Linke and Seidell, 1965).

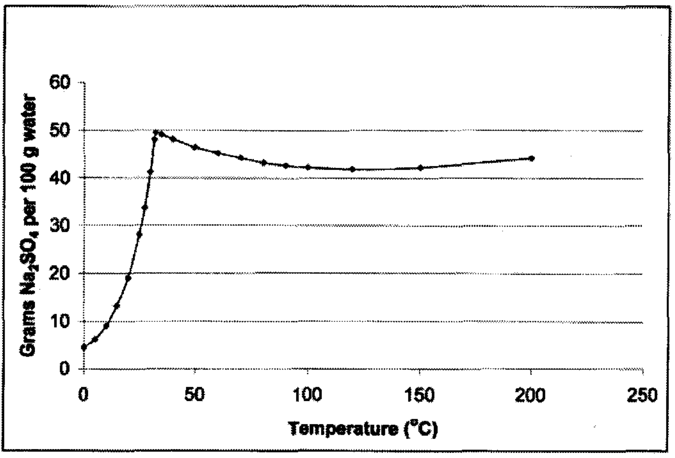

**Figure 24**. Solubility of sodium sulphate vs temperature (after Linke and Seidell, 1965) .

Thenardite may be formed by different processes and reactions. Sublimation of thenardite around volcanic gas vents occurs at high temperature and it persists during cooling (Williams-Jones et al., 2002). According to Stoiber and Rose (1974) thenardite sublimated at temperatures ≥330°C by reaction (9) around fumaroles of active Central Volcanoes. These authors suggested that the reaction involves purely gas-solid reactions which imply that participating cations are present in the gas as volatile halides, which is an unrealistic model.

$$2NaCl_{(g)} + SO_{3(gas)} + H_2O_{(g)} \leftrightarrow Na_2SO_{4(s)} + 2HCl_{(g)} \qquad (9)$$

**(2)** Thenardite associated with bloedite in more or less equal proportions (samples AV1443g and AV1443h). The coexistence of these sulphates is common in saline lakes and soil environments (Driessen and Schoorl, 1973; Mees, 1999) but very uncommon around coal fire gas vents. Microscopic and SEM images of the mineral assemblages have shown (Figs.11b, 11c) that thenardite crystals are grown in the bloedite matrix indicating that it has crystallized after the formation of bloedite.

**(3)** Thenardite and bloedite associated with aphthitalite (samples AV1443d and AV1443f), this indicates the high Mg, Na and K content in the aqueous solution. The optical and SEM images (Figs. 11 and 12) suggest that bloedite crystallized first and was followed by thenardite and aphthitalite. The salinity of the thenardite crystallizing solution seems to have been high in Cl, the fluid inclusions of this composition are trapped in crystals of thenardite in sample AV1443d (see Chapter VI).

Aphthitalite [$(K, Na)_3Na(SO_4)_2$], trigonal is a rare non-hydrated double salt. In view of its variability in composition, the question arises as to the constitution of aphthitalite whether it is a mixture of solid solution of two sulphates, or whether it represents, as is commonly supposed, a double salt (Washington and Merwin, 1921). Aphthitalite is reported to form as sublimates around fumarolic environment at very high temperatures (≥300°C) (Stoiber and Rose 1974; Williams-Jones 2002). Genge et al., (2001) reported fumarolic deposits of aphthitalite by $H_2O$-dominated gas on recent natrocarbonatite lava flows in northern Tanzania. These authors concluded that this salt mineral formed by sublimation process (gas-solid) and at ≈600°C.

**(4)** Thenardite, bloedite and aphthitalite associated with halite, langbeinite and unknown KNaMg-sulphate (samples AV1443e, Figs. 15, 16 and 17). Thenardite, bloedite, aphthitalite also occur in association with minor amounts of halite and arcanite (sample 1443i). The coexisting of NaCl with thenardite and bloedite indicates that the aqueous solution was not entirely saturated in NaCl, and its salinity was high. Halite in this assemblage seems to be the latest encrusted phase which has formed at reduced humidity (i.e. water vapour) conditions. Stoiber and Rose (1974) stated that halite in fumaroles of Central American Volcanoes formed at 100-200°C, a temperature range in good agreement with the field temperature measurements at the study site.

However, as described earlier, high chloride content decreases the solubility of thenardite. Zadanovskii et al. (1973) and Christov and Moller (2003) studied solute and solvent activities and solid-liquid equilibria in the H-Na-K-OH-Cl-$HSO_4$-$H_2O$ system from dilute to high solution concentration within the 0° to 250°C temperature range. They noted that from 0° to 200°C, the ternary solubility of thenardite decreases with increasing concentration of sodium hydroxide.

The crystallization of Mg-K-bearing minerals indicates relative abundance of $Mg^+$ and $K^+$ in the aqueous solution which has favoured the formation of langbeinite, aphthitalite and unknown KNaMg-sulphate. The coexistence of two K-bearing minerals aphthaitalite with langbeinite and/or aphthaitalite with arcanite indicates simultaneous formation of these sulphates at high temperature of the crystallization system (Stewart, 1963; Stoiber and Rose 1974; Rahimpour-Bonab and Kalantarzadeh, 2004). The occurrence of aphthitalite and arcanite is reported from a cave in Saudi Arabia (Forti et al. 2004). Unfortunately no experimental data are available to interpret the coexistence of langbeinite with aphthitalite and bloedite at temperature ≥100°C.

In addition to above minerals, well-crystallized possible new KNaMg-sulphate is found in sample AV1443e. This also indicates a $K^+$-rich solution. The composition of this new mineral is characterised by $K^+>Na^+>Mg^{2+}$ (Table 4). Extra investigations (XRD) are necessary to complete data of this possible new sulphate mineral prior to publication.

### *5.2.5. K-bearing Al sulphate mineral assemblage*

Sulphates occurring in samples AV1955 and AV 5204 at gas spots S3 and S4 are all hydrated $Al^{3+}$, $Mg^{2+}$, $K^+$ and $Ca^{2+}$ minerals. The coexisting of kalinite, pickeringite, alunogen, epsomite, hexahydrite and gypsum as cryptocrystalline fibrous material in sample AV1955 suggests that the resulting aqueous solution was acid and K-Al-Mg rich. All the minerals in this assemblage are hydrated sulphates, suggesting that initially formed phases were altered at some stage. In sample AV1955, gypsum is the first mineral to form from the solution of this assemblage since it is known to be the less soluble sulphate mineral (Spencer, 2000). Epsomite crystallized following gypsum.

Epsomite ($MgSO_4{\cdot}7H_2O$), orthorhombic, and hexahydrite ($MgSO_4{\cdot}6H_2O$), monoclinic are found in marine and lacustrine evaporite deposits, in weathering zones of coal and metallic deposits, in some soils and possibly on the surface of Europa (Chou and Seal, 2003). Hexahydrite bears a strong resemblance in physical and chemical properties to epsomite, a mineral with which it is often associated. Occurrences revealed by XRD analyses are not always easily confirmed by thin section studies.

Needle-like crystals of pickeringite in sample AV5204 (Figs. 22a and 22b) enclose small aggregates of alunogen, indicating that this phase crystallized before the formation of alunogen. Pickeringite or magnesium alum [$MgAl_2(SO_4)_4.22H_2O$], monoclinic, belongs to the mixed divalent-trivalent metal sulphate salts of the halotrichte group (Jambor et al 2000). It is often associated with alunogen and it has been reported from the Kateřina burning coal waste heaps in Radvanice, eastern Bohemia, Czech Republic (Žáček and Ondruš, 1997), Donets coal Basin, Ukraine (Panov et al. 1999) and Rieulay, northern France (Masalehdani et al., 2004).

Alunogen is not dominant phase at those locations. It appears as a late crystallized mineral phase.

Kalinite [$KAl(SO_4)_2.11H_2O$)], monoclinic also known as natural alum was discovered in 1868 (Dana's System of Mineralogy, 1951). It has been reported from partly related environments as an alteration product such as from Ruatapu cave, Orakei Korako geothermal field in New Zealand and from the crater lake of Kawah Ijen volcano, Indonasia; and from evaporative sulphate salts on Boulder Creek at Iron Mountain, California (Keith et al. 2001). The higher hydrate equivalent of kalinite is potash alum ($KAl (SO_4)_2.12H_2O$), which is reported to form near fumaroles of Melos geothermal field in Greece (Hall et al., 2003).

Kalinite in sample AV1995 could be a dehydration product of K-alum (9) which crystallized after the formation of pickeringite, and then later it has rapidly dehydrated to kalinite due to temperature increase as described above. The dehydration reaction can be presented as:

$$KAl\,(SO_4)_2.12H_2O \rightarrow KAl\,(SO_4)_2.11H_2O + H_2O\uparrow \qquad (9)$$

EDS element mapping (Fig. 10e) of some mixed fibrous phases in sample AV1955 showed occurrences of Fe. This indicates that some $Mg^{2+}$ was substituted by $Fe^{2+}$ (Fe:Mg = 6:7 wt%), the halotrichite-pickeringite series are known to be the most soluble salts among which extensive solid solution often takes place (Jambor et al. 2000).

### *5.2.6. Al-$NH_4$ sulphate mineral assemblage*

The Al-alkali-metal and $NH_4$-sulphate minerals crystallized at gas spot S6 are mainly salts of Al and Mg (samples AV5204 and AV5204a), a mixture of hydrous sulphates. Tschermigite is the main phase followed by alunogen and pickeringite.

Tschermigite, occurs as a groundmass constituent (sample AV5204). Individual crystals of this mineral were not observed in SEM images (see section 4.1.6). Pickeringite shows a similar occurrence as described earlier. Tschermigite [$(NH_4)Al(SO_4)_2.(H_2O)_{12}$], cubic, was discovered in 1853 at Tscherming, Kaaden, Ústi Region, Czech Republic (Amethyst

Galleries, Inc., 2006). Essential components of tschermigite are ammonia and sulfur that come from escaping coal-fire gas. The host environment where tschermigite forms is around burning coal seams and coal waste heaps such as at Inner Mongolia, China (Stracher et al. 2005), at eastern Bohemia, Czech Republic (Žáček and Ondruš, 1997), and at Rieulay, northern France (Masalehdani et al. 2004, 2005). Other occurrences of tschermigite, unrelated to this environment, are reported from the Te Kopia geothermal field, Taupo Volcanic Zone, New Zealand (Martin et al. 1999).

Alunogen [$Al_2(SO_4)_3.17H_2O$], triclinic, has been reported from numerous environments, at the Kateřina burning coal waste in Radvanice, eastern Bohemia, Czech Republic as a product of alteration of rock debris (Žáček and Ondruš, 1997); as incrustation around gas vents at Inner Mongolia, China (Stracher et al. 2005), and in hydrothermal and evaporitic settings at the Glen Lyon anthracite mine fire in eastern Pennsylvania Lamph et al. (1980). Other occurrence of this mineral includes fumaroles incrustations at active Central American volcanoes (Stoiber and Rose, 1974); around geothermal fields at Te Kopia in New Zealand and near fumaroles of Melos in Greece (Martin et al. 1999; Hall et al., 2003).

Alunogen is supposed to form under highly acidic (pH ≤3) and arid conditions in geothermal system, when steam condenses, alunogen is the principal stable Al sulphate phase to form (Nordstrom, 1982). In contrast, according to Martin et al. (1999) the formation of tschermigite requires either more specific conditions and/or favourable ionic activities that occur only locally, because it is more soluble than alunogen and it demands a more sheltered environment.

Chemical reactions through which alunogen or tschermigite crystallize around gas vents at burning coal seams or coal wastes, are non-existent. Stracher et al (2005) noted the resultant alunogen and tschermigite around gas vents at Wuda coalfield in China as products of hydrothermal alteration of metal bearing minerals in quartzofelspathic sand and sandstone followed by cooling of acid aqueous solution at ≥260°C and ≥230°C respectively. According to Nordstrom (1982), kaolinite in the host sediment of non-burning coal waste heaps may decompose in acid sulphate fluids, under appropriate conditions, to form alunogen :

$$Al_2Si_2O_5(OH)_4 + 6H^+ + 3SO_4^{2-} + 16H_2O \rightarrow Al_2(SO_4)_3.17H_2O + 2H_4SiO_4 \qquad (10)$$

Martin et al (1999) noted that this process is reversible and that alunogen exposed to fluids less acid than that from which it formed, in the presence of non-crystalline silica, it will itself react to yield kaolinite. Hall et al (2003) illustrated the following processes for the origin of alunogen near fumaroles in geothermal field at Melos in Greece, at ≤100°C and in wet weather conditions:

$H_2S_{(igneous)} + 1/2O_2 \rightarrow S° + H_2O$ (11)

$6S° + 6H_2O + 9O_2 \rightarrow 6H_2SO_4$ (12)

$6H_2SO_4 + Al_4Si_4O_{10}(OH)_8 \rightarrow 4AlSO_4^+ + 4SiO_2 + 10H_2O + 2SO_4^{2-}$ (13)

$2AlSO^+_4 + SO_4^{2-} + 17H_2O \rightarrow Al_2\,(SO_4)_3.17H_2O$ (14)

XRD patterns of selected altered baked rock debris from study area show no evidence peaks for existence of kaolinite, metakaolinite, and/or Al-spinel in samples AV5204 and AV5204a. This indicates the complete break down of primary cations of kaolinite in carbonaceous shales during thermal processes. This thermal (baking) process supplied $Al^{3+}$ for the formation of Al-sulphates at gas spots S3 and S6. Silica in kaolinite mineral was left in altered baked debris because its solubility is limited in low temperature acidic process (Halls et al., 2003).

Regardless of the precise chemical reaction, the formation of tschermigite, alunogen and pickeringite required a ready supply of $Mg^{2+}$, $Al^{3+}$, $SO_4^{2-}$, $H_2O$ and $NH_3$. The resulting aqueous solution contained water vapour, S, N, and $Al^{3+}$ from kaolinite and $Mg^{2+}$ from chlorite. Upon cooling, tschermigite and pickeringite and alunogen crystallized on altered baked rock debris. As described above, tschermigite occurs as the dominant phase, followed by pickeringite and/or alunogen. This implies that the activities of ammonia locally remained high and it was not removed from the aqueous solution. Similarly magnesium ions were available to crystallize pickeringite following tschermigite. Alunogen occurs as the late crystallized phase and it is not a dominant mineral at gas spot S6, because its formation acquired the depletion of $NH_3$ and Mg from the solution. Rodgers et al (2000) specified that for alunogen to be the dominant phase the activities of other ions should remain low.

### *5.2.7. Native elements and Gypsum*

The low temperature (80-100°C) yellow sulphur is the only native element found crystallized as monomineralic crust on altered rock debris around steam emitting vents in gas spot S6. The origin of sulphur is the substrate of the coal waste heap itself (coal, pyrite and carbonaceous shale) (Table 7). At the study site sulphur in the form of native (S°) does not occur as an abundant phase may be because it is lost as $SO_2$ during cooling of gas and/or was simply melted. Liquid sulphur forms at 175°C and is replaced by monoclinic sulphur at about 110°C (Africano and Bernard, 2000). Harris and Maciejewski (2000) noted that yellow sulphur i.e. monoclinic β-S8 and/or orthorhombic α-S8 allotropes melt at 112.8 and 119.6°C, respectively.

It should be noted that, the in-situ gas analysis (Table 5) has not revealed any $H_2S$ gas, indicating that it may have been oxidized by atmospheric oxygen to produce $SO_2$ (Masalehdani et al. 2005). According to Kusakabe and Komoda (1992) at low temperatures ($T \leq 200°C$) the following reactions (13) and (14) can produce elemental sulphur in the fumarolic environment:

$$4SO_{2(g/l)} + 3H_2O_{(g/l)} \leftrightarrow 3H_2SO_{3(l)} \qquad (15)$$

$$3H_2SO_{3(l)} \leftrightarrow 2H_2SO_{4\,(l)} + S^\circ + H_2O_{(g/l)}\uparrow \qquad (16)$$

Among all the minerals identified, gypsum is the least abundant sulphate. It occurs in association with other minerals and/or as a single phase. The minor occurrence of this sulphate is due to (1) the low calcium content of the original carbonaceous shale debris (2) the low solubility of gypsum.

## 6. IMPACTS

Sulphate salt and halides described herein are all soluble salts and therefore transient. The efflorescence dissolve leaving no residues in deionized water are thus removed in the first rainfall after their formation. All the minerals identified at the burning coal waste heap in Avion do have negative impacts on the environment and on the human health. In addition to metallic cations, S and N they also contain metallic trace elements.

Chemical analyses of selected sulphate minerals show that these minerals contain trace elements such as As, Ba, Cu, Mo, Cs, Ni, Rb, Th and U etc (Table 8). The salt minerals can be vectors for metal pollution of waters and soils and for toxins transmitted to humans by crop (food) grown in soils around the coal waste heap (Fig. 2b). Such pollutants resulted from coal fires (e.g. As poisoning or hyperkeratosis) already killed many people (Finkelman, 2004).

Slow dissolution of $NH_4$-bearing minerals (salammoniac, mascagnite and tschermigite) and their migration into groundwater and surrounding agricultural soils may increase the salt concentration and can destroy nearby flora and faunal habitats, further interaction of gas with oxygenated atmospheric precipitation results in $NO^{3-}$ and $NO^{2-}$ (Tables 1 and 5). The migration of nitrates and nitrites into the groundwater may increase the nitrogen content and cause local water pollution. Chemical analysis of collected drinking water (from tap water at the study site) is given in Table 9. It shows that the nitrate content of such drinking water is above the threshold level of 45 mg/l. Arsenic concentration at the moment remains below the threshold level of <0.05 mg/l (USPHS, 2002).

In addition, migration of Na-Mg-bearing minerals into surrounding soils may also increase salt content of the soil, dissolution of Al-bearing minerals are known to result acid mine drainage (AMD) (Bigham and Nordstrom, 2000).

Regular sampling and analysing of surface water and drinking water around burning coal waste heaps should be done in order to determine their ion and trace element contents in comparison to TLV (Threshold limit value). The burning coal waste heap may become a more important source of salinity and trace elements, considering the high concentration of dissolved sulphates and halides

Gas exhaled from surficial vents and fissures and different soluble minerals originated from cooling gas reveal important information about the chemical composition of burning coal and the possible interaction of the gas with rock and water on its way to the surface prior to exhalation. The chemistry of these minerals and the exhaled gas is reflective of elements and compounds that may be released as pollutants into the atmosphere, soil, streams, or ground water. Such pollutants may be responsible for a variety of environmental and human health problems including the destruction of floral and faunal habitats. Consequently, the study of the chemical nature, modes of formation of minerals associated with burning coal waste heaps can be critically useful in understanding environmental pollution problems associated with coal waste heap fires around the world.

**Table 8** . Chemical analyses of selected sulphate secondary minerals.

| **Major elements %** | **AV1443a** | **AV1443i** | **AV2503** |
|---|---|---|---|
| $SiO_2$ | 0.21 | 0.00 | 0.75 |
| $Al_2O_3$ | 0.42 | 0.00 | 0.42 |
| $Fe_2O_3$** | 0.00 | 0.00 | 0.12 |
| MnO | 0.04 | 0.00 | 0.01 |
| MgO | 0.00 | 8.59 | 13.73 |
| CaO | 0.00 | 0.00 | 0.07 |
| $Na_2O$ | 5.80 | 23.69 | 10.85 |
| $K_2O$ | 0.41 | 1.82 | 10.85 |
| $TiO_2$ | 0.00 | 0.00 | 0.013 |
| $P_2O_5$ | 0.00 | 0.47 | 0.035 |
| H20 | N.D. | N.D. | N.D. |
| LOI | 85.99 | 27.02 | 57.65 |
| Total | 92.87 | 60.95 | 83.90 |
| %N*** | 17.65 | N.D. | N.D. |
| %St**** | 22.38 | 19.94 | 17.10 |
| **Trace elements ppm** | | | |
| As | 2.17 | 4.55 | 14.0 |
| Ba | 3.90 | 6.10 | 12.90 |
| Co | 0.56 | 3.29 | 1.00 |
| Cr | 0.00 | 23.1 | 0.00 |
| Cu | 7.90 | 17.5 | 5.90 |
| Mo | 0.00 | 2.01 | 0.93 |
| Ni | 0.00 | 5.6 | 0.00 |
| Pb | 0.00 | 0.00 | 0.00 |
| Th | 0.13 | 0.09 | 0.29 |
| U | 0.44 | 0.23 | 0.28 |
| V | 1.60 | 2.90 | 3.60 |
| Zn | 0.00 | 0.00 | 0.00 |
| Zr | 0.00 | 31.10 | 3.81 |

N.D. No data    ** Total iron    *** Organic nitrogen
**** Total sulphur

**Table 9**. Chemical analysis of drinking water at the coal waste heap Avion.

| **Elements mg/L** | |
|---|---|
| Si | 6.46 |
| Ca | 142 |
| Fe | 0.02 |
| K | 2.37 |
| Na | 2.03 |
| Mg | 4.79 |
| Mn | N.D. |
| Al | 0.02 |
| Ba | 0.027 |
| As | 0.02 |
| Cu | 0.02 |
| Pb | 0.02 |
| Zn | 0.02 |
| **Ions mg/L** | |
| $Cl^-$ | 36.60 |
| $NO^{3-}$ | 46.50 |
| $SO_4^{2-}$ | 32.50 |

N.D: No data

## 7. CONCLUSIONS

Studies of burning coal waste heap at Avion demonstrate that mineral assemblages reminiscent of volcanic condensates and sublimates. The mineral assemblages are produced due to thermal metamorphism of fine-grained sedimentary rock debris by coal fire. Many elements (alkaline earths, sulphur and trace metals) are easily leached from the fine-grained carbonaceous shale debris by hydrothermal alteration (aqueous solution, with slightly acidic pH 4 to 5.5). Thus, most encrustations and crystalline phases are deposited in vapour-rich environment, with temperature ranges 40-265°C. Under this environment the vapour could become an effective hydrothermal fluid capable of leaching cations and anions from rock debris (Ellis and Mahon, 1967), fumarolic minerals form following cooling of the vapour upon reaching the surface of the coal waste heap. The difference in temperature is reflected in the mineralogy of the phases. We found that encrustations and/or crystallizations deposited at high temperatures (≥ 300°C) are less abundant than those deposited at lower temperatures (≤120°C°). These data are in agreement with the observations of Stoiber and Rose (1974).

21 efflorescence minerals, native sulphur and two possibly new sulphates found in association with this burning coal waste heap. The identified minerals are anhydrous or hydrous minerals suggesting that the mineralization achieved by more than one process and at varied temperature ranges. This includes:

- direct sublimation at temperature ≥265°C
- condensation (Gas-Liquid-Solid) at temperature ranges between 40-110°C. Following this mineralization process certain phases have undergone alteration (hydration and/or dehydration). The alteration has possibly occurred due to momentary temperature decrease and/or increase during mineralization process and/or due to removal of specimens from the gas spots and prior to analyses. Discovery of fluid inclusions trapped in crystals of thenardite revealed the high salinity and sulphate-rich aqueous solution. This also puts in evidence that the mineralization process of this new mineral assemblage occurred by gas-liquid-solid condensation process.

Variations between mineral assemblages are possibly due to (1) disproportionate of coal within the coal waste; continuous gas-rock interaction may have influenced the chemistry of escaping gas to the surface; (2) diversity of chemical composition within and among the rock debris; (3) temperature of cooling rate of the gas; influence of atmospheric conditions (i.e. seasons, meteoric water etc); and high salinity of the aqueous solution. The fluctuating temperatures and concomitant effects on the assemblage are accounted for by variations in combustion and atmospheric conditions and possibly removal (temperature decrease) of the assemblage from the vent during sample collecting.

Sulphates such as alunogen, tschermigite, pickeringite, halotrichite, epsomite and gypsum which occur encrusting on rock debris at the coal waste heap in Avion have already been reported elsewhere in association with coal fire gas (i.e. burning coal seams or coal waste heaps). Occurrence of unique rare mineral assemblage mascagnite, lecontite, thenardite, bloedite, aphthitalite, glauberite, langbeinite and halite are first known from coal fire gas. The same can also be said about kalinite which is not a product of coal fire gas. Thenardite, bloedite, aphthitalite, glauberite, langbeinite and halite are evaporitic or volcanogenic (with exception of bloedite) in origin. The present study gives them a new origin, minerals of coal fire gas from burning coal waste heaps. Further gas analyses and investigations are necessary to determine if the coal fire gas (including water vapour) can transport metallic cations as gaseous volatile oxides to the surface.

# REFERENCES

Africano, F. and Berbard, A. (2002). Acid alteration in the fumarolic environment of Usu volcano, Hokkaido, Japan. Journal of Volcanology and Geothermal Research, **97**, Iss. 1-4, 475-495.

Amethyst Galleries, Inc. (2006). Mineral Galleries, 830-13 AIA North no.322, Ponte Verda Beach, Florida.<http://mineral.galleries.com>

Arbor,A. (1990). Hand book of Chemistry and Physics, 7th edition, CRC Press, Michigan.

Arnold, A. (1976). Behavior of some soluble salts in stone monuments. In: T.H. Skoulikidis (Ed.), 2nd International symposium on the deterioration of building stones, National Technical University, Athens, 27-36.

Bell, F.G., Bullock, S.E.T., Hälbich, T.F.J. and Lindsay, P. (2001). Environmental impacts associated with an abandoned mine in the Witbank Coalfield, South Africa. International Journal of Coal Geology, **45**, 195-216.

Bigham, J.M. and Nordstrom, D.K. (2000). Iron and aluminium hydroxysulfates from acid sulfate waters, 351-403. In: Alpers, C.N., Jambor, J.L. and Nordstrom, D.K., Editors, (2000). Sulfate Minerals: Crystallography, Geochemistry, and Environmental Significance. Reviews in mineralogy and geochemistry, **40**.

Butts, D.(1997). In: Kirk-Othmer Encyclopedia of Chemical Technology, 4th edition; **22**, 403-411.

Carras, J.N., Day, S., Saghafi, A. and Williams, D.J., 1999. Spontaneouse combustion in spoil piles from open cut coal mines and the emission of greenhouse gases. In: 2nd International Symposium on the Operationalization of Remote Sensing, ITC, Enschede, 16-20 August, The Netherlands.

Chamberlain, E.A.C. and Hall, D.A. (1973). The ambient temperature oxidation of coal in relation to the early detection of spontaneous heating: Part 2, the Mining Engineer, **132**, 387-397.

Chipera, S.J. (2004). Experimental stability of magnesium sulfate hydrates that may be present in Mars. Geological society of America, Abstract with programs, **36**, n°5, 557.

Chou, M. and Seal, R.R. (2003). Determination of epsomite-hexahydrite equilibria by the humidity-buffer technique at 0.1 MPa with implications for phase equilibria in the system $MgSO_4$-$H_2O$. Astrobiology, **3**, n° 3, 619-630.

Cogema (1992). Evaluation du terril 76, rapport par Dupuis, J.C., pour Surchiste, 8p.

Cole, D.I. (1975). Observations on a burning cliff: Dorchester, Dorset, UK, Proceedings of the Dorset Natural History and Archaeological Society for 1974, Dorset Natural History and Archaeological Society, v. 96, p. 16-19, http://www.dor-mus.demon.co.uk (accessed July 2005).

Christov, C. and Moller, N. (2003). Chemical equilibrium model of solution behavior and solubility in the H-Na-K-OH-Cl-HSO4-SO4-H2O system to high concentration and temperature. Geochimica et cosmochimica Acta, 68, n°6, 1309-1331.

Dana's System of Mineralogy (1951). 7th edition, II, 404-407.

Driessen, P.M. and Schoorl.R. (1973). Mineralogy and morphology of salt efflorescences on saline soils in the Great Konya Basin, Turkey. Journal of Soil Science, **24**, n° 437-442.

Ellis, A.J. and Mahon, W.A.J. (1997). Chemistry and Geothermal Systems. In Energy Science and Engineering: Resources, Tecnnology, Management, An International Series. Editor, Denton, J. Academic Press, p.392.

Finkelman, R.B. and Marose, M. (1977). Downeyite, the first verified natural occurrence of $SeO_2$. American Mineralogist, **62**, 316-320.

Finkelman, R.B. (2004). Potential health impacts of burning coal beds and waste banks. International Journal of Coal Geology, **59**, Iss. 1-2, 19-24.

Forti, P., Galli, E., Rossi, A., Pint, J. and Pint, S. (2004). Ghar Al Hibashi lava tube: the richeset site in Saudi arabia for cave minerals. Acta Carsologica, 33/2, 189-205.

Gaines, R.V., Skinner, H.C., Foord, E.E., Mason, B., and Rosenzweig, A. (1997), Dana's New Mineralogy, ed. 8: New York, John Wiley and Sons, Inc., 1819 p., http://webmineral.com/danaclass.shtml (accessed July 2005).

Gaschnitz, R., Aeckersberg, R., Wirtgen, C., Verhoeven, M. and Rüter, H (2005). Burning waste dumps a potential source of energy. In: proceeding conference book , International conference on coal fire research, Beijing, China, p. 187-189.

Genge, M.J., Balme, M. and Jones, A.P. (2001). Salt-bearing fumarole deposits in the summit crater of Oldoinyo Lengai, northern Tanzania: interactions between natrocarbonatite lava and meteoric water. Journal of Volcanology and Geothermal Research, **106**, 111-122.

Gentzis, T. and Goodarzi, F. (1989). Organic petrology of a self-burning coal wastepile from Coleman, Alberta, Canada. International Journal of Coal Geology, **11**, 257-271.

Giardino, D.A. (1999). Estimating the rate of coal combustion in a mine fire. Informational Report 1249, U.S. Department of Labor, Mine Safety and Health Administration, Pittsburgh, Safety and Health Technology Center, Pittsburgh, PA, 30p.

Hall, A.J., Fallick, A.E., Perdikatsis, V. and Photos-Jones (2003). A model fort he origin of Al-rich efflorescences near fumaroles, Melos, Greece: enhanced weathering in a geothermal setting. Mineralogical Magazine, **67**, n°2, 363-379.

Harris, A.J.L. and Maciejewski, A.J.H. (2000). Thermal surveys of the Vulcano Fossa fumarole field 1994-1999: evidence for fumarole migration and sealing. Journal of Volcanology and Geothermal Reasearch, **102**, 119-147.

Hawley, G.G. (1971). The Condensed chemical dictionary, 8th edition: New York, N.Y., Van Nostrand Reinhold Company, 971 p.

Jambor, J.L., Nordstrom, D.K. and Alpers, C.N. (2000). Metal-sulfate salts from sulphide mineral oxidation, 303-350. In: Alpers, C.N., Jambor, J.L. and Nordstrom, D.K., Editors, (2000). Sulfate Minerals: Crystallography, Geochemistry, and Environmental Significance. Reviews in mineralogy and geochemistry, **40**.

Keith, D.C., Runnells, D.D., Esposito, K.J., Chermak, J.A., Levy, D.B., Hannula, S.,R., Watts M., and Hall, L. (2001). Geochemical models of the impact of acidic groundwater and evaporative sulfate salts on Boulder Creek at Iron Mountain, California. Applied Geochemistry **16**, 974-961.

Keller, L., McCarthy, G.J. and Richardson, J.L. (1986). Laboratory modelling of Northern Great Plains salt efflorescence mineralogy. Soil Science American, 50, 1363-1367.

Khalili, M. and Torabi, H. (2003). The exploration of sodium-sulphate in Aran Playa, Kashan, Central Iran. Carbonates and Evaporaites, **18**, n°18, 120-124.

Kim, A. (1973). The composition of coalbed gas. U.S. Bureau of Mines report of Investigations, 7762, U.S. Department of the interior, Bureau of Mines and Safety Research Center, Pittsburgh, PA, 9p.

Klein,C. (2002). Mineral Science, 22nd Ed. Wiley, New York, 641p.

Knacke, O. and Von Erdberg (1975). The crystallization pressure of sodium sulfate decahydrate, Ber Bunsen-Ges, Phys. Chem. **79**, 653-657.

Kusakabe, M. and Komoda, Y. (1992). Sulfur isotopic effects in the disproportionated reaction of sulfur dioxide at hydrothermal temperatures. Rept. Geological Survey Japan, **279**, 93-96.

Lapham, D.M., Barnes, J.H., Downey, W.F., Jr. and Finkelman, R.B. (1980). Mineralogy associated with burning anthracite deposits of eastern Pennsylvania. Pennsylvania Geological Survey Mineral Resources Report **78**, 82p.

Linke, W.F. (1965). Solubilities of inorganic and metal organic compounds. 2, American Chem. Society, Washington, D.C.

Linke, W.F. and Seidell,A.(1958). Solubilities of inorganic and organic compounds.**1**, American Chem. Society, Washington, D.C.

Martin, R., Rodgers, K.A., Browne, P.R.L. (1999). The nature and significance of sulphate-rich, aluminous efflorescences from the Te Kopia geothermal field, Taupo Volcanic Zone, new Zealand. Min. Mag. **63**, 413-419.

Masalehdani M.N.N.(1985).Thermal metamorphism associated with burnt coal seams, Rotowaro Coalfield, Huntly, New Zealand.Published MSc thesis, Auckland University,102 p.

Masalehdani, M.N.N. and Potdevin, J.L. (2004). Problèmes Géo-Environnentaux lies à la combustion des Terrils dans les Zones Miniers de la Région Nord-Pas-de-Calais, France. In: Conference proceeding book, Journées nationales de géotechnique et de géologie de l'ingénieur géotechnique et aménagement, 28-30 June , Lille, France, 209-218.

Masalehdani, M.N.N., Potdevin, J.L., Récourt, P. and Fialin, M. (2004). Products of oxidation and combustion within the burnig coal waste heaps in the Nord-Pas-de-Calais Coalfield, northern France. In: Conference proceeding abstract book, Joint Earth Sciences Meeting,20-25 September (2004), Strasbourg, France, 39.

Masalehdani, M.N.N., Potdevin, J.L., Cazier, F. and Courcot D. (2005). Coal waste heap fire: emission of toxic gases and condensation minerals, northern Franc: Measurements and analyses. In proceeding conference book, International conference on coal fire research, 101-103.

Mees, F. and Stoops, G. (1991).Mineralogical study of salt efflorescences on soils of the Jequetepeque Valley, northern Peru. Geoderma, **49**, 255-272.

Mees, F. (1999). Textural features of Holocene perennial saline lake deposits of the Taoudenni-Agorgott basin, northern Mali. Sedimentary Geology, **127**, 65-84.

Mees, F. (2003). Salt mineral distribution patterns in soils of the Otjomongwa pan, Namibia. Catena, **54**, 425-437.

Nichol D. and Tovey N.P. (1998). Remediation and monitoring of a burning coal refuse bank affecting the Southsea Looproad at Brymbo, North Walse. Engineering Geology **50**, 309-318.

Nordstrom,D.K. (1982). The effect of sulfate on aluminium concentrations in natural waters: some stability relations in the system $AL_2O_3$-$SO_3$-$H_2O$ at 298K. Geochimica et Cosmochimica Acta, **46**, 681-692.

Panov, B.S., Dudik, A.M., Shevchenko, O.A. and Matlak, E.S. (1999). On pollution of the biosphere in industrial areas: the example of the Donets Coal Basin. International Journal of Coal Geology, **40**, 199-210.

Palache, C, H. Berman, and C. Frondel. (1957). Dana's system of mineralogy, 7th edition. 2: 494, 509-513.

Pone, J.N., Stracher, G.B., Finkelman, R.B., Hein., K.A.A. and Annegarn, H.J.(2005). The environmental impact of coal fires, spontaneous combustion in South Africa. In: proceeding conference book, International conference on coal fire research, Beijing, China, 94-95.

Oftedal, I.(1922). Minerals from the burning coal seam at Mount Pyramide, Spitsbergen: Resultater Norges Statsunderstottede Spitsberg-Ekspedisjoner, **1**, 9-14.

Onac, B. P., White, W. B., Viehmann, I. (2001). Leonite, konyaite and syngenite from Tausoare Cave, Rodnei Mts., Romania. Mineralogical Magazine **65**(1), 1-7.

Orti, F., Gündogan, I. and Helvaci,C.(2002). Sodium sulphate deposits of Neogene age: the Kirmir formation, Beypazari basin, Turkey. Sedimentary Geology, **146**, 305-333.

Rahimpour-Bonab, H. and Kalantarzadeh, Z. (2004). Origin of secondary potash deposits; a case from Miocene evaporities of NW Central Iran. Journal of Asian Earth Sciences, **23**, 157-166.
Rodgers, K.A., Hamlin, K.A., Browne, P.R.L., Campbell, K.A. and Martin. R. (2000). The steam condensate alteration mineralogy of Ruatapu cave, Orakei Korako geothermal field, Taupo Volcanic Zone, New Zealand. Mineralogical magazine, **64**, n°1, 125-142.

Rost, R. (1937). Mineralály hořicich hald na Kladensku. Rozper. Čes. Akad. Věd Uměni, Tř. **47**, 1-19.

Rost, R. (1942). Dopiňky K mineralogii hořicich hald na Kladensku. Rozper. Čes. Akad. Věd Uměni, Tř., **52**, 25, 1-4.

Sejkora, J.I.Ř. and Kotrlŷ. M.(1998). A new cadmium sulfate natural phase from Radvanice near Truntnov (Czech Republic). Věstink Českého ústovu **73**, 4, 321-326.

Sharp, D.W.A. (1990). Dictionary of Chemistry, second edition 434 p.

Sinha, R. and Raymahashy, B.C. (2004). Evaporite mineralogy and geochemical evolution of the Sambhar Salt Lake, Rajasthan, India. Sedimentary Geology, **166**, 59-71.

Stewart, F.H. (1963). Marine Evaporites, US Geological Survey, professional paper, 440-Y, 52p.

Stoiber, E.E., and Rose, W.I. Jr. (1974). Fumarole incrustations at active Central American volcanoes. Geochimica et Cosmochimica Acta, **38**, 495-616.

Stracher, G.B. (1995). The anthracite smokers of eastern Pennsylvania: $P_{S2(g)}$ - T stability diagram by TL Analysis: Mathematically Geology, **27**, no. 4, 499-511.

Stracher, G.B. and Taylor, T.P. (2004). Coal fires burning out of control around the World: thermodynamic recipe for environmental catastrophe. International Journal of Coal Geology, **59**,7-17.,

Stracher, G.B., Pone, J.D.N., Finkelman, R.B., Annegarn, H.J., Mccormack, J., Blake, D.R., Rowland Hall, I. and Schroeder, P.(2005). Gas vent mineralogy and geochemistry: the burning culm banks of South Africa. Geological Society of America, Abstracts with Programs, **37**, n°. 7, 453.

Stracher,G.B., Prakash, A. Schroeder, P., MacCormack, J., Zhang,X., Van Dijk, P. and Blake, D. (2005). New mineral occurrences and mineralization processes: Wuda coal-fire gas vents of Inner Mongolia. American Mineralogist, **90**, 1729-1739.

Stracher,G.B., Prakash, A. (2006). The origine of gas-vent minerals: Isochemical and mass transfer processes. In: proceeding abstract book, Geological Society of America annual meeting, Philadelphia, 22-25 October, Paper N° 62-5.

Svensen, H., Dysthe, D.K., Bandlien, E.H., Sacko, S., Coulibaly. H., Planke, S. (2003). Subsurface combustion in Mali: Refutation of the active volcanism hypothesis in West Africa. Geology, **31**, no.7, 581-584.

Thalheim, K., Reichel, W., Witzke, T. (1991). Die Mineral des Döhlener Beckens. ISBN: 3910006078, 131p.
USPHS (2002). <www.sciencemag.org/cgi/content/full/296/5576/2145>

van Doesburg, J.D., Vergouwen, L. and van der Plas, L. (1982). Konyaite
$Na_2Mg(SO_4)_2.5H_2O$
a new mineral from Great Konya Basin, Turkey. American Mineral, **67**, 1035-1038.

Washington, H.S. and Merwin, H.E. (1921). Aphthitalite from Kilauea. American Mineralogist, **6**, 121-125.

West, I.M. (2001). Burning beach, burning cliffs and the Lyme volcano: oil-shale fires; geology of the Dorset Coast: United Kingdom, School of Ocean and Earth Sciences, Southampton University, 1-16, http://www.soton.ac.uk/~imw/kimfire.htm (accessed July 2005).

Williams-Jones, A.E., Migdisov, A., Archibald, M.S. and Xiao, Z. (2002). Vapor-transport of ore metals. Water-Rock Intractions, ore Deposits, and Environmental geochemistry: ATribute to david A. Crerar. The geochemical Society, Special Publication n°.7, Editor: Hellmann R. and Wood S.A., 279-305.

Winchell, H. and Benoit, R.J. (1951). Taylorite, mascagnite, aphthitalite, lecontite, and oxammite from guano. American Mineral, **36**, 590-602.

Witzke,T.(1990). Sekundärminerale und Haldenbranminerale des Döhlener Beckens (Secondary minerals and minerals from burning mine dumps of the Döhlen basin). Diploma thesis, Bergakademie Freiberg (Germany), Sektion Mineraloie/Geochemie, 1-71.

Žáček, V., Ondruš, P. (1997). Mineralogy of recently formed sublimites from Kateřina colliery in Radvanice, Eastern Bohemia, Czech Republic. Věstink Českého ústovu **72**, 3, 289-298.

Zanovskii, A., Soloveva, E., Liahovskaia., E., Shestakov, N., shleimovich, P. and Abutkova,L.(1973). Spravochnik po rastvorimosti solevykh system, I-1, II-1 and II-2. Izd.Khimyua.

# CHAPTER V

# A FLUID INCLUSION STUDY IN THENARDIT FROM BURNING COALWASTE HEAP, AVION, NORTHERN FRANCE

# A FLUID INCLUSION STUDY IN THENARDITE FROM BURNING COAL WASTE HEAP, AVION, NORTHERN FRANCE

Coquinot Y. University of Leoben, Department of Applied and Geophysics,
Mineralogy and Petrology Peter Tunner Strasse 5, A-8700 Leoben, Austria
**yvan.coquinot@hotmail.fr**

Dubois M. University of Lille 1, Department of Geology, UMR CNRS 8110,
Bâtiment SN5, 59655 Villeneuve d'Ascq CEDEX, France
**michel.dubois@univ-lille1.fr**

Masalehdani M.N.N. University of Lille1, Department of Geology, UMR CNRS
8110, Bâtiment SN5, 59655 Villeneuve d'Ascq CEDEX, France
**MN.Masalehdani@ed.univ-lille1.fr**

Blanchet A. University of Lille 1, Department of Geology, UMR CNRS 8110,
Bâtiment SN5, 59655 Villeneuve d'Ascq CEDEX, France
**aurelie-b.blanchet@laposte.net**

Potdevin J.L. University of Lille1, Department of Geology, UMR CNRS
8110 Bâtiment SN5, 59655 Villeneuve d'Ascq CEDEX, France
**Jean-Luc.Potdevin@ univ-lille1.fr**

Submitted for a poster presentation in RST meeting in Dijon, 2006. It will be included in the chapter presentation by M.N.N.Masalehdani et al., in «The First World Atlas of Coal Fires by Elsevier », 2007.

## 1. INTRODUCTION

Very few studies reported the occurrence of secondary minerals forming around gas vents from burning coal waste heaps (e.g. Finkelman and Mrose 1977; Žáček and Ondruš 1997; Panov et al. 1999; Masalehdani et al. 2005; Pone et al. 2005). Research involving the mineralogical studies, mode of formation of salt efflorescence minerals on burning coal waste heaps and the possible chemical reactions that occur during the crystallisation of the minerals is almost non-existent. Gas exhaled from surficial vents and fissures and different soluble minerals originated from cooling gas reveal important information about the chemical composition of burning coal and the possible interaction of the gas with rock and water on its way to the surface prior to exhalation. At the burning coal waste heap n°76 in Avion a variety of fumarole-related minerals (sulphates, halides and native sulphur) was identified depositing on the rock debris. Previous investigators identified minerals but none of them investigated or reported the occurrence of trapped fluid inclusions in efflorescent salt minerals originated from coal fire gas with exception of Masalehdani et al. (2005) who reported the occurrence of fluid inclusions in the crystals of sodium sulphate thus first documented from coal fire gas. In this chapter the preliminary studies of fluid inclusions in crystals of sodium sulphate (thenardite) is reported.

## 2. METHODOLOGICAL APPROACH

### *2.1. Sample collections and preparations*

10 samples of salt encrustations and/or crystalline solids Na-bearing minerals were carefully taken from gas spot S5 around the fumarole discharge in Front B at the top surface of the coal waste heap (Fig. 1a). After cooling in fresh air for about 5 minutes, specimens were placed into containers that were sealed and transported to the laboratory for analysis. The ephemeral nature of these salts and their sensitivity to temporal variations in temperature and humidity complicate attempts to find consistent relationships between mineral assemblages and render the preparation of samples difficult for various studies. Prior to analyses all samples were kept at ambient temperature in a shelter at the laboratory. A first series of analyses for all samples was done within a week of collection. Well crystalline specimens (e.g. sample AV1443d) contain fluid inclusions. In hand specimen the sample is transparent to translucent milky white, vitreous with concave outlines about 1cm long, contains snow white fine-grained granular overgrown crystals (Fig. 1b).

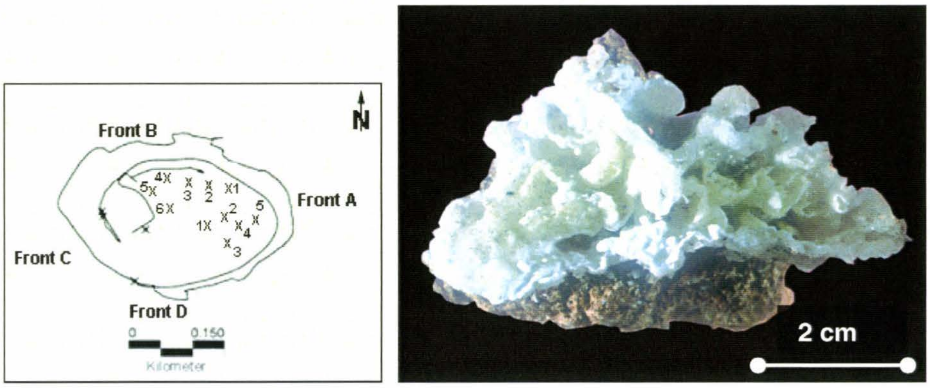

**Figure 1a and 1b**. Sample collection location (gas spot S5 front B), and a hand specimen of sample AV1443d from the coal waste heap n°76.

Taking into account the brittleness of the salt crystals and their high solubility in water, cautions have been taken in sample preparations. This acquired no water use. Polished uncovered thin and thick sections (60-100 µm and 50 µm) which permit both transmitted light viewing and fluid inclusion analyses were made at the Geology Department, University of Lille 1. Thickness of the sections depended on the granulometry of the sample. Preparations involved in making boxes (15x15x15 mm) which were used as a stand, then a fan-shaped sample was placed in a box which was then filled with epoxy. Using an abrasive the surface of the box was rectified, this makes a perfect flat surface. Coating of the sample, at room temperature required about 24 hours. Next step involved in rectification of the upper surface of the coated sample by coarse to very fine grain abrasive (size 1200 to 2400). It should be noted that during abrasion, impregnation of the sample may be required. Afterward, the sample is stuck on a frosted glass wafer. Levelling of the section processed using petrol. Final rectification and abrasing performed using abrasive paper. Petrol and diamond paste were used for polishing of the samples.

For the fluid inclusion analyses, sections were stuck on the glass wafer using a special resin ("géoptic" by Brot) which remains stable at relatively high temperature (200C°). As the chamber of the microthermometric stage requires a maximal size of 1 cm, small solid fragments were made using a glazier knife.

### *2.2. Analytical methods*

Fluid inclusions in thenardite were observed using a photonic microscope Olympus BX60 equipped with a digital video camera. They were studied on the microthermometric stage (FLUID INC, Co; United States) (Werre Jr, 1979). The stage was precisely calibrated using synthetic fluid inclusions (Syn Flinc Co). Standard used in this study are those pointed by Synflinc and include synthetic fluid inclusions in the $H_2O$ system and in the $H_2O$-$CO_2$ system. Estimated errors on measured temperatures are: ±0.1°C at low temperatures (-100 to +25°C) and increase to about +1°C at 400°C.

Raman spectrometry was performed at the LASIR laboratory, University of Lille 1 and at the University of Leoben in Austria. Raman spectroscopic measurements were done with a LABRAM (ISA Y. Jobin) instrument using a frequency-doubled Nd-YAG laser (100 mW source). Wavenumber measurements have an accuracy of 1.62 $cm^{-1}$ at low $\Delta\nu$ (Raman shift around 0 $cm^{-1}$) and 1.1 $cm^{-1}$ at high $\Delta\nu$ (around 3000 $cm^{-1}$). Low temperature Raman analysis was conducted with a Linkam THSMG 600 heating-freezing stage and an Olympus 100X long-working-distance objective (LMPlanFI, 0.80 numerical apertures) has been used. The stage was calibrated using synthetic fluid inclusions. Raman spectra of fluid inclusions were measured in a time span of 30 seconds, with five accumulations, at selected temperatures. During the freezing experiments, a vapour phase remained present within the analysed fluid inclusions. Each Raman measurement was performed with the focus providing the higher intensity. Slight displacement of the focus spot may have important effects on the absolute intensity of Raman spectra. Each spectra was analysed by the peak-fitting program. PeakFit, v. 4.12 (SYSTAT Software Inc.) to find the Gaussian-Laurentzian components contributions and to put in evidence the hidden peaks in complex shape spectra. The quality and definition of the Raman spectra are temperature dependent. For each phase analysed with the Raman, a spectra was measured at -180°C.

## 3. FLUID INCLUSION PETROGRAPHY

### *3.1. Description of fluid inclusions*

Fluid inclusions are relatively scarce in the samples. They were observed in two different habitus: in tubular and in rectangular (lozenge-shaped) thernardite crystals. The inclusion size reaches 60 µm, they occur either as isolated or along clusters composed of 3 to 15 objects. Some alignments are observed parallel to the elongation direction of the crystal.

Detailed observations indicate that inclusions are either isolated or occur in as clusters which are primary relative to the crystal growth. They can also be "pseudosecondary" (Roedder, 1984), i.e. formed by the sealing of a microcrack during the crystal growth. Fluid inclusion place crosscutting the crystal boundary has not been observed.

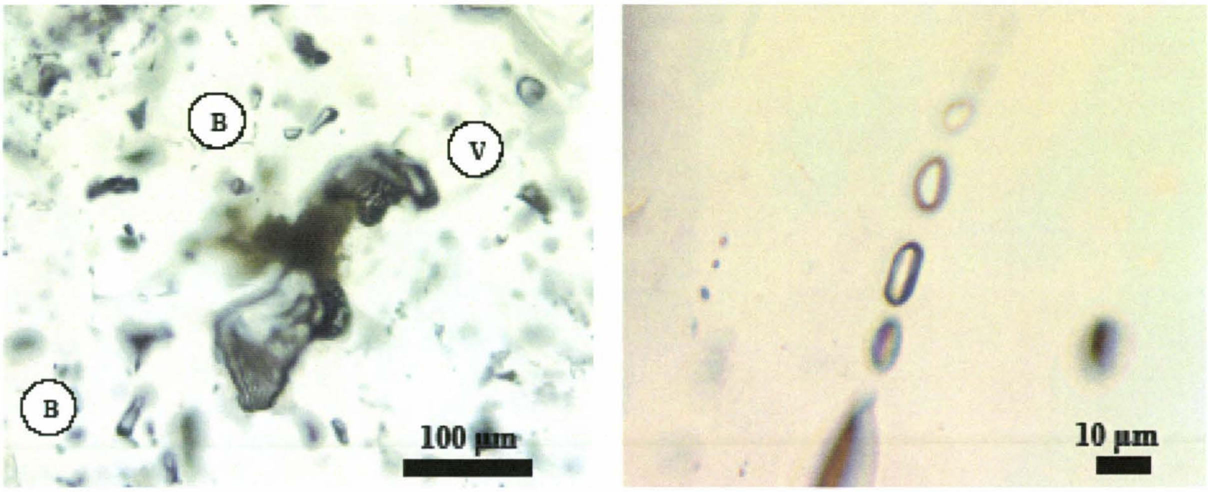

**A**. Cluster of inclusion with highly variable vapour filling ratio. V = vapour inclusions, B = two-phase inclusion.

**B**. A cluster of an aligned all-vapour inclusions.

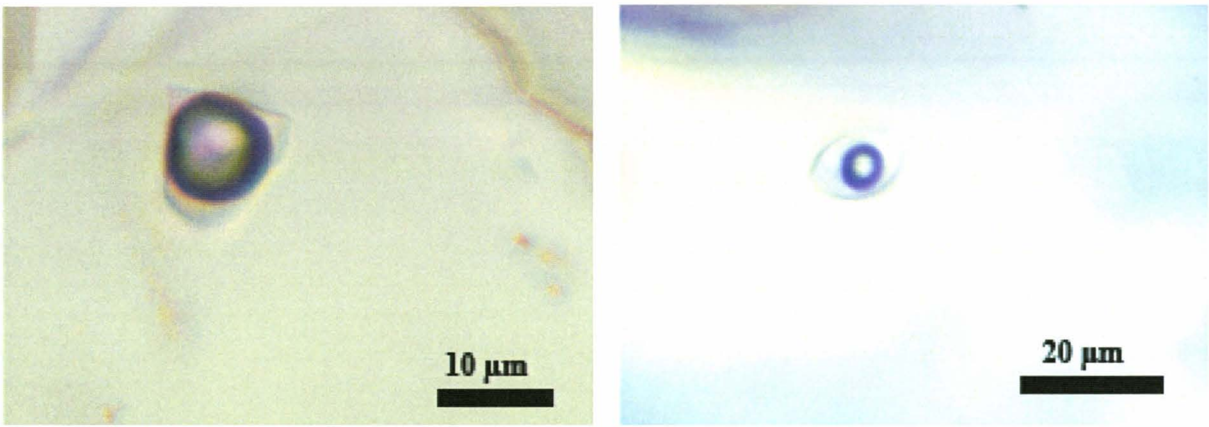

**C**. Isolated inclusion with high vapour filling ration.

**D**. Two phase (liquid + vapour) isolated inclusion (B-type)

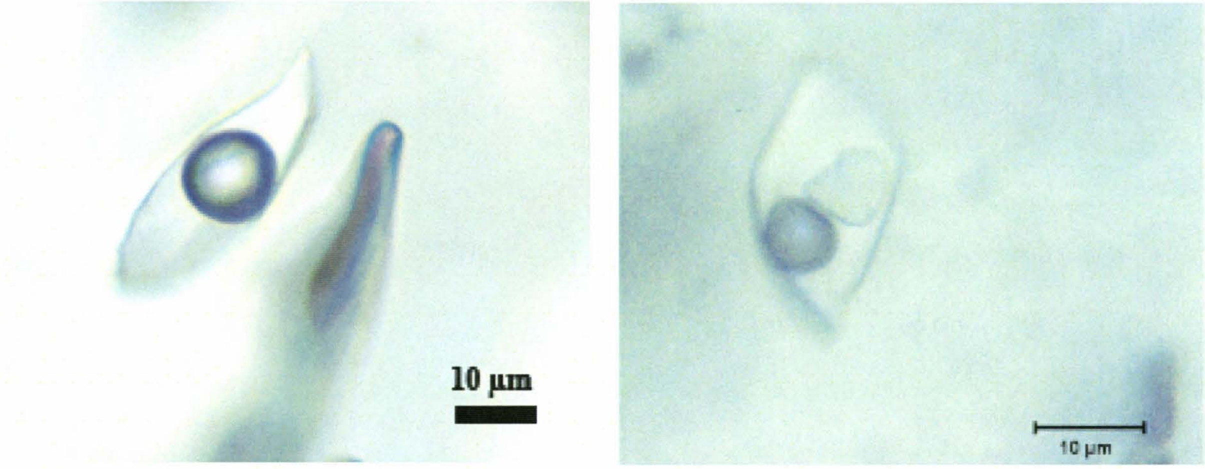

**E**. Two-phase inclusion of relatively large size (B-type).

**F**. Three phase (liquid + vapour + solid) inclusion (B-type).

**Figure 1:** Microphotographs of inclusions observed in thenardite crystals (sample AV1443d).

The main feature of the inclusions is the high variability of the vapour filling ratio ($R_{flv}$). $R_{flv}$ range from 0 (pure liquid) to 1 (pure vapour). The range is frequently observed within a single cluster.According to the $R_{flv}$ feature at room temperature, three fluid inclusion types have been distinguished :

- A-type which includes one-phase vapour inclusions;
- B-type is composed of two inclusion phases (liquid + vapour) and;
- C-type is defined as one-phase liquid inclusions.

It should be stressed that at room temperature, B-type inclusions sometimes contain a solid phase. The solid has generally a prismatic or tabular shape and presents a slight greenish sheen. It should be noted this classification does not take into account any chronological features, as two or three inclusion types can co-exist in a given alignment.

## 4. PHASE RELATIONS IN THE $Na_2SO_4$-NaCl-$H_2O$ SYSTEM

Analysed inclusions occur in thenardite $Na_2SO_4$, salt of high solubility in water. The interpretation of phase transitions in this case therefore requires primarily a perfect knowledge on the chemical systems including $Na_2SO_4$, as the dominant aqueous species, e.g. $Na_2SO_4$-$H_2O$, $Na_2SO_4$-NaCl-$H_2O$, and eventually $Na_2SO_4$-NaCl-$H_2O$, in addition to $MgSO_4$ and KCl.

### *4.1. The $Na_2SO_4$-$H_2O$ system*

The $NaSO_4$-$H_2O$ system has a eutectic point and various peritectic points, resulting from the existence of at least two reported hydrates, respectively $Na_2SO_4.10H_2O$ (decahydrate, also called mirabilite[1]) and $Na_2SO_4.7H_2O$ (heptahydrate), and anhydrous salt $Na_2SO_4$, (thenardite). In addition, three polymorph of thenardite have been noted (Schroeder et al., 1935), respectively orthorhombic 1 (named V), orthorhombic 2 (named III) and hexagonal (I). The heptahydrate is reported to be metastable. The co-ordinates of these invariant points are the listed in Table 1. The solubility of the decahydrate has been empirically calculated by Richards and Ingve (1918) in the range 14.731 to 24.845°C:

$$\log(s\,(\text{wt\%})) = 0.6600577 + 0.0296154 \times t(°C) + 0.0000696191 \times t(°C)^2$$

---

[1] Also called "admirable salt" by Johann Rudolph Glauber (1604-1668), German doctor and alchemist. In about 1625, in Vienna region (Austria), he was ill and he was cured by drinking water from a local source. After analysing water samples, he found salt crystals he called it "admirable salt or universal salt of philosophers"

The solubility curve of the heptahydrate, reported as metastable, is given by Loewel (1857) (Fig. 3). A polynomial fit of Loewel's data between the eutectic and the peritectic point has the expression:

$$(s(wt\%)) = 0.0106 \times t(°C)^2 + 1.0878 \times t\ (°C) + 18.763$$

**Table 1:** Co-ordinates of the invariant points in the $Na_2SO_4$-$H_2O$ system.

| Point | Ref. | Composition | | Temperature | | Coexisting phases* |
|---|---|---|---|---|---|---|
| | | wt% | molality[2] mol/kg | °C | K | |
| E | [1] | 3.288 | 0.240 | -1.2 | 271.95 | Ice+mir+L |
| $E^m$ | [2] | 14.5 | 1.195 | -3.5 | 269.65 | Ice+Na7+L |
| P1 | [3] | 49.7 | 6.962 | 32.383±0.001 | 305.533±0.001 | mir+then$^{(V)}$ + L |
| $P1^m$ | [4] | 51.80 | 7.572 | 24.4 | 297.55 | Na7+then$^{(V)}$+L |
| | [5] | | | 23.405±0.004 | 296.555±0.004 | |
| P2 | [6] | 44 | 5.536 | 185 | 458.15 | then$^{(V)}$+then$^{(III)}$+L |
| P3 | [6] | 45.6 | 5.906 | 241 | 514.15 | then$^{(III)}$ + then$^{(H)}$+L |

*mir = $Na_2SO_4.10H_2O$ (mirabilite) – Na7 = $Na_2SO_4.7H_2O$ (heptahydrate) – then = $Na_2SO_4$ (anhydrous salt = thenardite) – L = liquid. Superscripts $^{(V)}$, $^{(III)}$, $^{(H)}$ refer to the orthorhombic form V, orthorhombic form III and hexagonal form of thenardite. $^m$ refers to the metastable nature of the equilibrium.

References: [1]: Chrétien and Kohlmuler (1966); [2]: De Coppet (1872); [3]: Richards and Wells (1902); [4]: Loomis (1918); [5]: Washburn and Chem (1938) ; [5]: Kracek (1929), Kracek and Gibson (1930)

### *4.2. The ternary $Na_2SO_4$-NaCl-$H_2O$ system*

In the ternary $Na_2SO_4$-NaCl-$H_2O$ system, the eutectic temperature is significantly decreased down to the eutectic of the binary $H_2O$-NaCl. Some experimental data concerning the eutectic points are compiled in Table 4. Solubility relations in this system have been calculated by Marion and Farren (1999) and are re-drawn in Figure 4.

**Table 2:** Co-ordinates of the eutectic points (equilibrium Hydrohalite + Mirabilite + Ice) in the $Na_2SO_4$-NaCl-$H_2O$ system.

| Point | Composition | | Temperature | | Reference |
|---|---|---|---|---|---|
| | m($Na_2SO_4$) mol/kg | m(NaCl) mol/kg | °C | K | |
| E | 5.26 | 0.029 | -21.32 | 251.83 | [1] |
| | 5.06 | 0.011 | -21.7 | 251.45 | [1] |
| | 5.14 | 0.016 | -21.4 | 251.75 | [1] |
| | 5.16 | 0.014 | -21.34 | 251.81 | [2] (calculated) |

[1]: Bukshtein et al. (1953); [2]: Marion and Farren (1999)

---

[2] The molecular weight of $Na_2SO_4$ is 141.931 g/mol

## 5. RESULTS

### *5.1. Behaviour during microthermometric runs*

Microthermometry, *i.e.* observations of phase changes during temperature changes, is generally known to be difficult in brittle minerals, particularly in sulphates (Ulrich and Bodnar, 1988). Indeed, sulphate minerals are subject to stretching during cooling of the sample. In the samples studied, it has been observed that numerous fractures develop around inclusions during cooling runs, leading to a change of $R_{Flv}$ and modifying their bulk properties. Moreover, during heating above 100°C host crystals (mainly thenardite) turns into a brown-coloured phase. All these features have conducted to reject numerous inclusions. However, Microthermometric measurements include the following temperatures:

- homogenisation temperature ($T_h$): the temperature at which the liquid and the vapour phase of two-phase inclusions mix. This temperature is an indicator of the bulk inclusion density and of the trapping temperature $T_{trap}$ ($T_h \geq T_{trap}$)
- eutectic temperature ($T_e$): after freezing to very low temperatures (< -100°C), the temperature at which the first liquid droplet appear during heating. This temperature is characteristic of the main ions in solution
- ice meting temperature ($T_{mi}$): the temperature at which the last ice crystals melt into the solution. This temperature is a function of the salt content of the aqueous solution (except if saturated)
- solid melting temperature ($T_{ms}$): the temperature at which an included solid melts into the solution. The presence of this solid indicates a saturation of the solution relative to a given salt. The nature of the salt is optically unidentifiable. Raman microspectrometry is suitable for identification of numerous solids, but not for ionic solids except when they include water molecules (hydrates).

Bulk homogenisation temperature $T_h$ (B-type inclusions) are comprised in the range 82-133°C. In C-type inclusions (all-loquid inclusions) additional $T_h$ were measured in inclusions that have nucleated a vapour bubble during moderate cooling. These temperatures range from 40 and 84°C. During cooling, the solidification of the liquid phase is generally observed at about -55°C and is marked by a sudden contraction of the vapour phase jammed into ice. During subsequent heating, the frozen liquid becomes brownish at about -50°C. Eutectic temperatures ($T_e$) could rarely be precisely measured. However some data give a value between -40 and -30°C. Results are similar in B-type and C-type inclusions are similar.

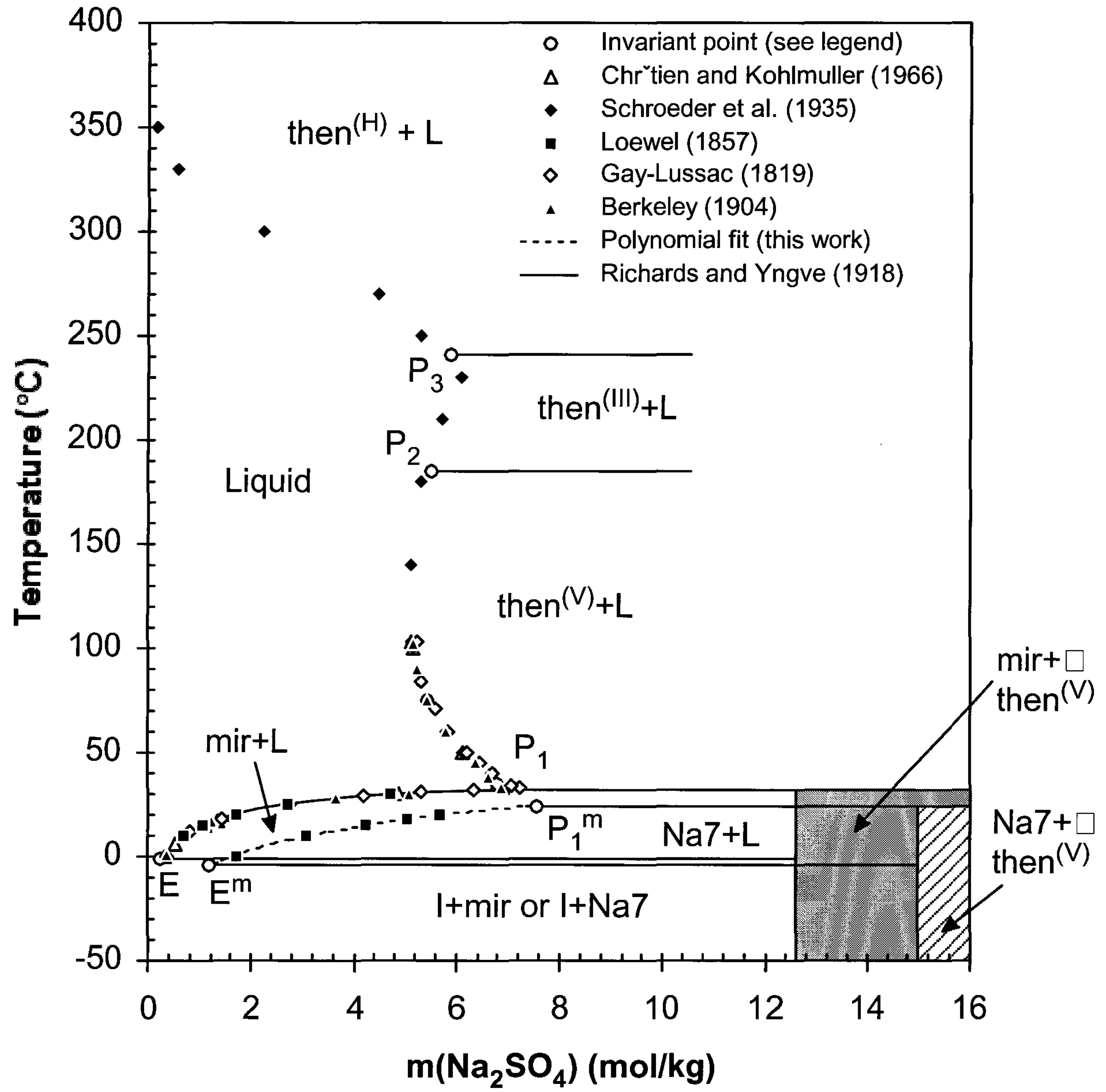

**Figure 3:** Phase diagram of the $H_2O$-$Na_2SO_4$ system. For the ice melting curve, see Figure 1. Phases: I=ice; $Na_2SO_4.10H_2O$; $Na_2SO_4$; (V) (III), (H) refer to the orthorhombic form V, orthorhombic form III and hexagonal form of thenardite. Invariant points: E=eutectic point I+L+mir. (Chrétien and Kohlmuller, 1966); E*=metastable eutectic I+L+Na7 (de Coppet, 1872); P1=peritectic point mir.→then.(V)+L (Richards and Wells, 1902); P1*=metastable peritectic point Na7→then.(V)+L (Wuite, 1914); P3=peritectic point then.(V) → then.(III) (Kracek, 1929; Kracek and Gibson, 1930); P4=peritectic point then.(V) → then.(H) (Kracek, 1929; Kracek and Gibson, 1930). Additional points of Loewel (1857) lying between P1* and P1 and beyond these two points were not reported because not visible at the diagram scale.

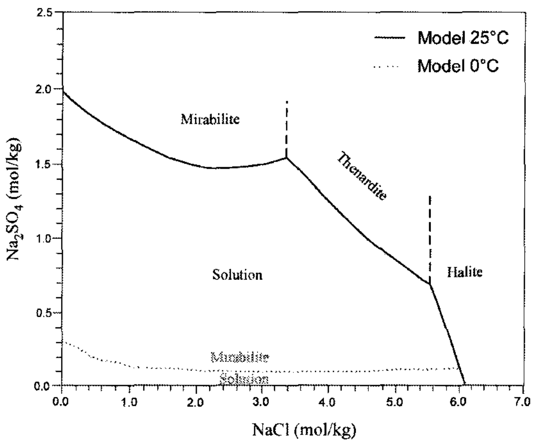

**Figure 4:** Phase relations in the $Na_2SO_4$-NaCl-$H_2O$ system (Marion and Farren, 1999).

Ice melting temperatures ($T_{mi}$) are low. Five temperatures have been measured between -24.5 and -23.4°C. Results are similar in B- and C- types. One inclusion of A-type indicates a value of +0.3°C. During cooling the formation of a solid has been noted in some inclusions (B-type). The observation of its disappearance during moderate heating has been made with great difficulty. The inclusion was submitted to numerous heating/cooling runs (*cycling procedure*; Haynes, 1985). This solid melts between +17.3 and +24°C. The nature of this solid phase could not be determined optically.

### *5.2. Raman microspectrometry*

Raman microspectrometry has been applied in order to:

- detect the presence of volatile constituents in the vapour phase of inclusions and,
- provide additional information on the nature of solid phases present in inclusions (initially or during cooling runs).

#### *5.2.1. Nature of the vapour phase*

The in-situ gas measurements and analyses at the coal waste heap n°76 in Avion revealed the presence of $CO_2$, $SO_2$, $NO_X$, $CH_4$, $H_2O$, and $O_2$ ( Masalehdani and Potdevin, 2004; Masalehdani et al., 2004 and 2005) but non of these volatile components were detected in the vapour phase of inclusions. This indicates that the fluid trapped in inclusions is only an aqueous solution without any detectable gas species.

#### *5. 2.2. Nature of the solid phase*

The nature of the solid phase can be suspected knowing the nature of the main components of the fluid. In water-bearing fluid inclusions solids present at temperature above 0°C are usually supposed to be clathrate (Roedder, 1984), gas hydrate. However in our case, the presence of clathrate can be excluded as no gas species have been detected in the vapour phase. Raman spectroscopy has revealed as a potential tool to identify phases appearing during freezing (Dubessy et al., 1982, 1992; Samson and Walker, 2000; Bakker, 2004). Three inclusions have been analysed at various temperatures. For each analysis, a spectrum has been obtained within the inclusion and a few micrometers distanced from the inclusions in the host crystal. The latter analysis can be considered as a "blank" and is necessary to remove the peaks due to the host mineral.

During cooling process of fluid inclusion analyses, thenardite (host mineral) should theoretically transform (i.e. dehydrate) into mirabilite, as it is not a stable sulphate phase at temperature ≤32.4°C (Marion and Farren, 1999). But it can subsist a few minutes at low to very low temperatures.

The host mineral analysed at low temperature is therefore certainly thenardite. Thus, the thenardite peaks in the Raman spectra have been taken away from the spectrum obtained on the frozen solution.

The frozen solution displays five additional peaks relative to the thenardite spectrum (Figure 4). These positions are: 3228.08, 3362.88, 3447.31, 3477.26 and 3512.67. A surprisingly result of the experiment is that whatever the location of the analysis spot, ice ($H_2O^s$) has not been detected.

**Table 3:** Microthermometric properties of inclusions analysed by Raman microspectrometry in cryoscopy

| N° | Type | $R_{flv}$ (%) | $T_e$ range (°C) | $T_{mi}$ (°C) | $T_{ms}$ (°C) | $T_h$ (°C) | Phase |
|---|---|---|---|---|---|---|---|
| 12 | C | 6 | - 40 ↔ -30 | n.o. | +23 ↔ +27 | 135±3 | Liquid |
| 10 | C | 8 | - 40 ↔ -30 | n.o. | 24.2 | 146±3 | Liquid |
| 9 | C | 10 | - 40 ↔ -30 | n.o. | 23.8 | 151±3 | Liquid |

n.o: not observed

The composition of the trapped solution probably belongs to the general $Na_2SO_4$-$NaCl$-$H_2O$ system. At temperature between 0°C the only stable phases are mirabilite, hydrohalite and ice formation and possibly heptahydrate (Figs, 4 and 5). Raman spectra of three inclusions have been obtained at various temperatures. Microthermometric properties of these inclusions are listed in Table 3. However Raman spectra obtained at various temperatures (Fig. 5) shows that freezing of the aqueous could results in the formation of a *brine glass* including amorphous ice and all ions present in the solution. These ions could be associated to form

NaCl, $Na_2SO_4$ molecules, and possible $MgSO_4$, $MgCl_2$, $K_2SO_4$ and KCl, taking into account the assumed composition of the mineralising fluid refer to composition of the fluid in the stockpile (Fig. 6). The presence of the spectra of these molecules could confusingly result in concluding that minerals of the same chemical composition at present. The presence of salt-like molecules in a the brine glass seems to be confirmed by the extreme variability of the spectrum depending on temperature, on analysis spot location, the successive steps of the cooling-heating procedure, at least. We conclude that there are a lot of difficulties to interpret spectra obtained at low temperatures, but the proposed approach is a promising tool for analysing the nature of the trapped solution.

## 6. INTERPRETATION OF DATA

Microthermometric analysis of inclusions has revealed a complex behaviour at low temperature. In addition Raman microspectrometry prevails to conclude that the frozen solution is probably a complex mixture of salt molecules scattered in brine glass. A systematic analysis of frozen solutions has to be performed.

Raman microspectrometry indicates that no volatile component is present in the vapour bubble of inclusions, and thus in the mineralising fluid. The fluid is therefore an aqueous solution. Even if phases are not in equilibrium during cooling runs, the low measured eutectic temperature (- 40 to -30°C) could indicate an aqueous solution dominated by $Na_2SO_4$ and NaCl (eutectic between -21 and - 22°C), with probably other salts which lower the eutectic temperature. The bulk composition can be deduced from the solid melting temperature. The last solid to melt is a hydrate one. If we assumed that this hydrate is mirabilite, then the reported temperature on the solubility curve of this salt (Figure 3) could give bulk salinity close to 50 wt%. The nature of the melting solid then has to be identified by Raman microspectrometry.

## 7. CONCLUSIONS

Study of fluid inclusions can provide useful information in the nature of the mineralising fluid most especially in the nature of the minerals forming from coal fire gas around burning coal waste heaps or coal seams. In our case detailed observations of thernardite crystals has revealed the presence of fluid inclusions, rather scarce but suitable for microthermometric analysis as well as other punctual methods. Result presented here are preliminary as experimental data are still incomplete. In deed, we should also verify the presence of trapped

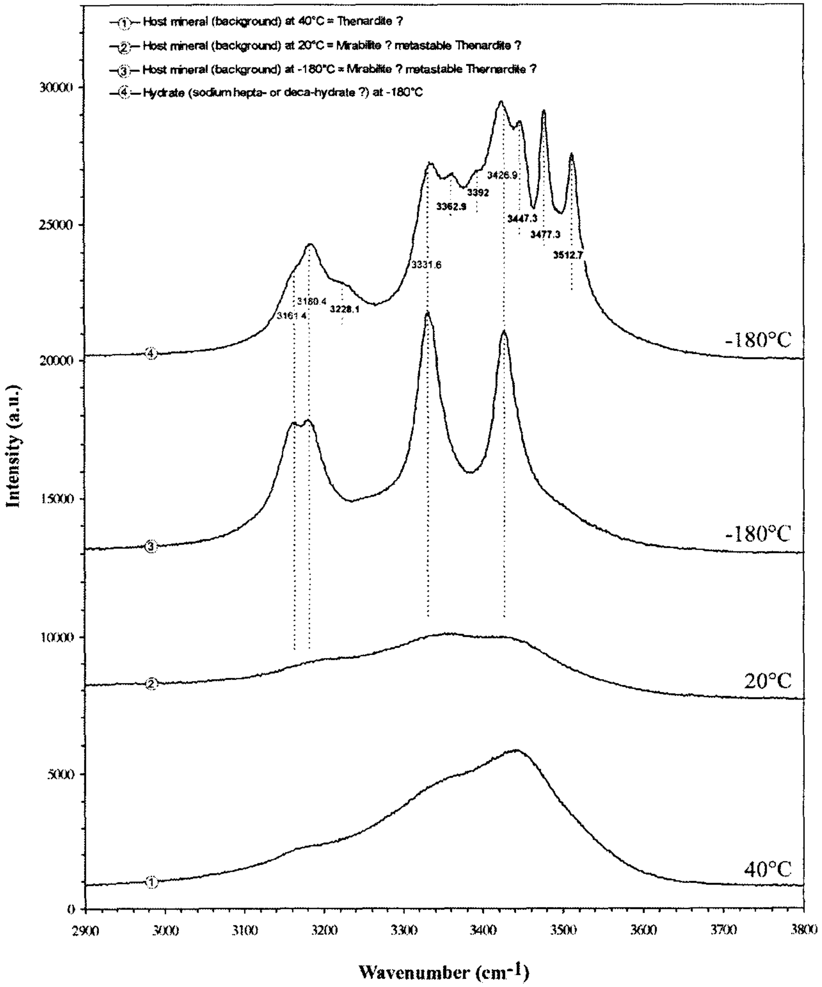

**Figure 5**. Raman spectra obtained at – 180°C in one inclustion in thenardite. The spectrum of thenardite was added as representing the host mineral.

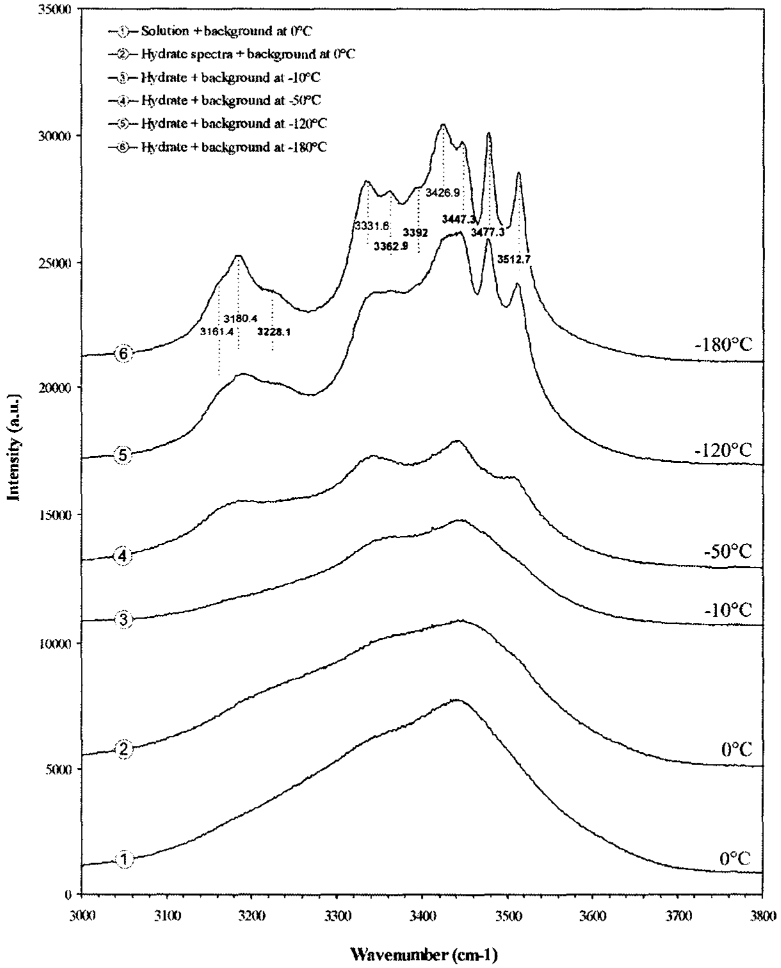

**Figure 6**. Raman spectra obtained at various temperatures in one inclusuion in thenardite.

fluid inclusions in other sulphate minerals. X-ray diffraction patterns of sample AV1443d do not reveal any peaks confirming the presence of mirabilite for example in this specimen.

Nevertheless, the latter mineral may coexist with thenardite in this sample but in smaller quantities. All observed inclusions have a primary or "pseudosecondary" origin. Both origins indicate a contemporaneity of the inclusions with the host mineral (Rodder, 1984). They therefore represent evidences of the fluid from which thenardite and some associated minerals have formed. icrothermometry combined with Raman microspectrometry results in concluding the following points:

- the mineralising fluid was essentially aqueous. No volatile species have been detected (above the detection limit of Raman and above the minimum concentration to nucleate gas hydrate),
- the eutectic temperature, although to be taken with caution, indicate a solution dominated by $Na_2SO_4$ and NaCl. Additional salt can not be however excluded,
- the concentration of the fluid is high (probably as high as 50 wt%),
- inclusions in thenardite crystals are characterised by a high variability of the vapour filling ratio. This is probably to the brittle property of the host crystals, rather than to boiling,
- homogenisation temperatures which reflect minimal trapping conditions are low (lower than 150°C, mainly lower than 100°C). In our environment, pressure is low, therefore no *pressure correction* (*i.e.* a correction on the temperature due to the pressure of the system) has been applied on homogenisation temperature and homogenisation temperatures can be considered as true trapping conditions. The temperature of the mineralising fluid is therefore relatively low (lower than 150°C). This point is corroborated by the present of all-liquid inclusions (considered as trapped below 70°C) (Goldstein and Reynolds, 1994). All-vapour inclusions and highly variable $R_{flv}$ coul 182 interpreted either as the results of an effervescence process (but the nature of the gas have not been identified) or a heterogeneous nature by mechanical mixture with air,
- the themardite crystals and the associated mineralization therefore result from the precipitation (and/or condensation) of an aqueous liquid-like fluid of moderate temperature.

# EFERENCES

Bakker, R. (2004). Raman spectra of fluid and crystal mixtures in the systems $H_2O$, $H_2O$-NaCl and $H_2O$-$MgCl_2$ at low temperatures: applications to fluid-inclusion research. Canadian Mineralogist, **42**, 1283-1314.

Berkeley, E. (1904). On some Physical constants of saturated solutions. Philosophical Transactions of the Royal Society (London), **203(A)**, 189-215.

Bukshtein, V.M., Valyashko, M.G., and Pel'sh, A.D., (Ed.) (1953). A Reference Book of Solubilities of Salt Systems. Vol. **I** and **II**. Izc. Vses. Nauch.-Issled. Inst. Goz., Goskhimizdat., Moscow-Leningrad, 1270 p.(in Russian).

Chrétien, A., and Kohlmuller, R. (1966). Composés sulfurés, séléniés et tellurés. In : Nouveau traité de chimie minérale (Ed. P. Pascal), Masson, Paris, 445-600.

De Coppet, M. (1872). Recherches sur la empérature de congélation des solutions salines. VII. Constitution chimique de quelques dissolutions salines, d'après les expériences sur leur congélation et leur maximum de densité. Annales de Chimie et de Physique **XXV**, 502-553.

Dubessy, J., Audeoud, S., Wilkins, R., and Kosztolanyi, C. (1982). The use of the Raman microprobe mole in the determination of the electrolytes dissolved in the aqueous phase of fluid inclusions. Chemical Geology, **37**: 137-150.

Dubessy, J., Boiron, M.C., Moissette, A., Monnin, C., and Sretenskaya, N. (1992). Determinations of water, hydrates and pH in fluid inclusions by micro-Raman spectroscopy. European Journal of Mineralogy **4**(5): 885-894.

Finkelman, R.B. and Marose, M. (1977). Downeyite, the first verified natural occurrence of $SeO_2$. American Mineralogist, **62**, 316-320.

Gay-Lussac, L. J. (1819). Annales de Physique et de Chimie **11**, 312 et suivantes (cité dans Wuite, 1914).

Goldstein, R. H., and Reynolds, T. J. (1994). Systematics of fluid inclusions in diagenetic minerals. Society for Sedimentary Geology. Society for Sedimentary Geology, 199 p.

Haynes, F. M. (1985). Determination of fluid inclusion composition by sequential freezing. Economic Geology **80**, 181-186.

Kracek, F.C. (1929). The polymorphism of sodium sulfate: I. Thermal analysis. J. Physical Chemistry, **33**, 2, 1281-1303.

Kracek, F.C., and Gibson, R.E. (1930). The polymorphism of sodium sulfate: III. Dilatometer investigations J. Physical Chemistry, **34**, 188-206.

Loewel, H. (1857). Observations sur la sursaturation des dissolutions salines. Annales de Chimie et de Physique **XLIV**, 32-58.

Loomis E. H. (1896). Ueber den Gefrierpunkt verdünnter wässeriger Lösungen. Annalen der Physik und Chemie, Neue Folge **57**, 495-520.

Marion, G. M. and Farren, R. E. (1999). Mineral solubilities in the Na-K-Mg-Ca-Cl-$SO_4$-$H_2O$ system: A re-evaluation of the sulfate chemistry in the Spencer-Møller-Weare model. Geochimica et Cosmochimica Acta, **63**(9), 1305-1318.

Masalehdani, M.N.N., Potdevin, J.L., Cazier, F., and Courcot D. (2005). Coal waste heap fire: emission of toxic gases and condensation minerals, northern Franc: Measurements and analyses. In proceeding conference book, International conference on coal fire research, 101-103.

Panov, B.S., Dudik, A.M., Shevchenko, O.A., and Matlak, E.S. (1999). On pollution of the biosphere in industrial areas: the example of the Donets Coal Basin. International Journal of Coal Geology, **40**, 199-210.

Pitzer, K. S. (1973). Thermodynamics of electrolytes. I. Theoretical basis and general equations. Journal of Physical Chemistry **77**, 268-277.

Pone, J.N., Stracher, G.B., Finkelman, R.B., Hein., K.A.A., and Annegarn, H.J.(2005). The environmental impact of coal fires, spontaneous combustion in South Africa. In: proceeding conference book, International conference on coal fire research, Beijing, China, 94-95.

Richards, T.W. and Wells, R.C. (1902). Redetermination of the inversion temperatures of sodium sulphate with reference to the international scale. Proceedings of the American Acadely of Arts and Sciences **38**, 481.

Richards, T.W. and Ingve, V. (1918). The solubility of sodium sulfate as a means of determining temperatures. Journal of the American Chemical Society **40**, 164-174.

Roedder E. (1984) Fluid inclusions. Mineralogical Society of America. pp. 544.

Samson, I. M. and Walker R. T. (2000). Cryogenic Raman spectroscopic studies in the system NaCl-$CaCl_2$-$H_2O$ and implications for low-temperature phase behavior in aqueous fluid inclusions. The Canadian Mineralogist **38**, 35-43.

Schroeder, W.C., Gabriel, Alton and Partridge, E.P. (1935). Solubility equilibria of sodium sulfate at temperatures of 150 to 350°. I. Effect of sodium hydroxide and sodium chloride. Journal of the American Chemical Society **57**, 1539-1546.

Ulrich, M. R. and Bodna,r R. J. (1988). Systematics of stretching of fluid inclusions II: Barite at 1 atm. confining pressure. Economic Geology, **83**, 1037-1046.

Washburn, E. R. and Clem, W. J. (1938). The transition temperature of sodium sulfate heptahydrate. Journal of the American Chemical Society, **60**, 754-757.

Werre Jr, R. W., Bodnar, R. J., Bethke, P. M., and Barton, P. B. (1979). A novel gas-flow fluid inclusion heating/freezing stage. Geol. Soc. Am. Abstr. Programs, 539.

Wuite, J.P. (1914). Das System Natriumsulfat-Wasser. Zeistchrift für physikalischer Chemie **86**, 349-382.

Žáček, V., Ondruš, P. (1997). Mineralogy of recently formed sublimites from Kateřina colliery in Radvanice, Eastern Bohemia, Czech Republic. Věstink Českého ústovu **72**, 3, 289-298.

# CHAPTER VI
# CASE STUDY
# MINERALOGY AND PETROGRAPHY OF IRON-RICH SLAGS AND PARALAVAS FORMED BY SPONTANEOUS COAL COMBUSTION, ROTOWARO COALFIELD, NORTH ISLAND, NEW ZEALAND

## ABSTRACT

Pyrometamorphism of coal measures overlying underground burnt-coal seams in the southern area of the Rotowaro Coalfield, New Zealand has produced porcellanites that enclose lenses of iron-rich magnetite and hematite-bearing slag-like rocks showing various degrees of oxidation. Paralavas that are associated with the iron-rich lenses form stalactites around fissures and gas-escape vents, and intrude the porcellanites. The slags are unusually rich in iron, and contain magnetite, hematite, hercynite, titaniferous magnetite, and minor fayalite and silicate glass. Iron oxides in these rocks exhibit a variety of textures and morphologies, including (dendritic, quench, exsolution, and oxidation) The paralavas contain abundant glass that encloses feathery crystals of fayalite and orthoferrosilite, plagioclase, tridymite, cristobalite, and minor magnetite. Phase equilibria data indicate that the paralavas and slags were formed at temperatue in the range of 1000-1600°C. Composition plots of local coal-measure sediments, a siderite nodule, and various porcellanites, slags and paralavas with respect to $SiO_2$, $Fe_2O_3$ and $Al_2O_3$ indicate that the porcellanites are all iron-rich with respect to the unmetamorphosed coal measures. The slags, irrespective of their oxidation state, plot on the iron enrichment trend shown by the porcellanites. Although the siderite nodule lies within the iron enrichment trend, most of the slags are more iron-rich than is the siderite nodule. The paralavas diverge from the iron enrichment trend, suggesting that they have formed by partial melting of the porcellanites. The Rotowaro samples represent some of the most iron-rich natural slags that have collected from a combustion-metamorphic environment.

**Keywords:** Spontaneous coal fire, combustion metamorphism, paralava, iron-rich slag, high temperature minerals

## 1. INTRODUCTION

Thermally baked and fused sediments that are produced by coal seam combustion are common geological features that have been described from many localities throughout the world, including the United States (Foit et al., 1987; Cosca et al., 1989 and Heffern and Coates 2004), Romania (Rădan and Rădan, 1998), Czech Republic (Tyráček, 1994), Australia (Ellyett and Fleming, 1974), New Zealand (Adams, 1978; Masalehdani, 1985) and China (Zhang, 1998; and de Bore et al., 2001). Combustion metamorphic rocks, also known as pyrometamorphic rocks, contain characteristic high-temperature minerals and silicate melts with a range of unusual physical features. These features have been described by a variety of terms including "paralavas" (Fermor, 1918; Sen Gupta, 1960; Essene et al, 1984); or "pseudo-igneous rocks" (Johnson and Bucknell, 1959), "scoria" (Adams, 1978) "buchites" (Hensen and Gray, 1979 and Foit et al., 1987), "melted-vitrified scoriaceous rocks" (Bustin and Mathews, 1982), and "clinker" (Lindqvist et al, 1985; Heffern and Coates, 1997). In many localities the baked and fused sediments are enriched in iron and in a few localities extreme iron enrichment has also led to the occurrence of iron-rich slag -like rocks (Cosca et al. 1989, Clark and Peacor, 1992).

Coal fires can occur in natural, near-surface exposures, underground and open pit mines, and in coal waste heaps and stockpiles. Phenomena such as lightning strikes and bush fires, may start coal seam fires directly or indirectly, however in situ spontaneous combustion of coal is more common. In situ combustion, results from heat generated by the exothermic oxidation of organic matter, and frequently also of pyrite, in the coal. A coal's propensity to combust spontaneously depends on the physical and chemical properties of the coal, the nature and condition of the surrounding sediments (e.g., capacity to dissipate heat) (Colaizzi, 2004), and access to oxygen. In the case of buried coal seams, atmospheric oxygen needs to penetrate into the rock sequence, often to a depth of several hundred meters for combustion to occur.

During in situ coal combustion overburden rocks also are affected by heating, which results in changes to their strength, composition and coherence. As baking and dehydration of sediments progress, shrinkage occurs that leads to the opening of large lateral fissures and cavities. These control the paths of escaping hot gases and lead to the formation of well-defined chimneys, through which toxic hot gases, water vapour and more volatile constituents are expelled from the underground coal combustion. The chimneys also facilitate the ingress of oxygen that is necessary to support and advance the sub-surface combustion of the coal seam, which eventually reduces it to a fused ash deposit. A reduction in volume of 40 to 60% may take place in the enclosing sediments that are being baked and/or melted; this reduces support for the overburden rock and often leads to local collapse.

In the northeastern and southeastern parts of the Rotowaro Coalfield, spontaneous combustion of coal seams have metamorphosed and melted the enclosing coal measure sediments. The degree of thermal alteration that is produced by burning of the coal is variable and very much localized. This study focuses on a single outcrop that is situated 2 km southeast of Rotowaro, Waikato coal region, in the North Island of New Zealand (Fig. 1). The pyrometamorphosed coal measures include baked, to partially melted and entirely melted rocks. Metamorphism has produced mineral assemblages that indicated crystallization under a range of oxidizing conditions. The objectives of this paper are to (1) describe the field occurrence of the porcellanites, melts (paralavas) and the exceptionally iron-rich slags, (2) explain in detail the mineralogy, petrography and chemistry and the mode of formation of different phases in the iron-rich slags and in the paralavas, (3) estimate the possible temperatures of pyrometamorphism under which different minerals and glass formed from the melt, in the slag, and in the paralavas, and (4) determine the origin of the iron-enrichment that produced these unusual pyrometamorphic slags and paralavas.

## 2. THE ROTOWARO COALFIELD

The Waikato Coal Region, North Island, New Zealand is made up of 13 coalfields that contain coals that range from subbituminous C to A. The Rotowaro Coalfield, defined as "the coal-bearing area entered around Rotowaro, Waikokowai, Glen Afton and Pukemiro" (Kear and Waterhouse, 1978), is situated 8 km southwest of Huntly (see Fig. 1) and is the Waikato Region's most productive coalfield. Underground mining began in 1915 and open pit mining commenced in 1936, approximately 55 million tons of coal have been removed.

The Waikato Coal Measures are an upper Eocene to Oligocene transgressive sequence onto Mesozoic basement rocks. They were deposited in a north to north-northwest–trending valley system, which is about 35 km wide and 200 km long and parallels the broad structural grain of the region. In the Rotowaro Coalfield the coal measures are confined by basement topography and syndepositional faulting (Edbrooke et al, 1994, p. 56-57). The gentle north to northwest regional dip of the coal measures (5-10°) is locally variable because of changes in seam thickness and uneven compaction, as well as irregular pre-coal measure topography and faults (Kear and Waterhouse, 1978). The coal in the Rotowaro Coalfield is entirely Eocene in age and is overlain by sediments of the upper Eocene to Oligocene Te Kuiti Group sediments.

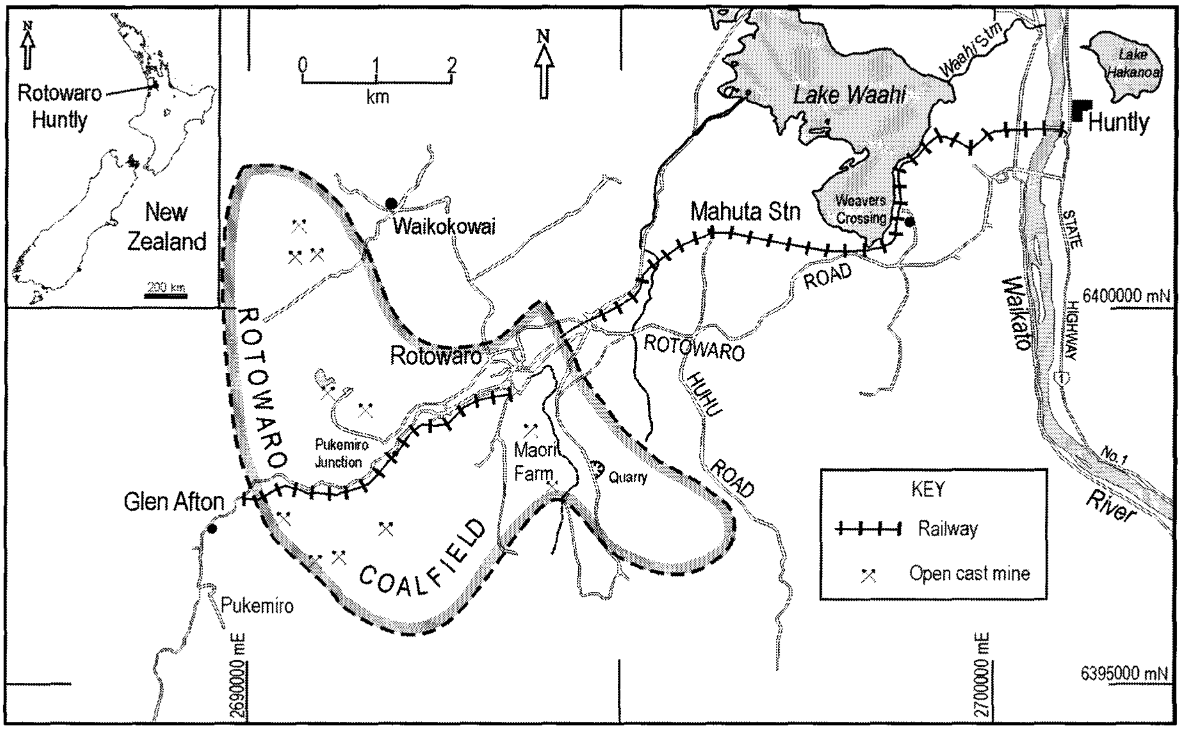

**Figure 1**. Location map of the Rotowaro Coalfield (redrawn from 1:50000 NZMS 260 S14 Hamilton 1979 and NZMS 260 S13 Huntly 1981).

Elsewhere in the Waikato Coal Region the Te Kuiti Group is unconformably overlain by Miocene sediments; however these are absent in the Rotowaro area. A regional unconformity separates the Miocene sediments from post Miocene fluviolacustrine peats, mud, gravel and volcanic ash deposits of the Tauranga Group. The general stratigraphic sequence of the Rotowaro area is presented in Figure 2.

The unmetamorphosed coal measure fireclays that enclose the coal seams in the Rotowaro Coalfield are high in silica and alumina. Mineralogically they are dominated by kaolin with quartz and lesser amounts of illite. Some of the sediments contain small amounts of hematite locally, a horizon that contains nodules of siderite with minor quartz is seen immediately above the coal seams.

Three main sets of coal seams are recognized. From bottom to top these include (1) Taupiri Coal Seams, enclosed in the Lower Waikato Coal Measures; (2) the Kupakupa Coal Seams towards the base of the upper Waikato Coal Measures and (3) the Renown Seam, which often is thin or absent at the top of the Upper Waikato Coal Measures. Coal from the Rotowaro Coalfield is largely is subbituminous A which is on the higher end of the range for the Waikato coal region. The properties of the coals in the Rotowaro Coalfield, given on an air-dried basis, are listed in Table 1a.

The chemistry of representative Waikato coals and coal ashes was described by Gray and Daley (1981). Although sulfides (notably pyrite and marcasite) occur in Waikato coals, 90% of the sulfur in the coals is organic (Gray and Daly, 1981). Many of the elements that are found in the coal that are complexed onto the organic material can be removed by cation exchange or leaching of the coal and are readily liberated readily by combustion. The major inorganic constituents of the Rotowaro coals have been determined using the methods described in Black (1982) and are shown below in Table 1b.

Testing of the spontaneous-combustion propensity of New Zealand coals, showed that the subbituminous coals of the Waikato Coalfield could be classified as "extremely prone to spontaneous combustion" (Beamish et al., 2001).

## 3. COMBUSTION METAMORPHISM

The principal outcrop of pyrometamorphics is a natural scarp face that is about 25 meters long and 2 m to 6 m high (Figs. 3A and 3B). Although neither unmetamorphosed sediments nor the coal seam itself is exposed, it is likely that the combusted coal seam was an extension of the major Taupiri coal seam that is restricted to the wider surroundings of the study site (quarry).

The major portion of the exposure consists of a variety of thermally metamorphosed sediments (porcellanites) that range in color from cream, to yellow, orange and red and reflect different amounts of iron-enrichment and degree of oxidation. The porcellanites, although variable in color, contain similar minerals: mullite, cristobalite, tridymite, and hematite with residual minerals such as low quartz, rutile and zircon. Very high-temperature rocks contain cristobalite, mullite and glass. Many of the porcellanites show disseminations of black iron-rich spots that are mainly composed mainly of hematite (Masalehdani, 1985).

In the main exposure solid yellow porcellanites form discontinuous beds that are up to 50 cm thick, with well-developed horizontal and vertical prismatic cracks that formed as a result of shrinkage during the baking process. The complete combustion of the underlying coal led to the collapse of the overburden and created large cavities. Locally the strata are highly disturbed with well-preserved breccias and broken rocks.

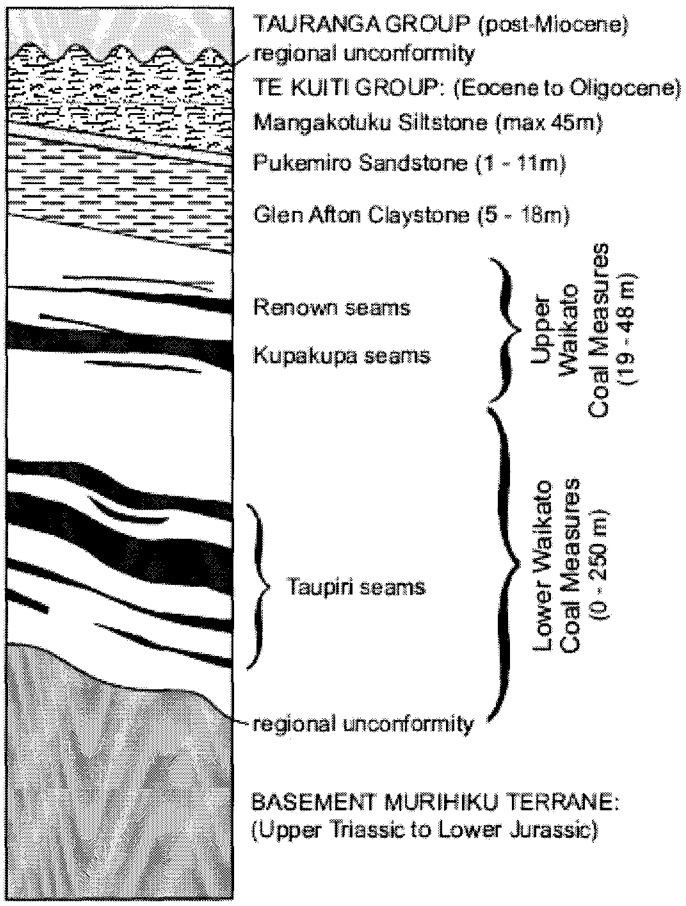

**Figure 2.** General stratigraphic sequence of the Rotowaro area (data supplied by Solid Energy NZ for the Callaghanssector, Rotowaro, Edbrooke et al., 1994).

**Table 1**

**a)** The properties of the coals in the Rotowaro Coalfield on an air dried-basis (after Gray and Daly, 1981).

| Seam | % Moisture | % Ash | % VM | % FC | % S | SP.E. MJ/kg |
|---|---|---|---|---|---|---|
| **Renown** | 11.9 | 8.8 | 40.4 | 38.9 | 1.25 | 24.11 |
| **Kupakupa** | 13.6 | 2.2 | 39.2 | 45.0 | 0.27 | 24.61 |
| **Taupiri** | 14.3 | 3.8 | 37.2 | 44.7 | 0.27 | 24.19 |

**b)** The major inorganic constituents of the Rotowaro coals (after Black, 1982).

| Element abundance in coal (Wt %) | Cl | F | Fe | Ca | Mg | Na | K | Al |
|---|---|---|---|---|---|---|---|---|
|  | 0.04 | 0.01 | 0.4 | 1.2 | 0.1 | 0.1 | 0.05 | 0.07 |

**Figure 3A**. General view of quarry face. Arrows point to the photos taken from the central part of the quarry and sample collection locations from profile E.

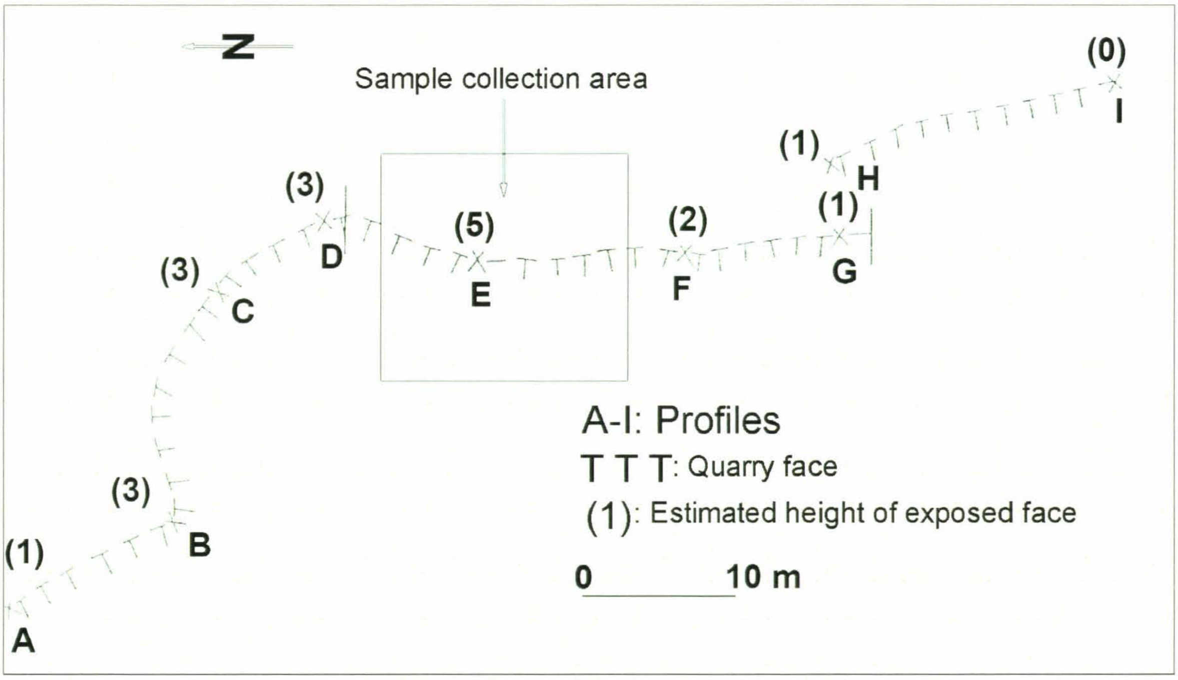

**Figure 3B**. Quarry face shown in Fig. 3a and sample collections area (profile E).

A lensoid body (2.5 m x 0.4m) in the lower part of the outcrop within the light colored baked porcellanites contains the main exposure of iron-rich, magnetite and hematite-bearing, pyrometamorphics (Fig. 4). These rocks are black- blue and magnetite-rich at the bottom and ends of the lens, whereas they are red hematite-rich in the middle of the lens which indicated variable oxidation conditions.

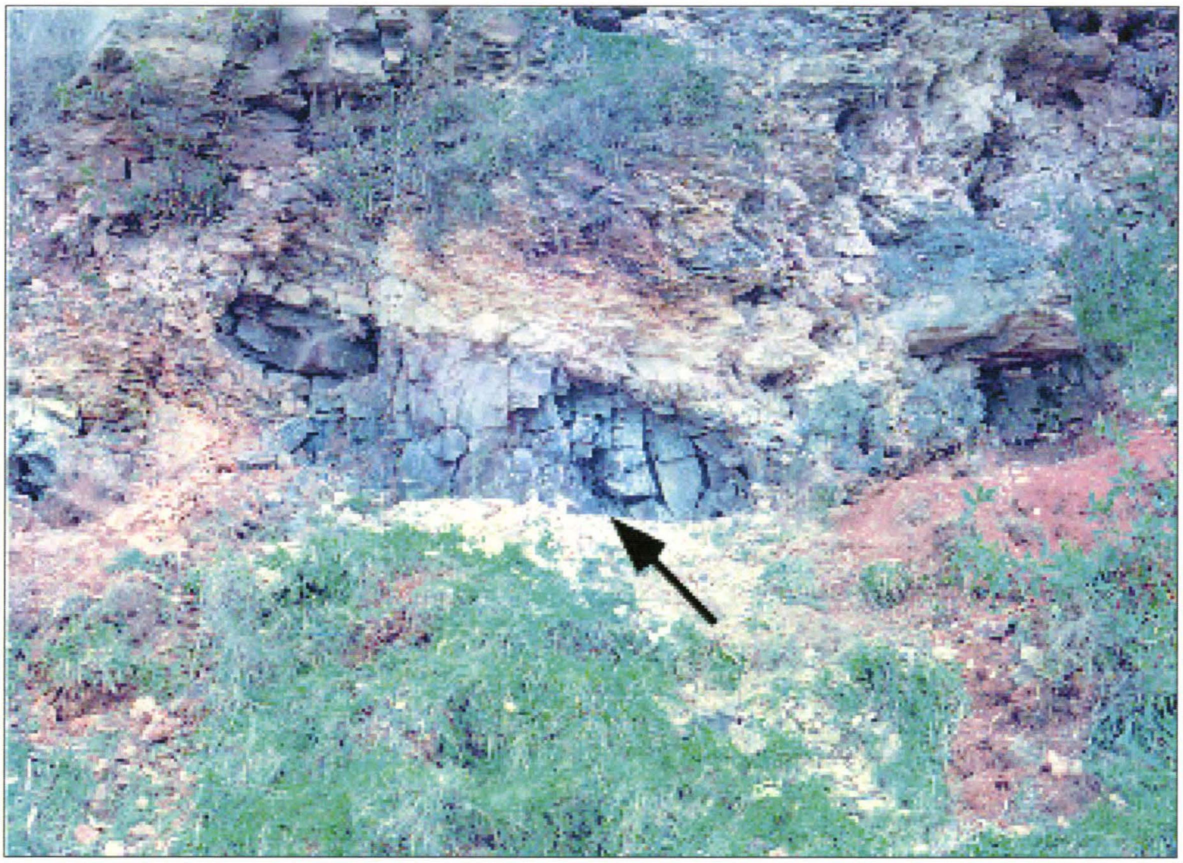

**Figure 4.** A lensoid body of baked (dark blue-black) iron-rich pyrometamorphosed rocks (arrow). Scale: 2.5m x 0.4m at the highest point (see also Fig. 6b).

In hand specimens, melted iron-rich rock (the slag) is hard, heavy, vesicular and dark gray to black with a dull luster. Except for its vesicularity, it is similar in appearance to a furnace slag (Fig. 5). Vesicles in the slag are cavities that are less than 1 cm in diameter, with either spherical or irregular that shapes result from the trapping of gas bubbles.

Melts of iron-rich silicate rock that appear in irregular masses on both sides of the lens of slag and porcellanites (Fig. 6A, B) are here referred to herein as paralava. The paralavas are dark gray to black with a ropy, lobate, rounded pod-like form and have dull, glazed, smooth surfaces (Fig.7). The dark color of the most paralavas indicates that they were formed in a reducing environment. "Stalactites" of the solidified paralavas were observed around vents, tongues of paralava have penetrated the overlying porcellanites along horizontal fissures (Fig. 8A, B) and fill the cavities of brecciated rocks (Fig. 7C). Ropy paralava coats the surface of some fissures (Fig. 8C). In the outcrop in profile E (Fig. 3A) the slags and the paralavas occur in close vicinity to fissures, cracks, and crevices (chimneys) where most of the hot gasses from underground coal combustion have escaped to the atmosphere. This indicates that the combustion gasses were the source of the heat that produced the very high-temperature pyrometamorphism, rather than the combustion of the coal itself, and that the gasses transported the elements that are concentrated in the slags and paralavas.

## 4. METHODS OF STUDY

For this study, samples of the pyrometamorphics were taken mainly from profile E (see Fig. 3a, 3b; Tables 2 and 3). Samples of unmetamorphosed fireclays and siderite-rich nodules from open pit mines in the Rotowaro Coalfield (see section 3) were provided by the State Coal Mines, Huntly.

X-ray powder diffraction data were obtained using a Phillips PW 1130 diffractometer. For petrographic studies of polished sections and polished thin sections, Leitz Labor Lux II transmitted light and Reichert reflected light microscopes were used. Quantitative electron microprobe determinations of the mineralogy of slag and paralava samples were performed using a JEOL JXA-5A electron microprobe. Data acquisition and analysis were carried out using a "Link System" energy dispersive analyser, and software.

Bulk rock major element chemical analyses were obtained using an automated Philips PW 1410 x-ray fluorescence spectrometer. Data reduction was carried out by the methods described in Parker and Willis (1977).

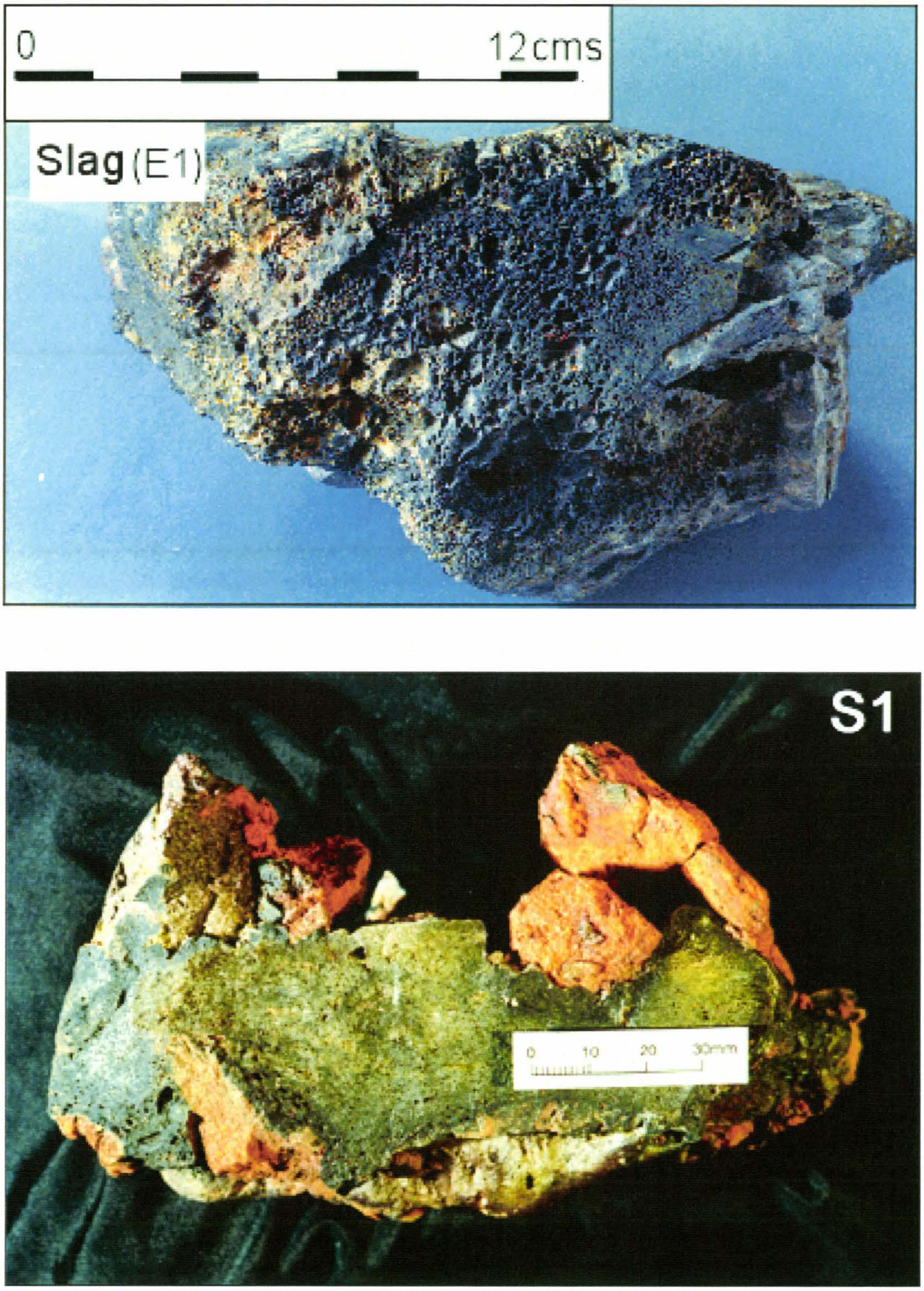

**Figure 5**. Cut slabs of selected melted iron-rich slags. Note vesicular slaggy material in sample S1 is surrounded by reddish porcellanite.

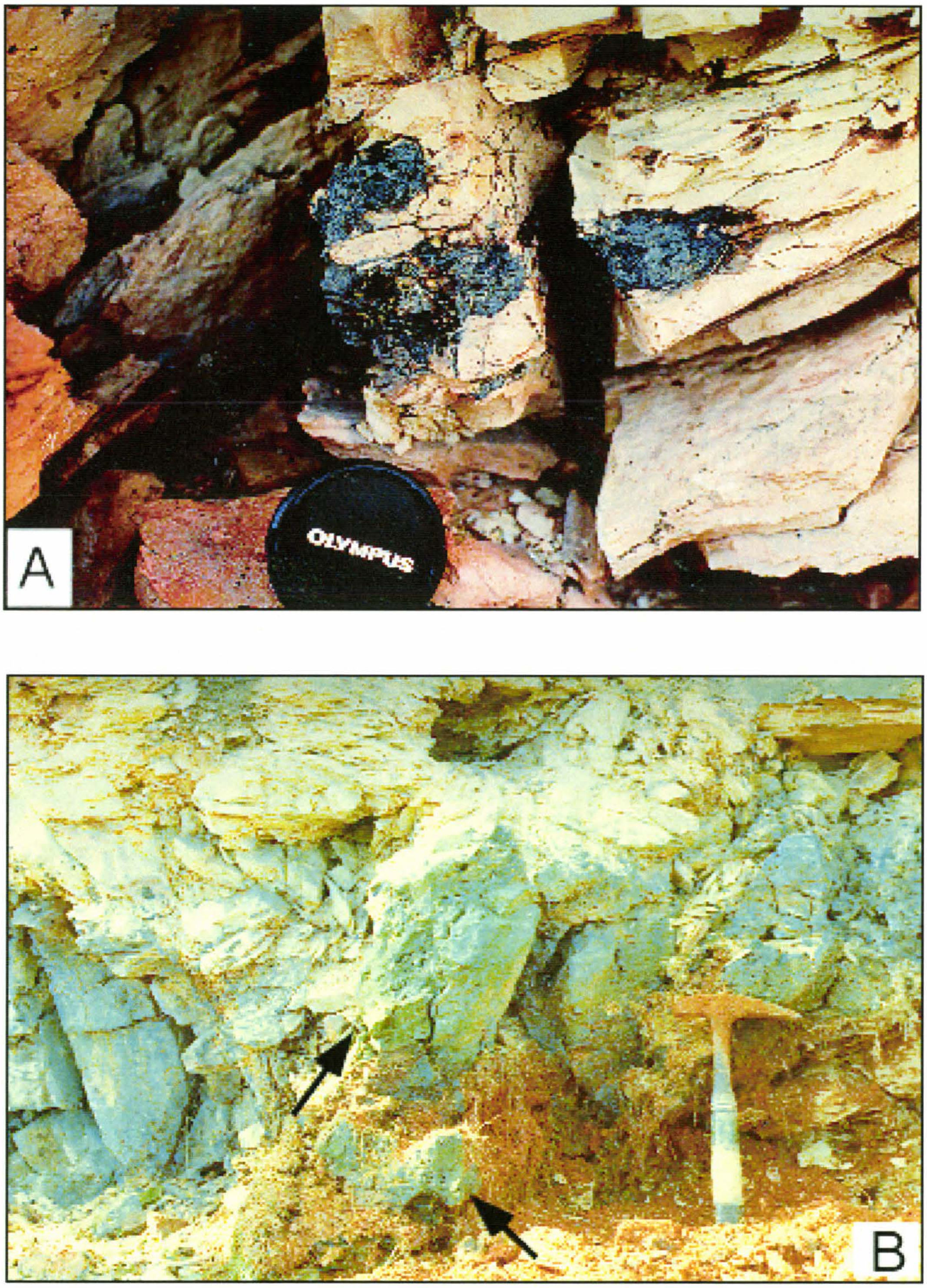

**Figure 6. (A)** Shrinkage cracks along and across porcellanites (creamy-yellow) containing irregular slaggy masses of melted rock (gray-black). Lens cap 5cm. **(B)** Highly vesicular slaggy masses of iron-rich rock (arrows).Enlargement of center portion of Figure 4 of profile E. Hammer 30 cm.

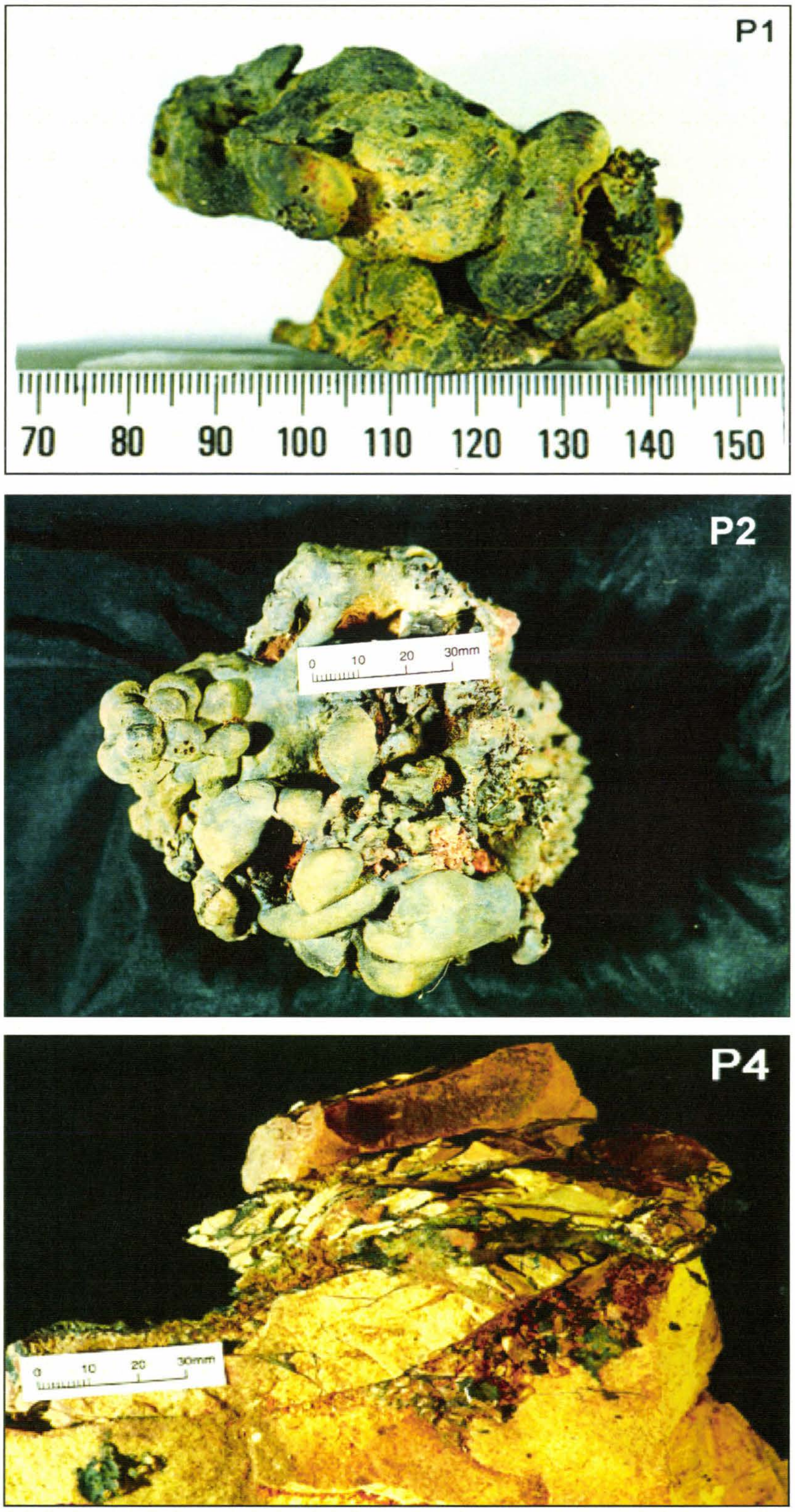

**Figure 7**. **(A, B)** Cut slabs of the selected pyrometamorphic, the paralavas (samples P1 and P2). Note gray-black color, ropy, lobate, rounded pod-like shape and dull glazed surfaces of the paralavas. **(C)** Filling of spaces by paralava (gray-black) in brecciated porcellanite (yellow) in sample P4.

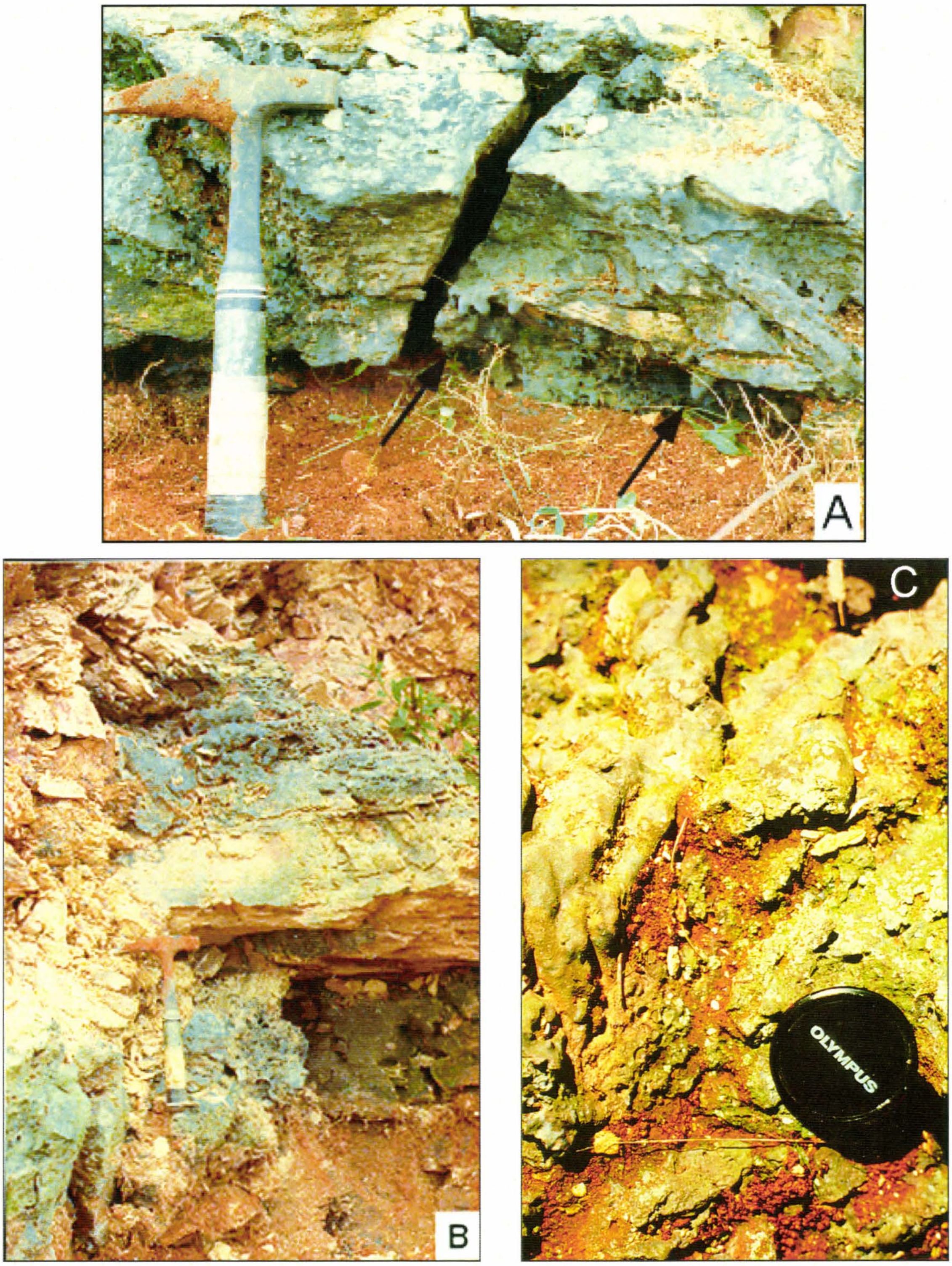

**Figure 8**. Profile E. **(A)** "Stalactites" (arrows) of solidified paralavas in a cavity (note the open vertical crack). **(B)** Paralava (gray-black) associated with and/or flowing over porcellanites. Hammer for scale, 40 cm. **(C)** Ropy paralava coats the surface of some fissures in profile E at the study area. Lens cap for scale 5cm.

**Table 2**. Sample descriptions of selected slags and paralavas and identified minerals.

| Sample n° | Descriptions and minerals |
|---|---|
| **E1 (Slag)** | Numerous circular vesicles <1cm in diameter, dark gray to black, dull luster, heavy and hard.<br>Magnetite, hematite, Al-spinel, Ti-spinel ± fayalite ± glass |
| **RO1 (Slag)** | Vesicular, dark gray to, dull luster, heavy and hard, dark gray, surrounded by reddish porcellanite.<br>Magnetite, hematite, Al-spinel, Ti-spinel, ± fayalite ± glass ± unknown Fe-Al-Ti-Si-oxide |
| **RO2 (Slag)** | Circular vesicles <1cm in diameter, rough surface, dark gray-black, dull luster.<br>Magnetite, hematite, Al-spinel, Ti-spinel, ± fayalite ± glass |
| **P1 (Paralava)** | Dark gray to black in color, has a ropy, lobate, rounded pod-like form, dull glazed smooth surface, is hollow and light.<br>Fayalite, orthoferrosilite, anorthide, tridymite, cristobalite, glass ± magnetite |
| **P2 (Paralava)** | Gray color, has a ropy, lobate round or ellipsoidal shape, dull glazed luster smooth surface, is hollow and light.<br>Fayalite, orthoferrosilite, anorthide,tridymite, cristobalite, glass ± magnetite |

**Table 3**. Methods of identification of minerals in selected slags and paralavas.

| Identified minerals | Methods | | |
|---|---|---|---|
| | XRD | OP | EMP |
| Magnetite | x | x | x |
| Hematite | x | x | x |
| Al-spinel | x | x | x |
| Ti-spinel | x | x | x |
| Fayalite | x | x | x |
| Orthoferrosilite | x | x | x |
| Anorthide | x | x | x |
| Tridytmite | x | x | |
| Cristobalite | x | x | |
| Glass | | x | x |
| *Un. Fe-Al-Ti-Si-Oxide | | x | x |

XRD: X-ray diffraction    OP: Optical microscope

* Un : Unknown    EMP: Electron microprobe

## 5. CHEMISTRY

Chemical analyses of selected slags, paralavas, porcellanites and fireclays are given in Table 4. Figure 9 shows a $SiO_2$, $Fe_2O_3$, $Al_2O_3$ ternary diagram of the Rotowaro slags, paralavas and porcellanites plotted with unmetamorphosed Rotowaro sediments. The various fields show little overlap. The trends indicate that the porcellanites are iron-rich with respect to the coal measures. Although the paralavas show a similar an amount of iron-enrichment that is similar to the porcellanites, their trend diverges towards enrichment in $SiO_2$ with decreasing $Fe_2O_3$. The slags show much more iron-enrichment and lie on the extension of the porcellanite field toward the $Fe_2O_3$ corner of the ternary diagram. The Rotowaro examples of slags represent some of the most iron-rich natural slags that have been observed in a combustion metamorphic environment.

The variations in chemistry of the main rock groups also are reflected in their petrography. The iron-rich slags are composed dominantly of magnetite accompanied by other iron-rich oxides and fayalite. The iron oxides show a range of different textural features that indicates that complex oxidation and exsolution effects took place as the slag cooled. The paralavas differ from the slags and other pyrometamorphics in that they contain abundant glass enclosing quench-textured silicate minerals, which include plagioclase, tridymite, feathery crystals of fayalite and orthoferrosilite, with only minor amounts of magnetite.

## 6. PETROGRAPHY AND MINERALOGY OF THE FE – RICH SLAGS

The iron-rich slags have assembages that are dominated by magnetite, hematite, and spinels. These minerals occur in many different textural associations with each other, and reflect the original crystallization of the slags at high temperatures and under a range of oxidation conditions followed by periods of re-equilibration of the primary phases as the rocks cooled. In addition to oxides, minor amounts of fayalite and silicate glass are found in the slags. Iron silicate (fayalite) in slags is an accessory phase. It appears as fine-grained, dark gray inclusions in magnetite hosts and /or the matrix (see Fig. 10C).

## Table 4

**a)** Chemical analyses of selected slag (E1) and paralavas (P1 and P2).

| | (E1) | (P1) | (P2) |
|---|---|---|---|
| $SiO_2$ | 32.48 | 55.24 | 54.92 |
| $TiO_2$ | 0.63 | 0.86 | 0.77 |
| $Al_2O_3$ | 12.80 | 17.2 | 16.78 |
| $Fe_2O_3^*$ | 46.13 | 21.39 | 21.49 |
| MnO | 0.54 | 0.01 | 0.01 |
| MgO | 1.42 | 1.7 | 1.89 |
| CaO | 0.42 | 0.2 | 0.22 |
| $Na_2O$ | 0.28 | 0.03 | 0.07 |
| $K_2O$ | 0.25 | 1.39 | 1.83 |
| $P_2O_5$ | 0.20 | 0.19 | 0.28 |
| Cl | N.D. | 0.017 | 0.029 |
| $SO_3$ | N.D. | 0.027 | 0.029 |
| $H_2O$ | 2.06 | N.D. | N.D. |
| LOI | 1.61 | N.D. | N.D. |
| Total | 98.82 | 98.254 | 98.318 |

*$Fe_2O_3$ refers to total iron     N.D: No data

**b)** Chemical analyses of selected siderite-nodule (SQ8) fireclays (F1 and F2) and porcellanites (E10 and B2).

| | (SQ8) | (F1) | (F2) | (E10) | (B2) |
|---|---|---|---|---|---|
| $SiO_2$ | 9,16 | 62.52 | 62.60 | 43.12 | 52.44 |
| $TiO_2$ | 0.25 | 1.26 | 1.25 | 0.79 | 1.11 |
| $Al_2O_3$ | 5.08 | 26.08 | 26.26 | 19.68 | 24.87 |
| $Fe_2O_3$* | 62,99 | 3.99 | 3.98 | 29.15 | 16.25 |
| MnO | 1,58 | 0.01 | 0.02 | 0.48 | 0.30 |
| MgO | 0,45 | 0.69 | 0.70 | 1.14 | 1.01 |
| CaO | 0,82 | 0.05 | 0.06 | 0.11 | 0.06 |
| $Na_2O$ | N.D. | 0.02 | 0.04 | 0.00 | 0.14 |
| $K_2O$ | 0,29 | 1.73 | 1.72 | 0.19 | 0.18 |
| $P_2O_5$ | 0,25 | 0.18 | 0.70 | 0.16 | 0.11 |
| $H_2O$ | 0.6 | 0.18 | 0.18 | 2.77 | 2.13 |
| LOI | 17,83 | 3.19 | 3.19 | 2.85 | 2.13 |
| Total | 100 | 99.89 | 100.70 | 100.42 | 100.73 |

*$Fe_2O_3$ refers to total iron

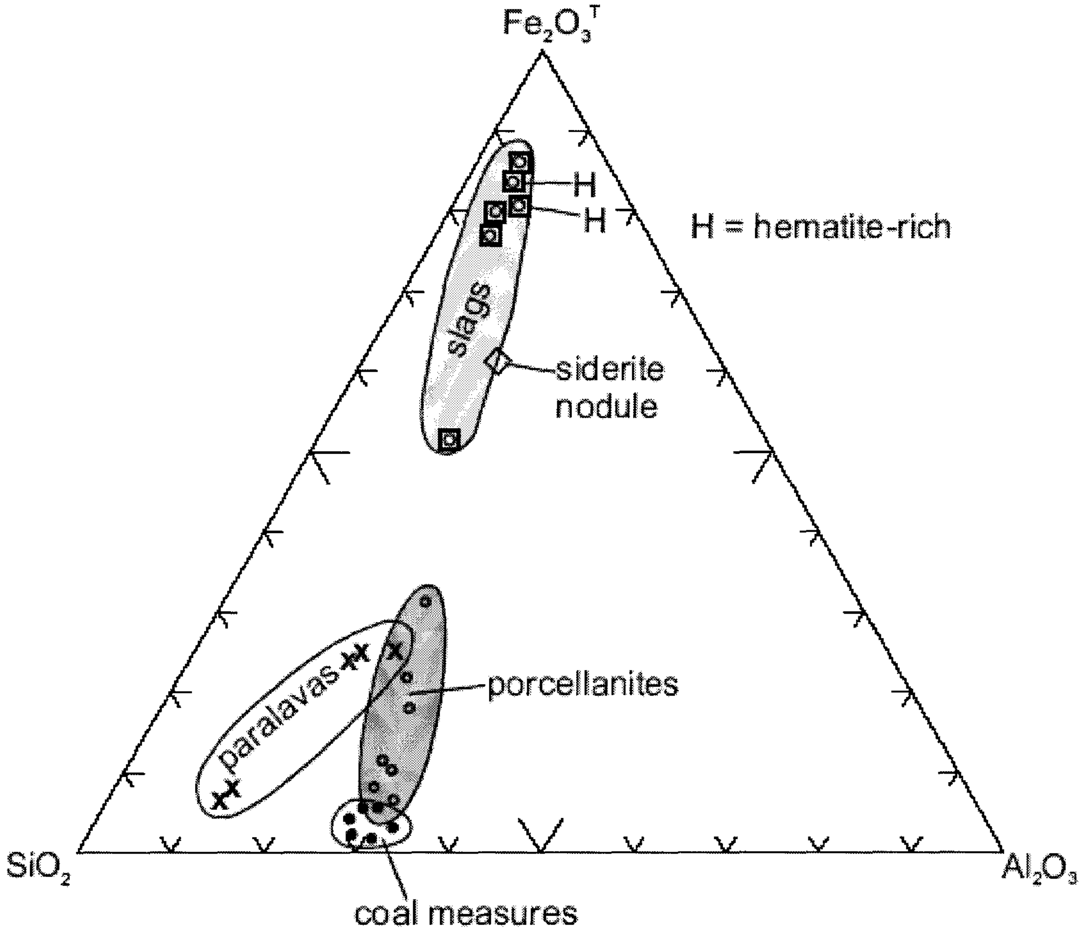

**Figure 9**. Plot of $SiO_2$, $Fe_2O_3$ and $Al_2O_3$ of the various Rotowaro pyrometamorphics and coal measure sediments.

The principal associations and textural relationships of opaque oxides that are observed in the slags are:

### *6.1. Magnetite-hematite-spinel assemblages*

- Relatively coarse skeletal and fine dendritic intergrowth of magnetite-hematite-spinel set in a microcrystalline silicate mineral or silicate-rich glass matrix is a common occurrence. Typically, the skeletal crystals are elongate, and consist of a simple set of cross-arms at right angles that correspond to the cubic crystallographic axes; it appears that growth was initiated from the interior surface and proceeded toward the arms and arrow-heads. The outlines of these skeletal crystal face-boundaries often are incomplete (Fig. 10).

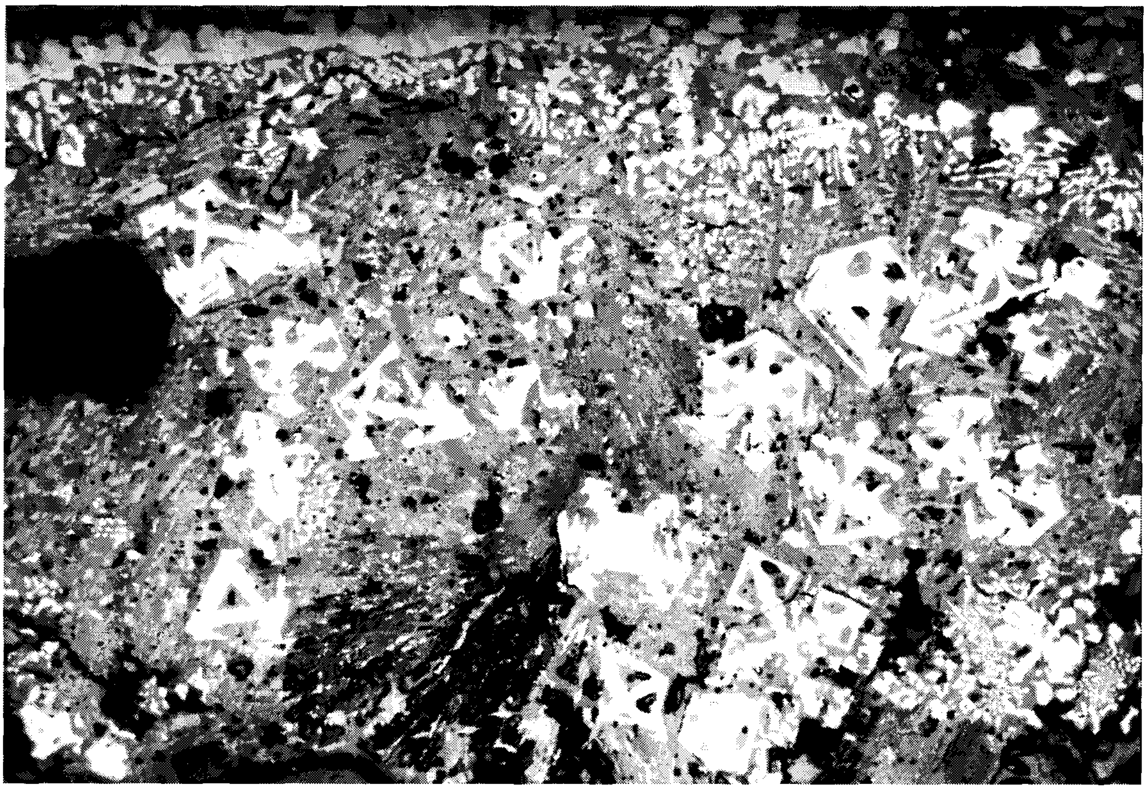

**Figure 10**. Reflected light micrograph x 22 (sample E1). Skeletal crystals of exsolved magnetite-hematite-spinel assemblages (white) in silicate matrix (gray) of the slag. The black areas are vesicles.

- Exsolved intergrowths of the fine hematite and Al-spinel lamellae that are oriented parallel to crystallographic planes in the host magnetite commonly occur in the central portion of the slag lens (Fig. 11). The spinel lamellae were identified in polished section by their isotropic nature and grey color. Fine exsolved and tabular hematite intergrowths in magnetite appear white-gray and anisotropic and are highly reflective. Qualitative scanning traverses across a selected crystal (Fig. 12) showed a good negative correlation between Al and Fe. The concentration of Al toward the center of the crystal could be evidence of crystallization at very high temperatures. The exsolved fine spinel lamellae in host magnetite are aluminous spinels. Unfortunately, because of the size of the spinel it has not been possible to obtain an electron microprobe analysis of the individual spinel lamellae.

- Fine intergrowths of magnetite-hematite-spinel having myrmekitic textures are present as interstitial crystals in a silicate matrix. The grain boundaries of these crystals are mutually rounded, so that in thin sections the texture resembles a finely woven fabric. Although it is difficult to observe the details of the exsolution textures of these assemblages, they are considered to be the same as described above. These dendrites often form "coronas" around coarse central solid crystals of the same phases; in some cases they form sub parallel acicular branches in the "corona" (see Fig. 11A).
- Euhedral crystals (up to 0.4mm in diameter) of an exsolved magnetite-hematite spinel assemblage occur as aggregates of fine equant crystals, grouped together and having a mosaic texture (see Fig. 11B), or have hexagonal outlines enclosed in a silicate matrix (see Fig. 11C). The interior and interstices between the hollow hexagonal dendritic crystals are filled with silicates and/or glass (see Fig.11D).

### *6.2. Hematite and Ti-spinel assemblages*

Ti-spinel with a relatively homogeneous composition, which contains 9.6 to 11.8% $TiO_2$ and less than 4% $Al_2O_3$ occurs with hematite as anhedral "mosaic" textured aggregates that are concentrated at the rims of the vesicles in the slag sample E1 (Fig. 13). Minerals in this assemblage lack the exsolution features observed in the magnetite-hematite-spinel assemblages.

### *6.3. Late oxidation of magnetite to hematite and zoning effects*

Oxidation of magnetite to hematite occurs as relatively broad lamellae and often extends from one edge of the magnetite crystal to the other (see Fig. 11). This particular oxidation process apparently took place while the combustion of the coal seam was in progress, as evidenced by similar occurrences that were observed in the "furnace slags of a central heating system, from places where the draft has been especially intermittent" (Ramdohr, 1982).

Some large euhedral magnetite crystals (up to 0.4 mm in diameter) show a very characteristic zoning that is expressed most obviously by color variation: the inner most part of the magnetite crystals is gray-brown, whereas the margins are whitish-blue (Fig. 14). These optical variations indicate the presence of hematite at the margins of the magnetite crystals. This incipient "martitization" has most likely resulted from oxidation of magnetite to hematite during the cooling process at temperatures 600°C of at least (Haggerty, 1976).

## 7. PETROGRAPHY AND MINERALOGY OF THE PARALAVAS

The paralavas are distinct in that they contain more glass, and an abundance of silicate minerals including orthoferrosilite, fayalite, tridymite and cristobalite, occasional high-temperature feldspar, and only minor amounts of magnetite. All minerals in the paralavas show ubiquitous feathery quench textures.

### *7.1. Iron silicates*

Fayalite in thin sections, fayalite appears as pale yellow crystals with high relief and high birefringence. Orthoferrosilite is colorless to pale yellow, with nearly parallel extinction (0-8°) and with 2Vα, as measured by universal stage method, ranging from 82° to 108° (average 90°). Skeletal crystals of fayalite and orthoferrosilite, which vary in size from a few microns to phenocrysts of up to 0.3 mm in diameter occur in all paralavas. These crystals may be embayed at their extremities or cellular (filled with glass) throughout much of their length and elongated parallel to the a-axis, or form as large hopper-shaped crystals generally with the gross outline of the common dome and prismatic forms of olivine (Fig. 15).

Electron microprobe analyses of fayalite and orthoferrosilite have been recalculated to give an empirical structural formula, calculated on the basis of 4 oxygens atoms for fayalite and 3 oxygens atoms for orthoferrosilite, of $(Fe_{1.91}\ Mn_{0.03}\ Mg_{0.06})\ (Al_{0.07}\ Si_{0.92})\ O_4$ and $(Fe_{0.80}\ Mn_{0.01}\ Mg_{0.15}\ Ca_{0.01})\ (Al_{0.13}\ Si_{0.90})\ O_3$ respectively.

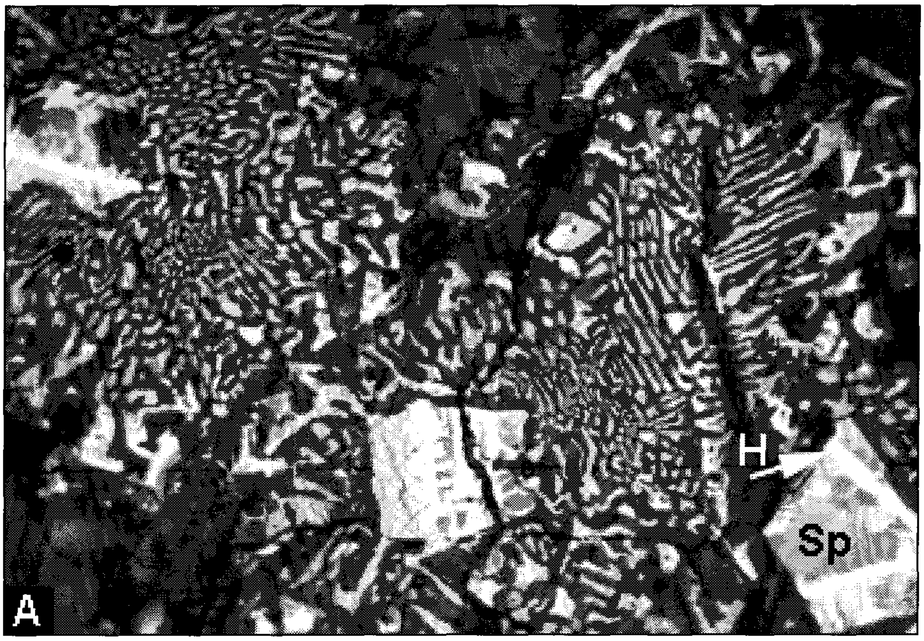

**Figure 11A**. Reflected light micrograph of slags x 45 (sample E1). Exsolved magnetite-hematite-spinel assemblages (white) in granophyric-like intergrowth relation with silicate minerals (gray). H, Hematite; Sp, Spinel.

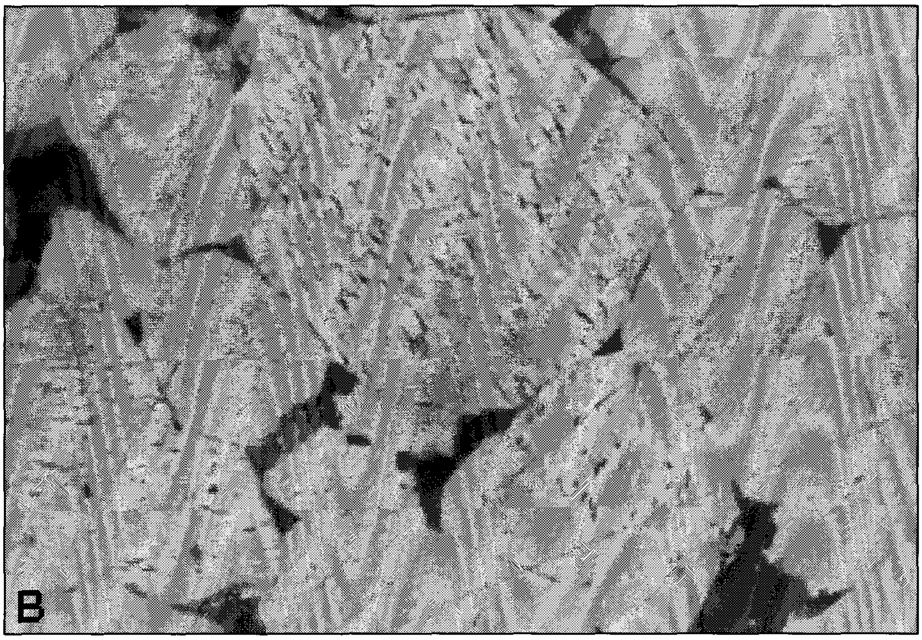

**Figure 11B**. Reflected light micrograph of slags x 110 (sample RO2). Crystals of magnetite with finely exsolved hematite (white) and spinel (gray), arranged in a mosaic texture. The black areas between the crystals are silicates.

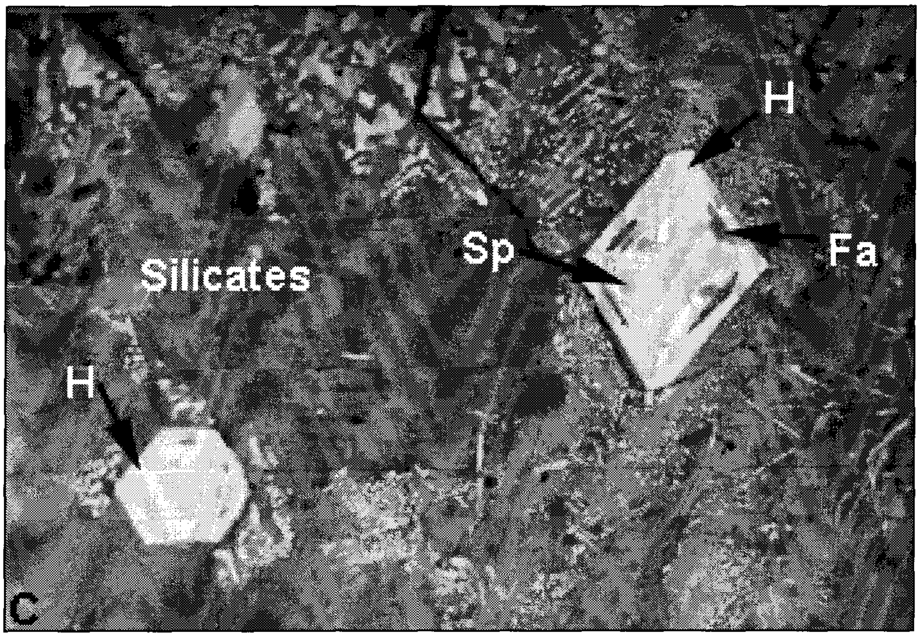

**Figure 11C**. Reflected light micrograph of slag x 45 (sample E1). Euhedral magnetite with finely exsolved spinel (Sp) lamellae (light gray) and tabular intergrowths of hematite (H) (white) in silicates (cristobalite, fayalite and glass) matrix (dark gray). The dark gray inclusions in these crystals are fayalite (Fa).

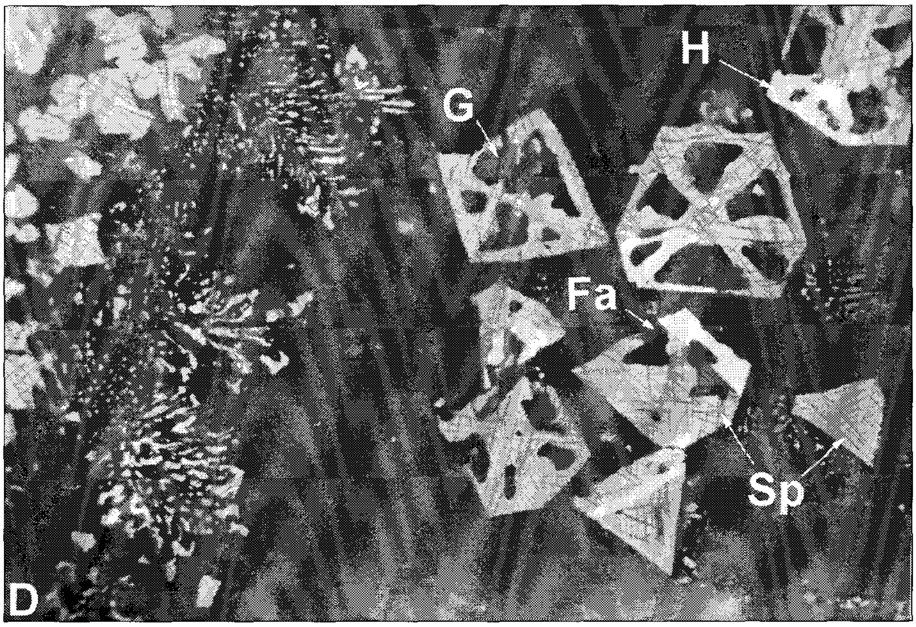

**Figure 11D**. Reflected light micrograph of slag x 45 (sample E1). Euhedral magnetite crystals with finely exsolved spinel (Sp) lamellae (light gray) and tabular intergrown hematite (H) (white) in silicate matrix (dark gray). The areas between the internal dendrite within these crystals are filled with fayalite (Fa) and /or glass (G)..

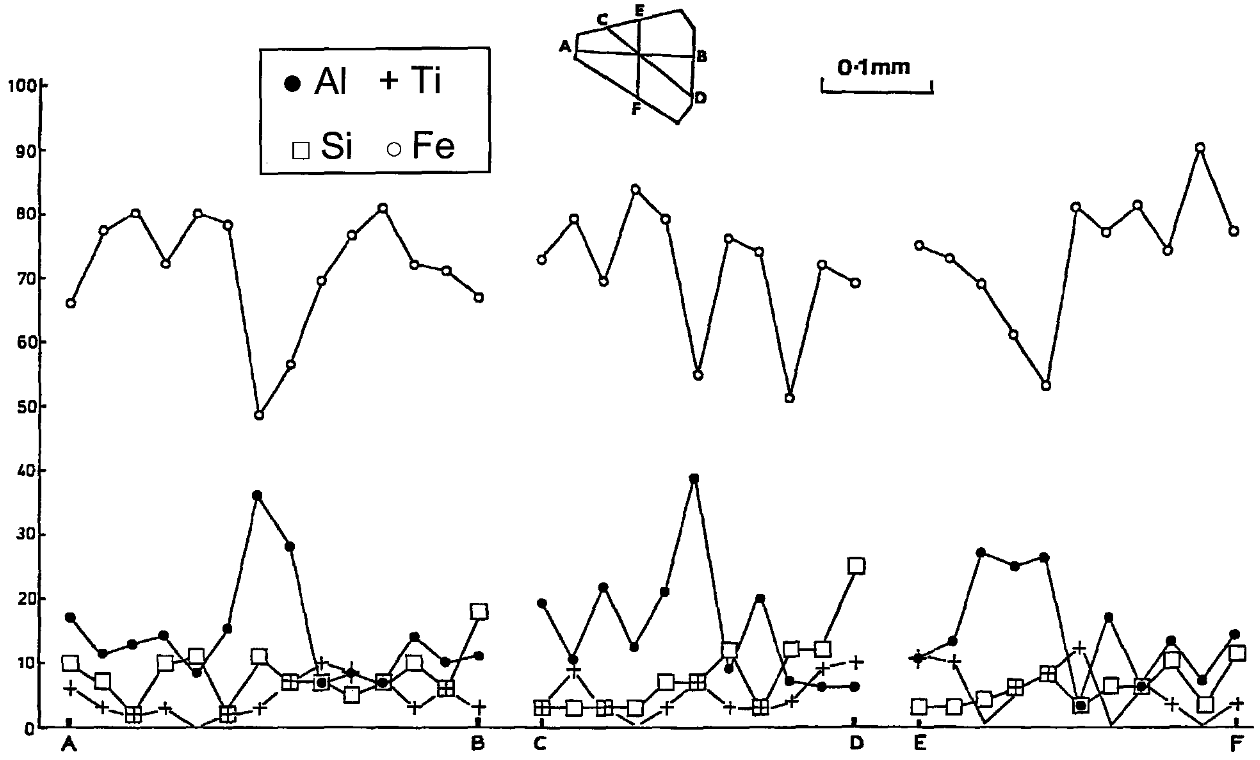

Figure 12. Plot of the qualitative electron microprobe analyses of selective exsolved magnetite-hematite-spinel assemblages in the slag (sample E1).

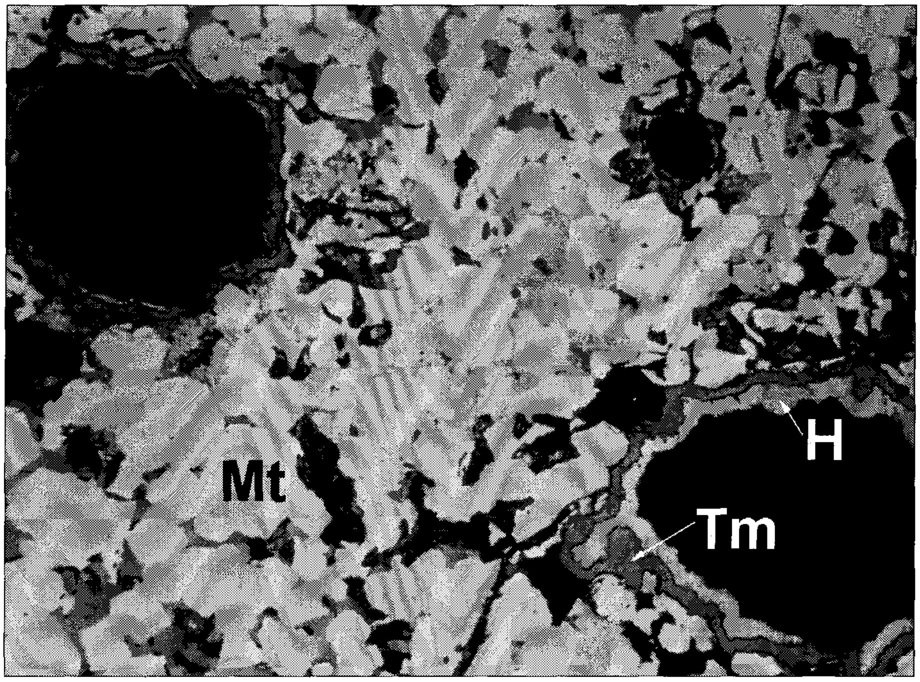

**Figure 13**. Reflected light micrograph x 45 (sample E1). Hematite (H) and titaniferous magnetite (Tm) crystals concentrated around the vesicles (black). Matrix (dark gray) consists of tridymite, fayalite and glass. Black spots are cavities. Mt, Magnetite.

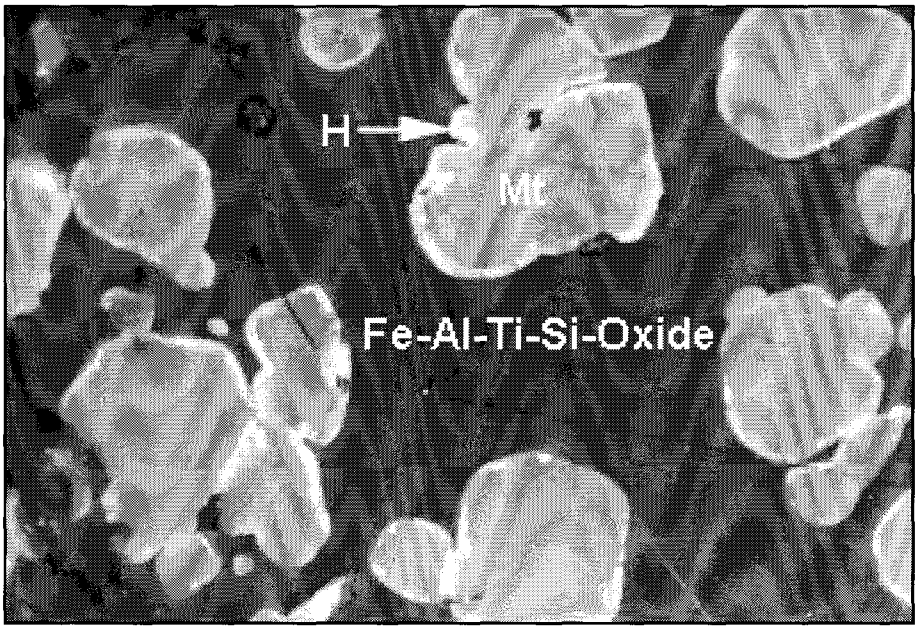

**Figure 14**. Reflected light micrograph x 110 (sample RO1). Magnetite (Mt) crystals with rims of hematite (H). Matrix consists of unknown Fe-Al-Ti-Si-oxide. Black spots are dirt on the surface of sample.

### *7.2. Feldspar, silica minerals, opaques and glass*

High-calcium feldspar crystals occur as colorless low relief and birefringence laths or as tabular crystals intergrown with orthoferrosilite and fayalite and enclosed by reddish-brown glass. The tabular plagioclase crystals, when viewed in sections cut perpendicular to their a-axes, show a characteristic hollow, rectangular "belt-buckle" form (see Fig. 15A).

Electron microprobe analyses reveal that the plagioclase contains notable, although variable, amounts of iron (1.9-3.97% total iron calculated as $Fe_2O_3$). Feldspars in melted sediments that were associated with coal seams were reported by Phemister (1942), Bishop (1965), Bentor and Kastner (1976), Bustin and Mathews (1982), Mason and Davis (1983), Essene et al (1984), Cosca et al. (1989), and Grapes (2004).

Cristobalite and tridydmite were identified by their X-ray powder diffraction data. In thin section tridymite occurs as acicular (up to 0.3 mm long) or "fan"-shaped arrays, containing fine feather-like orthoferrosilite (see Fig. 15D). Cristobalite in paralavas possibly crystallized from the residual silicate melt in the temperature range of 1500°C to 1600°C, whereas tridymite, in the same specimens, could have been formed directly from the melt at lower temperatures (1500-1400°C) or by conversion of cristobalite during the cooling process according to Schairer and Bowen (1947) (Fig.16).

Magnetite in paralavas forms fine feathery inclusions, intergrown on the rims and/or the concave embayments of lobate crystals of fayalite and orthoferrosilite. Glass occurs in the interstices between the silicates (see Fig. 15).

The glass enclosing the high-temperature silicate and oxide minerals is high in silica (60 wt %) and contains variable amounts of iron ($\leq 7$ wt %). Notably all glasses contain substantial amounts of $K_2O$ ($\leq 4$ wt %) and very low amounts of $Na_2O$ ($\leq 1$ wt %) (Table 5).

## 8 DISCUSSION OF CONDITIONS OF FORMATION OF SLAGS AND PARALAVAS

It is clear that the paralavas and slags from Rotowaro Coalfield in New Zealand formed from high-temperature melting at atmospheric pressure, but there is no direct way to determining the melting temperatures or the conditions of melting or the temperature of crystallization of the various mineral assemblages. Occurrences of mineral assemblages in these rocks and phase equilibria studies from the literature do allow us to make estimates of temperatures for the formation of the slags and paralavas at the study site.

The concentration of Al toward the center of the magnetite crystals in the slags is good evidence of crystallization at very high temperatures. Phase relations in the system Fe-Al-O at temperatures ≥1000°C were studied by Richards and White (1954), Hoffmann and Fisher (1956), Muan and Gee (1956) and Atlas and Sumida (1958); they observed that at these temperatures and atmospheric pressure complete solid solution between the spinels, magnetite ($Fe_2O_3$) and hercynite ($FeAl_2O_4$) occurred. Exsolution between $Fe_3O_4$ and $FeAl_2O_4$ is reported to begin at T≤1000°C at a given composition of 55 mole % hercynite (Turnock and Eugster, 1962).

The concentration of homogeneous crystals of hematite and titaniferous magnetite around the vesicles indicates that these mineral assemblages have crystallized later than did assemblages in the slag itself, and under more oxidizing conditions than controlled the magnetite-hercynite exsolved assemblages that are found in the interior of the slag samples. It also is possible that the titaniferous magnetite and hematite rapidly quenched around the vesicles and remained unexsolved. Similar occurrences of unexsolved Ti-spinel are described in (Ramdohr 1982, p.924,) from extrusive or plutonic rocks brought rapidly from the high-temperature zones to the Earth's surface.

The crystallization of the titaniferous magnetite in basalt is a function of temperature and partial pressure of oxygen ($PO_2$) (Haggerty, 1976). To determine the $PO_2$ during development of this mineral within the slag sample E1, the composition of Ti-magnetite obtained from the electron microprobe analyses was plotted in the system $FeO$-$TiO_2$-$Fe_2O_3$ at 1200°C (Fig. 17), assuming the temperature of the crystallization was the same. From this figure it seems likely that the crystallization of titaniferous magnetite occurred under high $PO_2$ conditions as also is evidenced by the presence of coexisting hematite.

**Figure 15A.** Transmitted light micrographs x 220 PPL of paralava (sample P1). Typical branching dendritic texture of fayalite (Fa) containing an overgrown skeletal anorthide (A). The gray phase at right top corner is orthoferrosilite (Fs) with inclusions of glass (G) black.

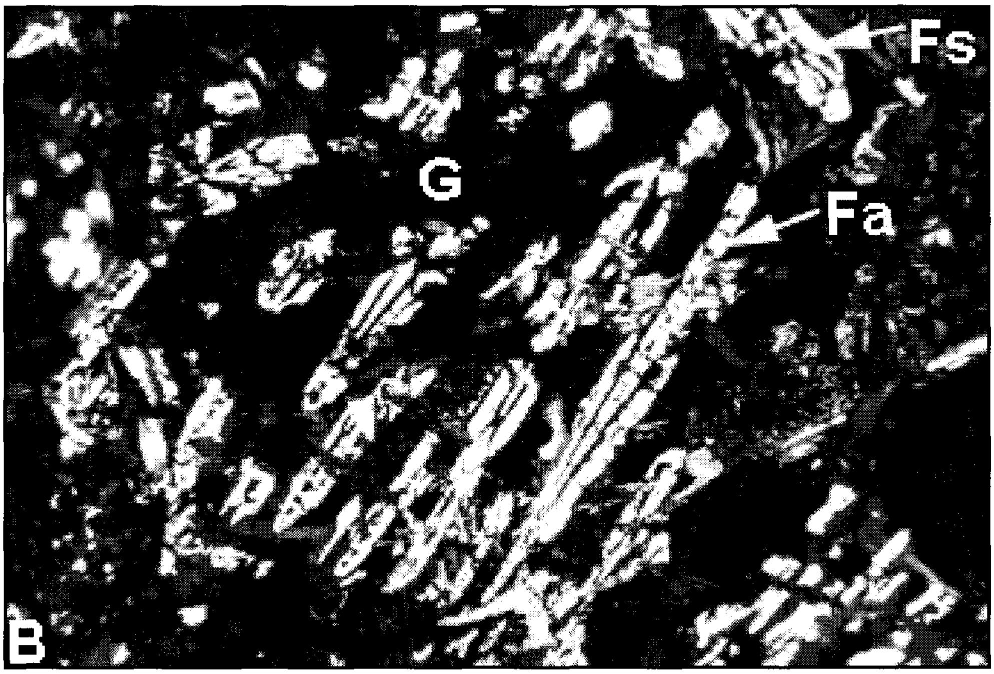

**Figure 15B.** Transmitted light micrographs x 220 PPL of paralava (sample P1). Elongated skeletal crystals of fayalite (Fa) and orthoferrosilite (Fs) in glass (G) matrix.

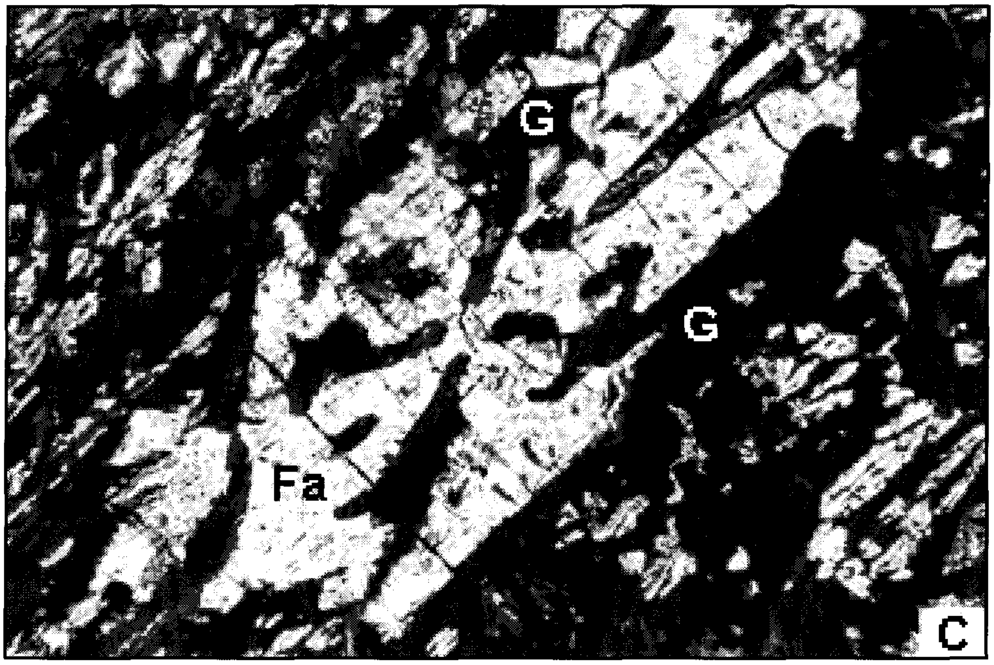

**Figure 15C**. Transmitted light micrographs x 80 PPL of paralava (sample P1). Large skeletal fayalite (Fa), the black material in and around the crystals is glass (G).

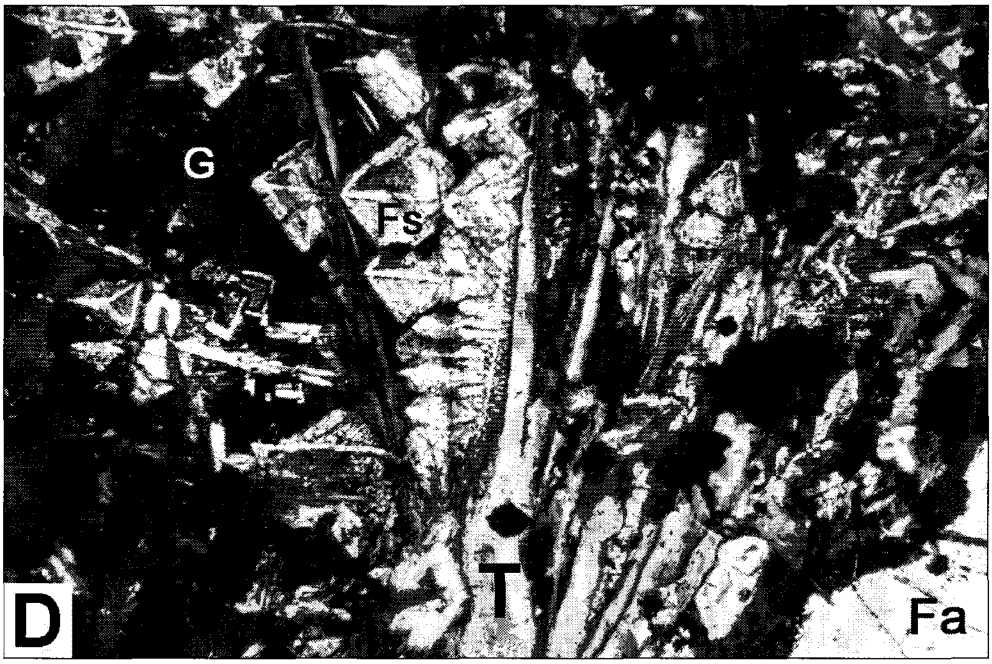

**Figure 15D**. Transmitted light micrographs of paralava x 220 PPL (sample P1). Dendrites of orthoferrosilite (Fs) concentrated between acicular tridymite (T) crystals. The white phase at right bottom corner is fayalite (Fa).

The appearances of silicate minerals in the paralavas also provide some evidence of temperatures higher than 1000°C. Investigations by Smith (1971) showed that orthoferrosilite ($FeSiO_3$) crystallizes from fayalite and silica at $T \geq 900°C$ and a pressure of 1kbar. Higher pressures (12-73 kbar) increase the stability of $FeO.SiO_2$ at high temperatures (620-1270°C) as found by Akimoto et al (1964). Bohlen et al. (1980a) determined a temperature and pressure that was lower (700°C and 8kbar) than estimated previously for the coexistence of the fayalite-orthoferrosilite assemblage.

The coexistence of orthoferrosilite and fayalite and their dependence on temperature and pressure have been the subject of extensive investigation since the initial work of Bowen and Schairer (1932). Later they studied the ternary system $MgO$-$FeO$-$SiO_2$ under atmospheric pressure and high temperatures ($\geq 1200°C$) and found that pure or substantially pure $FeO.SiO_2$ dissociates into fayalite and silica under such conditions (Bowen and Schairer, 1935).

In the Rotowaro paralava specimens there is no textural evidence to support the hypothesis that orthoferrosilite ($FeSiO_3$) crystallized after fayalite ($Fe_2SiO_4$). Simultaneous crystallization of orthoferrosilite and fayalite may have taken place from the reaction of iron and silica present in the paralava melt at atmospheric pressure and temperature $\leq 1200°C$ (Fig. 18). The reaction could have been stabilized by partitioning of the other components such as Mg, Mn and Al into the fayalite and orthoferrosilite structures as described by Bohlen et al (1980b). Rapid quenching of these minerals might then have inhibited their decomposition.

The occurrences of (tridymite + anorthite + orthoferrosilite + fayalite) assemblages in the paralavas indicate very high temperatures certainly above 1000°C. Crystallization of anorthite from a silicate melt probably occurs at $\leq 1470°C$ (Morse 1980) (see Fig. 16).

The general convergence of the data indicates formation of the slags and paralavas in the temperature range of1000°C to 1600°C.

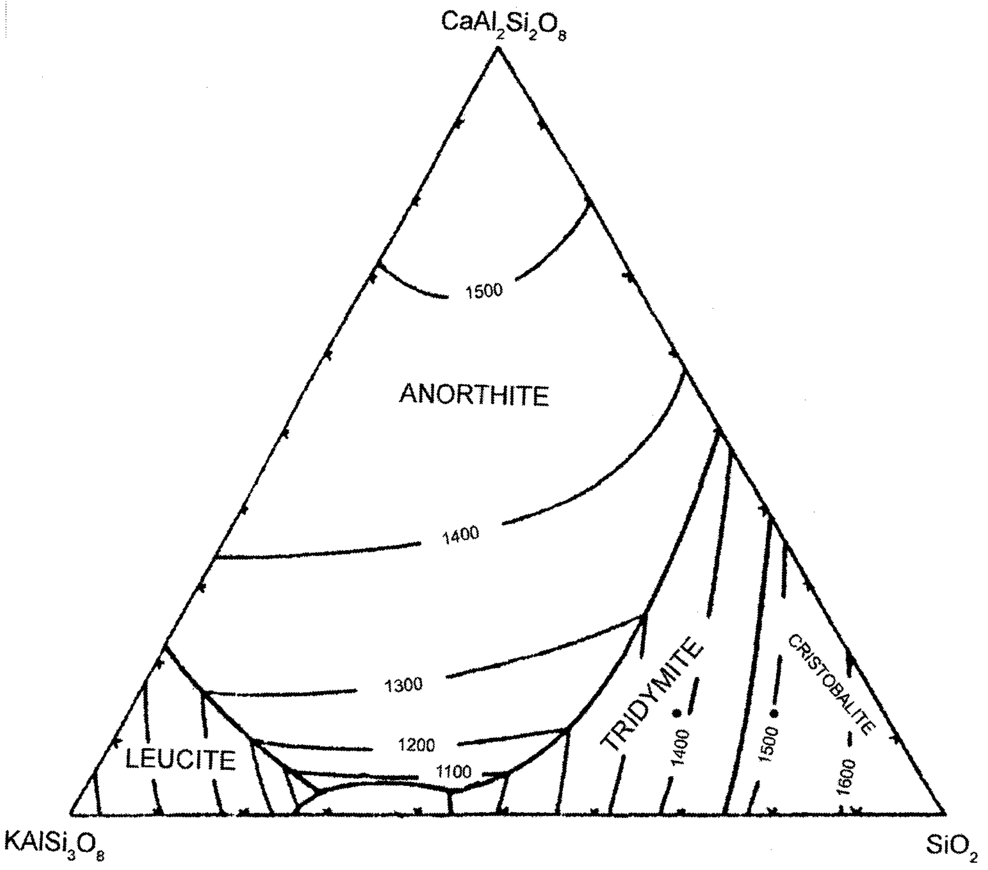

**Figure 16**. Plot of composition of glass (filled circles) in paralavas (Table 5) projected onto the liquidus of the system $CaAl_2Si_2O_8$-$KAlSi_3O_8$-$SiO_2$ (redrawn from Schairer and Bowen, 1947).

**Table 5**. Chemical analyses of glass in selected paralava samples.

| | **(P1)** | **(P2)** |
|---|---|---|
| $SiO_2$ | 60.75 | 49.13 |
| $TiO_2$ | 0.28 | 0.30 |
| $Al_2O_3$ | 19.11 | 17.89 |
| FeO* | 5.81 | 6.76 |
| MnO | 0.40 | 0.35 |
| MgO | 0.00 | 0.39 |
| CaO | 8.38 | 9.90 |
| $Na_2O$ | 0.00 | 0.60 |
| $K_2O$ | 3.94 | 2.94 |
| $P_2O_5$ | 0.09 | 0.25 |
| Total | 98.76 | 88.51 |

* FeO: refers to total iron

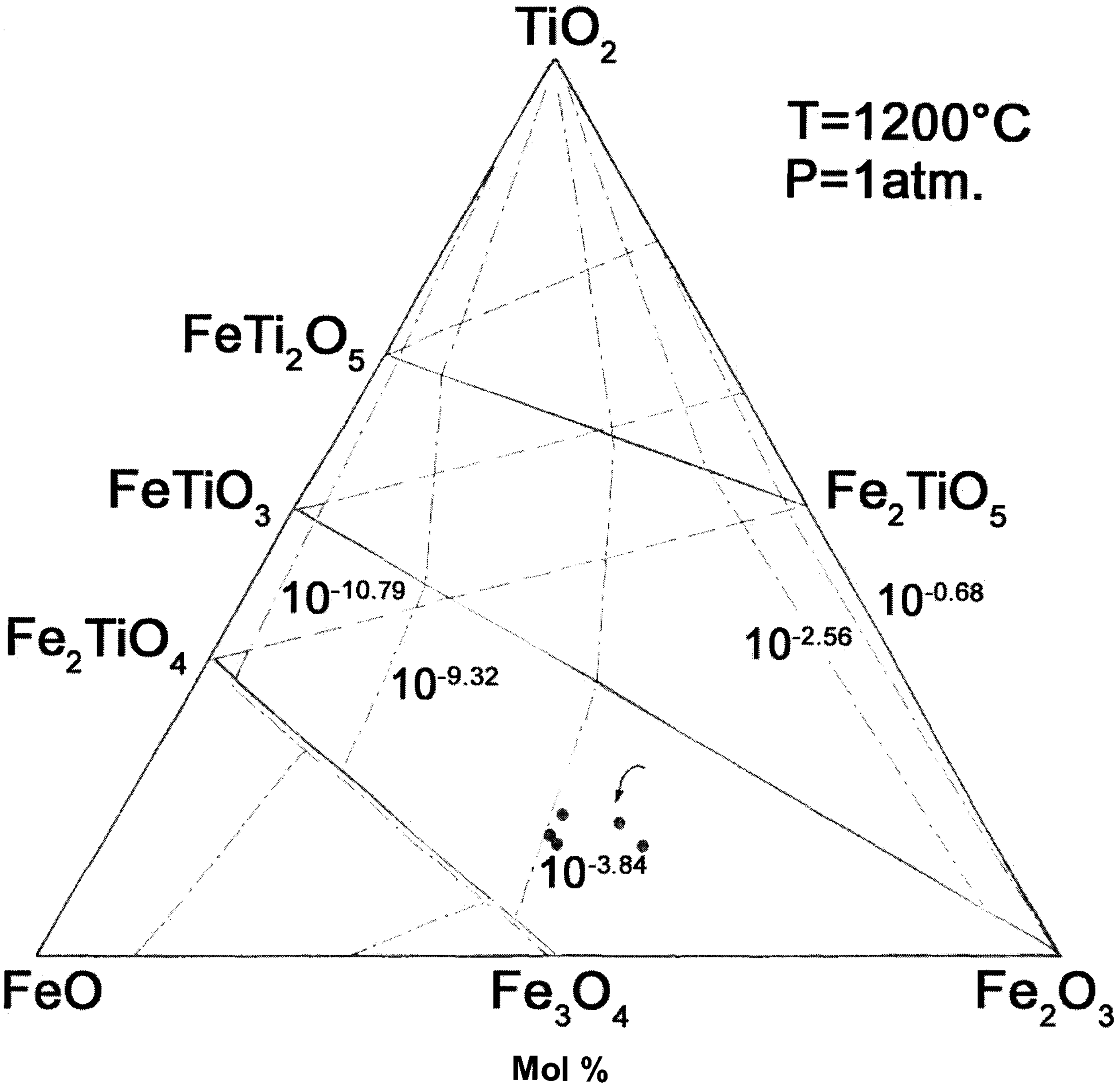

**Figure 17**. Plot of composition of titaniferous magnetite in the slag (sample EI) from electron microprobe analyses (redrawn from Haggerty, 1976).

Ulvöspinel = $Fe_2TiO_4$
Magnetite = $Fe_3O_4$
Ilmenite = $FeTiO_3$
Hematite = $Fe_2O_3$
Pseudobrookite series = $FeTiO_2O_5$ – $Fe_2TiO_5$
Oxidation-reaction lines = dashed
Solid solution lines = straight

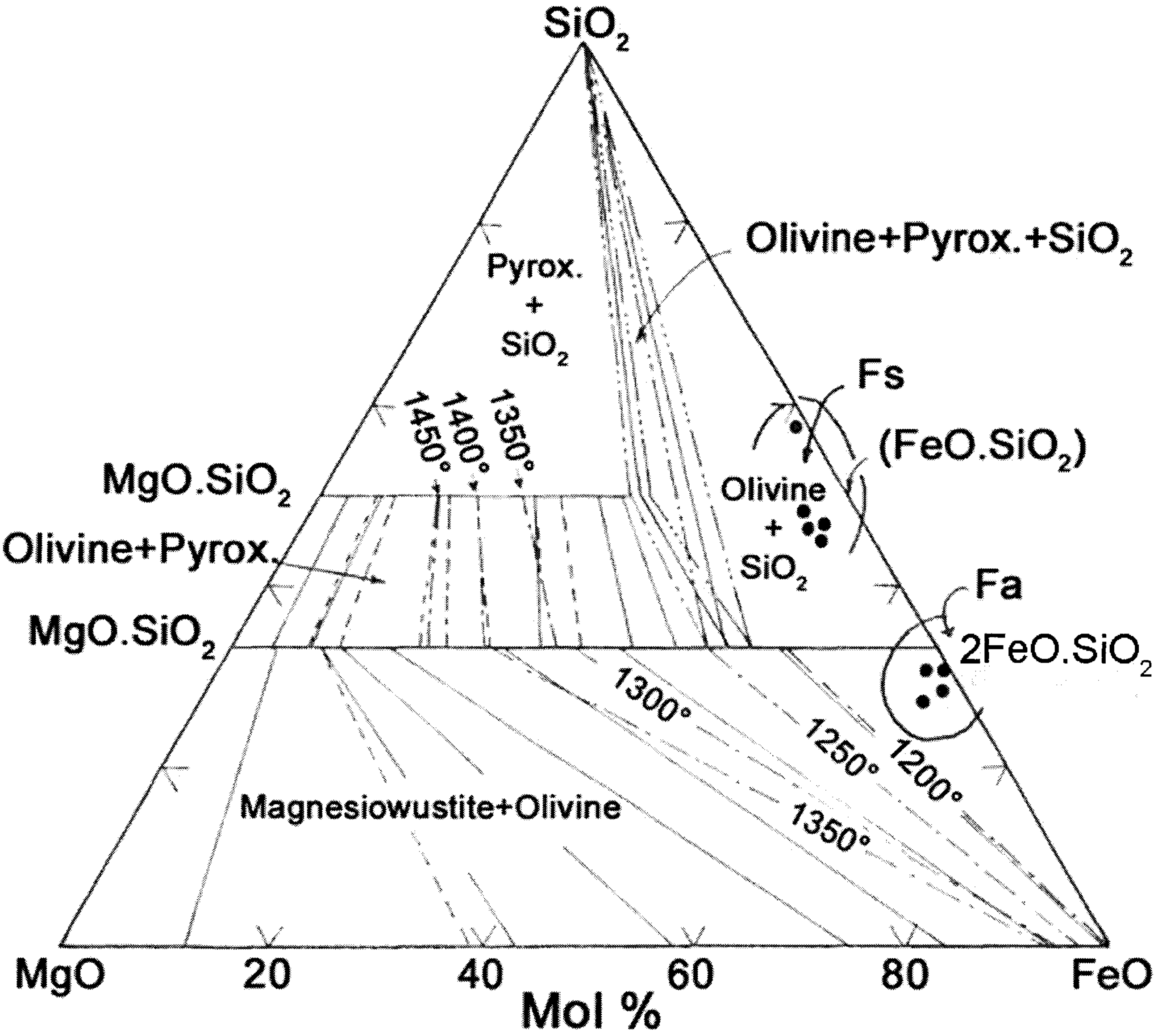

**Figure 18**. Plot of electron microprobe compositions of fayalite (Fa) and orthoferrosilite (Fs) in the slag (sample P1) (redrawn from Nafziger and Muan, 1967).

# 9. SUMMARY AND CONCLUSIONS

Thermal metamorphism of coal measures immediately overlying burnt coal seams in the Rotowaro Coalfield, North Island, New Zealand produced unusual iron-rich slags that contain the crystalline phases: magnetite, hematite, hercynite, titaniferous magnetite and accessory fayalite. Silicate melts (paralavas) that are associated with the slags contain abundant glass fayalite, orthoferrosilite, anorthite, cristobalite and tridymite and minor magnetite. Evidence from known equilibrium relationships between these phases indicates that the slags and paralavas were formed at ultra-high temperatures in the range 1000°C to 1600°C and at atmospheric pressure.

The iron oxides that occurr in the slags show variation in texture and composition. In the interior of the slags the magnetite crystals show very well-developed exsolution and oxidation textures whereas near the surface around the vesicles, hematite and titaniferous magnetite coexist and these minerals do not show any oxidation or exsolution textures. The observed variations in the iron oxides indicate differences in composition, $PO_2$ conditions, time of crystallization, and cooling rate between the area immediately adjacent to the vesicles and the central portion of the slag. The occurrence of high-Ti minerals near the surface around the vesicles indicates that the Ti must have been transported by hot gases. It is suggested that, as a result of the early high- emperature crystallization of high-Al phases in the slag, the relative proportion of Ti increased in the residual system. It may have been transported by the hot gasses escaping from the slag melt to be precipitated near the surface around the vesicles as titaniferous magnetite.

Exceptionally iron-rich slag-like rocks are unusual and the Rotowaro examples represent some of the most iron-rich natural slags that are known from a combustion metamorphic environment. The plotted trends of Rotowaro slag and porcellanite chemistries indicate that some iron mobilization process occurred during the pyrometamorphism, as also was suggested by Clark and Peacor (1992) in their study of similar rocks from the Powder River Basin in Wyoming. The source of the iron that is required to produce these iron-rich slags is an enigma, because the coal measures themselves are relatively poor in iron. Nevertheless the slags, irrespective of their oxidation state, lie on a continuation of the iron-enrichment trend observed in the porcellanites, which suggests that iron was concentrated by the coal combustion process.

During coal combustion, at atmospheric pressure and ultra-high (>1000°C) temperatures, hot gasses escaped into the open surficial fractures and cracks. The combination of the escaping gasses with atmospheric oxygen resulted in sustained high temperatures that caused intensive melting of the protolith sediments in an environment similar to that of a blast furnace. Melting of the sediments also may have been fluxed by alkali elements that are known to be complexed into the coal (see Table 1b) and liberated by its combustion. Evidence for this is seen in the high content of $K_2O$ in the paralava glasses (see Table 5). The hot gasses that were vented to the surface through open fissures also may have leached out elements from the enclosing sediments and transported them to be deposited in the melt and pyrometamorphics.

## ACKNOWLEDGEMENTS

The authors gratefully acknowledge Prof. Dr Glenn Stracher of East Georgia College, Swainsboro, Georgia, the USA, who encouraged us to contribute this article. Thanks are due to Drs J. Swope, M.J. Hibbard and R. McDowell for comments and reviewing this paper. We wish to acknowledge staff of the Geology Department, Auckland University who provided help with the electron microprobe and X-ray fluorescence analyses. Dr S. Maquiné de Souza and Ms. L. Cotterall provided assistance with figure preparations. The first author would like to express very special thanks to Prof. Dr Jean-Luc Potdevin of the Geology Department, University of Lille and Daniel Milhau for their help and support.

# REFERENCES

Adams, J., 1978. A melt rock near Murchison, New Zealand basalt or fused sandstone? New Zealand Journal of Geology and Geophysics, 21, N°6, p. 743-745.

Akimoto, S., Fujisawa, H., and Katsura, T., 1964. Synthesis of $FeSiO_3$ pyroxene (ferrosilite) at high pressures. Proc. Japan Acad, 40, p. 272-275.

Atlas, L.M. and Sumida, W.K., 1958. Solidus, subsolidus, and subdissociation phase equilibria in the system Fe-Al-O. Journal of the American Ceramic Society, 41, p. 150-160.

Beamish, B. B., Barakat, M.A., and St. George, J.D., 2001. Spontaneous-combustion propensity of New-Zealand coals under adiabatic conditions. International Journal of Coal Geology, 45, p. 217-224.

Bentor, Y.K., and Kastner, M., 1976. Combustion metamorphism in Southern California. Science 193, p. 486-488.

Black, P.M., 1982. Petrology and inorganic chemistry of South Island lignites, New Zealand. Geological Society of Australia. Coal Group Symposium (1982: Melbourne, Vic.) p.131-144.

Bishop, D.G., 1965. The geology of the Clinton District, South Otago. Transactions Royal Society of New Zealand, Geological series 2, p. 205-230.

Bohlen, S.R., Essene, E.J., and Boettcher, A.L., 1980a. Reinvestigation and application of olivine-quartz-orthopyroxene barometry. Earth and Planetary Science Letters, 47, p. 1-10.

Bohlen, S.R., Boettcher, W.A.., Dollase, W.A. and Essene, E.J., 1980b. The effect of manganese on olivine-quartz-orthopyroxene stability. Earth Planet Sci. Letters, 47, p.11-20.

Bowen, N.L., and Schairer, J.F., 1932. The system FeO- $SiO_2$. American Journal of Sciences, 24, p. 177-213.

Bowen, N.L., and Schairer, J.F., 1935. The system MgO-FeO-$SiO_2$. American Journal of Sciences, 29, p. 151-217.

Bustin, R.M., and Mathews, W.H., 1982. In situ gasification of coal, a natural example: history, petrology and mechanics of combustion. Canadian Journal of Earth Sciences, 19, p. 514-523.

Clark, B.H., and Peacor, D.R., 1992. Pyrometamorphism and partial melting of shales during combustion metamorphism: mineralogical, textural, and chemical effects. Contributions to Mineralogy and Petrology, 112, p. 558-568.

Colaizzi J.G., 2004. Prevention, control and/or extinguishment of coal seam fires using cellular grout. International Journal of Coal Geology, 59, p. 75-81.

Cosca, M.A., Essene, E.J., Geissman, J.W., Simmons, W.B., and Coates, D.A., 1989. Pyrometamorphic rocks associated with naturally burned coal beds, Powder River Basin, Wyoming. American Mineralogist 74, p. 85-100.

de Bore, C.B., Dekkers, M.J., and van Hoof, T.A.M., 2001. Rock-magnetic properties of TRM carrying baked and molten rocks straddling burnt coal seams. Physics of the Earth and Planetary Interiors, 126, p. 93-108.

Edbrooke, S.W., Sykes, R. and Pocknall, D.T. 1994. Geology of the Waikato Coal Region, New Zealand. Institute of Geological and Nuclear Sciences monograph 6. Lower Hutt, New Zealand. 236 p. (plus index and 8 map sheets).

Ellyett, C.D., and Fleming, A.W., 1974. Thermal infrared imagery of the burning mountain coal fire. Remote Sensing of Environment, 11, p. 221-229.

Essene, E.J., Coates, D.A., Geissman, J.W., and Simmons, W.B., 1984. Paralavas formed by burning of coal beds. EOS, 65, No 16, 17 April, V32A-13, p. 300.

Fermor, L.L., 1918. Preliminary note on the burning of coal seams at the outcrop. Transactions of the Mining, Geological, and Metallurgical Institute of India, 12, p. 50-63.

Foit, F.F.Jr., Hooper, R.L., and Rosenberg. P.E., 1987. An unusual pyroxene, melilite, and iron oxide mineral assemblage in a coal-fire buchite from Buffalo, Wyoming. American, Mineralogist, 72, p. 137-147.

Grapes, R., 2004. Marl to basalt: a case of extreme pyrometamorphism. In: Annual report, Institute for mineralogy, petrology and geochemistry, Albert-Ludwigs-Universität Freiburg, p. 26-27.

Gray, V.R., and Daly, T.A., 1981. Chemical properties and composition of Waikato Coals. New Zealand Journal of Science 24, p. 179-202.

Haggerty, S.E., 1976. Opaque mineral oxides in terrestrial igneous rocks. Mineralogical Society of America, short course notes: oxide minerals Ed. Rumble, 3, p. Hg-101-277.

Heffern, E.L., and Coates, D.A., 1997. Clinker- its occurrence, uses, and effects on coal mining in the Powder River Basin. In: Jones, R.W., Harris, R.E., (Ed.), Proceeding of the 32nd Annual Forum on the Geology of Industrial Minerals. Public Information Circular No38, p. 151-165. Wyoming State Geological Survey, Laramie, WY, USA.

Heffern, E.L., and Coates, D.A., 2004. Geological history of natural coal-bed fires, Powder River basin, USA. International Journal of Coal Geology 59, p. 25-47.

Hensen, B.J., and Gray, D.R., 1979. Clinohypersthene and hypersthene from a coal buchite near Ravensworth, New South Wales, Australia. American Mineralogist, 64, no 1-2; p. 131-135.

Hoffmann, A., and Fisher, W.A., 1956. Bildung des spinels $FeOAl_2O_3$ und seiner Mischkristalle mit $Fe_2O_4$ und $Al_2O_3$, Z. Phys. Chem, NF, 7, p. 80-90.

Kear, D., and Waterhouse, B, C., 1978. Waikato Coalfields: Rotowaro Coalfield 1:15840 New Zealand DSIR, Wellington, New Zealand, 24 p.

Johnson, W., and Bucknell, M.J., 1959. Pseudo-igneous rocks in the Triassic succession of the Springfield Basin, Gordon-Cradock district. Transactions Royal Society of South Australia, p.245-257.

Lindqvist, J.K., Hatherton, T. and Mumme, T.C., 1985. Magnetic anomalies resulting from baked sediments over burnt coal seams in southern New Zealand. New Zealand Journal of Geology and Geophysics, 28, p. 404-412.

Masalehdani M.N., 1985. Thermal metamorphism associated with burnt coal seams, Rotowaro Coalfield, Huntly, New Zealand. (Unpublished MSc Thesis, Auckland University, p.102.

Mason, D.R., and Davis, R., 1983. Geology and mineral chemistry of fused shale within overburden strata of Liddel seam in the Bowman's Creek Area, Hunter Valley, NSW. 17th Newcastle Symposium on advances in the study of the Sydney Basin, 29 April-1 May, 4 p.

Morse, S.A., 1980. Basalts and phase diagrams. An introduction to the quantitative use of phase diagrams in igneous petrology. Springer, New York, 493 p.

Muan, A., and Gee, C.L., 1956 Phase equilibrium studies in the system iron oxide – $\gamma$ $Al_2O_3$ in air at 1 atmosphere $O_2$ pressure. Journal of the American Ceramic Society 39, 207-214.

Nafziger, R.H. and Muan, A. 1967. System MgO-"FeO"-SiO2. American Mineral, 52 (9-10), 1377.

Parker, R.J. and Willis, J,P., 1977. Computer programs sort, REORD and MW for major element XRF data processing. Computer Geoscience 3, 115-171.

Phemister, J., 1942. Note on fused spent shale from a retort at Pumpherston, Midlothian. Transactions-Geological Society of Glasgow, No 18 (XVIII), p. 238-246.

Rãdan, S.C., and Rãdan, M., 1998. Rock magnetism and paleomagnetism of porcellanites/clinkers from the western Dacic Basin (Romania). Geol.Carpat. 49. p. 209-211.
Ramdohr, P., 1982. The ore minerals and their intergrowths. Pergamon Press, 2nd Ed.,

1250 p.

Richards, R.G. and White, J., 1954. Phase relations of iron-oxide containing spinels. I. relations in the system Fe-Al-O. Transactions British Ceramic Society, 53, p. 233-270.

Schairer, H., and Bowen, N.L., 1947. The system leucite-anorthide-silica. Geological Society of Finland Bulletin, 20, p. 67-87.

Sen Gupta, S., 1960. Petrography of the Para-Lavas of the Eastern Part of Jharia Coalfield. Geol. Min. Met. Soc. Ind.Q.J.23, p. 79-101.

Smith, D., 1971. Stability of the assemblage iron-rich orthopyroxene- olivine- quartz. American Journal of Sciences, 271, p. 370-383.

Turnock, A.C., and Eugster, H.P., 1962. Fe-Al oxides: Phase relationships below 1000°. Journal of Petrology, 3 (3), p. 533-565.

Tyráček. J., 1994. Stratigraphical interpretation of the paleomagnetic measurements of the porcellanites of the Most basin, Czech Republic.Vestink Ceského geologického ústavu 69 (2), p. 83-87.

Zhang, Xiangmin, 1998. Coal fires in northwest China: Detection, monitoring, and prediction using remote sensing data. PhD. Thesis, Delft University of Technology, Delft, The Netherlands, 135 p.

# 1. SUMMARY, CONCLUSION AND RECOMMENDATIONS

At the two selective study coal waste heaps in the Nord-Pas-de-Calais region (Avion n°76 and Fouquiére-les-Lens n°83) features like: development of the surficial fissures, opining of large gas vents, baked debris, emission of various gases (including water vapour) and the encrustations of secondary salt minerals are observed and taken as evidence of subsurface coal fire associated with these sites. Both physical and chemical properties of the coal waste heaps' materials influenced and facilitated their spontaneous subsurface combustion. External factor such as lightning may have also initiated the coal fire within these coal waste heaps. These include:

- coal rank
- coal volatile matter
- petrographic composition of coal
- coal moisture content
- pyrite content in coal and in rock debris
- petrographic composition of rock debris and their carbon content
- mining and construction method
- available air and atmospheric conditions
- particle size, void ratio and surface area

Seasonal surface temperature measurements around selected gas spots (fumarole discharges) within the coal waste heap n°76 were recorded at the top surface of the site for one year. The temperatures gradient in the range of 40- 255.7°C showed that combustion is more important in the northeast and southeast of this site. It should be stressed that the temperature 255.7°C is a surface measured temperature, in the other words the self-sustained heating temperature but not the thermal baking temperature of coal waste heap rock debris (see below).

At atmospheric pressure and at temperature ranges 500-900°C, upon the combustion, the original coal measures black carbonaceous shales associated with the coal waste heap n°76 in Avion are baked and modified into variegated reddish, pinkish and orange baked rock debris (the porcellanites). Quartz-bearing sandstones are less affected by heating. The mineralogical composition of the black carbonaceous shales is: quartz, kaolinite, muscovite, illite ± calcite ± gypsum ± siderite, in addition to pyrite and organic carbon. The porcellanites are hematite-rich and contain quartz. Molten rock debris (i.e. the slag and/or the paralava) were not observed associated in this coal waste heap. This clearly indicates that in-situ subsurface combustion in this site resulted at temperature ≤ 900°C, as described below.

Laboratory baking and dehydration experiments on carbonaceous shale samples from coal waste heap in Avion, revealed that dehydration of clay minerals appears at 500°C. At this temperature all water molecules and (OH) ions in kaolinite are driven off and it disappears from the XRD patterns, illite, muscovite and calcite persist until temperature 700°C, above temperature 900°C the latter minerals are completely decomposed. As baking temperature increases, at 1200°C XRD patterns reveal the presence of new phases, such as mullite, cordierite, spinel, tridymite ± quartz, and the sample shows ropy surface containing spherical vesicles ≤2mm in diameter indicating the gas escape from the sample.

Although, man-mad, the mineralogical investigations of baked rock samples collected from coal waste heap n°144 in Rieulay confirm perfectly the baking and dehydration temperature of heating and combustion processes and the formation of high temperature minerals, as described above. In other words in this site intentional baking and combustion attended by temperature in ≥1200°C.

In-situ gas measurements and analyses around selected gas spots were performed using the chamber method. Gas measurements were carried out three times at the coal waste heap n°76 and twice at the coal waste heap n°83. Gas temperature recording and the quantification of concentrations of emitted gases such as $H_2S$, $SO_2$, $NO_x$, CO, $CO_2$, hydrocarbons, $O_2$ and $H_2O$ were determined. The concentrations of the various gases were compared to each other and to TLV (Threshold limit value) in order to determine the negative impacts of such gases on the human health and on the environment. Field measured surface temperatures around active events (56-255.5°C) showed heterogeneity of combustion at both sites. $H_2S$ was absent, the most important finding was the concentration of $CO_2$ (7%) much higher than TLV; the concentrations of $SO_2$ (<5 to 25 ppmv) and $NO_x$ (8 to 25 ppmv) are also above TLV. CO concentration is in order of 20-110 ppmv therefore, below and/or above TLV. $CH_4$ is the main emitted hydrocarbon; methane concentrations were measured (47 to 260 ppmv) outside the explosion limit. Further, the level of $O_2$ (<1% to 19%) around the gas vents is below the atmospheric level it requires that access to the sites must be limited to authorised people only.
The results of laboratory oxidation experiments on selected medium-volatile bituminous coal and carbonaceous shale samples from coal waste heap in Avion showed that concentration

and emission of each gas are rank and temperature depended. On the other hand the higher the temperature the higher the CO concentration, for example. This is also valid for the emission of other hydrocarbon gases from coal combustion (e.g. methane, ethylene etc). It is demonstrated that carbonaceous shales are source of gas emissions (e.g. $SO_2$, CO, O) and heat. The oxidation tests on coal samples revealed mass loss then mass gain of solid, the phenomena is believed to be due to the formation of different gases which are not released and/or the formation of sulphates (e.g. iron sulphate).

In 3 years of sampling from coal waste heap n°76 in Avion, 21 secondary salt efflorescence minerals were identified as encrustations and crystalline phases depositing principally on baked carbonaceous shale debris and around fumaroles discharges at top surface of the site. The most abundant and most frequently found minerals are thenardite and bloedite, others include konyaite, glauberite, aphthitalite, langbeinite, arcanite, gypsum, epsomite, hexahydrite, alunogen, kalinite, pickeringite, tschermigite, mascagnite, lecontite, and two possible new minerals, as well as halides (salammoniac, halite) and native sulphur. The major chemical components making up the fumarole-related deposits are $SO_4$, $NH_4$, $H_2O$, Cl, Mg, K, Na, Al, Ca, Fe, Mn and S.

It is concluded here that the secondary mineral association of burning coal waste heap at Avion and processes of their origin are to a considerable extent analogous with condensates and sublimates that are produced by volcanic fumaroles. Alkaline earths, sulphur and trace metals are hydrothermally leached from the fine-grained rock debris by continuous gas-rock interaction. Thus, most encrustations and crystalline phases are deposited in vapour-rich and slightly acidic pH (4 to 5.5) environment; and at temperature ranges between 40-265°C. Fumarolic minerals form following cooling of the gas (S,N,O,C compounds, water vapour originally in the gas and hydrothermally leached cations and trace elements) upon reaching the surface of the coal waste heap. It is found that encrustations and/or crystallizations deposited at high temperatures ($\geq$ 300°C) are less abundant than those deposited at lower temperatures ($\leq$150°C°). The difference in temperature is reflected in the mineralogy of the phases.

However, the processes of mineralization occurred from a complex solution chemistry (acid-rich aqueous solution) and sequence of processes. Salammoniac formed by direct gas sublimation. Thenardite, bloedite, aphthitalite, langebenite, arcanite, glauberite, halite, gypsum, epsomite, pickeringite, alunogen, tschermigite, mascagnite and native sulphur formed from a cooling gas-liquid system (i.e. condensation). Konyaite and hexahydrite formed from partial alteration (minerals begin to crystallize during cooling and dehydrate immediately after deposition and/or after sampling: hydration of bloedite, dehydration of epsomite). Kalinite can be a dehydration product of K-alum, and lecontite may be an alteration (hydration) product of pre-existing ammonium aphthitalite.

Occurrences of trapped fluid inclusions in crystals of thenardite in sample AV1443d indicates low crystallisation temperature $\leq 150°C$ and high salinity of aqueous solution of the mineral assemblage thenardite-bloedite-aphthitalite.

Variation in the mineral assemblages between locations at coal waste heap n°76 indicate: variations in coal content within the waste; influence of continuous gas-rock interaction on the chemistry of gas escaping to the surface; variations in temperature and cooling rate of the gas; influence of atmospheric conditions (i.e. seasons, meteoric water etc); and variable composition of the aqueous solution.

It should be noted that sulphate salt and halides described herein are all soluble salts and therefore transient. The efflorescence dissolve leaving no residues in deionized water are thus removed in the first rainfall after their formation. All the minerals identified at the burning coal waste heap in Avion have negative impacts on the environment and on the human health. In addition to metallic cations, S and N they also contain metallic trace elements. Chemical analyses of selected sulphate minerals show that these minerals contain trace elements such as As, Ba, Cu, Mo, Cs, Ni, Rb, Th and U. Coal fire salt minerals can be vectors for metal pollution of groundwater and soils and for toxins transmitted to humans by crop (food) grown in soils around the coal waste heap. Slow dissolution of Na-Mg-bearing minerals (thenardite, bloedite etc) and $NH_4$-bearing minerals (salammoniac, mascagnite and tschermigite) and their migration into groundwater and surrounding agricultural soils may increase the salt concentration and can destroy nearby flora and faunal habitats. Interaction of gas with oxygenated atmospheric precipitation results in $NO^{3-}$ and $NO^{2-}$ formation. The migration of nitrates and nitrites into the groundwater may increase the nitrogen content and cause local water pollution. Chemical analysis of collected drinking water (tap water at coal waste heap in Avion) showed the nitrate content above the threshold level of 45 mg/l. Arsenic concentration at the moment remains below the threshold level of <0.05 mg/l.

The salt occurrences may represent potential environmental and health hazards. The study of chemical nature and mutual interactions of the phases carrying harmful elements should be investigated.

Most of the sulphate minerals, and the presence of fluid inclusions in thenardite crystals, are documented for first time from coal-fire gas.

The present research study was carried out in time limited therefore it still remains further scientific investigations about coal fires within coal waste heaps regionally or nationally. This includes:

1) annual in-situ gas measurements and quantification of greenhouse gases and heat flux measurements at the coal waste heap n°83 in Fouquiéres les-Lens.
2) research and analysis of collected condensate waters and transport of cations and trace elements by coal fire gas and their forms (i.e. volatile)
3) further laboratory tests on carbonaceous shale their potential heat source,
4) regular sampling and analysis of drinking water and groundwater around coal waste heaps n°76, n°83 and n°144,
5) detailed studies about processes of mineralization of the secondary minerals from coal fire gas,
6) finally, it is highly recommended to investigate possible soil-water pollutions and the formation of secondary by-products at the coal waste heap n°144 in Rieulay. This site and its tailings may be polluted and may contain AS or As-pyrite and other harmful metals and/or trace elements.

## 2. PREVENTIONS

Coal fires induced by spontaneous combustion emit various greenhouse gases. The emission of carbon dioxide due to coal burning produces 38% of the world's annual total emissions of $CO_2$. No single estimation has yet been compiled as to the effect of emission derived solely from spontaneous combustion of coal on a global basis. Indeed, such a figure would be hard to achieve, given the fragmented nature of the information available. Coal fires evoked by spontaneous combustion affect many nations, although each isolated incident is only a minor contributor to overall emissions since it is a point source of pollution.

Each fire is unique. It will emit quantities of $CO_2$, $CH_4$, $SO_2$, $NO_X$, $H_2S$ and other gases at rates that reflect its current state. Any fire, regardless of its cause, is controlled by three fundamental factors: fuel, heat and oxygen. The removal of any one of these will extinguish the fire, a principal upon which all fire-fighting techniques are founded. The relationship between these factors is commonly referred to as the fire triangle (Fig. 1), together with various ways in which each side of the relationship can be successfully addressed.

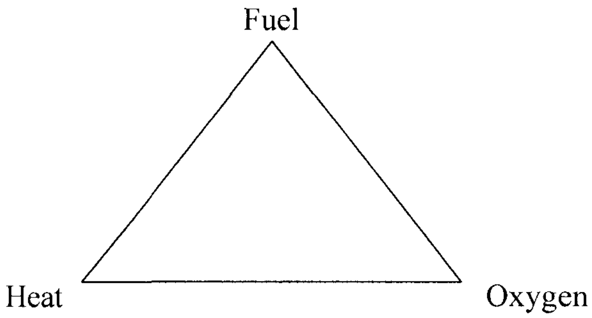

**Figure 1**. The fire triangle.

Next steps to deal with the problem of spontaneous combustion associated with coal waste heaps may be:

- try to extinguish the existing relatively new fires
- try to isolate the existing old fires
- try to take a scientific approach to mining practices and give due consideration to proposed fire prevention plans
- try to bring about awareness of the hazards and risks of coal fires (e.g. policy makers and people living in vicinity of burning coal waste heaps)
- carry out routines monitoring the coal waste heaps areas using new scientific techniques (e.g. in-situ gas measurements, heat-flux measurements, remote sensing etc)
- disseminate the acquired knowledge to help other affected countries (e.g. scientific publications, conference presentations)
- find funding to invest in further research on the phenomenon of spontaneous combustion and occurrences of toxic by-products (e.g. harmful trace elements, metal-bearing secondary-minerals etc).

On the basis of all the problems caused by spontaneous combustion like greenhouse gas emissions, the financial losses and the threat to local population, numerous investigations were internationally made to prevent coal from self-heating and to quench caused coal fires. Here in France hazards caused by coal fires and emission of various gases and the formation of secondary by-products were not scientifically researched. It is hoped that the results and investigations methods described in this study will be some of assistance in the recognition of similar occurrences elsewhere.